ANISOTROPIC SCATTERING, VOIDS AND HYBRID PRINCIPLES IN FINITE ELEMENT NEUTRON TRANSPORT

BY

Navtej Singh Riyait

Thesis submitted in fulfilment of the
requirement for the degree of
Doctor of Philosophy

of

The University of London

and the

Diploma of Imperial College

1987

Nuclear Power Section
Department of Mechanical Engineering
Imperial College of Science and
Technology, London.
SW7 2BX

A B S T R A C T

The treatment of anisotropic scattering for the multigroup form of the even parity equation and methods for solution of void problems have been considered within the framework of the finite element method. The maximum principle functional $K^{+}(\phi^{+})$ of Ackroyd has been used.

Anisotropic scattering in the multigroup approximation is investigated in one dimensional slab geometry. Treatment of within group and intergroup anisotropic scattering in the finite element method is illustrated. Proof tests on one dimensional multigroup neutron transport problems are reported for strong anisotropic scattering. The in-group scattering is checked using the so called backward-forward-isotropic scattering law for source and eigenvalue problems. With this law anisotropic scattering problems can be transformed into equivalent isotropic scattering problems. In this way the well validated isotropic version of the finite element code FELTRAN is used to validate the anisotropic version. Intergroup scattering effects are checked by solving few group source problems for P_1, P_3 scattering and backward-forward-isotropic scattering law. For P_1 and P_3 scattering, checks are made with the discrete-ordinate finite difference code ANISN and the spherical harmonics finite element/finite-difference code MARC/PN. For the backward-forward-isotropic

scattering law, comparison is made with the two group exact solution of Williams (1985) for one dimensional systems.

In the case of solutions of the even parity equation for systems with voids the conventional finite element method tends to give physically unacceptable results as the void cross section tends to zero. An explanation of this effect is proposed. Two new methods for voids using biased trial functions are described and tested. Firstly, the iterative method which synthesises a finite element solution using a sequence of related problems with constant absorption cross section in the void regions. Secondly, the extrapolation method which obtains a best approximation to the void solution by combining two or more independent biased trial functions in an optimum way. The extrapolation method is further divided into elementary, sequential and nodal or multiparameter extrapolation. The theory of both the iteration and extrapolation method is given and discussed. Several two dimensional X-Y geometry test problems using the above methods are investigated. Results are compared with those obtained with other numerical methods, e.g. discrete-ordinates and Monte Carlo, and the almost exact results of the point kernel method for voids surrounded by purely absorbing media.

Finally hybrid principles, using a trial function and a trial vector are briefly studied together with the synthesis

method of solution for reducing computer storage requirements. The synthesis method uses the idea of nodal or multiparameter extrapolation. In this method higher moment solutions can be built-up starting with a diffusion theory solution. Using the N^{+-} functional, this building up of the solution can be done on an element level allowing discontinuous solution, for the even parity angular flux across element interfaces.

ੴ

ਸਤਿਨਾਮੁ ਕਰਤਾ ਪੁਰਖੁ

ਨਿਰਭਉ ਨਿਰਵੈਰ

ਅਕਾਲ ਮੂਰਤਿ

ਅਜੂਨੀ ਸੈਭੰ

ਗੁਰ ਪ੍ਰਸਾਦਿ ॥

ACKNOWLEDGEMENTS

Firstly the author wishes to thank Professor A.J.H Goddard for providing the opportunity to carry out this research work and his overall support during the project. The author is also indebted to Professor R.T. Ackroyd for his careful and close supervision and advice throughout the course of this study. I also wish to thank him for much of the theoretical work in the methods for voids.

I would like to express my thanks to Dr. J.G. Issa for much support and advice and many valuable discussions concerning the code FELTRAN and implementation of multi-group anisotropic scattering. Here I am also grateful to Mr. K. Fletcher of UKAEA, Risley for his advice and solutions to multigroup anisotropic scattering test problems using the code MARC/PN. My thanks also go to Mr. G.E. Stott for his assistance relating to a later version of FELTRAN; to Mr. P.J. Robinson of UKAEA, Risley, for providing RANKERN solutions to void test problems and Mr. M.H. Watmough of British Nuclear Fuels for providing McBEND solutions to void test problems.

Also I would like to thank the Science and Engineering Research Council and United Kingdom Atomic Energy Authority, Risley for providing financial support for this study.

Last but not least I would like to thank my wife for typing the thesis.

C O N T E N T S

ABSTRACT
ACKNOWLEDGEMENTS
CONTENTS

PAGE

1 INTRODUCTION

1.1 Scope of Thesis 13
1.2 Review of Previous Work 16
1.3 Neutron Interactions 21
1.3.1 Angular Distribution of Scattered Neutrons 23
1.3.2 Kinematics of Neutron Scattering 25
References to Chapter 1 29

2 NEUTRON TRANSPORT

2.1 Neutron Transport Equation 35
2.2 Even and Odd Parity Equations 39
2.3 Boundary Conditions 42
2.4 Source and Eigenvalue Problems 43
2.5 Numerical Methods for Neutron Transport 45
2.5.1 Discrete Ordinates Method 46
2.5.2 Integral Transport Method 48
2.5.3 Spherical Harmonics Method 49
2.5.4 Monte Carlo Method 52
2.5.5 Finite Element Method 53
References to Chapter 2 55

PAGE

3 GENERALISED LEAST SQUARES METHOD FOR GENERATING VARIATIONAL PRINCIPLES

3.1 Introduction 61
3.2 Conventional Least Squares Method 61
3.3 Generalised Least Squares Method 64
3.3.1 The Basic Idea 64
3.3.2 The $W^{+-}(\phi^+,\phi^-)$ Functional 68
3.3.3 The $K^{+-}(\phi^+,\phi^-)$ Maximum Principle 68
3.3.4 Maximum Principle for ϕ^+ 70
3.3.5 Maximum Principle for ϕ^- 71
3.3.6 Geometrical Interpretation of $K^{+-}(\phi^+,\phi^-)$ 71
3.4 First Order Principles 74
3.4.1 The $\hat{K}(\phi)$ and $\bar{K}(\phi)$ Principles 74
3.4.2 Conventional Least Squares Method for the First Order Equation 78
3.4.3 Generalised Least Squares Method for the First Order Equation 80
References to Chapter 3 83

4 ANISOTROPIC SCATTERING IN ONE DIMENSIONAL SLAB GEOMETRY

4.1 Introduction 85
4.2 The $K^+(\phi^+)$ Functional 89
4.3 The Reduced Functional 91
4.4 Finite Element Approximation 96
4.4.1 Choice of Elements 101
4.5 Derivation of Angular Matrices 106
4.6 The Odd Parity Flux 118
4.7 The Multigroup Approximation 121
4.7.1 The Multigroup Equation 122
4.8 Even and Odd Parity Downscatter Sources 125
4.8.1 Local Source Matrices 131

PAGE

4.9 Extension to Higher Dimensions 134
4.10 One Group Test Cases 137
4.10.1 BFI Scattering Law Test Problem I 137
4.10.2 BFI Scattering Law Test Problem II 145
4.10.3 Forward Scattering Source Problem 149
4.11 Multigroup Test Cases 152
4.11.1 Benchmark Problem with BFI Scattering Law 152
4.11.2 P1 and P3 Scattering Source Problems 158
4.11.3 P1 Scattering Multiregion Source Problem 177
4.11.4 P3 Scattering Eigenvalue Problem 188
References to Chapter 4 190

5 TREATMENT OF VOIDS

5.1 Introduction 196
5.2 Conventional FEM for Voids 196
5.3 Iteration Method for Voids 203
5.3.1 Introduction 203
5.3.2 Iteration for the First Order Equation 203
5.3.3 Iteration for the Even Parity Equation 207
5.3.4 Lower Bounds to the Exact Solution in Voids 209
5.4 Extrapolation Method for Voids 212
5.4.1 Extrapolation Method Outlined 212
5.4.2 Motivation for the Method 214
5.4.3 Geometrical Interepretation 219
5.4.4 Derivation of Parameters 222
5.5.5 Extrapolation for First Order Equation 228
5.4.6 Improved Solution in the Void 230
5.4.7 Sequential Extrapolation 232
5.4.8 Multiparameter Extrapolation 238

PAGE

5.4.9 Choice of Trial Functions for Extrapolation 249
5.5 Void Test Problems 251
5.5.1 Introduction 251
5.5.2 Square Source Void Problem with Pure Absorber 252
5.5.3 Straight Duct Source Problem with Pure Absorber 272
5.5.4 Dog-Leg Duct Source Problem with Pure Absorber 284
5.5.5 Square Source Void Problem with Scattering Media 296
References to Chapter 5 301

6 HYBRID VARIATIONAL PRINCIPLES FOR THE FINITE ELEMENT METHOD

6.1 Introduction 304
6.2 Least Squares Method for Hybrid Variational Principles 306
6.2.1 A Hybrid Maximum Principle for Diffusion Theory 306
6.2.2 Classical Maximum Principle 309
6.2.3 Minimum Principle 310
6.3 Hybrid Principles for Transport Theory 312
6.3.1 The H+-(ϕ^+, ϕ^-) Maximum Principle 312
6.3.2 Neutron Conservation 316
6.3.3 The E+-(ϕ^+, ϕ^-) Minimum Principle 318
6.3.4 The E-+(θ^-, θ^+) Minimum Principle 320
6.3.5 The N+-(ϕ^+, ϕ^-) Functional 322
6.4 Generating Higher Moment Solutions from Lower Moments 323
6.4.1 Maximisation of H+-(ϕ^+, ϕ^-) 323
6.4.2 Synthesis Method 325

PAGE

6.4.3 Synthesis Method in One Dimensional Slab Geometry 328

6.4.4 Synthesis Using N+-(ϕ^+,ϕ^-) 332

References to Chapter 6 337

7 CONCLUSIONS AND RECOMMENDATIONS

7.1 Discussion 340

7.2 Recommendations for Further Study 341

APPENDICIES 344

A Derivation of the Even Parity Equations for the Iteration Method

B Theoretical Lower Bounds to the Even Parity Flux

C Derivation of Parameters for Elementary Extrapolation

D Detailed Point Kernel and Extrapolation Method Solutions

List of Joint Publications

CHAPTER 1

1. INTRODUCTION

1.1 Scope of Thesis
1.2 Review of Previous Work
1.3 Neutron Interactions
1.3.1 Angular Distribution of Scattered Neutrons
1.3.2 Kinematics of Neutron Scattering

References to Chapter 1

1. INTRODUCTION

1.1 Scope of Thesis

This thesis is mainly concerned with the solution of the even parity neutron transport equation using the finite element method. Both fixed source and eigenvalue problems are considered. The maximum principle functional $K^{+}(\phi^{+})$ of Ackroyd [1] is employed for problems with anisotropic scattering and voids. More precisely anisotropic scattering is treated mathematically in one dimensional slab geometry in the multigroup approximation and is implemented and tested. Also new methods for solution of void problems are developed and tested. The thesis concludes with an application of the hybrid principles proposed by Ackroyd [2].

After a brief review of previous work done in finite element neutron transport with isotropic and anisotropic scattering and also voids, there follows a brief discussion on neutron scattering interactions.

In chapter two, the first order and the even and odd parity second order neutron transport equations are introduced. The boundary conditions are also stated. Subsequently various numerical methods widely used in neutron transport calculations are outlined and their advantages and disadvantages discussed. These include the discrete-

ordinates finite-difference, integral transport, spherical harmonics, Monte Carlo and the finite element method.

Chapter three is concerned with the various functionals introduced by Ackroyd [3]. The generalised least squares method for obtaining variational principles is considered. The functional $W^{+-}(\phi^+, \phi^-)$, which provides a least squares measure of the error made by the approximations ϕ^+ and ϕ^- is considered. Also the physical and geometrical interpretations of W^{+-} and the functional K^{+-} are given. Finally, other functionals arising from the W^{+-} functional are reviewed.

Chapter four is concerned mainly with anisotropic scattering in one dimensional slab geometry, both for one group and the multigroup case. Angular integration is performed in the $K^+(\phi^+)$ functional leading to the reduced functional. Matrices for the angular constants are derived subsequently, after introduction of the finite element approximation. Also even and odd parity down-scatter source matrices are evaluated. Extension of multigroup anisotropic downscatter to higher spatial dimensions is then discussed. Next, results of test problems in one dimensional slab geometry for both one group and the multigroup case are presented and compared with those obtained with other numerical methods or analytical results.

In chapter five, the problem encountered when solving the even parity equation for voided regions using the conventional finite element method is discussed. An explanation of the almost flat flux profile obtained from the conventional finite element method is proposed. Two new methods, iteration and extrapolation, for obtaining improved solutions, for systems with voids, are presented. The theory of both the methods is given and discussed. Subsequently several test problems are considered. These include a straight duct problem, a dog-leg duct problem and also two square source void problems. Results of the iteration and extrapolation (global and nodal) methods are compared with point kernel, discrete ordinates and Monte Carlo methods, and are discussed.

Hybrid principles of Ackroyd [2] which involve a trial function and a trial vector are discussed in chapter six. Also the method of synthesis is illustrated for one dimensional slab geometry. This method involves just one unknown per node, even for higher moment solutions and hence reduces computer storage requirements. The idea of nodal extrapolation, used in the solution of void problems is also employed here in the synthesis method.

In chapter seven, there is a discussion and recommendations for further study which is followed by the Appendices.

1.2 Review of Previous Work

The finite element method has been applied to neutron transport calculations for many years. Major effort has been directed towards solution of the neutron transport equation with isotropic scattering. A brief review of some of the work carried out in the area of finite element neutron transport is given below. Particular emphasis is given to anisotropic scattering work and treatment of voided regions in finite element neutron transport.

The finite element solution of the neutron transport equation has been investigated by several researchers including Ohnishi [4], Kang and Hansen [5], Deppe and Hansen [6] and Grenfell [7] for diffusion problems. Transport theory work includes that of Miller, Lewis, Rossow, [8], Kaper et al [9], Briggs et al [10] and Mordant [11].

Ziver [12] and Ziver and Goddard [13] have developed the finite element method for neutron transport in two dimensional X-Y geometry. Their work includes the multigroup scheme with isotropic scattering. Issa [14] has developed the method for two dimensional R-Z geometry and has also solved some three dimensional multigroup diffusion problems with prism shaped elements. Quah [15] has produced a modular code for multigroup finite element neutron transport with isotropic scattering.

Wilson [16] has used the K^{+-} principle in one dimensional slab geometry with discontinuous finite elements. He has developed the code DUPLEX and has solved several one group problems.

With anisotropic scattering, especially in the multigroup case, it is only recently that much effort has been directed at incorporating anisotropic scattering within the finite element method. Lillie and Robinson [17] have solved two dimensional multigroup problems with anisotropic scattering. They used a spatial discretisation of the even parity transport equation as their basis. They constructed a functional with the property that the stationary value of the functional gave an approximate solution. Both the position and angular space were discretised, finite elements for the former and discrete ordinates for the latter.

Galliara [18] has used the $K^{+}(\phi^{+})$ maximum principle functional of Ackroyd [1] to solve one group neutron transport problems in one dimensional slab geometry. He used finite elements for the spatial variable and Legendre polynomials for the angular variable. He also treated anisotropic scattering in the one group case and used upto eight even moments expansion for the even parity angular flux.

Fletcher [19,20] has developed the code MARC/PN for

multigroup neutron transport calculations, using a weighted residual technique stemming from the $K^{+}(\phi^{+})$ principle. He initially used a finite difference scheme for neutron position but now has the finite element option. Spherical harmonics are used for neutron direction. MARC/PN can be used to solve multigroup anisotropic scattering problems.

Splawski [21], and Ackroyd and Splawski [22] investigated the use of orthogonal functions for approximating the angular dependence of the even parity flux. Simple one dimensional examples were considered. Splawski also demonstrated Ackroyd's method of bracketing local reaction rates, (i.e. local error bounds) using complementary principles, in one dimensional slab geometry.

Wood and Williams [23,24] have developed the one group and multigroup anisotropic scattering equations, for R-Z geometry and Wood [25] has implemented this in the code FELICIT. Many one group and multigroup source and eigenvalue test problems have been solved and reported.

De Oliviera [26] has recently extended multigroup anisotropic scattering for arbitrary geometry and has reported solutions to a few test problems. Williams and Wood, and De Oliviera have all used the $K^{+}(\phi^{+})$ functional for the even parity transport equation.

Independently Riyait [27] and Issa [28] have worked on multigroup anisotropic scattering using the $K^{+}(\phi^{+})$ functional. Riyait [29] has considered multigroup anisotropic scattering in one dimensional slab geometry and obtained solutions to several problems. Comparison of finite element solutions is made with analytical and other numerical solutions. Anisotropic scattering theory for the even parity equation and results of test problems are discussed in detail in this thesis. Issa et al [28] have extended the multigroup anisotropic scattering to two and three dimensions. The capability of the finite element code FELTRAN is demonstrated by Issa et al, by solving several practical source and eigenvalue problems.

Stott [30] has worked on cylindrical R-Z and Cartesian X-Y geometries, and has produced a semi-commercial code FELTRAN. He has also implemented the multigroup anisotropic scattering option into FELTRAN.

Relatively little work has been done in improving the solution of the even parity transport equation for voids. The discrete ordinates methods suffer from ray effects. Watanabe and Maynard [31] have developed the discrete cones method for voids, using the first order equation and have mitigated the ray effect to some extent. The direct use of the even parity equation gives physically unacceptable results for void problems due to the division of the leakage

term by the total macroscopic cross section, which is usually set to a low value ($\sim 10^{-8}$) for void regions. Ackroyd and Grenfell [32] have solved duct problems using the finite element method for the even parity equation. They used a macroscopic absorption cross section in the void which was one tenth of the total macroscopic cross section of the surrounding region (a pure absorber). Reasonable flux profiles were obtained for the void system.

Chucas [33] has developed a method for void regions and implemented it in the diffusion code FENDER, originally developed by Shuttleworth [34]. His method combines diffusion theory in material regions with line-of-sight kernels in a void region. Emergent currents at the void boundary are calculated and combined with line-of-sight kernels to produce incident currents on void boundaries. These are subsequently used as additional sources for a further diffusion theory calculation in the non-void regions.

1.3 Neutron Interactions

Since part of the work reported in this thesis concerns anisotropic scattering, it is appropriate to look briefly at interaction involving neutrons and nuclei. Neutrons can interact with nuclei in a variety of ways. Neutrons may disappear in a reactor or shield as a result of absorption reactions. An important absorption reaction is that of radiative capture in which the nucleus is left in an excited state after neutron capture and becomes stable by emitting a γ-ray. This reaction is of course denoted by (n, γ). Other ways in which neutrons disappear is by charged particle reactions like (n, p) and (n, α) reactions. Also, when a neutron collides with certain heavy nuclei (e.g. ^{235}U), the nuclei split into two lighter fragments releasing a large amount of energy and radiation. This of course is the fission process.

The scattering interactions are also extremely important for the principle applications of this thesis to shielding problems. Scattering is a mechanism which is used by reactor designers to slow fast neutrons down to thermal energies (0.025eV) where they can be absorbed by (n, γ) reactions. Hence, neutron scattering mechanisms and neutron kinetics need to be considered. This is done briefly below in Sections 1.3.1 and 1.3.2. In <u>elastic</u> scattering the nucleus remains unchanged in isotopic composition and internal energy

after interacting with a neutron. In the case of inelastic scattering, the nucleus is left in an excited state after the interaction. Each of these processes can occur by three different mechanisms viz., compound nucleus formation, potential scattering and direct interaction.

In compound nucleus formation the incident neutron is absorbed by the nucleus. The compound nucleus subsequently decays. If the nucleus returns to the ground state then it is compound elastic scattering, but, if the emitted neutron leaves the nucleus in an excited state this is termed compound inelastic scattering.

Potential scattering is an elastic type scattering which can occur at any incident neutron energy. The incident neutron here is scattered without penetrating the nucleus itself. In direct interaction scattering the neutron energy is much higher than that encountered in reactor physics. In this process the incident neutron collides directly with one of the nucleons in the nucleus and emerges with reduced energy.

1.3.1 Angular Distribution of Scattered Neutrons

It has been observed that elastic scattering of neutrons is always or nearly always isotropic in the centre of mass (c.of m.) system for sufficiently low energies, below 100keV. In fact for hydrogen, the scattering in the centre of mass system is isotropic upto 30 MeV. In general, the heavier the nuclide, the lower the energy above which elastic scattering becomes anisotropic. As the energy of the incident neutrons increases the scattering becomes more forward peaked (anisotropic) in the centre of mass system. Also the variations of the angular distribution of neutrons with increasing mass number of the scattering nucleus is similar to that occuring with increasing energy. Broadly speaking, for light nuclei, the differential elastic scattering cross sections in the centre of mass system are relatively flat. With increasing mass number of the incident nucleus, the scattering cross sections are forward peaked with successive maxima and minima. Illustration of differential cross section variation for ^{12}C and ^{238}U with scattering angle in the centre of mass system, for different energies, is given by Lamarsh [35]. In regions of resonance scattering it is difficult to make general statements regarding differential elastic scattering cross sections. For inelastic scattering the angular distribution of scattered neutrons is relatively simple for most of the energy range of interest in reactor physics. It can generally

be assumed that inelastic scattering is isotropic in the centre of mass system for reactor physics application. Finally, potential scattering of fast neutrons is never isotropic in the centre of mass system, but highly peaked in the forward direction.

The above statements about scattering cross sections are all referred to in the centre of mass system. Since the frame of neutron transport calculation is the laboratory system, then it is necessary to transform the differential cross section from the centre of mass system to the laboratory system. This is relatively straight forward. The transformation from the centre of mass frame to laboratory system itself introduces scattering anisotropy. This effect is not so significant for heavy nuclei, but is very important for light nuclei. A thorough discussion of neutron scattering interactions can be found in [35,36].

1.3.2 Kinematics of Neutron Scattering

As mentioned in the previous section the transformation from centre of mass system to the laboratory system introduces anisotropy of scattering. Since neutron transport calculations are performed in the laboratory system, scattering cross sections are required in this system. Consider a stationary nucleus in the laboratory system as shown in Fig. 1.1. Application of conservation of momentum in the laboratory system leads to the following relations for the cosines of the scattering angle θ_L [36].

$$\mu_L(E,E') = \frac{1}{2}\left[(A+1)\sqrt{\frac{E'}{E}} - (A-1)\sqrt{\frac{E}{E'}} - \frac{QA}{\sqrt{EE'}} \right] \qquad (1.3\text{-}1)$$

where E and E' are the initial and final laboratory system neutron energies respectively, $\mu_L = \cos\theta_L$ and $A = {}^{M}/_{m}$. For elastic scattering, the reaction Q value is set to zero. Solving for E', the final neutron energy, from above, gives

$$E'(\mu_L,E) = \frac{1}{(1+A)^2}\left[\mu_L\sqrt{E} \pm \sqrt{E(\mu_L^2+A^2-1)+A(A+1)Q} \right]^2 \qquad (1.3\text{-}2)$$

The threshold energy for in-elastic scattering is then given by

$$E_{th} = \frac{-A(A+1)Q}{\mu_L^2+A^2-1} \qquad (1.3\text{-}3)$$

and the minimum threshold energy occurs at $\theta_L = 0$, i.e.

$$E_{th\,min}(\mu_L = 1) = -\frac{(A+1)Q}{A} \qquad (1.3\text{-}4)$$

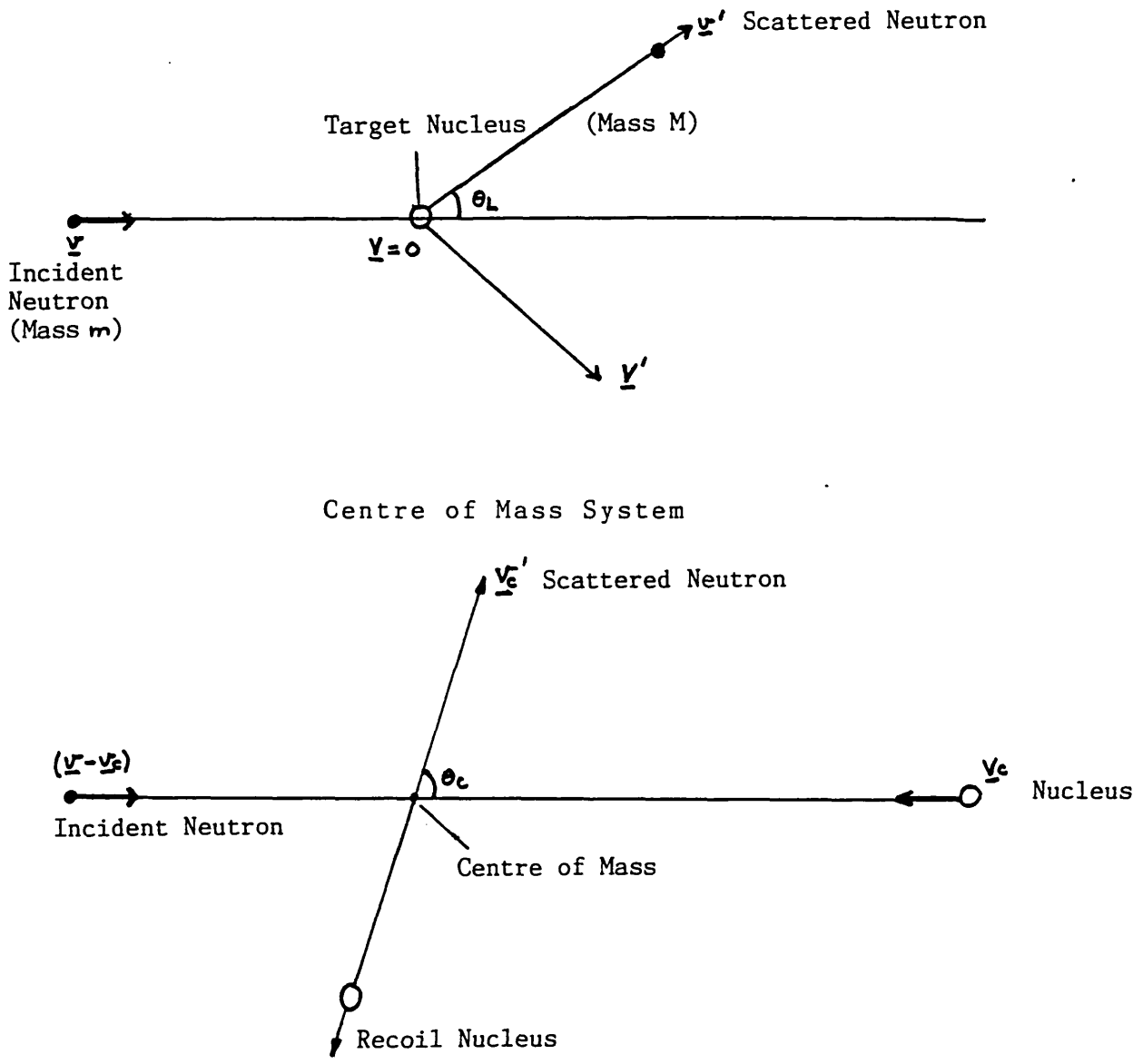


Fig. 1.1 Laboratory and Centre of Mass System for Neutron Scattering

Now the relation between the cosine of scattering angle in the centre of mass and laboratory system is given by

$$\mu_L = \frac{1 + \mu_c \gamma}{(1 + 2\gamma\mu_c + \gamma^2)^{\frac{1}{2}}} \qquad (1.3\text{-}5)$$

where

$$\gamma(E) = A \left(1 + \frac{(A+1)}{A} \frac{Q}{E} \right)^{\frac{1}{2}} \qquad (1.3\text{-}6)$$

So, whereas all possible angles $-1 \leq \mu_c \leq 1$ are possible for scattering in centre of mass system, this is not so for the laboratory system as can be seen from the above relationship between μ_L and μ_c. When the incident neutron energy is less than or equal to

$$Ec = \frac{- AQ}{(A-1)} \qquad (1.3\text{-}7)$$

it is found that $0 \leq \gamma(E) \leq 1$, and only forward scattering is possible. When the neutron energy rises from E_{th} to Ec, μ_L ranges from 1 to 0. For $E > E_{th}$, $\gamma(E) > 1$ and all scattering angles are allowed.

As a consequence of near isotropic scattering of neutrons in centre of mass system, the differential scattering cross section is fairly well represented by low order Legendre polynomial expansion, viz.,

$$\sigma_s(E,\mu_c) = \sigma_s(E) \sum_l \left(\frac{2l+1}{4\pi}\right) f_l(E)\, P_l(\mu_c) \qquad (1.3\text{-}8)$$

$\sigma_s(E,\mu_c)$ is the differential scattering cross section for elastic or inelastic scattering and $f_l(E)$ are the expansion coefficients.

REFERENCES TO CHAPTER 1

1. ACKROYD, R.T.
"A Finite Element Method for Neutron Transport-I. Some Theoretical Considerations".
Ann. Nucl. Energy, 5, p75 (1978)

2. ACKROYD, R.T.
"The Why and How of Finite Elements".
Ann. Nucl. Energy, 8, p539 (1981)

3. ACKROYD, R.T.
"A Finite Element Method for Diffusion Theory Embracing Nodal and Difference Methods".
Prog. Nucl. Energy, 18, 1/2, p7 (1986)

4. OHNISHI, T.
"Application of Finite Element Solution Technique to Neutron Diffusion and Transport Equations".
Proc. Conf. on New Developments in Reactor Mathematics and Applications, Idaho Falls, Idaho, March 29-31,1971.

5. KANG, C.M. and HANSEN, K.F.
"Finite Element Methods for Reactor Analysis".
Nucl. Sci. Engng. 51, p456 (1973)

6. DEPPE, O and HANSEN, K.F.
"Application of the Finite Element Method to Two-Dimensional Diffusion Problems".
Nucl. Sci. Engng. 54, p56 (1975)

7. GRENFELL, D.T.
"The Application of the Finite Element Method to the Solution of Radiation Shielding Problems".
Ann. Nucl. Energy, 8, p581 (1981)

8. MILLER, W.F., LEWIS, E.E. and ROSSOW, E.C.
"Application of Phase-Space Finite Elements to the Two-Dimensional Neutron Transport Equation in X-Y Geometry".
Nucl. Sci. Engng. 52, p12 (1973)

9. KAPER, H.G., LEAF, G.K. and LINDERMAN, A.J.
"Application of Finite Element Methods in Reactor Mathematics".
ANL-8126, Argonne National Laboratory, 1974.

10. BRIGGS, L.L., MILLER, W.F. and LEWIS, E.E.
"Ray Effect Mitigation in Discrete Ordinate-Like Angular Finite Element Approximations in Neutron Transport".
Nucl. Sci. Engng. 57, p205 (1975)

11. MORDANT, M.
"Some Efficient Lagrangian Mesh Finite Elements Encoded in ZEPHYR for Two-Dimensional Transport Calculations".
Ann. Nucl. Energy, 8, 11/12, p657 (1981)

12. ZIVER, A.K.
"Solution of the Boltzmann Transport Equation by Finite Elements".
PhD. Thesis, University of London.

13. ZIVER, A.K. and GODDARD, A.J.H.
"A Finite Element Method for Multigroup Diffusion - Transport Problems in Two Dimensions".
Ann. Nucl. Energy, 8, p689-698 (1981)

14. ISSA, J.G.
PhD Thesis
Imperial College, University of London. (1983)

15. QUAH, C.S.
PhD Thesis
Imperial College, University of London. (1983)

16. WILSON, E.W.
PhD Thesis
Queen Mary College, University of London. (1985)

17. LILLIE, R.A. and ROBINSON. J.C.
"A Linear Triangle Finite Element Formulation for Multigroup Neutron Transport Analysis with Anisotropic Scattering".
ORNL/TM - 5281, Oak Ridge National Laboratory. (1976)

18. GALLIARA, J.S.
PhD Thesis
Queen Mary College, University of London. (1978)

19. FLETCHER, J.K.
"Solution of the Time Independent Multi-Group Neutron Transport Equation Using Spherical Harmonics".
Ann. Nucl. Energy, 4, p401 (1977)

20. FLETCHER, J.K.
"Recent Developments of the Transport Code MARC/PN".
Prog. Nucl. Energy, 18, 1/2, p75 (1986)

21. SPLAWSKI, B.A.
PhD Thesis
Queen Mary College, University of London. (1982)

22. ACKROYD, R.T. and SPLAWSKI, B.A.
"A Finite Element Method for Neutron Transport -VI. Upper and Lower Bounds for Local Characteristics of Solutions".
Ann. Nucl. Energy, 9, p315 (1982)

23. WOOD, J. and De OLIVEIRA, C.R.E.
"A Multigroup Finite-Element Solution of the Neutron Transport Equation - Part I".
Ann. Nucl. Energy, 11 p229 (1984)

24. WOOD, J. and WILLIAMS M.M.R.
"Recent Progress in the Application of the Finite Element Method to the Neutron Transport Equation".
Ann. Nucl. Energy, 14, p21 (1984)

25. WOOD, J.
"Multigroup Anisotropic Scattering in the Finite Element Method".
Prog. Nucl. Energy, 18, 1/2, p91 (1986)

26. De OLIVEIRA, C.R.E.
"An Arbitrary Geometry Finite Element Method for Multigroup Neutron Transport With Anisotropic Scattering".
Prog. Nucl. Energy, 18, 1/2, p227 (1986)

27. RIYAIT, N.S.
"The Finite Element Method for Multigroup Neutron Transport: Anisotropic Scattering in One Dimensional Slab Geometry".
Report SAF 072, Imperial College, London (1985)

28. ISSA, J.G., RIYAIT, N.S., GODDARD, A.J.H.and STOTT, G.E.
"Multigroup Application of the Anisotropic FEM code FELTRAN to 1,2 and 3D Problems".
Prog. Nucl. Energy, 18, 1/2, p251 (1986)

29. RIYAIT, N.S.
"The Finite Element Method for Multigroup Transport: Few Group Test Problems with Anisotropic Scattering".
Report SAF 076. Imperial College, London. (1985)

30. STOTT, G.E.
PhD Thesis
University of London. To be published.

31. WATANABE,Y. and MAYNARD, C.W.
"The Discrete Cones Method in Two-Dimensional Neutron Transport Computation".
University of Wisconsin, Report UWFDM - 574 (1984)

32. ACKROYD, R.T. and GRENFELL, D.T.
"A Finite Element Method for Neutron Transport - III. Two Dimensional One-Group Test Problems.
Ann. Nucl. Energy, p563 (1979)

33. CHUCAS, S.J.
"The Treatment of Voided Regions in the Finite Element Diffusion Code FENDER".
Prog. Nucl. Energy, 18, 1/2, p185 (1986)

34. SHUTTLEWORTH, E.
"FENDER: A Finite Element Code for the Solution of the Diffusion Equation in Shield Design Applications".
Ann. Nucl. Energy, 8, p597 (1981)

35. LAMARSH, J.R.
"Introduction to Nuclear Reactor Theory".
Addison Wesley Publishing Co. (1960)

36. BELL, G.I. and GLASSTONE, S.
"Nuclear Reactor Theory"
Van Nostrand Reinhold Co. (1970)

CHAPTER 2

2. NEUTRON TRANSPORT

2.1 Neutron Transport Equation
2.2 Even and Odd Parity Equations
2.3 Boundary Conditions
2.4 Source and Eigenvalue Problems
2.5 Numerical Methods for Neutron Transport
2.5.1 Discrete Ordinates Method
2.5.2 Integral Transport Method
2.5.3 Spherical Harmonics Method
2.5.4 Monte Carlo Method
2.5.5 Finite Element Method

References to Chapter 2

2. NEUTRON TRANSPORT

2.1 Neutron Transport Equation

One of the central problems of reactor physics is to predict the distribution of neutrons in a reactor, since it is the neutron distribution that determines the rate at which various nuclear reactions occur within the reactor. Neutron distribution is in general a function of neutron direction, position, energy and time. The basic equation for determining neutron distribution is the Boltzmann transport equation. This is simply a balance equation which equates neutron sources in a given system to the net losses due to absorption and leakage out of the system. In the present work we are interested in time independent problems and hence consider the steady state form of the transport equation. The mono-energetic form of this may be written as

$$\underline{\Omega} \cdot \nabla \phi_o(\underline{r}, \underline{\Omega}) + \sigma_T(\underline{r})\, \phi_o(\underline{r}, \underline{\Omega}) = \int_{\Omega'} \sigma_s(\underline{r}, \underline{\Omega} \cdot \underline{\Omega}')\, \phi_o(\underline{r}, \Omega')\, d\underline{\Omega}' + S(\underline{r}, \underline{\Omega}) \qquad (2.1\text{-}1)$$

*

where

$\phi_o(\underline{r}, \underline{\Omega})$ is the angular flux at position $\underline{r}$ and direction $\underline{\Omega}$.

$\sigma_T(\underline{r})$ is the macroscopic total cross section at $\underline{r}$.

$\sigma_s(\underline{r}, \underline{\Omega} \cdot \underline{\Omega}')$ is the differential scattering cross section for scattering at position $\underline{r}$ from direction $\underline{\Omega}'$ to $\underline{\Omega}$.

$S(\underline{r}, \underline{\Omega})$ is the extraneous source at position $\underline{r}$ and direction $\underline{\Omega}$.

The co-ordinate system for $\underline{r}$ and $\underline{\Omega}$ is shown in Fig. 2.1.

* Los Alamos notation for cross sections.

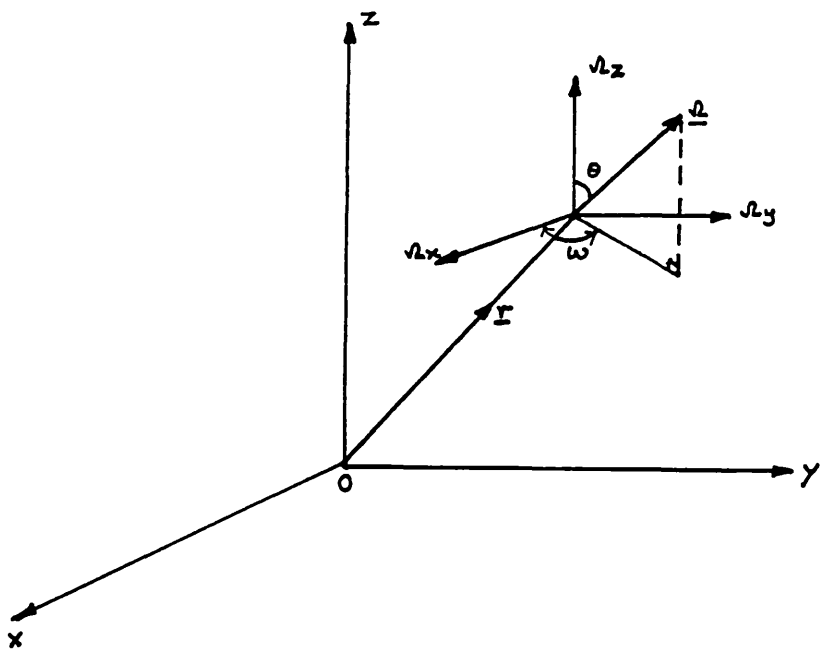


Fig. 2.1 Co-ordinate System for $\underline{r}(x,y,z)$ and Spherical System used for $\underline{\Omega}(\theta, \omega)$.

Assumptions made in obtaining the transport equation are that particles may be considered as points, that particles travel in straight lines between collisions and that particle-particle interactions may be neglected. It is also assumed in applications that σ_T and σ_s are region-wise constant. The scattering cross section $\sigma_s(r, \Omega \cdot \Omega')$ is usually expanded in terms of Legendre polynomials $P_l(\mu_0)$ as

$$\sigma_s(r, \Omega \cdot \Omega') = \sum_{l=0}^{\infty} \left(\frac{2l+1}{4\pi} \right) \sigma_{sl}(r) P_l(\mu_0) \qquad (2.1\text{-}2)$$

where $\mu_0 = \Omega \cdot \Omega' = \cos\theta$, θ being the angle between directions Ω and Ω' . The coefficients σ_{sl} are calculated from

$$\sigma_{sl} = 2\pi \int_{-1}^{1} \sigma_s(r, \mu_0) P_l(\mu_0) \, d\mu_0$$

The angular flux, $\phi_0(r, \Omega)$, is a useful quantity since it is a starting point for calculations of both reaction rates and boundary crossings in nuclear reactors and radiation shields. The scalar or total flux is obtained by integration of $\phi_0(r, \Omega)$ over all directions Ω . Hence

$$\Phi_0(r) = \int_{4\pi} \phi_0(r, \Omega) \, d\Omega \qquad (2.1\text{-}3)$$

$\Phi_0(r)$ is used in obtaining reaction rates. The neutron current $J(r)$ is defined as

$$J(r) = n \cdot \int_{4\pi} \Omega \, \phi_0(r, \Omega) \, d\Omega \qquad (2.1\text{-}4)$$

and is the net number of neutrons crossing a unit area, with outward normal $\underline{n}$, per unit time,in the direction of $\underline{n} \cdot \underline{J}(\underline{r})$ is required at the outer boundary and interface crossings. Detailed analysis of the neutron transport equation is given by several authors [1,2,3].

2.2 Even and Odd Parity Equations

The neutron transport equation (2.1-1) is true for all directions $\underline{\Omega}$ and in particular for direction $-\underline{\Omega}$.

$$-\underline{\Omega}\cdot\nabla\phi_o(r,-\underline{\Omega}) + \sigma_T\phi_o(r,-\underline{\Omega}) = \int_{\Omega'}\sigma_s(r,-\underline{\Omega}\cdot\underline{\Omega}')\phi_o(r,\underline{\Omega}')d\Omega' + S(r,-\underline{\Omega}) \tag{2.2-1}$$

Adding and subtracting (2.1-1) and (2.2-1) leads to the following pair of coupled equations for the even and odd parity fluxes, $\phi_o^+(r,\underline{\Omega})$ and $\phi_o^-(r,\underline{\Omega})$, respectively.

$$\underline{\Omega}\cdot\nabla\phi_o^-(r,\underline{\Omega}) + c\,\phi_o^+(r,\underline{\Omega}) = S^+(r,\underline{\Omega})$$

and
$$\underline{\Omega}\cdot\nabla\phi_o^+(r,\underline{\Omega}) + \zeta^{-1}\phi_o^-(r,\underline{\Omega}) = S^-(r,\underline{\Omega}) \tag{2.2-2}$$

where $\psi^{\pm}(r,\underline{\Omega}) = [\psi(r,\underline{\Omega}) \pm \psi(r,-\underline{\Omega})]$

for any function $\psi(r,\underline{\Omega})$. The superscript + denotes even parity component and - denotes odd parity component of the function $\psi(r,\underline{\Omega})$. Eliminating $\phi_o^-(r,\underline{\Omega})$ from the Eqns. (2.2-2) gives a second order integro-differential equation for $\phi_o^+(r,\underline{\Omega})$ called the even parity equation.

$$-\underline{\Omega}\cdot\nabla[\zeta\,\underline{\Omega}\cdot\nabla\phi_o^+] + c\,\phi_o^+ = S^+ - \underline{\Omega}\cdot\nabla\zeta\,S^- \tag{2.2-3}$$

Similarly the odd parity equation for $\phi_o^-(r,\underline{\Omega})$ is

$$-\underline{\Omega}\cdot\nabla\left[C^{-1}\underline{\Omega}\cdot\nabla\phi_o^-\right] + G^{-1}\phi_o^- = S^- - \underline{\Omega}\cdot\nabla C^{-1}S^+ \qquad (2.2\text{-}4)$$

The operators C and G, termed removal and leakage operators, are positive definite and self adjoint. These properties also hold for the inverse operators C^{-1} and G^{-1}. The C and G operators are defined by

$$C\psi(r,\underline{\Omega}) = \sigma_T(r)\,\psi(r,\underline{\Omega}) - \int_{\Omega'} \sigma_s^+(r,\underline{\Omega}\cdot\underline{\Omega}')\,\psi(r,\underline{\Omega}')\,d\Omega' \qquad (2.2\text{-}5)$$

with

$$\sigma_s^{\pm}(r,\underline{\Omega}\cdot\underline{\Omega}') = \tfrac{1}{2}\left\{\sigma_s(r,\underline{\Omega}\cdot\underline{\Omega}') \pm \sigma_s(r,-\underline{\Omega}\cdot\underline{\Omega}')\right\}$$

and

$$G\psi(r,\underline{\Omega}) = \frac{\psi(r,\underline{\Omega})}{\sigma_T(r)} + \int_{\Omega'} g(r,\underline{\Omega}\cdot\underline{\Omega}')\,\psi(r,\underline{\Omega}')\,d\Omega'$$

Here g is defined in terms of a function f as

$$g(r,\underline{\Omega}\cdot\underline{\Omega}') = \tfrac{1}{2}\left\{f(r,\underline{\Omega}\cdot\underline{\Omega}') - f(r,-\underline{\Omega}\cdot\underline{\Omega}')\right\} \qquad (2.2\text{-}6)$$

where f is the non-negative solution of the integral equation

$$f(r,\underline{\Omega}\cdot\underline{\Omega}') = \frac{\sigma_s(r,\underline{\Omega}\cdot\underline{\Omega}')}{(\sigma_T)^2} + \int_{\Omega''} f(r,\underline{\Omega}''\cdot\underline{\Omega}')\,\frac{\sigma_s(r,\underline{\Omega}\cdot\underline{\Omega}'')}{\sigma_T}\,d\Omega'' \qquad (2.2\text{-}7)$$

See for instance Ackroyd [4].

The inverse operators are given by

$$C^{-1}\psi(r,\underline{\Omega}) = \frac{\psi(r,\underline{\Omega})}{\sigma_T} + \int_{\Omega'} d(r,\underline{\Omega}\cdot\underline{\Omega}')\,\psi(r,\underline{\Omega}')\,d\Omega' \qquad (2.2\text{-}8)$$

with

$$d(r,\underline{\Omega}\cdot\underline{\Omega}') = \frac{1}{2}\left\{ f(r,\underline{\Omega}\cdot\underline{\Omega}') + f(r,-\underline{\Omega}\cdot\underline{\Omega}') \right\} \qquad (2.2\text{-}9)$$

and

$$\mathcal{G}^{-1}\psi(r,\underline{\Omega}) = \sigma_T\,\psi(r,\underline{\Omega}) - \int_{\Omega'} \sigma_s^-(r,\underline{\Omega}\cdot\underline{\Omega}')\,\psi(r,\underline{\Omega}')\,d\Omega' \qquad (2.2\text{-}10)$$

At this stage no assumption is made on $\sigma_s(r,\underline{\Omega}\cdot\underline{\Omega}')$ except that it is a continuous function of $\underline{\Omega}\cdot\underline{\Omega}'$. If, however, $\sigma_s(r,\underline{\Omega}\cdot\underline{\Omega}')$ is expanded in Legendre polynomials as in (2.1-2), then the kernels $g(r,\underline{\Omega}\cdot\underline{\Omega}')$ and $d(r,\underline{\Omega}\cdot\underline{\Omega}')$ take the following form:

$$g(r,\underline{\Omega}\cdot\underline{\Omega}') = \sum_{\substack{l=1\\ \text{odd}}}^{\infty} \left(\frac{2l+1}{4\pi}\right) \frac{\sigma_{sl}}{\sigma_T(\sigma_T - \sigma_{sl})} P_l(\underline{\Omega}\cdot\underline{\Omega}') \qquad (2.2\text{-}11)$$

and

$$d(r,\underline{\Omega}\cdot\underline{\Omega}') = \sum_{\substack{l=0\\ \text{even}}}^{\infty} \left(\frac{2l+1}{4\pi}\right) \frac{\sigma_{sl}}{\sigma_T(\sigma_T - \sigma_{sl})} P_l(\underline{\Omega}\cdot\underline{\Omega}')$$

The even and odd parity scattering cross section expansions are simply

$$\sigma_s^+(r,\underline{\Omega}\cdot\underline{\Omega}') = \sum_{\substack{l=0\\ \text{even}}}^{\infty} \left(\frac{2l+1}{4\pi}\right) \sigma_{sl}(r)\,P_l(\mu_0) \qquad (2.2\text{-}12)$$

$$\sigma_s^-(r,\underline{\Omega}\cdot\underline{\Omega}') = \sum_{\substack{l=1\\ \text{odd}}}^{\infty} \left(\frac{2l+1}{4\pi}\right) \sigma_{sl}(r)\,P_l(\mu_0)$$

Although $\phi_o^+(r,\underline{\Omega})$ and $\phi_o^-(r,\underline{\Omega})$ are mathematical functions they can be related to physical quantities used in reactor physics. Integrating $\phi_o^+(r,\underline{\Omega})$ over all $\underline{\Omega}$ gives the scalar flux $\bar{\phi}_o(r)$. In addition, the net number of neutrons, per unit time, crossing a unit area in the same direction as $\underline{n}$, the outward normal to the unit area, is

$$\frac{1}{2}\underline{n}\cdot\int_{\underline{\Omega}\cdot\underline{n}>0}\underline{\Omega}\,\phi_o^-(r,\underline{\Omega})\,d\Omega \qquad (2.2\text{-}13)$$

2.3 Boundary Conditions

Two types of external boundary conditions are met in neutron transport. At a bare surface S_b of a system there is the non re-entrant condition

$$\phi_o(r,\underline{\Omega}) = 0 \qquad \text{for } \underline{\Omega}\cdot\underline{n}<0 \qquad (2.3\text{-}1)$$

where $\underline{n}$ is the outward normal to S_b. If there is an inward source $T(r,\underline{\Omega})$ on a bare surface S_s, then we have

$$\phi_o(r,\underline{\Omega}) = T(r,\underline{\Omega}) \qquad \text{for } \underline{\Omega}\cdot\underline{n}<0 \qquad (2.3\text{-}2)$$

These boundary conditions are for the first order form of the transport equation. The even parity forms of (2.3-1) and (2.3-2) are

$$\phi_o^+(r,\underline{\Omega}) + \zeta\left[S^- - \underline{\Omega}\cdot\nabla\phi_o^+(r,\underline{\Omega})\right] = 0 \qquad \text{for } \underline{\Omega}\cdot\underline{n}<0 \text{ on } S_b$$

and (2.3-3)

$$\phi_o^+(r,\underline{\Omega}) + \zeta\left[S^- - \underline{\Omega}\cdot\nabla\phi_o^+(r,\underline{\Omega})\right] = T(r,\underline{\Omega}) \qquad \text{for } \underline{\Omega}\cdot\underline{n}<0 \text{ on } S_s.$$

The second boundary condition represents symmetry of a system and is the perfect reflector condition on a surface S_{pr}, viz.,

$$\phi_o(r,\underline{\Omega}) = \phi_o(r,\underline{\Omega}^*) \qquad (2.3\text{-}4)$$

where $\underline{\Omega}^*$ is the reflected direction to $\underline{\Omega}$, at r, on S_{pr}. The even parity form of this is

$$\zeta\left[S^-(r,\underline{\Omega}) - \underline{\Omega}\cdot\nabla\phi_o^+(r,\underline{\Omega}) - S^-(r,\underline{\Omega}^*) + \underline{\Omega}^*\cdot\nabla\phi_o^+(r,\underline{\Omega}^*)\right] = 0 \qquad (2.3\text{-}5)$$

In addition, at interfaces of regions, $\phi_o(r,\underline{\Omega})$ is continuous for all directions $\underline{\Omega}$ crossing the interface, i.e. $\phi_o^+(r,\underline{\Omega}) + \phi_o^-(r,\underline{\Omega})$ is continuous for all $\underline{\Omega}\cdot\underline{n} \neq 0$.

2.4 Source and Eigenvalue Problems

Fixed source problems in reactor physics and radiation shielding calculations involve an extraneous distributed neutron source which is usually isotropic. When the source term, $S(r,\underline{\Omega})$, in (2.1-1), is expanded in spherical harmonics

only the angle independent term is non-zero for isotropic sources. Hence

$$S(r, \underline{\Omega}) = \frac{S_0(r)}{4\pi} \tag{2.4-1}$$

Similarly the even parity extraneous source $S^+(r, \underline{\Omega})$ also equals $S_0(r)/4\pi$ for isotropic sources. The transport equation with an extraneous source represents an inhomogeneous problem. In the present work the extraneous (fixed) source is assumed to be regionwise constant. In multigroup problems $S(r, \underline{\Omega})$ is replaced by an effective source, $S^{eff}(r, \underline{\Omega})$, in a particular group. $S^{eff}(r, \underline{\Omega})$ contains a fixed source contribution and a downscatter contribution from the higher groups.

In multigroup systems containing fission sources only, we are interested in the condition when there exists a balance between the source of neutrons produced in fission and the total loss due to absorption and leakage. The fission source, assumed isotropic, is given by

$$\frac{\nu \sigma_f(r)}{4\pi} \int_{\Omega} \phi_0(r, \underline{\Omega}) \, d\Omega \tag{2.4-2}$$

where $\sigma_f(r)$ is the macroscopic fission cross section and ν is the average number of neutrons produced per fission. The one group even parity equation then becomes

$$-\underline{\Omega} \cdot \nabla \left[S \underline{\Omega} \cdot \nabla \phi_0^+ \right] + c \phi_0^+ = \frac{\nu \sigma_f(r)}{4\pi} \int_{\Omega} \phi_0^+(r, \underline{\Omega}) \, d\Omega \tag{2.4-3}$$

where the source term is replaced by

$$\frac{\nu\sigma_f}{4\pi}\int_{\Omega} \phi_0^+(r, \Omega)\, d\Omega$$

and σ_f is the fission cross section. Dividing ν by k_{eff}, where k_{eff} is the effective multiplication factor, leads to an eigenvalue problem for the eigenvalue $1/k_{eff}$, using Eqn. (2.4-3). The iterative scheme to determine the effective multiplication factor and the corresponding flux ϕ_0^+ is known as the power iteration method [2]. A critical system is obtained when $k_{eff}=1$. In this case there is a balance of source neutrons from fission and the total loss of neutrons. When k_{eff} is greater (or less) than unity a supercritical (or subcritical) system is obtained.

2.5 Numerical Methods for Neutron Transport

In the following sections various methods used for neutron transport calculations are outlined. The methods divide into two broad classes; deterministic and stochastic methods. The methods sketched below include discrete ordinates, spherical harmonics, integral transport, Monte Carlo and the finite element method. Existing codes using the above methods include:

(a) ANISN [5] and DOT [6]	- discrete ordinates finite difference
(b) WIMS [7]	- integral transport collision probability
(c) MARC/PN [8]	- spherical harmonics finite difference

(d) MONK [9], MORSE [10] and McBEND [11] - Monte Carlo

(e) RANKERN [12] - stochastic integration point kernel

(f) FELTRAN [13], FELICIT [14] and FENDER [15] - finite element spherical harmonics

A comprehensive review of neutron transport approximations is given by Sanchez and McCormick [16].

2.5.1 Discrete Ordinates Method

The discrete ordinates method is a name given to several closely related numerical techniques for obtaining an approximate solution to the transport equation. The method is based on discretisation of the continuous angular variable $\underline{\Omega}$. The continuous $\underline{\Omega}$ is replaced by the discrete ordinates (directions) $\underline{\Omega}_i$, i=1,2,3,.....,N. In the spatial domain either a finite difference or a finite element scheme may be used [1]. The first step in the discrete ordinates method is to select a finite set of directions $\underline{\Omega}_i$ and quadrature weights ω_i , i= 1,2,3,.....,N, such that all the terms in the transport equation may be evaluated numerically. Hence,

$$\int_{4\pi} \sigma_s(\underline{r}, \underline{\Omega}\cdot\underline{\Omega}')\,\phi_e(\underline{r}, \underline{\Omega}')\,d\Omega' \approx \sum_{j=1}^{N} \omega_j\, \sigma_s(\underline{r}, \underline{\Omega}_j \rightarrow \underline{\Omega}_i)\,\phi_e(\underline{r}, \underline{\Omega}_j) \qquad (2.5\text{-}1)$$

and the scalar flux is

$$\Phi_0(r) = \int_{\Omega} \phi_0(r, \underline{\Omega})\, d\Omega \approx \sum_{i=1}^{N} w_i\, \phi_0(r, \underline{\Omega}_i) \qquad (2.5\text{-}2)$$

The transport equation

$$\underline{\Omega}_i \cdot \nabla \phi_0(r, \underline{\Omega}_i) + \sigma_T\, \phi_0(r, \underline{\Omega}_i) = \sum_{j=1}^{N} w_j\, \sigma_s(r, \underline{\Omega}_j \rightarrow \underline{\Omega}_i)\, \phi_0(r, \underline{\Omega}_j) + S(r, \underline{\Omega}_i) \qquad (2.5\text{-}3)$$

is then solved along each direction $\underline{\Omega}_i$. The scattering cross section, which can include anisotropic scattering, is usually expanded in spherical harmonics, viz.,

$$\sigma_s(r, \underline{\Omega}_j \rightarrow \underline{\Omega}_i) = \sum_{l} \sum_{m=-l}^{l} Y_l^m(\underline{\Omega}_i)\, Y_l^{m*}(\underline{\Omega}_j)\, \sigma_{sl}(r) \qquad (2.5\text{-}4)$$

Diamond difference schemes for the spatial dependence lead to good accuracy relative to the computational effort required. Coupling of the different directions for the first order equation is simpler than the second order even parity equation. The discrete ordinates method is easily extended to orthogonal multidimensional systems. Although codes based on the discrete ordinates finite difference methods are widely used for multi-group anisotropic scattering reactor physics and radiation shielding calculations, the method does have its limitations. It is difficult to treat problems of irregular boundaries with this method. In higher dimensions, the method suffers from oscillations in the solution, termed the 'ray effect'. This effect shows up in problems with localised sources, highly absorbing media and void problems. The ray effect seems to be due to the inability of the quadrature formula to approximate reasonably the scalar flux from the angular

flux. For higher angular quadrature approximation, the frequency of the oscillations increases while the magnitude decreases. Lathrop [17] has proposed some remedies for the ray effect. Recently Watanabe and Maynard [18] have developed the discrete cones method and have had some success in mitigating ray effects even for low angular quadrature.

2.5.2 Integral Transport Method

This method differs from the other numerical methods in the sense that an integral equation for the angular flux is derived. The angular variable in the integrand can be treated to a high degree of accuracy depending upon the angular integration. In the case of isotropic scattering a further simplification occurs and a scalar flux equation can be derived. Usually the integral transport method is applied to situations where affects of anisotropic scattering are small, in order to keep the integral equation for the angular flux relatively simple. The most widely used method for solving the integral transport equation is the method of collision probabilities [19]. This leads to a matrix equation for the collision rates where the coefficient matrix, containing the collision probabilities, is dense and unsymmetric. This implies large computer time and memory. Hence the integral transport method is most widely used in infinite lattice problems where the spatial domain, which is a single cell, is sufficiently small that it requires relatively few spatial mesh points. The method has limited use

in deep penetration shield problems, where there may be a high degree of anisotropic scattering and many spatial mesh points may be required. See [19] for details of the method.

2.5.3 Spherical Harmonics Method

The spherical harmonics method has been used by Fletcher [8] with a finite difference treatment of spatial dependence to obtain numerical solutions of the transport equation for complex systems, but more frequently it is used to provide analytical solutions for simpler problems with, for instance, linear anisotropic scattering. In this method the angular flux, extraneous source and the scattering kernel are expanded in spherical harmonics. In one dimensional slab geometry the angular flux is a function of x and μ (cosine of angle neutron direction makes with the x axis) only. It is expanded in a Legendre series as

$$\phi_0(x,\mu) = \sum_{l=0}^{\infty} \left(\frac{2l+1}{4\pi}\right) \phi_l(x) P_l(\mu) \qquad (2.5\text{-}5)$$

and the scattering cross section $\sigma_s(x, \underline{\Omega}\cdot\underline{\Omega}')$ is expanded as in Eqn. (2.1-2). The coefficients $\phi_l(x)$ in (2.5-5) are given by

$$\phi_l(x) = 2\pi \int_{-1}^{1} \phi_0(x,\mu) P_l(\mu)\, d\mu \qquad (2.5\text{-}6)$$

The advantage in using Legendre series expansion for $\phi_0(x,\mu)$ is that the first two coefficients, $\phi_0(x)$ and $\phi_1(x)$, have a physical meaning. The scalar or total flux is given by $\phi_0(x)$, while

$\phi_1(x)$ gives the neutron current.

$$\phi_1(x) = J(x) = 2\pi \int_{-1}^{1} \mu \phi_0(x,\mu)\, d\mu \qquad (2.5\text{-}7)$$

Substitution for $\phi_0(x,\mu)$ and $\sigma_s(x, \underline{\Omega}\cdot\underline{\Omega}')$ into the first order transport equation leads to the following set of linear differential equations for the coefficients $\phi_L(x)$.

$$\frac{(L+1)}{(L+2)} \frac{d\phi_{L+1}(x)}{dx} + \frac{L}{(2L+1)} \frac{d\phi_{L-1}(x)}{dx} + (\sigma_T - \sigma_{sL})\, \phi_L(x) = S_L(x) \qquad (2.5\text{-}8)$$

$L=0,1,2,\ldots\ldots,N.$

These are known as the P_N equations and the spherical harmonics method as the P_N method [2]. For instance, in the P_1 approximation, all the ϕ_L's for $L \geq 2$ are set to zero and we obtain

$$\frac{d\phi_1}{dx} + (\sigma_T - \sigma_{s0})\, \phi_0 = S_0 \qquad (2.5\text{-}9)$$

and $$\frac{1}{3} \frac{d\phi_0}{dx} + (\sigma_T - \sigma_{s1})\, \phi_1 = 0$$

for isotropic extraneous source and linear (P_1) anisotropic scattering.

Boundary conditions in the P_N method cannot be satisfied exactly since the coefficients $\phi_L(x)$ extend over the whole range of μ ($-1 \leq \mu \leq 1$) while the boundary condition, e.g.

a bare surface, applies for only half the range of μ ($-1 \leq \mu$ or $\mu \leq 1$). One choice for the boundary conditions (Marshak boundary condition) is to set

$$\int_0^1 P_i(\mu)\, \phi_0(x,\mu)\, d\mu = 0 \qquad (2.5\text{-}10)$$

i=1,2,3,....,N (odd N).

on a bare surface on the right hand side of a slab system. Another condition used on a bare surface is to set

$$\phi(x,\mu_i) = 0 \qquad (2.5\text{-}11)$$

i=1,2,3,....,(N+1)/2 (odd N)

for a finite number of points μ_i . These are the Mark boundary conditions [3]. Although anisotropic scattering can be handled easily by the spherical harmonics method, it has the disadvantage that the equations become complex for higher order approximations in multidimensional geometry.

2.5.4 Monte Carlo Method

In contrast to the deterministic methods, e.g. discrete ordinates finite difference, spherical harmonics, integral transport and finite elements, the Monte Carlo method is a stochastic method. In this method particles are tracked until they are absorbed within the system or are lost due to leakage from the system. The method has the advantage that it is capable of treating complex three dimensional systems, whereas deterministic methods, until the advent of the finite element method, have been largely confined to regular two dimensional systems. The Monte Carlo method has two disadvantages, in that it is slow and that it gives only a statistical estimate of the correct answer rather than a precise value. For some problems Monte Carlo is particularly suited to flux determination in a local region whereas deterministic methods give a flux profile across a system. The efficiency of Monte Carlo calculations has been improved by attaching weights to the particles and playing Russian roulette to terminate the history of particles or using splitting techniques [19,20] to produce weighted particles which are in a favourable position and direction for detector response. Scattering is handled by sampling randomly from neutron differential cross section which is expanded in a truncated Legendre series.

2.5.5 Finite Element Method

The finite element method is a general technique for constructing solutions to boundary value problems [21,22]. The method involves dividing the solution region into simpler subregions, called finite elements, and using variational concepts or weighted residual methods or the hypercircle method [23] to construct an approximation to the solution over the finite elements. The latter are connected together at certain nodal points and the variational problem is formulated approximately for arbitrary boundary conditions over each sub-domain. The problem requires only a choice of simple local co-ordinate functions, called shape functions, for each element. The shape functions are usually polynomials. The global model is then obtained by simply fitting together the elements representing a given domain and by summing contributions from each element within the domain or region. The process of building a global approximation from local ones gives rise to a systematic technique for constructing shape functions for arbitrary domains. The shape functions chosen are usually piecewise polynomials with local support, i.e. they have non-zero value only in a relatively small neighbourhood of certain nodal points. In the case of linear elliptic equations the method leads to a banded system of linear algebraic equations, which can be solved in a variety of ways [22,24].

The finite element method has had condiderable success in solving a wide range of problems in engineering [24]. During

the mid-fifties finite element analysis originated as a discipline for solving problems in structural engineering. It soon became apparent that the method had implications beyond those considered originally and that it was a powerful technique for numerical solution of differential equations. In the mid-sixties the finite element method was based on variational methods [24]. In the early seventies the method was given a functional analysis basis [21,22]. Early work using functional analysis was by Prager and Synge [25] on approximations in elasticity theory. The early work on neutronics using a functional approach was by Ackroyd [26] using the method of the hypercircle to optimise approximate solutions and to obtain local error bounds. Some papers on finite element neutron transport work in the sixties and seventies include those of Pomraning and Clark [27], Kaper et al [28], Ohnishi [29], Ackroyd [30] and Martin and Duderstadt [31]. Recent works include those of Ackroyd [32], Mordent [33], Lewis and Dilber [34] and Kavenoky and Lautard [35].

In neutron transport theory the finite element approximation is usually introduced in the spatial domain to represent complex geometrical boundaries. In the angular space spherical harmonics or discrete ordinates approximations are used. Details of the finite element method are given in Section 4.4.

REFERENCES TO CHAPTER 2

1. DUDERSTADT, J.J. and MARTIN, W.R.
"Transport Theory".
John Wiley and Sons. (1979)

2. DUDERSTADT, J.J. and HAMILTON, L.J.
"Nuclear Reactor Analysis".
John Wiley and Sons. (1976)

3. BELL, G.I. and GLASSTONE, S.
"Nuclear Reactor Theory".
Van Nostrand Reinhold Co. (1970)

4. ACKROYD, R.T.
"The Why and How of Finite Elements".
Ann. Nucl. Energy, 8, p539 (1981)

5. ENGLE, W.W.
"ANISN-ORNL A One Dimensional Discrete Ordinates Transport Code".
CCC-254 Computer Technology Centre, Union Carbide Corporation, Oak Ridge. (1973)

6. RHOADES, W.A. and MYNATT, F.R.
"The DOT-II Two Dimensional Discrete Ordinates Transport Code".
ORNL-TM-4280. Oak Ridge National Laboratory. (1973)

7. ASKEW, J.R. and ROTH, M.J.
"WIMS-E Scheme for Neutronics Calculations".
UKAEA, Winfrith. Report AEEW-R1315. (1982)

8. FLETCHER, J.K.
"Recent Developments of the Transport Theory Code MARC/PN".
Prog. Nucl. Energy, 18, 1/2, p75 (1986)

9. SHERRIFS, V.S.W.
"MONK- A General Purpose Monte Carlo Neutronics Program".
SRD R 86. (1978)

10. STRAKER, E.A., STEVENS, P.N., IRVING, D.C. and CHAIN, V.R.
"The MORSE Code- A Multigroup Neutron and Gamma-Ray Monte Carlo Transport Code".
ORNL-4585. (1970)

11. BENDALL, D.E. and BRISSENDEN, R.T.
"MCBEND Program User's Guide". (Unpublished)
UKAEA, Winfrith.

12. MILLER, P.C. and SUMNER, V.
"RANKERN-A Point Kernel Code for Complicated Geometry Problems".
AEEW-R1313. (1980)

13. ISSA, J.G., RIYAIT, N.S., GODDARD, A.J.H. and STOTT, G.E.
"Multigroup Application of the Anisotropic FEM Code FELTRAN to One, Two and Three Dimensional and R-Z Problems".
Prog. Nucl. Energy, 18, 1/2, p251 (1986)

14. WOOD, J.
"Multigroup Anisotropic Scattering in the Finite Element Method".
Prog. Nucl. Energy, 18, 1/2, p91 (1986)

15. SHUTTLEWORTH, E.
"FENDER: A Finite Element Code for the Solution of the Diffusion Equation in Shield Design Applications".
Ann. Nucl. Energy, 8, 11/12, p597 (1981)

16. SANCHEZ, R. and McCORMICK, N.J.
"A Review of Neutron Transport Approximations".
Nucl. Sci. Engng., 80, p481 (1982)

17. LATHROP, K.D.
"Remedies for Ray Effects".
Nucl. Sci. Engng., 45, p255 (1971)

18. WATANABE, Y. and MAYNARD, C.W.
"The Discrete Cones Method for Two Dimensional Neutron Transport Computation in General Media".
University of Wisconsin, Report UWFDM-599. (1984)

19. LEWIS, E.E. and MILLER, N.F.
"Computational Methods of Neutron Transport".
John Wiley and Sons. (1984)

20. CHILTON, A.B., SHULTIS, J.K. and FAW, R.E.
"Principles of Radiation Shielding".
Prentice-Hall.

21. CAREY, G.F. and ODEN, J.T.
"The Texas Finite Element Series-Vol. II.
A Second Course".
Prentice-Hall.(1983)

22. AXELSSON, O. and BARKER, V.A.
"Finite Element Solution of Boundary Value Problems".
Academic Press Inc. (1984)

23. SYNGE, J.L.
"The Hypercircle in Mathematical Physics".
Cambridge University Press. (1957)

24. ZIENKIEWICZ, O.C.
"The Finite Element Method".
McGraw Hill, London. (1977)

25. PRAGER, W, and SYNGE, J.L.
Quart. Appl. Math. 5(3), p241 (1947)

26. ACKROYD, R.T.
"Geometrical Methods for Determining the Accuracy of the Approximate Solution of the Boltzmann Equation."
UKAEA Internal Document, (1960)

27. POMRANING, G.C., and CLARK, M. Jr.
"The Variational Method Applied to the Monoenergetic Boltzmann Equation. Part I."
Nucl. Sci Engng 16, p147. (1963)

28. KAPER, H.G., LEAF, G.K., and LINDERMANN, A.J.
"Application of Finite Element Methods in Reactor Mathematics".
ANL - 8126, Argonne National Laboratory. (1974)

29. OHNISHI, T.
"Finite Element Solution Technique for Neutron Transport Approximations. Numerical Reactor Calculations."
IAEA-SM - 154/56, Vienna. (1972).

30. ACKROYD, R.T.
"A Finite Element Method for Neutron Transport I. Some Theoretical Considerations".
Ann. Nucl. Energy, 5, p75. (1978)

31. MARTIN, W.R., and DUDERSTADT, J.J.
"Finite Element Solutions of the Neutron Transport Equation with Application to Strong Heterogeneties."
Nucl. Sci. Engng, 62, p371. (1977)

32. ACKROYD, R.T.
"A Finite Element Method for Diffusion Theory Embracing Nodal and Difference Methods."
Prog. Nucl. Energy, 18, 1/2, p7. (1986)

33. MORDENT, M.
"Phase-space Finite Elements Encoded in ZEPHYR for X-Y and R-Z Transport Calculations."
Prog. Nucl. Energy, 18, 1/2, p27. (1986)

34. LEWIS, E.E., and DILBER, I.
"Finite Element, Nodal and Response Matrix Methods: A Variational Synthesis for Neutron Transport."
Prog. Nucl. Energy, 18, 1/2, p63. (1986)

35. KAVANOKY, A., and LAUTARD, J.J.
"New Developments in Finite Element Reactor Calculations".
Prog. Nucl. Energy, 18, 1/2, p3. (1986)

CHAPTER 3

3. GENERALISED LEAST SQUARES METHOD FOR GENERATING VARIATIONAL PRINCIPLES

3.1 Introduction

3.2 Conventional Least Squares Method

3.3 Generalised Least Squares Method

- 3.3.1 The Basic Idea
- 3.3.2 The $W^{+-}(\phi^+, \phi^-)$ Functional
- 3.3.3 The $K^{+-}(\phi^+, \phi^-)$ Maximum Principle
- 3.3.4 Maximum Principle for ϕ_o^+
- 3.3.5 Maximum Principle for ϕ_o^-
- 3.3.6 Geometrical Interpretation of $K^{+-}(\phi^+, \phi^-)$

3.4 First Order Principles

- 3.4.1 The $\hat{K}(\phi)$ and $\bar{K}(\phi)$ Principles
- 3.4.2 Conventional Least Squares Method for First Order Equation
- 3.4.3 Generalised Least Squares Method for First Order Equation

References to Chapter 3

3. GENERALISED LEAST SQUARES METHOD FOR GENERATING VARIATIONAL PRINCIPLES

3.1 Introduction

In this Chapter the Generalised Least Squares (GLS) Method is reviewed. Starting with the conventional Least Squares (LS) method, the limitations of this method are discussed. Later the basic idea of the GLS method is given before introducing the $W^{+-}(\phi^{+}, \phi^{-})$ functional for neutron transport calculations. The K^{+-} maximum principle is then derived together with maximum principles for ϕ^{+} and ϕ^{-} separately. It is also shown how weighted residual schemes can be derived using K^{+-}. Subsequently a geometrical interpretation of K^{+-} is given. Next the conventional least squares method for the first order equation is shown with its limitations. The conventional LS method raises the order of the associated Euler equation. How this can be avoided is subsequently shown using the GLS method for the first order neutron transport equation.

3.2. Conventional Least Squares Method

Of the various methods used in the solution of boundary value problems, e.g. weighted residual, collocation, the least squares method offers an alternative. Although the method has been mentioned and briefly discussed in various texts, see for example Carey and Oden [1], Zienkiewicz [2], Mitchell and

Wait [3], it has not been widely used. One of the reasons for its unpopularity could be in the fact that the conventional LS method raises the order of the original equation to be solved. So for instance, a second order differential equation for a boundary value problem becomes a fourth order equation. This requires smoother trial functions, i.e. the conventional least squares method raises the continuity requirements of the trial function across element interfaces.

Consider an equation of the form

$$L\phi_o = S \tag{3.2-1}$$

Then the conventional least squares method requires the functional

$$J(\phi) = \int_V (L\phi - S)^2 dv = \text{Minimum} \tag{3.2-2}$$

where ϕ is an approximation to ϕ_o. The integral of the residual squared is to be a minimum. Assume L is self adjoint and without including any boundary conditions, for simplicity, consider arbitrary admissible variation in ϕ. In other words $\phi_o + \epsilon\psi$ is a nearby admissible function for small ϵ. Here ψ is also an admissible function. Then $J(\phi_o + \epsilon\psi)$ becomes

$$\begin{aligned} J(\phi_o + \epsilon\psi) &= \int_V [L(\phi_o + \epsilon\psi) - S]^2 dv \\ &= \int_V [(L\phi)^2 + S^2 - 2L\phi_o S + 2\epsilon(L\phi_o L\psi - L\psi S) \\ &\quad + \epsilon^2 (L\psi)^2] dv \end{aligned} \tag{3.2-3}$$

The minimum condition is that the first variation of $J(\phi_0+\epsilon\psi)$ is zero, i.e.

$$\lim_{\epsilon\to 0} \frac{\partial J(\phi_0+\epsilon\psi)}{\partial \epsilon} = 0$$

This implies from (3.2-3) that

$$2\int_V (L\phi_0 L\psi - L\psi S)\,dv = 0 \qquad (3.2\text{-}4)$$

The terms in (3.2-4) can be evaluated as follows, using Green's Formula,

$$\int_V v\,Lu\,dv = \int_V uL^*v\,dv + \Gamma(u,v) \qquad (3.2\text{-}5)$$

$\Gamma(u,v)$ contains boundary terms obtained from integration by parts. Hence, (3.2-4) becomes

$$\int_V \psi L^* L\phi_0\,dv = \int_V \psi L^* S\,dv - \Gamma(L\phi_0 - S, \psi)$$

This implies an Euler equation of the form

$$L^*L\phi_0 = L^*S \qquad (3.2\text{-}6)$$

Hence the conventional least squares method has raised the order of the equation. So for instance, if L was a second order differential operator, L*L would be a fourth order operator.

3.3. Generalised Least Squares Method

3.3.1. The Basic Idea

In order to avoid the difficulties encountered in the simple least squares method for generating variational principles, i.e. raising the order of the original equation, the generalised least squares method is considered. The generalised least squares is applied here to generate variational principles and weighted residual methods for $K^+(\phi^+)$ and $K^-(\phi^-)$. In the GLS method, operator weights are associated with the least squares process. In the previous example we could have

$$J(\phi) = \int_V (L\phi - s).W.(L\phi - s)\, dv = \text{minimum} \qquad (3.3\text{-}1)$$

where W is an operator weight. Consider the pair of parity equations for neutron transport [4]

$$\underline{\Omega}\cdot\nabla\phi_o^- + c\phi_o^+ - s^+ = 0 \qquad (3.3\text{-}2)$$

$$\underline{\Omega}\cdot\nabla\phi_o^+ + \sigma^{-1}\phi_o^- - s^- = 0 \qquad (3.3\text{-}3)$$

For an approximation (ϕ^+, ϕ^-) to the pair (ϕ_o^+, ϕ_o^-) we have the residuals

$$R^+ = \underline{\Omega}\cdot\nabla\phi^- + c\phi^+ - s^+ \qquad (3.3\text{-}4)$$

and

$$R^- = \underline{\Omega}\cdot\nabla\phi^+ + \sigma^{-1}\phi^- - s^- \qquad (3.3\text{-}5)$$

In this case, the operator weights chosen are C^{-1} with R^+ and G with R^-. So the functional becomes

$$J(\phi^+, \phi^-) = \int_\Omega \int_V R^+ C^{-1} R^+ \, d\Omega \, dV \qquad (3.3\text{-}6)$$

and

$$I(\phi^+, \phi^-) = \int_\Omega \int_V R^- G R^- \, d\Omega \, dV \qquad (3.3\text{-}7)$$

The reason for choosing the particular weights C^{-1} and G is, firstly, it makes it possible to obtain classical variational principles as simple cases of the generalised variational principle obtained from the GLS method; secondly the GLS method does not lead to the raising of the differential operators involved [4]. The functionals I and J can give a measure of the local error, if applied to an element, or the global error made by the trial functions, ϕ^+ and ϕ^-, as

$$\int_\Omega \int_V (R^+ C^{-1} R^+ + R^- G R^-) \, d\Omega \, dV \qquad (3.3\text{-}8)$$

Similarly the measure of error or mismatch at surfaces is as follows:

(a) Surface Source

$$I_S(\phi^+, \phi^-) = \int_{S_S} \left\{ \int_{\underline{\Omega}\cdot\underline{n}>0} |\underline{\Omega}\cdot\underline{n}| \left[\phi^+ - \phi^- - T(\underline{r}, -\underline{\Omega}) \right]^2 d\Omega \right.$$
$$\left. + \int_{\underline{\Omega}\cdot\underline{n}<0} |\underline{\Omega}\cdot\underline{n}| \left[\phi^+ + \phi^- - T(\underline{r}, \underline{\Omega}) \right]^2 d\underline{\Omega} \right\} dS$$

(3.3-9)

(b) Bare Surface (Special case of (a))

$$I_b(\phi^+,\phi^-) = \int_{S_b}\left\{\int_{\underline{\Omega}\cdot\underline{n}>0} |\underline{\Omega}\cdot\underline{n}|\,[\phi^+-\phi^-]^2\,d\Omega + \int_{\underline{\Omega}\cdot\underline{n}<0} |\underline{\Omega}\cdot\underline{n}|\,[\phi^++\phi^-]^2 d\Omega\right\} ds \tag{3.3-10}$$

(c) Interfaces Between Elements

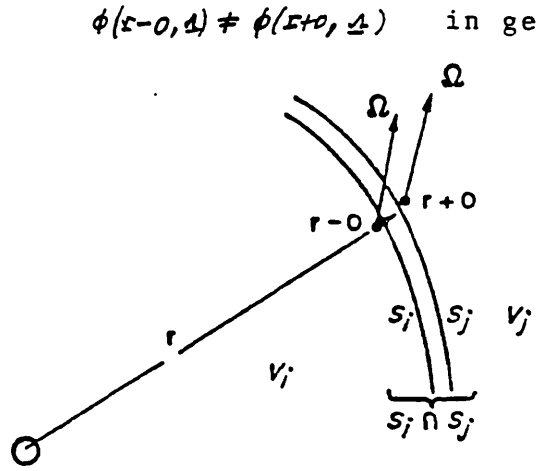
$$I_f(\phi^+,\phi^-) = \int_{\cup(S_i\cap S_j)}\int_{\Omega} |\underline{\Omega}\cdot\underline{n}|\left\{\omega^+(r,\underline{\Omega})\,[\phi^+(r+o,\underline{\Omega})-\phi^+(r-o,\underline{\Omega})]^2 + \omega^-(r,\underline{\Omega})\,[\phi^-(r+o,\underline{\Omega})-\phi^-(r-o,\underline{\Omega})]^2\right\} d\Omega\, ds \tag{3.3-11}$$

See Fig 3.1 for the notation used for discontinuities.

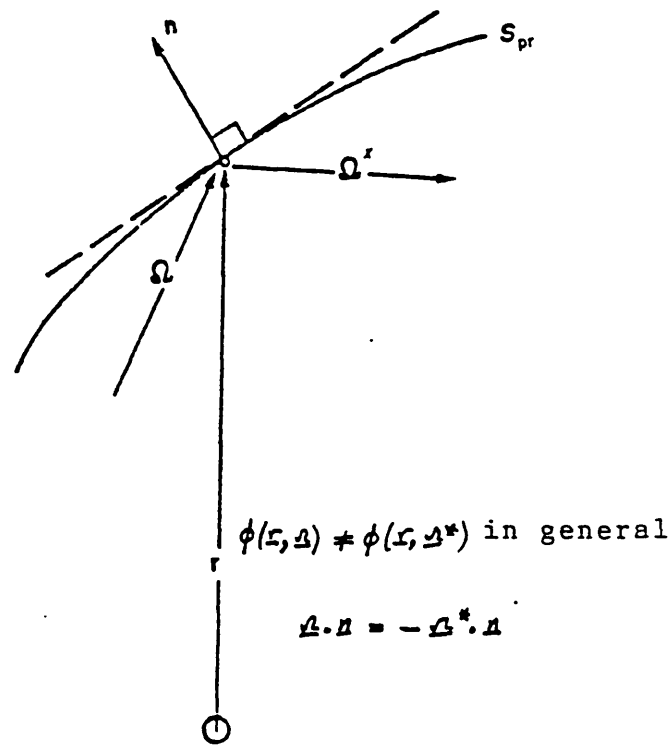
(d) Perfect Reflector

$$I_{pr}(\phi^+,\phi^-) = \int_{S_{pr}}\int_{\Omega} |\underline{\Omega}\cdot\underline{n}|\left\{\omega^+(r,\underline{\Omega})\,[\phi^+(r,\underline{\Omega})-\phi^+(r,\underline{\Omega}^*)]^2 + \omega^-(r,\underline{\Omega})\,[\phi^-(r,\underline{\Omega})-\phi^-(r,\underline{\Omega}^*)]^2\right\} d\Omega\, ds \tag{3.3-12}$$

The interface and perfect reflector conditions can be enforced as closely as required by increasing the penalty weights.



Jump in $\phi(r,\Omega)$ at the interface $S_i \cap S_j$ of subregions V_i and V_j bounded by surfaces S_i and S_j respectively.



Jump at r on a perfect reflector S_{pr} between incident beam $\phi(r,\Omega)$ and reflected beam $\phi(r,\Omega^*)$.

Fig. 3.1 Jumps in ϕ for interfaces and a perfect reflector.

3.3.2 The W^{+-} Functional

We can now define a functional which provides a least squares measure of the errors made by the approximations ϕ^+ and ϕ^- as

$$W^{+-}(\phi^+,\phi^-) = I(\phi^+,\phi^-) + J(\phi^+,\phi^-) + I_s(\phi^+,\phi^-) + I_b(\phi^+,\phi^-) + I_{pr}(\phi^+,\phi^-) + I_f(\phi^+,\phi^-) \quad (3.3\text{-}13)$$

Expanding $W^{+-}(\phi^+,\phi^-)$ leads to the identity (See Ackroyd [1])

$$K^{+-}(\phi^+,\phi^-) + W^{+-}(\phi^+,\phi^-) = \int_V \{ \langle c^{-1}s^+, s^+ \rangle + \langle \varsigma s^-, s^- \rangle \} dV + 2\int_{S_s}\int_{\underline{\Omega}\cdot\underline{n}<0} |\underline{\Omega}\cdot\underline{n}|\, T^2\, d\Omega\, ds \quad (3.3\text{-}14)$$

The right hand side of the above is a known quantity involving the sources S^+, S^-, T and material data.

3.3.3. K^{+-} Maximum Principle

$K^{+-}(\phi^+,\phi^-)$ may be written in full as

$$K^{+-}(\phi^+,\phi^-) = K^+(\phi^+) + K^-(\phi^-) + L(\phi^+,\phi^-) + M(\phi^+,\phi^-) - I_f(\phi^+,\phi^-) - I_{pr}(\phi^+,\phi^-) \quad (3.3\text{-}15)$$

Here $K^+(\phi^+)$ and $K^-(\phi^-)$ are the functionals used to obtain classical maximum principles.

$$K^+(\phi^+) = 2\int_V \{ \langle \phi^+, s^+ \rangle + \langle \underline{\Omega}\cdot\nabla\phi^+, \varsigma s^- \rangle \} dV - F^+(\phi^+,\phi^+) + 4\int_{S_s}\int_{\underline{\Omega}\cdot\underline{n}<0} |\underline{\Omega}\cdot\underline{n}|\, \phi^+ T\, d\Omega\, ds \quad (3.3\text{-}16)$$

and

$$K^-(\phi^-) = 2\int_V \{ \langle \phi^-; s^- \rangle + \langle \underline{\Omega}\cdot\nabla\phi^-, c^{-1}s^+ \rangle \} dV - F^-(\phi^-;\phi^-) + 4\int_{S_S}\int_{\underline{\nu}\cdot\underline{n}<0} |\underline{\Omega}\cdot\underline{n}|\,\phi^-\tau\, d\underline{\Omega}\, ds \tag{3.3-17}$$

where

$$F^+(\phi^+,\phi^+) = \int_V \{ \langle \underline{\Omega}\cdot\nabla\phi^+, \varsigma(\underline{\Omega}\cdot\nabla\phi^+)\rangle + \langle \phi^+, c\phi^+\rangle \} dV \tag{3.3-18}$$

and

$$F^-(\phi^-,\phi^-) = \int_V \{ \langle \underline{\Omega}\cdot\nabla\phi^-, c^{-1}(\underline{\Omega}\cdot\nabla\phi^-)\rangle + \langle \phi^-, \varsigma^{-1}\phi^-\rangle \} dV \tag{3.3-19}$$

The surface integrals L and M are defined as

$$L(\phi^+,\phi^-) = -2\int_{US_i}\int_{\underline{\Omega}} \underline{\Omega}\cdot\underline{n}_i\,\phi^+\phi^-\, d\Omega\, ds \tag{3.3-20}$$

and

$$M(\phi^+,\phi^-) = -2\int_{S_{pr}}\int_{\underline{\Omega}} \underline{\Omega}\cdot\underline{n}\,\phi^+\phi^-\, d\Omega\, ds \tag{3.3-21}$$

These integrals arise from the expansion of the integrand of the volume integral in $W^{+-}(\phi^+,\phi^-)$. The cross term

$$\int_\Omega\int_V 2(\phi^+\underline{\Omega}\cdot\nabla\phi^- + \phi^-\underline{\Omega}\cdot\nabla\phi^+)\, d\Omega\, dV$$

can be written as

$$2\iint \operatorname{div}(\underline{\Omega}\,\phi^+\phi^-)\, d\Omega\, dV$$

Then the divergence theorem gives

$$2\iint \operatorname{div}(\underline{\Omega}\,\phi^+\phi^-)\, d\underline{\Omega}\, dV = 2\iint_{US_i} \underline{\Omega}\cdot\underline{n}_i\,\phi^+\phi^-\, d\Omega\, ds + 2\iint_{S_{pr}} \underline{\Omega}\cdot\underline{n}\,\phi^+\phi^-\, d\Omega\, ds$$

Hence these terms appear on the right hand side of (3.3-13). Since $W^{+-}(\phi^+, \phi^-)$ is positive definite, all the component functionals in (3.3-13) are positive definite. Then from (3.3-14)

$$K^{+-}(\phi^+, \phi^-) \leq 2\alpha \tag{3.3-22}$$

Hence $K^{+-}(\phi^+, \phi^-)$ defines a maximum principle. Equality is obtained in (3.3-22) if and only if $\phi^+ = \phi_o^+$ and $\phi^- = \phi_o^-$.

3.3.4 Maximum Principle for ϕ^+

The classical variational principle can be obtained from the identity

$$J(\phi^+, \phi^-) + I(\phi^+, \phi^-) + K^+(\phi^+) + K^-(\phi^-) + L(\phi^+, \phi^-) + M(\phi^+, \phi^-) + I_b(\phi^+, \phi^-) + I_s(\phi^+, \phi^-) = 2\alpha \tag{3.3-23}$$

by making suitable choices for ϕ^+ and ϕ^-. If $\phi^+(\underline{r}, \underline{\Omega})$ satisfies the following conditions:

(a) ϕ^+ is continuous at each interface for all directions $\underline{\Omega}$ across the interface.

(b) ϕ^+ satisfies the reflection condition

$$\phi^+(\underline{r}, \underline{\Omega}) = \phi^+(\underline{r}, \underline{\Omega}^*) \quad \text{for all} \quad \underline{\Omega} \cdot \underline{n} = -\underline{\Omega}^* \cdot \underline{n} \quad \text{on} \quad S_{pr}.$$

(c) $\phi^- = \phi_o^-$,

then

$$K^+(\phi^+) \leq F^+(\phi_o^+, \phi_o^+) \tag{3.3-24}$$

This is the classical maximum principle for ϕ^+.

3.3.5 Maximum Principle for ϕ^-.

If $\phi^-(r, \underline{\Omega})$ satisfies the conditions given in (a) and (b) above and we choose

(c) $\phi^+ = \phi_o^+$

then

$$K^-(\phi^-) \leq F^-(\phi_o^-, \phi_o^-) \qquad (3.3\text{-}25)$$

Hence, a maximum principle for ϕ^- is obtained.

On the other hand, if both ϕ^+ and ϕ^- satisfy conditions (a) and (b) above, and

$$\phi^- = S[S^- - \underline{\Omega}\cdot\nabla\phi^+]$$

from the parity equations, then

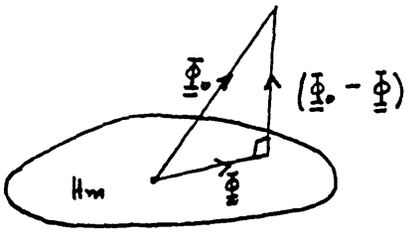
$$K^+(\phi^+) \leq F^+(\phi_o^+, \phi_o^+) \leq E^+(\phi^+) \qquad (3.3\text{-}26)$$

where $E^+(\phi^+)$ is the functional associated with the classical minimum principle. See Ackroyd [4] for further details.

3.3.6 Geometrical Interpretation of $K^{+-}(\phi^+, \phi^-)$

A simple geometrical interpretation of the K^{+-} maximum principle can be obtained by considering a Hilbert space with a suitable scalar product [4]. If the pair (ϕ^+, ϕ^-) is represented by the vector $\underline{\Phi}$ and the exact solution vector by

$\underline{\Phi}_o$, then the generalised least squares error is given by $\sqrt{(\underline{\Phi} - \underline{\Phi}_o)^2}$.



$$\underline{\Phi} = \sum_m a_m \underline{\Phi}_m$$

Fig. 3.2 Hilbert space interpretation of max $K^{+-}(\phi^+, \phi^-)$.

If this distance is minimised, by appropriate choice of ϕ^+ and ϕ^-, as it is if $\underline{\Phi}_o$ projects orthogonally on Hm, the subspace of $\underline{\Phi}_m$, then

$$(\underline{\Phi} - \underline{\Phi}_o) \cdot \underline{\Phi}_m = 0 \qquad \text{for m= 1,2.....,M.}$$

Here $\{\underline{\Phi}_m\}$ are the set of basis functions for Hm. Minimising $(\underline{\Phi} - \underline{\Phi}_o)^2$ maximises $K^{+-}(\phi^+, \phi^-)$.

The K^{+-} boundary free principle not only generates a boundary free least squares method and classical variational principles, but, also generates Galerkin and Petrov - Galerkin schemes (Ackroyd [5]). If the trial functions ϕ^+ and ϕ^- are independent, then the following weighted residual equations are obtained

$$0 = \int_V \int_\Omega \left[\phi_i^+ \{ -\underline{\Omega} \cdot \nabla [\zeta \underline{\Omega} \cdot \nabla \phi^+] + C\phi^+ - S^+ + \underline{\Omega} \cdot \nabla \zeta S^- \} \right.$$
$$\left. + \phi_i^- \{ -\underline{\Omega} \cdot \nabla [C^{-1} \underline{\Omega} \cdot \nabla \phi^-] + \zeta^{-1} \phi^- - S^- + \underline{\Omega} \cdot \nabla C^{-1} S^+ \} \right] d\Omega dV$$
$$+ \text{ surface terms} \qquad (3.3\text{-}27)$$

If the boundary and interface conditions are satisfied, then the weighted residual equations, above, reduce to Glerkin form. If $\phi^- = \phi_o^-$ and the interface conditions for ϕ^+ is satisfied, then the following weighted residual equations are obtained.

$$0 = \int_V \int_\Omega \phi_m^+ \left[-\underline{\Omega}\cdot\nabla\left[\varsigma\left(\underline{\Omega}\cdot\nabla\phi^+\right)\right] + c\,\phi^+ - s^+ + \underline{\Omega}\cdot\nabla\varsigma s^-\right] d\Omega\, dV$$

$$+ \text{surface terms} \qquad (3.3\text{-}28)$$

When ϕ^- is made dependent on ϕ^+, to reduce the number of unknowns, then the weighted residual equations of Galerkin type for the second order even parity equations are replaced by ones for the first order equations with more general weights. Since

$$\phi^- = \varsigma\left[s^- - \underline{\Omega}\cdot\nabla\phi^+\right]$$

with

$$\phi_m^- = -\varsigma\,\underline{\Omega}\cdot\nabla\phi_m^+$$

then the weighted residual equations may be written as

$$0 = \int_V \int_\Omega \left(\phi_m^+ + c^{-1}\left[\underline{\Omega}\cdot\nabla\phi_m^-\right]\right)\left(\underline{\Omega}\cdot\nabla\phi + \Sigma\phi - s\right) d\Omega\, dV \qquad (3.3\text{-}29)$$

$$+ \text{surface terms}$$

3.4 First Order Principles

3.4.1 The $\tilde{K}(\phi)$ and $\bar{K}(\phi)$ Principles

In this section two maximum principles, $\tilde{K}(\phi)$ and $\bar{K}(\phi)$ for the first order transport equation are briefly discussed. Usually the finite element solutions of the first order neutron transport equation are obtained by a weighted residual scheme, although Kaplan [6] has used a stationary principle for the first order Boltzmann equation. The generalised least squares method canbe used to derive a maximum principle for the first order equation. The first principle is the boundary tied $\bar{K}(\phi)$ principle. Consider a trial function which has the following properties:

(a) ϕ and its first derivatives are continuous within the finite elements for given $\underline{\Omega}$.

(b) $\phi(\underline{r}, \underline{\Omega})$ is continuous across element interfaces for all directions $\underline{\Omega}$ crossing the interface.

Define a functional $V(\phi)$ as

$$V(\phi) = \int_V \langle \Sigma^{-1}(\underline{\Omega}\cdot\nabla\phi + \Sigma\phi - S), (\underline{\Omega}\cdot\nabla\phi + \Sigma\phi - S)\rangle \, dV + 2\iint_{S_b}\iint_{\underline{\Omega}\cdot\underline{n}<0} |\underline{\Omega}\cdot\underline{n}|\,\phi^2\, d\underline{\Omega}\, ds + 2\iint_{S_s}\iint_{\underline{\Omega}\cdot\underline{n}} |\underline{\Omega}\cdot\underline{n}|\,(T-\phi)^2\, d\Omega\, ds \qquad (3.4\text{-}1)$$

where

$$\Sigma\phi(\underline{r}, \underline{\Omega}) = \sigma_T\phi(\underline{r}, \underline{\Omega}) - \int_{\Omega'} \sigma_S(\underline{r}, \underline{\Omega}\cdot\underline{\Omega}')\,\phi(\underline{r}, \underline{\Omega}')\, d\Omega' \qquad (3.4\text{-}2)$$

and

$$\Sigma^{-1}\phi(r,\Omega) = \frac{\phi(r,\Omega)}{\sigma_T} + \int_{\Omega'} f(r,\Omega\cdot\Omega')\,\phi(r,\Omega')\,d\Omega' \tag{3.4-3}$$

Let $\theta = \phi - \phi_0$, then $V(\phi)$ can be written as

$$\int_V \left[\langle \Omega\cdot\nabla\theta, \Sigma^{-1}\Omega\cdot\nabla\theta\rangle + \langle\theta,\Sigma\theta\rangle \right] dV + \int_{S_b}\int_{\Omega} |\Omega\cdot n|\,\theta^2\,d\Omega\,ds. \tag{3.4-4}$$

Since Σ and Σ^{-1} are positive then

$$V(\phi) \geq 0.$$

Defining a bilinear form $\tilde{F}(\phi,\psi)$, see Ackroyd [8], and a functional $\tilde{K}(\phi)$ as

$$\begin{aligned}\tilde{K}(\phi) = {} & 2\int_V \left[\langle \phi^+, S\rangle + \langle \Omega\cdot\nabla\phi^+, \Sigma^{-1}S\rangle \right] dV \\ & - \tilde{F}(\phi,\phi) + 4\int_{S_s}\int_{\Omega\cdot n<0} |\Omega\cdot n|\,\phi_T\,d\Omega\,ds\end{aligned} \tag{3.4-5}$$

leads to the following:

$$V(\phi) + \hat{K}(\phi) = \int_V \langle S, \Sigma^{-1}S\rangle\,dV + 2\int_{S_s}\int_{\Omega\cdot n<0} |\Omega\cdot n|\,T^2\,d\Omega\,ds \tag{3.4-6}$$

Since $V(\phi)$ is non-negative, then

$$\hat{K}(\phi) \leq \hat{K}(\phi_0) = \int_V \langle S, \Sigma^{-1}S\rangle\,dV + 2\int_{S_s}\int_{\Omega\cdot n<0} |\Omega\cdot n|\,T^2\,d\Omega\,ds \tag{3.4-7}$$

is the maximum principle for the Boltzmann equation.

The $\bar{K}(\phi)$ principle is completely boundary free and can

be derived from the $K^{+-}(\phi^+,\phi^-)$ maximum principle. Here an alternative expression for K^{+-} is used, viz.,

$$K^{+-}(\phi^+,\phi^-) = \int_V [2\langle\phi,s\rangle + 2\langle\underline{\Omega}\cdot\nabla\phi, \Sigma^{-1}s\rangle]\,dv - \hat{F}(\phi,\phi)$$
$$+4\int_{S_s}\int_{\underline{\Omega}\cdot\underline{n}<0} |\underline{\Omega}\cdot\underline{n}|\,\phi T\,d\Omega\,ds - \int_{\cup S_i}\int_{\underline{\Omega}} \phi^2\,\underline{\Omega}\cdot\underline{n}_i\,d\Omega\,ds$$
$$-\int_{S_{pr}}\int_{\Omega}\phi^2\,\underline{\Omega}\cdot\underline{n}\,d\underline{\Omega}\,ds - \int_{\cup(S_i\cap S_j)}\int_{\underline{\Omega}} |\underline{\Omega}\cdot\underline{n}|\,w(r,\underline{\Omega})\,[\phi(r+o,\underline{\Omega})-\phi(r-o,\underline{\Omega})]^2 d\Omega ds$$
$$-\int_{S_{pr}}\int_{\Omega} |\underline{\Omega}\cdot\underline{n}|\,w(r,\underline{\Omega})\,[\phi(r,\underline{\Omega})-\phi(r,\underline{\Omega}^*)]^2 d\Omega\,ds$$
$$= \bar{K}(\phi) \qquad (3.4\text{-}8)$$

Also $W^{+-}(\phi^+,\phi^-)$ may be written as

$$W^{+-}(\phi^+,\phi^-) = \int_V \langle\Sigma^{-1}(\underline{\Omega}\cdot\nabla\phi+\Sigma\phi-s),\ \underline{\Omega}\cdot\nabla\phi+\Sigma\phi-s\rangle\,dv$$
$$+2\int_{S_b}\int_{\underline{\Omega}\cdot\underline{n}<0} |\underline{\Omega}\cdot\underline{n}|\,\phi^2\,d\underline{\Omega}\,ds + 2\int_{S_e}\int_{\underline{\Omega}\cdot\underline{n}<0} |\underline{\Omega}\cdot\underline{n}|\,[T-\phi]^2\,d\Omega\,ds$$
$$+\int_{\cup(S_i\cap S_j)}\int_{\Omega} |\underline{\Omega}\cdot\underline{n}|\,w(r,\underline{\Omega})\,[\phi(r+o,\underline{\Omega})-\phi(r-o,\underline{\Omega})]^2\,d\Omega\,ds$$
$$+\int_{S_{pr}}\int_{\Omega} |\underline{\Omega}\cdot\underline{n}|\,w(r,\underline{\Omega})\,[\phi(r,\underline{\Omega})-\phi(r,\underline{\Omega}^*)]\,d\Omega\,ds$$
$$= \bar{V}(\phi). \qquad (3.4\text{-}9)$$

Then the following identity is obtained

$$\bar{K}(\phi) + \bar{V}(\phi) = \int_V \langle\Sigma^{-1}s, s\rangle\,dv + 2\int_{S_s}\int_{\underline{\Omega}\cdot\underline{n}<0} |\underline{\Omega}\cdot\underline{n}|\,T^2\,d\Omega\,ds$$

Since $\bar{V}(\phi)$ is non negative, then

$$\bar{K}(\phi) \leq \int_V \langle \Sigma^{-1} S, S \rangle + 2 \iint_{S_S} \int_{\underline{\Omega}\cdot\underline{n}<0} |\underline{\Omega}\cdot\underline{n}| \, T^2 \, d\Omega \, dS \tag{3.4-10}$$

which is the boundary free maximum principle for ϕ. See Ackroyd [7,8] for a complete derivation of this maximum principle. When the continuity condition across interfaces is applied to the trial funciton, then the $\bar{K}(\phi)$ principle reduces to the $\tilde{K}(\phi)$ maximum principle.

3.4.2 Conventional Least Squares Method for the First Order Equation

The conventional least squares method is applied to the first order form of the transport equation as an illustration before considering the generalised least squares method. Consider the least squares functional for a system with a bare surface only.

$$U(\phi) = \int_V \int_\Omega (\underline{\Omega}.\nabla\phi + \Sigma\phi - S)^2 d\underline{\Omega}\, dV + \int_{S_b} \int_\Omega |\underline{\Omega}.\underline{n}|\phi^2 d\Omega ds \quad (3.4\text{-}11)$$

The operator Σ has been defined earlier. If we consider an arbitrary variation in ϕ i.e. $\phi+\epsilon\Psi$, then the minimum condition for $U(\phi+\epsilon\Psi)$ gives

$$\int_V \int_\Omega (\underline{\Omega}.\nabla\phi + \Sigma\phi - S)(\underline{\Omega}.\nabla\Psi + \Sigma\Psi) d\underline{\Omega}\, dV + \int_{S_b} \int_\Omega |\underline{\Omega}.\underline{n}|\phi\Psi\, d\Omega ds = 0 \quad (3.4\text{-}12)$$

Let $P\phi \equiv \underline{\Omega}.\nabla\phi + \Sigma\phi$.

Then

$$\int_V \int_\Omega (P\phi - S) P\Psi\, d\Omega dV + \int_{S_b} \int_\Omega |\underline{\Omega}.\underline{n}|\phi\Psi\, d\Omega ds = 0 \quad (3.4\text{-}13)$$

Using Green's formula

$$\int_\Omega \int_V v\, Pu\, dV d\underline{\Omega} = \int_\Omega \int_V u\, P^* v\, dV d\underline{\Omega} + \int_{S_b} \int_\Omega \underline{\Omega}.\underline{n}\, uv\, d\underline{\Omega} ds \quad (3.4\text{-}14)$$

with $u = \Psi$ and $v = P\phi$ gives from (3.4-13)

$$\int_V \int_{\underline{\Omega}} (P^* P\phi - P^* S)\,\psi \, d\underline{\Omega}\, dV = \int_{S_b} \int_{\Omega} \underline{\Omega}\cdot\underline{n}\,(S - P\phi)\,\psi \, d\Omega\, dS - \int_{S_b} \int_{\underline{\Omega}\cdot\underline{n}<0} |\underline{\Omega}\cdot\underline{n}|\,\phi\,\psi \, d\Omega\, dS \tag{3.4-15}$$

Hence, the Euler equation corresponding to (3.4-15) is

$$P^* P\phi = P^* S \qquad \text{in} \qquad V. \tag{3.4-16}$$

with

$$\phi - (P\phi - S) = 0 \quad \text{on } S_b \text{ for } \underline{\Omega}\cdot\underline{n} < 0$$

and (3.4-17)

$$(P\phi - S) = 0 \quad \text{on } S_b \text{ for } \underline{\Omega}\cdot\underline{n} > 0$$

Hence the order of the original equation increases from one to two because of the $-\underline{\Omega}\cdot\nabla(\underline{\Omega}\cdot\nabla\phi)$ term in (3.4-16).

Note that

$$\int_V \int_{\Omega} (\underline{\Omega}\cdot\nabla\phi + \Sigma\phi - S)^2 \, d\Omega\, dV$$

can also be written in terms of the even and odd parity components ϕ^+ and ϕ^- as

$$\int_V \int_{\underline{\Omega}} \left\{ (\underline{\Omega}\cdot\nabla\phi^+ + S^{-1}\phi^- - S^-)^2 + (\underline{\Omega}\cdot\nabla\phi^+ + c\,\phi^+ - S^+)^2 \right\} d\Omega\, dV \tag{3.4-18}$$

3.4.3 Generalised Least Squares Method for the First Order Equation

Here it is shown how the generalised least squares method, using the functional $V(\phi)$ can give rise to the first order Boltzmann equation, together with its boundary conditions. The Euler-Lagrange equations for $V(\phi)$ imply the first order transport equation. The functional $V(\phi)$ is defined as

$$V(\phi) = \int_V \int_\Omega (\underline{\Omega}.\nabla\phi + \Sigma\phi - s)\Sigma^{-1}(\underline{\Omega}.\nabla\phi + \Sigma\phi - s)\, d\Omega\, dV + \int_{S_b}\int_{\underline{\Omega}.\underline{n}<0} |\underline{\Omega}.\underline{n}|\,\phi^2\, d\Omega\, ds \qquad (3.4\text{-}19)$$

The operator weight used here is Σ^{-1} as opposed to the unit operator weight in the conventional least squares method. Following a procedure similar to the one in Section 3.4.2, we set $\phi_\epsilon = \phi + \epsilon\psi$ and use the minimising condition

$$\lim_{\epsilon\to 0} \frac{\partial V(\phi+\epsilon\psi)}{\partial\epsilon} = 0$$

This gives

$$2\int_V\int_\Omega (\underline{\Omega}.\nabla\phi + \Sigma\phi - s)\Sigma^{-1}(\underline{\Omega}.\nabla\psi + \Sigma\psi)\, d\Omega\, dV + \int_{S_b}\int_{\underline{\Omega}.\underline{n}<0} |\underline{\Omega}.\underline{n}|\,\phi\psi\, d\Omega\, d\underline{s} = 0 \qquad (3.4\text{-}20)$$

Again if P is the operator $(\underline{\Omega}.\nabla+\Sigma)$, then its adjoint is $P^* = (-\underline{\Omega}.\nabla+\Sigma)$. Using Green's formula, (3.4-14), results in

$$\int_V\int_\Omega (\underline{\Omega}.\nabla\psi + \Sigma\psi)\Sigma^{-1}(\underline{\Omega}.\nabla\phi + \Sigma\psi - s)\, d\Omega\, dV + \int_{S_b}\int_{\underline{\Omega}.\underline{n}<0} |\underline{\Omega}.\underline{n}|\,\phi\psi\, d\Omega\, ds = \int\int \psi P^*\Sigma^{-1}(P\phi - s)\, d\underline{\Omega}\, dV + \int_{S_b}\left\{\int_{\underline{\Omega}.\underline{n}<0} |\underline{\Omega}.\underline{n}|\,\phi\psi + \int_\Omega \underline{\Omega}.\underline{n}\,\phi\,\Sigma^{-1}(P\phi - s)\, d\Omega\right\} ds \qquad (3.4\text{-}21)$$

for arbitrary ψ . Hence,

$$\begin{aligned} &(a)\quad P^{*}\Sigma^{-1}(P\phi - S) = 0 \qquad \text{in} \quad V \\ &(b)\quad \phi^{-} - \Sigma^{-1}(P\phi - s) = 0 \quad \text{on} \quad S_b \ \text{for} \ \underline{\Omega}\cdot\underline{n} < 0 \\ &(c)\quad \Sigma^{-1}(P\phi - S) = 0 \quad \text{on} \quad S_b \ \text{for} \ \underline{\Omega}\cdot\underline{n} > 0 \end{aligned} \tag{3.4-22}$$

From condition (a) we have

$$-\underline{\Omega}\cdot\nabla\left(\Sigma^{-1}\underline{\Omega}\cdot\nabla\phi\right) + \Sigma\phi + \underline{\Omega}\cdot\nabla\left(\Sigma^{-1}\right)S - S = 0 \tag{3.4-23}$$

Using the even and odd parity components of ϕ , i.e. ϕ^{+} and ϕ^{-} gives

$$\underline{\Omega}\cdot\nabla\left(\Sigma^{-1}\underline{\Omega}\cdot\nabla\phi\right) = \underline{\Omega}\cdot\nabla\left(\zeta\,\underline{\Omega}\cdot\nabla\phi^{+}\right) + \underline{\Omega}\cdot\nabla\left(c^{-1}\underline{\Omega}\cdot\nabla\phi^{-}\right).$$

Also

$$\Sigma\phi = c\phi^{+} + \zeta^{-1}\phi^{-}$$
$$S = s^{+} + s^{-}$$

and

$$\underline{\Omega}\cdot\nabla\left(\Sigma^{-1}S\right) = \underline{\Omega}\cdot\nabla\left(\zeta s^{-}\right) + \underline{\Omega}\cdot\nabla\left(c^{-1}s^{+}\right).$$

Using these relations, the even parity components of (3.4-23) give

$$-\underline{\Omega}\cdot\nabla\left(\zeta\,\underline{\Omega}\cdot\nabla\phi^{+}\right) + c\phi^{+} = s^{+} - \underline{\Omega}\cdot\nabla\left(\zeta s^{-}\right) \tag{3.4-24}$$

while the odd components give

$$-\underline{\Omega}\cdot\nabla\left(c^{-1}\underline{\Omega}\cdot\nabla\phi^{-}\right) + \zeta^{-1}\phi^{-} = s^{-} - \underline{\Omega}\cdot\nabla\left(c^{-1}s^{+}\right) \tag{3.4-25}$$

Eqns. (3.4-24) and (3.4-25) are like the equations for the even and odd parity fluxes ϕ_o^+ and ϕ_o^-.

The boundary conditions are now

$$\phi^+ + \phi^- - C^{-1}(\underline{\Omega}.\nabla\phi^- - S^+) - \zeta(\underline{\Omega}.\nabla\phi^+ - S) = 0 \quad \text{for} \quad \underline{\Omega}.\underline{n} < 0$$

and $$C^{-1}(\underline{\Omega}.\nabla\phi^- - S^+) + \zeta(\underline{\Omega}.\nabla\phi^+ - S^+) = 0 \quad \text{for} \quad \underline{\Omega}.\underline{n} > 0$$

whereas the interface condition is $\Sigma^{-1}(\underline{\Omega}.\nabla\phi + \Sigma\phi - S)$ continuous across interfaces for $\underline{\Omega}.\underline{n} \neq 0$.

These conditions can be shown (Ackroyd [9]) to be disguised forms of the boundary and interface conditions for the even and odd parity equations by defining

$$\phi' = \Sigma^{-1}(S - \underline{\Omega}.\nabla\phi) . \qquad (3.4\text{-}26)$$

Then ϕ' satisfies the interface continuity condition. It can then be shown that

$$\phi = \phi' \quad \text{within} \quad V \qquad (3.4\text{-}27)$$
$$\phi = \phi' \quad \text{on} \quad S_b .$$

Hence

$$\underline{\Omega}.\nabla\phi + \Sigma\phi = S \qquad (3.4\text{-}28)$$

i.e. ϕ satisfies the first order transport equation.

REFERENCES TO CHAPTER 3

1. CAREY, G.F., and ODEN, J.T.
"Finite Elements: A Second Course Vol II".
Prentice-Hall, Inc. (1983)

2. ZIENKIEWICZ, O.C.
"The Finite Element Method".
McGraw Hill. (1977)

3. MITCHELL, A.R., and WAIT, R.
"The Finite Element Method in Partial Differential Equations".
Wiley & Sons. (1977)

4. ACKROYD, R.T.
"The Why and How of Finite Elements".
Ann. Nucl. Energy, 8, 11/12, p539 (1981)

5. ACKROYD, R.T.
"Generalised Least Squares as a Generator of Variational Principles and Weighted Residual Methods in FEM Transport Methods".
Prog. Nucl. Energy, 18, 1/2, p45. (1986)

6. KAPLAN, S.
"A New Derivation of Discrete Ordinate Approximations".
Nucl. Sci. Engng, 34, p76. (1968)

7. ACKROYD, R.T.
"Least Squares Derivation of Extremum and Weighted Residual Methods for Equations of Reactor Physics - I".
Ann. Nucl. Energy, 10, p65 (1982)

8. ACKROYD, R.T.
"A Finite Element Method for Neutron Transport VII. Completely Boundary-Free Maximum Principle for the First-Order Boltzmann Equation.
Ann. Nucl. Energy, 10, 5, p243 (1982)

9. ACKROYD, R.T.
Private Communication (1986)

CHAPTER 4

4. ANISOTROPIC SCATTERING IN ONE DIMENSIONAL SLAB GEOMETRY

4.1 Introduction
4.2 The $K^+(\phi^+)$ Functional
4.3 The Reduced Functional
4.4 Finite Element Approximation
    4.4.1 Choice of Elements
4.5 Derivation of Angular Matrices
4.6 The Odd Parity Flux
4.7 The Multigroup Approximation
    4.7.1 The Multigroup Equation
4.8 Even and Odd Parity Downscatter Sources
    4.8.1 Local Downscatter Source Matrices
4.9 Extension To Higher Dimensions
4.10 One Group Test Cases
    4.10.1 BFI Scattering Law Test Problem I
    4.10.2 BFI Scattering Law Test Problem II
    4.10.3 Forward Scattering Source Problem
4.11 Multigroup Test Cases
    4.11.1 Benchmark Problem with BFI Scattering Law
    4.11.2 P1 and P3 Scattering Source Problems
    4.11.3 P1 Scattering Multiregion Source Problem
    4.11.4 P3 Scattering Eigenvalue Problem

References to Chapter 4

4. ANISOTROPIC SCATTERING IN ONE DIMENSIONAL SLAB GEOMETRY

4.1. Introduction

In the study of neutron transport through media there are many situations where anisotropic scattering of neutrons is important. There are two differenct types of anisotropies of scattering depending on which frame of reference the collision process is investigated. See Section 1.3. In the centre of mass system the scattering is isotropic for low energy neutrons. At higher energies, above approximately 1 MeV the scattering becomes anisotropic. Then the angular distribution of neutrons is generally forward peaked. As seen earlier a second type of anisotropy occurs in the transformation from the centre of mass system to the laboratory system. This effect is most important for neutrons scattering off light nuclei. It is the laboratory system of course in which the transport equation is solved. In the laboratory system anisotropy is pronounced in the scattering of fast neutrons from nuclei of all mass numbers and in the scattering of neutrons of all energies from light nuclei. Anisotropic scattering effects are important in the distribution of neutrons deep within shield regions and small critical systems. See Brockmann [1].

Anisotropic scattering also tends to make the scattered neutron travel in directions biased towards the direction

of the incident neutron. In testing the mathematical process employed, it is convenient to consider the so called backward-forward-isotropic (BFI) scattering model. The forward bias in real anisotropic scattering tends to make the escape of a scattered neutron, from a system, more likely when the incident neutron is travelling in an escape direction. For example, consider the escape probability of a neutron in a slab shield system, as shown in Fig 4.1, with a source on the left and a bare surface on the right. In comparing isotropic and anisotropic scattering the absorption and scattering cross-sections are taken to be the same in both shield regions. In the case of anisotropic scattering the backward scattering is zero and the probability of forward scattering in the direction of the incident neutron is a half.

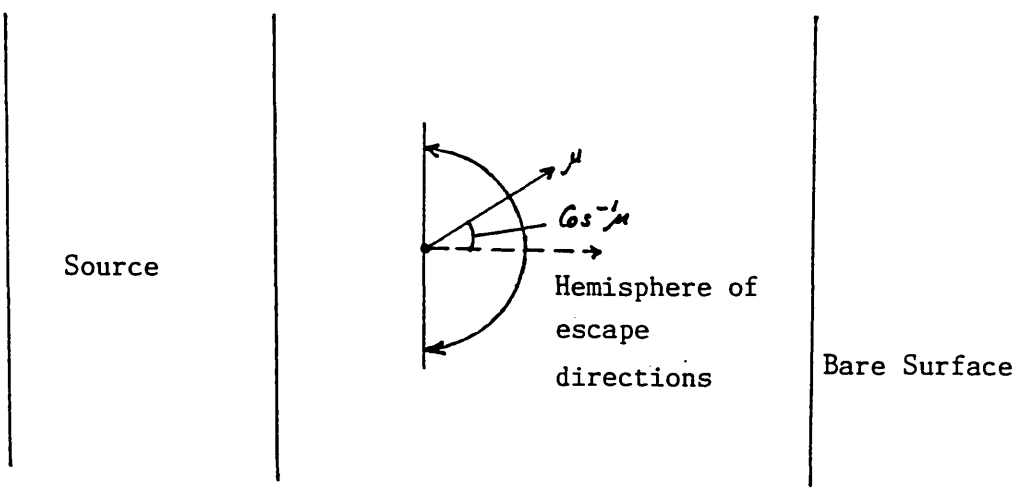


Fig. 4.1 Source-Shield Geometry.

After scattering the components of the isotropically scattered neutron are the same for both shield components. If the probability of the isotropically scattered neutron having an escape direction is α ($< \frac{1}{2}$), then the probability of the anisotropically scattered neutron having an escape direction is ($\frac{1}{2} + \alpha$). See Fig. 4.2.

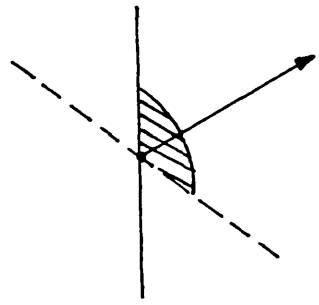


Fig. 4.2 Angular Distribution of Forward Scattered Neutrons.

In the present work the angular dependence of the scattering cross section is expanded in series of Legendre polynomials, viz.,

$$\sigma_s(x,\mu_0) = \sum_{l=0}^{\infty} \left(\frac{2l+1}{4\pi}\right) \sigma_{sl}(x)\, P_l(\mu_0) \qquad (4.1\text{-}1)$$

$\mu_0 = \mu.\mu'$ is the cosine of angle between incident and scattered neutrons in the laboratory system.
The $l=0$ term represents isotropic scattering since then $\sigma_s(x,\mu_0)$ is independent of μ_0. The $l=1$ term represents

linear anisotropic scattering, and so on for $l \geq 2$. A large number of terms are required in the expansion of $\sigma_s(x,\mu_0)$ if anisotropy of scattering is severe. In many practical calculations of reactor physics, the first three terms in the expansion are adequate.

In this Chapter the treatment of multigroup anisotropic scattering in one dimensional slab geometry is presented in detail and several test problems with severe anisotropic scattering are analysed. In the case of one dimensional slab geometry, as shown below in Fig. 4.3, the even parity equation becomes

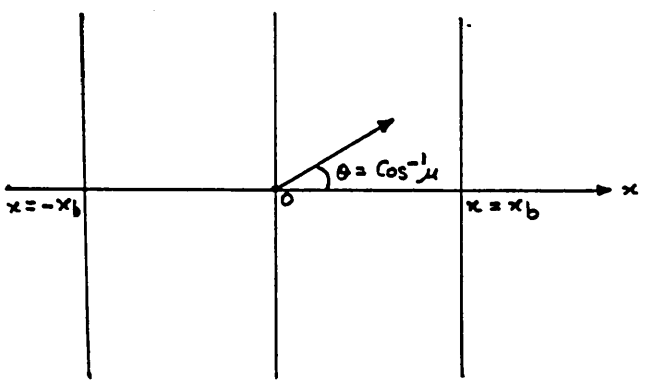


Fig. 4.3 One Dimensional Slab Geometry.

$$\mu \frac{d}{dx}\left\{ \Sigma_s (s^-(x,\mu) - \mu \frac{d\phi_0^+(x,\mu)}{dx} \right\} + C\,\phi_0^+(x,\mu) = S^+(x,\mu) \qquad (4.1\text{-}2)$$

with the bare surface boundary condition

$$\begin{aligned} \phi_0(x_b,\mu) &= 0 \quad \text{for} \quad -1 \leq \mu < 0 \\ \phi_0(-x_b,\mu) &= 0 \quad \text{for} \quad 0 < \mu \leq 1 \end{aligned} \qquad (4.1\text{-}3)$$

At a perfect reflector at x_r , we have

$$\phi_0(x_r, \mu) = \phi_0(x_r, -\mu) . \qquad (4.1\text{-}4)$$

4.2 The $K^+(\phi^+)$ Functional

The even parity form of the neutron transport equation lends itself to a variational treatment since it is a second order elliptic equation. Ackroyd [2] has obtained boundary free maximum and minimum principles for $\phi_0^+(x,\mu)$ using the Cauchy-Schwarz inequality, and the fact that the bilinear functional $F^+(\phi^+, \phi_0^+)$ is independent of ϕ_0^+ . The maximum principle is

$$K^+(\phi^+) \leq N(\phi^+) \leq F(\phi_0^+, \phi_0^+) \qquad (4.2\text{-}1)$$

where F is the functional associated with ϕ_0^+ . $N(\phi^+)$ is a more complicated functional than $K^+(\phi^+)$ and so the latter is used for computational purposes. For a derivation of the maximum principle and an explicit expression for $N(\phi^+)$, see Ackroyd [2]. For a function $\phi^+(x,\mu)$ to be admissible in the K^+ principle it has to satisfy the following conditions:

(i) be continuous and piecewise differentiable in x.

(ii) be continuous in μ except at interfaces in the direction $\mu = 0$.

(iii) satisfy the perfect reflector boundary condition at $x = x_r$, i.e. $\phi^+(x_r, \mu) = \phi^+(x_r, -\mu)$.

An explicit expression for $K^+(\phi^+)$ is

$$K^+(\phi^+) = \int_V \{ 2\langle \phi^+, s^+\rangle + 2\langle \underline{\Omega}\cdot\nabla\phi^+, \varsigma s^-\rangle - \langle \underline{\Omega}\cdot\nabla\phi^+, \varsigma(\underline{\Omega}\cdot\nabla\phi^+)\rangle - \langle \phi^+, C\phi^+\rangle \} dV$$
$$+2\int_{S_s}\int_{\underline{\Omega}\cdot\underline{n}<0} \{\phi^+(\underline{r},\underline{\Omega}) + \phi^+(\underline{r},-\underline{\Omega})\} |\underline{\Omega}\cdot\underline{n}| T\, d\underline{\Omega}\, d\underline{S} \qquad (4.2\text{-}2)$$
$$-\int_{S_b \cup S_s}\int_{\Omega} (\phi^+)^2 |\underline{\Omega}\cdot\underline{n}|\, d\Omega\, d\underline{S}$$

where $\phi^+(\underline{r},\underline{\Omega})$ is the approximate even parity flux, T is an inward surface source at a bare surface S_b. In the case of one dimensional slab geometry with no surface sources $K^+(\phi^+)$ becomes

$$K^+(\phi^+) = \int_x \{ 2\langle \phi^+, s^+\rangle + 2\langle \mu\frac{d\phi^+}{dx}, \varsigma s^-\rangle - \langle \mu\frac{d\phi^+}{dx}, \varsigma(\mu\frac{d\phi^+}{dx})\rangle$$
$$- \langle \phi^+, C\phi^+\rangle \} dx - \int_{S_b}\int_{\mu} (\phi^+)^2 \mu\, d\mu\, dx \qquad (4.2\text{-}3)$$

The inner product $\langle u,v\rangle$ is defined as

$$\langle u,v\rangle \equiv \int_{\Omega} u(\underline{r},\underline{\Omega})\, v(\underline{r},\underline{\Omega})\, d\Omega \qquad (4.2\text{-}4)$$

The positive definite and self adjoint properties of G,C with their inverses are fundamental for the construction of maximum and minimum principles, Ackroyd [2,3].

4.3 The Reduced Functional

The first step in the procedure for obtaining a solution is to integrate the $K^+(\phi^+)$ functional over μ and then over x for the finite elements. The contribution from an element is conveniently obtained by carrying out the integration using local co-ordinates for the element. In this section the integration over μ is discussed and in Section 4.5 is shown the integration over the finite elements. $K^+(\phi^+)$ may be written as

$$K^+(\phi^+) = \int_x \int_{-1}^{1} \Big\{ -\frac{1}{\sigma_T}\left(\mu \frac{d\phi^+}{dx}\right)^2 - \sigma_T (\phi^+)^2 + \frac{S_0^+}{2\pi}\phi^+ + \phi^+ \sum_{\substack{l=0 \\ \text{even}}}^{\infty} \left(\frac{2l+1}{4\pi}\right) \int_0^{2\pi}\int_{-1}^{1} \sigma_{sl}^+ P_l(\mu_0)\, \phi^+(x,\mu')\, d\mu' d\omega' - \frac{d\phi^+}{dx} \sum_{\substack{l=1 \\ \text{odd}}}^{\infty} \left(\frac{2l+1}{4\pi}\right) \int_0^{2\pi}\int_{-1}^{1} \frac{\sigma_{sl}}{\sigma_T(\sigma_T - \beta_{sl})} P_l(\mu_0)\, \mu' \frac{d\phi^+(x,\mu')}{dx}\, d\mu' d\omega' \Big\} dx$$

$$- \int_{-1}^{1} |\mu| \left[l_i\, \phi^+(x,\mu) \right]^2 d\mu \qquad (4.3\text{-}1)$$

where $l_i = 0 \Rightarrow$ reflective boundary condition

and $l_i = 1 \Rightarrow$ bare surface boundary condition.

In (4.3-1) it has been assumed that the extraneous source $S(x,\mu)$ is isotropic, hence $S^-(x,\mu) = 0$. The above functional applies to the one group case. The angular integrals are as follows:

$$I_1(x) = -\frac{1}{\sigma_T} \left\langle \mu \frac{d\phi^+}{dx}, \mu \frac{d\phi^+}{dx} \right\rangle \qquad (4.3\text{-}2)$$

$$I_2(x) = -\sigma_T \langle \phi^+, \phi^+ \rangle \tag{4.3-3}$$

$$I_3(x) = 2\langle \phi^+, s^+ \rangle \tag{4.3-4}$$

$$I_4(x) = \langle \phi^+, \langle \sigma_s^+, \phi^+ \rangle \rangle \tag{4.3-5}$$

$$I_5(x) = -\left\langle \mu \frac{d\phi^+}{dx}, \left\langle g, \mu \frac{d\phi^+}{dx} \right\rangle \right\rangle \tag{4.3-6}$$

and a bare surface boundary term integral I_{BT}.

The reduced functional, i.e. the functional obtained after angular integration, is then

$$K_R^+(\phi^+) = \int_x (I_1 + I_2 + I_3 + I_4 + I_5)\, dx + I_{BT}.$$

The trial function is expanded in a Legendre series

$$\phi^+(x,\mu) = \sum_{\substack{l=0 \\ \text{even}}}^{\infty} \left(\frac{2l+1}{4\pi} \right) \phi_l^+(x)\, P_l(\mu) \tag{4.3-7}$$

and the kernels $\sigma_s^+(x,\mu_0)$ and $g(x,\mu_0)$ have the expansions given in (2.2-12) and (2.2-11) respectively. In (4.3-7) $\phi_l^+(x)$ are referred to as the even moments of the expansion for the even parity angular flux. The integrals I_1 to I_5 are readily evaluated using the recurrence relations for the Legendre polynomials,

$$\mu P_l(\mu) = \frac{1}{(2l+1)} \left[(l+1) P_{l+1}(\mu) + l P_{l-1}(\mu) \right] \tag{4.3-8}$$

using the addition theorem for spherical harmonics

$$P_l(\mu_0) = P_l(\mu) P_l(\mu') + 2 \sum_{m=1}^{l} \frac{(l-m)!}{(l+m)!} P_l^m(\mu) P_l^m(\mu') \cos m(\omega - \omega') \tag{4.3-9}$$

and the orthonormality property of the Legendre polynomials,

$$\int_{-1}^{1} P_l(\mu)\, P_{l'}(\mu)\, d\mu = \frac{2\delta_{ll'}}{2l+1} \tag{4.3-10}$$

Results of the angular integration are:

$$\begin{aligned} I_1(x) = \frac{-1}{8\pi^2 \sigma_T} \sum_{n=0}^{\infty} \Bigg\{ & \left[\frac{(2n+1)^2}{(4n+3)} + \frac{4n^2}{(4n-1)} \right] \left(\frac{d\phi^+_{2n}}{dx} \right)^2 \\ & + \left[\frac{(2n+1)(2n+2)}{(4n+3)} \right] \frac{d\phi^+_{2n+2}}{dx} \frac{d\phi^+_{2n}}{dx} \\ & + \left[\frac{2n(2n-1)}{(4n-1)} \right] \frac{d\phi^+_{2n-2}}{dx} \frac{d\phi^+_{2n}}{dx} \end{aligned} \tag{4.3-11}$$

with $\frac{d\phi^+_n}{dx} = 0$ for $n < 0$ and $\phi^+_n \equiv \phi^+_n(x)$.

$$I_2(x) = \frac{-\sigma_T}{8\pi^2} \sum_{n=0}^{\infty} (4n+1) \left(\phi^+_{2n} \right)^2 \tag{4.3-12}$$

$$I_3(x) = \frac{S_0^+ \phi_0^+}{4\pi^2} \tag{4.3-13}$$

$$I_4(x) = \frac{1}{8\pi^2} \sum_{n=0}^{\infty} (4n+1) \varpi^+_{2n} \left[\phi^+_{2n} \right]^2 \tag{4.3-14}$$

$$I_5(x) = \sum_{n=0}^{\infty} \frac{\Delta_S (2n+1)}{8\pi^2 (4n+3)} \left[(2n+1) \frac{d\phi^+_{2n}}{dx} + (2n+2) \frac{d\phi^+_{2n+2}}{dx} \right]^2 \tag{4.3-15}$$

where $\Lambda_{s(2n+1)} = \dfrac{\sigma_{s(2n+1)}}{\sigma_T\,(\sigma_T - \sigma_{s(2n+1)})}$

The boundary term is

$$I_{BT} = \int_0^1 \mu\, I_i \Big[\sum_{m=0}^{\infty} \sum_{n=0}^{\infty} a_{2n} P_{2n}(\mu)\, \phi^+_{2n}(x)\, a_{2m} P_{2m}(\mu)\, \phi^+_{2m}(x) \Big]\, d\mu \qquad (4.3\text{-}16)$$

where $a_{2n} = (4n+1)/4\pi$

I_{BT} can be evaluated using the recurrence relation (4.3-8) and the result below [4,5] for Legendre polynomials.

$$\int_0^1 P_\gamma(\mu) P_\lambda(\mu)\, d\mu = (-1)^{\frac{1}{2}(\gamma+\lambda+1)} \left[\frac{\gamma!\,\lambda!}{2^{\gamma+\lambda-1}(\gamma-\lambda)(\gamma+\lambda+1)\left[(\gamma/2)!\right]^2\left[\left((\lambda-1)/2\right)!\right]^2} \right] \qquad (4.3\text{-}17)$$

The boundary term then becomes

$$I_{BT} = -\frac{I_i}{8\pi^2} \sum_{n=0}^{\infty} \phi^+_{2n}(a_i)(4n+1) \sum_{m=0}^{\infty} \phi^+_{2m}(a_i) \left[(2m+1) I_{2n,2m+1} + 2m\, I'_{2n,2m-1} \right] \qquad (4.3\text{-}18)$$

where $i = 0, 1$ and

$$I_{2n,2m+1} = \int_0^1 P_{2n} P_{2m+1}\, d\mu = \left[\frac{(-1)^{n+m+1}(2n)!\,(2m+1)!}{2^{2(n+m)+1}(2n-2m-1)(n+m+1)\,(m!)^2(n!)^2} \right] \qquad (4.3\text{-}19)$$

and

$$I'_{2n,2m-1} = \int_0^1 P_{2n} P_{2m-1}\, d\mu = \left[\frac{(-1)^{(n+m)}(2n)!\,(2m-1)!}{2^{2(n+m)-1}(n+m)(2n-2m+1)(n!)^2\left[(m-1)!\right]^2} \right] \qquad (4.3\text{-}20)$$

In practice the Legendre series expansions for $\sigma_s(x,\mu_0)$ and $\phi^+(x,\mu)$ are truncated after a finite number of terms.

In particular

$$\phi^{+}(x,\mu) = \sum_{l=0}^{M-1} \left(\frac{4l+1}{4\pi}\right) \phi_{2l}^{+}(x) \; P_{2l}(\mu) \tag{4.3-21}$$

where M is the number of even moments included in the expansion.

The fission source term for eigenvalue problems leads to an integral

$$I_6(x) = \frac{\nu\sigma_f}{8\pi^2}\int_{-1}^{1} \phi_0^{+}(x) P_0(\mu)\, d\mu$$

i.e.

$$\frac{\nu\sigma_f \, \phi_0^{+}(x)}{4\pi^2} \; . \tag{4.3-22}$$

4.4 Finite Element Approximation

Consider a boundary value problem of the form

$$L\phi_o = f\phi_o \qquad \phi_o \in V \qquad (4.4\text{-}1)$$

and

$$M\phi_o = g\phi_o \qquad \phi_o \in \partial V \qquad (4.4\text{-}2)$$

with ϕ_o, the unknown function belonging to the space H of admissible functions. Then the Galerkin approximation is obtained by considering the problem in a finite dimensional subspace H^h of H. In Eqns. (4.4-1) and (4.4-2) L is a linear differential operator, M is a boundary operator, f and g are given data. V is the domain under consideration with boundary ∂V. The parameter h decreases as the dimension of the subspace increases. The Galerkin approximation [6,7] to ϕ_o is

$$\phi_h(x) = \sum_{j=0}^{N} \alpha_j \chi_j(x) \qquad (4.4\text{-}3)$$

where N is the dimension of H^h. The α_j are unknown coefficients and χ_j are linearly independent basis functions spanning H^h. Although the Galerkin method provides an approximation to the solution, it does not specify how to construct H^h, i.e. the basis functions $\chi_j(x)$. The finite element method provides a general and systematic technique for constructing the basis functions χ_j.

The main idea is that the basis functions X_j can be defined piecewise over subregions of the domain, called finite elements, and that over the subregion the X_j can be chosen to be simple functions, such as polynomials of low degree. To construct the basis functions, replace the domain V by a collection V_h of simpler domains V_e, the finite elements, such that

$$V_h \approx V \qquad \text{and} \qquad \overline{V}_h = \bigcup_{e=1}^{N} \overline{V}_e \ .$$

Here $\overline{V}_e$ is the element V_e together with its boundary. N is the total number of elements in the domain. In one dimension consider a closed interval [a,b] divided into N elements with $a = x_0 < x_1 < x_2 \cdots < x_N = b$, then $\overline{V}_e = [x_{i-1}, x_i]$. The basis functions X_j are now chosen to be piecewise polynomials. Over each element $\overline{V}_e$, local shape functions ψ_i^e, $i=1,2,3,\ldots,N_e$ are constructed. The approximation solution $\phi_h^e(x)$ over element $\overline{V}_e$ is then

$$\phi_h^e(x) = \sum_{j=1}^{N_e} \alpha_j^e \psi_j^e(x) \qquad (4.4\text{-}4)$$

N_e is the number of degrees of freedom for the element. In the case of the simplest elements, linear Lagrange elements, $N_e = 2$. Local shape functions have the property that

$$\psi_{ij}^e(x_j^e) = \delta_{ij} \qquad (4.4\text{-}5)$$

i.e. shape functions have value 0 or 1 at nodal points within each element. The basis functions of adjacent elements, constructed using local shape functions, are related through nodal parameters. The global basis functions are obtained by patching together the local shape functions.

The problem stated in (4.4-1) and (4.4-2) may also be considered as one of minimisation of a functional. See for instance, Carey and Oden [6]. In this case the finite element approximation is a simple variant of the classical Rayleigh-Ritz method. The functional K^+ over a finite element mesh can be written as

$$K^+(\phi_h) = \sum_{e=1}^{N} K_e^+(\phi_h^e) \qquad (4.4\text{-}6)$$

i.e. the functional over the whole finite element domain is simply the sum of functionals for each element. This means that we need only consider the element functional and the contiguous element when deriving angular and spatial matrices. Write

$$\phi_h^e(x) = \sum_{j=1}^{N_e} \bar{\phi}_j^e \, \psi_j^e(x)$$

where $\bar{\phi}_j^e = \bar{\phi}_j^e(x_j)$ are nodal values and $x_j \in \bar{V}_e$. The set $\{x_j\}_{j=1}^{N_e}$ are the nodes in element $\bar{V}_e$. $\psi_j^e(x)$ are of course the shape functions. Inserting $\phi_h^e(x)$ into K_e^+ and applying the condition that K_e^+ be stationary with respect to nodal parameters,

$$\frac{\partial K_e^+}{\partial \bar{\phi}_j^e} = 0 \qquad j = 1, 2, 3, \ldots, N_e \qquad (4.4\text{-}7)$$

leads to a system of linear algebraic equations for element $\bar{V}_e$.

$$\sum_{j=1}^{N_e} K_{ij}^{e+} \bar{\phi}_j^e = S_i^e \qquad i = 1, 2, 3, \ldots, N_e. \qquad (4.4\text{-}8)$$

K_{ij}^{e+} are entries in the element stiffness matrix and S_i^e are entries in the element load vector. $\bar{\phi}_j^e$ is a nodal vector for the unknowns.

For example, consider $N_e = 2$. We then have

$$\begin{bmatrix} K_{e11}^+ & K_{e12}^+ \\ K_{e21}^+ & K_{e22}^+ \end{bmatrix} \begin{bmatrix} \bar{\phi}_1^e \\ \bar{\phi}_2^e \end{bmatrix} = \begin{bmatrix} S_1^e \\ S_2^e \end{bmatrix} \qquad (4.4\text{-}9)$$

The final system of equations is obtained by summing the contributions for each element, viz.,

$$\sum_{e=1}^{N} K_{lk}^{e+} = K_{lk}^+ \qquad (4.4\text{-}10)$$

$$\sum_{e=1}^{N} S_l^e = S_l \qquad (4.4\text{-}11)$$

where l, k refer to a global numbering scheme. Then the following matrix equation is obtained

$$K^{+}\underline{\phi} = \underline{S} \qquad (4.4\text{-}12)$$

K^{+} is the global stiffness matrix and $\underline{S}$ the load vector. In general the global stiffness matrix is banded due to the coupling of the finite elements. In the present neutron transport finite element work the trial function is

$$\phi^{+e}(x,\mu) = \sum_{l=0}^{\infty} \left(\frac{4l+1}{4\pi}\right) \phi_{2l}^{+e}(x) P_{2l}(\mu)$$

where of course ϕ_{2l}^{+e} are the even spatial moments and are the nodal values in the finite element approximation. In the case of linear finite element approximation the number of degrees of freedom of the number of unknowns is equal to the number of even moments computed.

4.4.1 Choice of Elements

On the work reported here on anisotropic scattering in one dimensional slab geometry only linear Lagrange elements have been used. The Lagrange C^0 elements are the most common class of elements. They are based on Lagrange interpolation [6,7,8]. With these elements only continuity of the interpolant across interelement boundaries is required. The simplest case is one of piecewise linear interpolation locally on each element $\bar{V}e$. Then the flux moments have the following expansion

$$\phi_k^e(x) = \bar{\phi}_1^e \psi_1^e(x) + \bar{\phi}_2^e \psi_2^e(x) \qquad (4.4\text{-}13)$$

where ψ_1^e and ψ_2^e are termed local shape functions.

$$\psi_1^e = (1 - x/h_e)$$
$$\psi_2^e = x/h_e \qquad (4.4\text{-}14)$$

h_e being the length of element $\bar{V}e$.
The shape functions for a linear element are illustrated below in Fig 4.4. They have the property that

$$\psi_1^e(x_{i-1}) = 1 \;, \quad \psi_1^e(x_i) = 0$$
$$\psi_2^e(x_{i-1}) = 0 \;, \quad \psi_2^e(x_i) = 1. \qquad (4.4\text{-}15)$$

Global basis functions are constructed from the shape functions on elements adjacent to node j as shown below in Fig. 4.4.

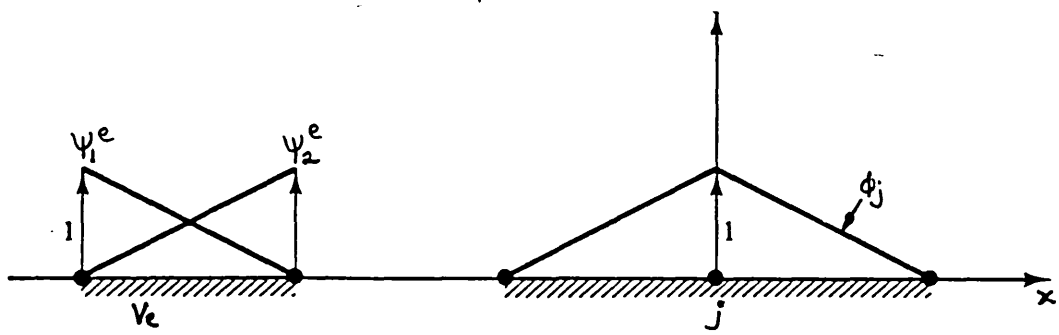


Fig. 4.4 Local and global basis functions for a linear Lagrange element

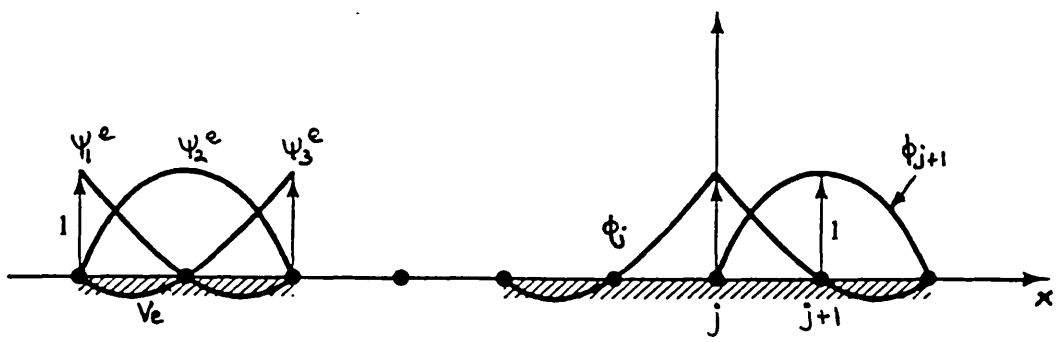


Fig. 4.5 Local and global basis functions for a quadratic Lagrange element

Globally, the piecewise linear interpolant has the form

$$\phi_h(x) = \sum_{j=0}^{N} \bar{\phi}_j \chi_j(x) \qquad (4.4\text{-}16)$$

where N is the number of linear elements.

The next type of Lagrange elements have piecewise quadratic interpolation on element $\bar{V}_e$. In this case

$$\phi_h^e(x) = \bar{\phi}_1^e \psi_1^e(x) + \bar{\phi}_2^e \psi_2^e(x) + \bar{\phi}_3^e \psi_3^e(x)$$

with $\psi_i^e(x_j) = \delta_{ij}$ at node j.

The shape functions on element $\bar{V}_e$ are

$$\psi_1^e(x) = \frac{2}{h^2}\left(x - h/2\right)\left(x - h\right)$$

$$\psi_2^e(x) = -\frac{4x}{h^2}\left(x - h\right) \qquad (4.4\text{-}17)$$

$$\psi_3^e(x) = \frac{2x}{h^2}\left(x - h/2\right)$$

Both the shape functions and basis functions for quadratic interpolation are shown in Fig. 4.5. In general, using a k^{th} degree polynomial interpolation, the piecewise interpolant ϕ_h^e over element $\bar{V}_e$ is

$$\phi_h^e(x) = \sum_{i=1}^{k+1} \psi_i^e(x) \bar{\phi}_i^e \qquad (4.4\text{-}18)$$

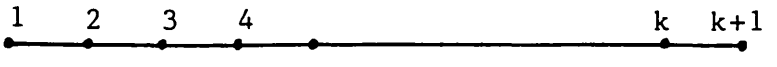


Fig. 4.6. k+1 Nodes on Element $\bar{V}_e$

where

$$\psi_i^e(x) = \prod_{\substack{j=1 \\ (j\neq i)}}^{k+1} \frac{(x-x_j)}{(x_i-x_j)} = L_i(x) \qquad (4.4\text{-}19)$$

the Lagrange interpolation polynomials. The degree of an element is the degree of complete polynomial defining an approximation on an element.

The other type of elements are the Hermite class of elements. These are used in fourth order problems where the variational functional involves second derivatives of the trial functions. Hence the second derivative trial function must be square integrable over an element $\overline{V}_e$. The finite element trial function, i.e. the basis functions, must have continuous first derivatives at interface nodes. The function and its derivatives of various orders are interpolated in Hermite elements. There are then two unknowns per each node of the element. Hence, the finite element trial function on $\overline{V}_e$ takes the form

$$\phi_h^e(x) = \sum_{i=1}^{k+1} \bar{\phi}_i^e \hat{\psi}_{oi}^e(x) + \sum_{i=1}^{k+1} \bar{\phi}_i^{e\prime} \hat{\psi}_{1i}^e(x) \qquad (4.4\text{-}20)$$

where $\hat{\psi}_{oi}^e$ and $\hat{\psi}_{1i}^e$ are the shape functions on $\overline{V}_e$ and $\bar{\phi}_i^e$ are the nodal values of the function being approximated, and $\bar{\phi}_i^{e\prime}$ the nodal values of the derivative. The element has $k+1$ nodes. The shape functions $\hat{\psi}_{oi}^e$ and $\hat{\psi}_{1i}^e$ satisfy the following relations:

$$\hat{\psi}_{oi}^e(x_j) = \begin{cases} 1 & i=j \\ 0 & i\neq j \end{cases} \qquad \hat{\psi}_{1i}^e(x_j) = 0 .$$

and $\hat{\psi}^e_{oi}(x_j) = 0$ $\qquad$ $\hat{\psi}^e_{1i}(x_j) = \begin{matrix} 1 & i=j \\ 0 & i\neq j \end{matrix}$. (4.4-21)

These conditions are satisfied by the Hermite polynomials [6,7,8]. Hence,

$$\hat{\psi}^e_{oi}(x) = \prod_{\substack{j=1 \\ (j\neq i)}}^{k+1} \frac{(x-x_j)^2}{(x_i-x_j)^2}\left[1 + 2\sum_{\substack{j=1 \\ (j\neq i)}}^{k+1} \frac{(x_i-x)}{(x_i-x_j)}\right] \tag{4.4-22}$$

and $$\hat{\psi}^e_{1i}(x) = \prod_{\substack{j=1 \\ (j\neq i)}}^{k+1} \frac{(x-x_j)^2}{(x_i-x_j)}(x-x_i)$$

In the case of an element with two nodes (k=1) and length h_e, the shape functions are as follows:

$$\hat{\psi}^e_{o1}(x) = \left(1+\frac{2x}{h_e}\right)\left(1-\frac{x}{h_e}\right)^2$$

$$\hat{\psi}^e_{o2}(x) = \frac{x^2}{h_e^2}\left(3-\frac{x}{h_e}\right)$$

$$\hat{\psi}^e_{11}(x) = x\left(1-\frac{x}{h_e}\right)^2$$

$$\hat{\psi}^e_{12}(x) = \frac{x^2}{h_e}\left(1-\frac{x}{h_e}\right) \tag{4.4-23}$$

Apart from the fact that with Hermite elements, there are two unknowns per node, the rest of the finite element calculation proceeds in the same way as for Lagrange C^o elements.

4.5 Derivation of Angular Matrices

Matrices for the angular constants of the reduced functional $K_R^+(\phi^+)$ can be obtained by substituting the finite element basis functions in $I_1(x), I_2(x), \ldots, I_5(x)$, performing the spatial integration and maximising the reduced functional with respect to nodal parameters. This process is illustrated below, using linear Lagrange elements. The ideas are essentially the same for higher order one dimensional elements and for higher dimensions. For two dimensions, e.g. x-y geometry, analytical derivation may be difficult. We choose the piecewise linear basis functions.

$$\phi_{2n}(x) = \left(1-\frac{x}{h}\right)\bar{\phi}_{2n+1} + \frac{x}{h}\bar{\phi}_{2n+2} \qquad (4.5\text{-}1)$$

for a typical element shown below in Fig 4.7. The superscript + on $\phi^+(x)$ has been dropped for convenience. $h = h_e$ is the length of element $\bar{V}_e$. The local node numbering is as shown in Fig 4.7.

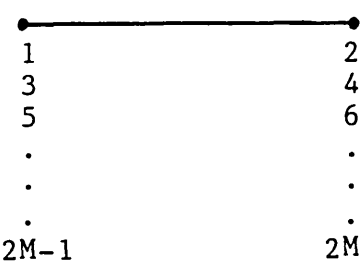


Fig. 4.7 Local Node Numbering for M Moments for a Linear Element

$\bar{\phi}_i$ are the nodal values of the flux expansion coefficients, $\phi(x)$. So for example, n=o gives the first even moment coefficient, n=1 the second, and so on. The number of unknowns per node increases directly as the number of moments for the flux increases, for Lagrangian elements in one dimension.

We start the angular constants matrix derivation by looking at the I_1 term. This can be written as

$$I_1(x) = \sum_{n=0}^{M-1} \left[\alpha_{2n} (\phi'_{2n})^2 + \beta_{2n} \phi'_{2n+2} \phi'_{2n} + \gamma_{2n} \phi'_{2n-2} \phi_{2n}\right] \quad (4.5\text{-}2)$$

where

$$\begin{aligned} \alpha_{2n} &= \frac{-1}{8\pi^2 \sigma_T} \left[\frac{(2n+1)^2}{(4n+3)} + \frac{4n^2}{(4n-1)} \right] \\ \beta_{2n} &= \frac{-1}{8\pi^2 \sigma_T} \left[\frac{(2n+1)(2n+2)}{(4n+3)} \right] \\ \gamma_{2n} &= \frac{-1}{8\pi^2 \sigma_T} \left[\frac{2n(2n-1)}{(4n-1)} \right] \end{aligned} \quad (4.5\text{-}3)$$

and

$$\phi'_i \equiv \frac{d\phi_i(x)}{dx} .$$

Substituting for ϕ'_{2n}, ϕ'_{2n+2}, ϕ'_{2n-2} into (4.5-2) gives

$$I_1(x) = \sum_{n=0}^{M-1} \frac{\alpha_{2n}}{h^2} \left[-\bar{\phi}_{2n+1} + \bar{\phi}_{2n+2} \right]^2 + \frac{\beta_{2n}}{h^2} \left[-\bar{\phi}_{2n+3} + \bar{\phi}_{2n+4} \right] \times \left[-\bar{\phi}_{2n+1} + \bar{\phi}_{2n+2} \right] + \frac{\gamma_{2n}}{h^2} \left[-\bar{\phi}_{2n-1} + \bar{\phi}_{2n} \right] \left[-\bar{\phi}_{2n+1} + \bar{\phi}_{2n+2} \right]$$

and the first term in the reduced functional

$$K_{1R}^{+}(\phi^{+}) = \int_{0}^{h} I_1(x)\,dx$$

becomes

$$K_{1R}^{+}(\phi^{+}) = \sum_{n=0}^{M-1} \frac{\alpha_{2n}}{h}\left[\bar{\phi}_{2n+1}^{2} - 2\bar{\phi}_{2n+1}\bar{\phi}_{2n+2} + \bar{\phi}_{2n+2}^{2}\right]$$
$$+ \frac{\beta_{2n}}{h}\left[\bar{\phi}_{2n+3}\bar{\phi}_{2n+1} - \bar{\phi}_{2n+3}\bar{\phi}_{2n+2} - \bar{\phi}_{2n+4}\bar{\phi}_{2n+1} + \bar{\phi}_{2n+4}\bar{\phi}_{2n+2}\right] \quad (4.5\text{-}4)$$
$$+ \frac{\gamma_{2n}}{h}\left[\bar{\phi}_{2n-1}\bar{\phi}_{2n+1} - \bar{\phi}_{2n-1}\bar{\phi}_{2n+2} - \bar{\phi}_{2n}\bar{\phi}_{2n+1} + \bar{\phi}_{2n}\bar{\phi}_{2n+2}\right].$$

For two even moments expansion of the angular flux

$$K_{1R}^{+}(\phi^{+}) = \frac{\alpha_0}{h}\left[\bar{\phi}_1^{2} - 2\bar{\phi}_1\bar{\phi}_2 + \bar{\phi}_2^{2}\right] + \frac{\beta_0}{h}\left[\bar{\phi}_3\bar{\phi}_1 - \bar{\phi}_3\bar{\phi}_2 - \bar{\phi}_4\bar{\phi}_1 + \bar{\phi}_4\bar{\phi}_2\right]$$
$$+ \frac{\alpha_2}{h}\left[\bar{\phi}_3^{2} - 2\bar{\phi}_3\bar{\phi}_4 + \bar{\phi}_4^{2}\right] + \frac{\gamma_2}{h}\left[\bar{\phi}_1\bar{\phi}_3 - \bar{\phi}_1\bar{\phi}_4 - \bar{\phi}_2\bar{\phi}_3 + \bar{\phi}_2\bar{\phi}_4\right] \quad (4.5\text{-}5)$$

Differentiating $K_{1R}^{+}(\phi^{+})$ with respect to $\bar{\phi}_1, \bar{\phi}_2, \bar{\phi}_3, \bar{\phi}_4$ gives

$$\frac{\partial K_{1R}^{+}}{\partial \bar{\phi}_1} = \frac{2\alpha_0}{h}\bar{\phi}_1 - \frac{2\alpha_0}{h}\bar{\phi}_2 + \frac{(\beta_0+\gamma_2)}{h}\bar{\phi}_3 - \frac{(\beta_0+\gamma_2)}{h}\bar{\phi}_4$$

$$\frac{\partial K_{1R}^{+}}{\partial \bar{\phi}_2} = -\frac{2\alpha_0}{h}\bar{\phi}_1 + \frac{2\alpha_0}{h}\bar{\phi}_2 - \frac{(\beta_0+\gamma_2)}{h}\bar{\phi}_3 + \frac{(\beta_0+\gamma_2)}{h}\bar{\phi}_4$$

$$\frac{\partial K_{1R}^{+}}{\partial \bar{\phi}_3} = \frac{(\beta_0+\gamma_2)}{h}\bar{\phi}_1 - \frac{(\beta_0+\gamma_2)}{h}\bar{\phi}_2 \quad \frac{2\alpha_2}{h}\bar{\phi}_3 \quad -\frac{2\alpha_2}{h}\bar{\phi}_4$$

$$\frac{\partial K_{1R}^{+}}{\partial \bar{\phi}_4} = -\frac{(\beta_0+\gamma_2)}{h}\bar{\phi}_1 + \frac{(\beta_0+\gamma_2)}{h}\bar{\phi}_2 - \frac{2\alpha_2}{h}\bar{\phi}_3 + \frac{2\alpha_2}{h}\bar{\phi}_4$$

These equations may also be written in matrix form as

$$\begin{bmatrix} \frac{\partial K_{1R}^{+}}{\partial \bar{\phi}_1} \\ \frac{\partial K_{1R}^{+}}{\partial \bar{\phi}_2} \\ \frac{\partial K_{1R}^{+}}{\partial \bar{\phi}_3} \\ \frac{\partial K_{1R}^{+}}{\partial \bar{\phi}_4} \end{bmatrix} = \begin{bmatrix} \frac{2\alpha_0}{h}\begin{bmatrix} 1 & -1 \\ -1 & 1 \end{bmatrix} & \frac{(\beta_0+\gamma_2)}{h}\begin{bmatrix} 1 & -1 \\ -1 & 1 \end{bmatrix} \\ \frac{(\beta_0+\gamma_2)}{h}\begin{bmatrix} 1 & -1 \\ -1 & 1 \end{bmatrix} & \frac{2\alpha_2}{h}\begin{bmatrix} 1 & -1 \\ -1 & 1 \end{bmatrix} \end{bmatrix} \begin{bmatrix} \bar{\phi}_1 \\ \bar{\phi}_2 \\ \bar{\phi}_3 \\ \bar{\phi}_4 \end{bmatrix} \tag{4.5-6}$$

By defining the finite element local matrix for the leakage term as $\frac{2}{h}\begin{bmatrix} 1 & -1 \\ -1 & 1 \end{bmatrix}$, we obtain the angular matrix as

$$\begin{bmatrix} \alpha_0 & (\beta_0+\gamma_2)/2 \\ (\beta_0+\gamma_2)/2 & \alpha_2 \end{bmatrix} . \tag{4.5-7}$$

In the case of three moments expansion of $\phi^t(x,\mu)$, the angular constants matrix becomes

$$\begin{bmatrix} \alpha_0 & (\beta_0+\gamma_2)/2 & 0 \\ (\beta_0+\gamma_2)/2 & \alpha_2 & (\beta_2+\gamma_4)/2 \\ 0 & (\beta_2+\gamma_4)/2 & \alpha_4 \end{bmatrix}.$$

(4.5-8)

In general for M moments, the angular matrix is of dimension M x M

$$\begin{bmatrix} \alpha_0 & (\beta_0+\gamma_2)/2 & 0 & 0 & \cdots \\ (\beta_0+\gamma_2)/2 & \alpha_2 & (\beta_2+\gamma_4)/2 & 0 & \cdots \\ 0 & (\beta_2+\gamma_4)/2 & \alpha_4 & & \\ 0 & 0 & \ddots & & \\ \vdots & \vdots & & \ddots & \\ \vdots & \vdots & & & (\beta_{2M}+\gamma_{2M-2})/2 \\ \vdots & \vdots & & (\beta_{2M}+\gamma_{2M-2})/2 & \alpha_{2(M-1)} \end{bmatrix}.$$

(4.5-9)

As we have seen the spatial, finite element part and the angular part has been separated. The angular matrices have to be calculated once only and combined with finite

element matrices to obtain local matrices.

Similar procedure to the one described above can be used to derive the angular constants matrices for other terms in the reduced functional. For $K^{+}_{2R}(\phi^{+})$ the following diagonal angular matrix is obtained

$$\begin{bmatrix} \gamma_0 & & & \\ & \gamma_2 & & 0 \\ & & \gamma_4 & \\ & 0 & & \ddots \\ & & & & \gamma_{2(M-1)} \end{bmatrix} \qquad (4.5\text{-}10)$$

where $\gamma_{2n} = -\frac{\sigma_T (4n+1)}{8\pi^2}$. The finite element local matrix is

$$2h \begin{bmatrix} 1/3 & 1/6 \\ 1/6 & 1/3 \end{bmatrix} \qquad (4.5\text{-}11)$$

$K^{+}_{2R}(\phi^{+})$ represents part of the removal term. Since the extraneous source is isotropic then the $K^{+}_{3R}(\phi^{+})$ or $I_3(x)$ term simply gives $\frac{S_0}{4\pi^2}$ for the angular constant, with a finite element load vector

$$h \begin{bmatrix} \frac{1}{2} \\ \frac{1}{2} \end{bmatrix} .$$

Here S_o is the source strength.

$K_{4R}^{+}(\phi^{+})$ is the other part of the removal term and so the finite element matrix is as given in (4.5-11) whereas the angular matrix is

$$\begin{bmatrix} \sigma'_{s0} & & & & \\ & \sigma'_{s2} & & \mathbf{0} & \\ & & \sigma'_{s4} & & \\ & & & \ddots & \\ & \mathbf{0} & & & \sigma'_{s2(M-1)} \end{bmatrix} \tag{4.5-12}$$

where $\sigma'_{s2n} = \dfrac{(4n+1)\,\sigma_{s2n}}{8\pi^2}$.

In the case of isotropic scattering only, σ'_{s0} term is required from (4.5-12), whereas, say for P_3 anisotropic scattering, both σ'_{s0} and σ'_{s2} are needed.

The next term in the reduced functional is $K_{5R}^{+}(\phi^{+})$, and involves $I_5(x)$. This is the anisotropic scattering leakage term. $I_5(x)$ may be written as

$$I_5(x) = -\sum_{n=0}^{(M-1)} \lambda_{2n+1}\left[\delta_{2n}\,\phi'_{2n} + \epsilon_{2n}\,\phi'_{2n+2}\right]^2 \tag{4.5-13}$$

where $\delta_{2n} = (2n+1)/4\pi$

$\epsilon_{2n} = (2n+2)/4\pi$

and

$$\lambda_{2n+1} = \frac{2\,\Lambda_{s(2n+1)}}{(4n+3)}$$

Here, as in $K_{IR}^{+}(\phi^{+})$, the finite element local matrix is

$$\frac{2}{h}\begin{bmatrix} 1 & -1 \\ -1 & 1 \end{bmatrix}.$$

Now consider the angular matrix. If the scattering is linearly anisotropic, i.e. P_1 scattering, for a one moment expansion of $\phi^{+}(x,\mu)$ the angular constant is $-\lambda_1 \delta_0^2$. For two moments the angular matrix becomes

$$\begin{bmatrix} -\lambda_1 \delta_0^2 & -\lambda_1 \delta_0 \epsilon_0 \\ -\lambda_1 \delta_0 \epsilon_0 & -\lambda_1 \epsilon_0^2 \end{bmatrix}. \qquad (4.5\text{-}14)$$

If now the scattering order is increased to P_3, while keeping a two moment flux expansion, then the bottom right hand corner entry in (4.5-14) becomes $-(\lambda_1 \epsilon_0^2 + \lambda_3 \delta_2^2)$. In general the angular constants matrix for the anisotropic leakage term can be written as

$$\begin{bmatrix} -\lambda_1 \delta_0^2 & -\lambda_1 \delta_0 \epsilon_0 & 0 & 0 & \cdot & \cdot \\ -\lambda_1 \delta_0 \epsilon_0 & -(\lambda_1 \epsilon_0^2 + \lambda_3 \delta_2^2) & -\lambda_3 \delta_2 \epsilon_2 & 0 & \cdot & \cdot \\ 0 & -\lambda_3 \delta_2 \epsilon_2 & -(\lambda_3 \epsilon_2^2 + \lambda_5 \delta_4^2) & & & \\ 0 & 0 & \cdot & & & \\ \cdot & \cdot & \cdot\ \cdot & & & \\ \cdot & \cdot & \cdot & & & \\ \cdot & \cdot & \cdot & & & \\ & & & & \cdot\ -\lambda_{2M-1}\delta_{M-1}\epsilon_{M-1} & \\ & & -\lambda_{2M-3}\delta_{M-1}\epsilon_{M-1} & & \cdot & -(\lambda_{2M+3}\delta_{2M-4}^2 + \lambda_{2M-1}\delta_{2M-2}^2) \end{bmatrix} \qquad (4.5\text{-}15)$$

for M moments.

The final term in the reduced functional is the boundary term (B.T.). This may be written as

$$I_{B.T.} = -2L_i \sum_{n=0}^{M-1} \sum_{k=0}^{M-1} \phi_{2n}(x)\, \phi_{2k}(x)\, a_{2n}\, a_{2k} \left[J_{2n,2k+1} + K_{2n,2k-1} \right] \quad (4.5\text{-}16)$$

where

$$J_{2n,2k+1} = \frac{(2k+1)}{(4k+4)} I_{2n,2k+1}$$

$$K_{2n,2k-1} = \frac{2k}{(4k+1)} I'_{2n,2k-1}$$

and $a_{2n} = (4n+1)/4\pi$.

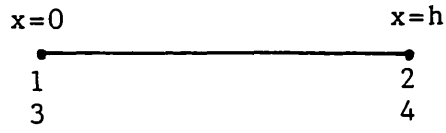
The integrals $I_{2n,2k+1}$ and $I'_{2n,2k-1}$ have been defined in Section 4.3. In one dimensional geometry, the bare surface boundary term will affect only the end nodes on the boundary. Suppose, that the extreme left element begins at $x=0$ and that there is a bare surface here. Then

$$\phi_{2n}(0) = \bar{\phi}_{2n+1}(0)$$

and

$$I_{BT.} = -2L_0 \sum_{n} \sum_{k} \bar{\phi}_{2n+1}\, \bar{\phi}_{2k+1}\, a_{2n}\, a_{2k} \left[J_{2n,2k+1} + K_{2n,2k-1} \right] . \quad (4.5\text{-}17)$$

Consider the case of two moments. Only nodes 1 and 3 will be affected.



$$\therefore I_{BT} = -2L_0 \Big\{ a_0 \bar{\phi}_1 \left[a_0 \bar{\phi}_1 \left(J_{0,1} + K_{0,1} \right) + a_2 \bar{\phi}_3 \left(J_{0,3} + K_{0,1} \right) \right]$$
$$+ a_2 \bar{\phi}_3 \left[a_0 \bar{\phi}_1 \left(J_{2,1} + K_{2,-1} \right) + a_2 \bar{\phi}_3 \left(J_{2,3} + K_{2,1} \right) \right] \Big\}$$

Since $K_{0,-1} = K_{2,-1} = 0$, then

$$\frac{\partial I_{BT}}{\partial \bar{\phi}_1} = -2l_0 \left\{ 2\,(a_0)^2 \bar{\phi}_1 \left(J_{0,1}\right) + a_0 a_2 \left(J_{0,3} + K_{0,1} + J_{2,1}\right) \bar{\phi}_3 \right\}$$

and

$$\frac{\partial I_{BT}}{\partial \bar{\phi}_3} = -2l_0 \left\{ 2\,(a_2)^2 \bar{\phi}_3 \left(J_{2,3} + K_{2,1}\right) + a_0 a_2 \left(J_{0,3} + K_{0,1} + J_{2,1}\right) \bar{\phi}_1 \right\}.$$

Hence the angular matrix is in this case

$$-2l_0 \begin{bmatrix} 2(a_0)^2 \left(J_{0,1}\right) & a_0 a_2 \left(J_{0,3} + K_{0,1} + J_{2,1}\right) \\ a_0 a_2 \left(J_{0,3} + K_{0,1} + J_{2,1}\right) & 2(a_2)^2 \left(J_{2,3} + K_{2,1}\right) \end{bmatrix}. \qquad (4.5\text{-}18)$$

For four moments we have

$$-2l_0 \begin{bmatrix} 2(a_0)^2 J_{0,1} & a_0 a_2 \left(J_{0,3} + K_{0,1} + J_{2,1}\right) & a_0 a_4 \left(J_{0,5} + K_{0,3} + J_{4,1}\right) & a_0 a_6 \left(J_{0,7} + K_{0,5} + J_{6,1}\right) \\ & 2(a_2)^2 \left(J_{2,3} + K_{2,1}\right) & a_2 a_4 \left(J_{2,5} + K_{2,3} + J_{4,3} + K_{4,1}\right) & a_2 a_6 \left(J_{2,3} + K_{2,5} + J_{6,3} + K_{6,1}\right) \\ & & 2(a_4)^2 \left(J_{4,5} + K_{4,3}\right) & a_4 a_6 \left(J_{4,7} + K_{4,5} + J_{6,5} + K_{6,3}\right) \\ & \text{Symmetric} & & 2(a_6)^2 \left(J_{6,7} + K_{6,5}\right) \end{bmatrix}$$

(4.5-19)

In general, for M moments the angular matrix for the boundary term has the following entries

$$a_{ii} = -4l_o (a_{2i})^2 \left(J_{2i,2i+1} + K_{2i,2i-1} \right) \tag{4.5-20}$$

along the diagonal, with $i=1,2,3,\ldots\ldots(M-1)$. The off diagonal terms are

$$a_{ij} = -2l_o\, a_{2i}\, a_{2j} \left[J_{2i,2j+1} + K_{2i,2j-1} + J_{2j,2i+1} + K_{2j,2i-1} \right], \quad i \neq j. \tag{4.5-21}$$

We can compare the two moments case with the angular matrix given by Galliara [9]. He only went up to eight even moments expansion, whereas, the present work is more general and also extends to the multigroup scheme. The following quantities are required for the angular matrix:

$$J_{0,1} = I_{0,1} = 1/2$$

$$J_{0,3} = 3/5\, I_{0,3} = -3/40$$

$$J_{2,1} = I_{2,1} = 1/8$$

$$K_{0,1} = 2/5\, I'_{0,1} = 1/5$$

$$J_{2,3} = 3/5\, I_{2,3} = 3/40$$

$$K_{2,1} = 2/5\, I'_{2,1} = 1/20.$$

Hence

$$\begin{bmatrix} \frac{\partial I_{BT}}{\partial \bar{\phi}_1} \\ \\ \frac{\partial I_{BT}}{\partial \bar{\phi}_3} \end{bmatrix} = \frac{-l_4}{16\pi^2} \begin{bmatrix} 2 & 5/2 \\ \\ 5/2 & 25/2 \end{bmatrix} \begin{bmatrix} \bar{\phi}_1 \\ \\ \bar{\phi}_3 \end{bmatrix} \tag{4.5-22}$$

This is same as the expression obtained by Galliara [9].

Finally, there is the fission source term $\nu\sigma_f \phi_0^+(x)/4\pi$. In this case the finite element local matrix is given by

$$2h \begin{bmatrix} 1/3 & 1/6 \\ 1/6 & 1/3 \end{bmatrix}$$

and the angular term is $\frac{\nu\sigma_f}{k_{eff}\ 8\pi^2}$, where $\frac{1}{k_{eff}}$ constitutes the eigenvalue and keff is the effective multiplication factor.

In actual implementation of the above, each angular matrix is multiplied by each entry in the spatial matrix. This generates the full local matrix which is then inserted into the global matrix to give the relevant contribution from a particular element.

4.6 The Odd Parity Flux

The odd parity flux $\phi^-(x,\mu)$ may be required if the full angular flux $\phi(x,\mu)$ is to be calculated. It is also used implicitly in treating anisotropic down-scatter in the multigroup scheme for the even parity equation. In one group theory, with an isotropic extraneous source

$$\phi_0^-(x,\mu) = -\zeta\left[\mu\frac{d\phi_0^+(x,\mu)}{dx}\right] \qquad (4.6\text{-}1)$$

The above expression becomes approximate when an approximation to $\phi_0^-(x,\mu)$ is introduced. Using the definition of ζ, we have,

$$\phi^-(x,\mu) \approx -\frac{\mu}{\sigma_T}\frac{d\phi^+(x,\mu)}{dx} - 2\pi\int_{-1}^{1}\left\{\mu'\sum_{\substack{l=1\\ \text{odd}}}^{\infty}\left(\frac{2l+1}{4\pi}\right)\Lambda_{sl}P_l(\mu)P_l(\mu')\frac{d\phi^+(x,\mu')}{dx}\right\}d\mu' \qquad (4.6\text{-}2)$$

Using the Legendre series expression for $\phi^+(x,\mu)$, the first term in (4.6-2) becomes

$$-\frac{\mu}{\sigma_T}\left[\sum_{n=0}^{\infty}\left(\frac{4n+1}{4\pi}\right)\frac{d\phi_{2n}^+(x)}{dx}P_{2n}(\mu)\right]$$

while the second term gives

$$-\sum_{n=0}^{\infty}\frac{P_{2n+1}(\mu)\Lambda_{s(2n+1)}}{4\pi}\left[(2n+1)\frac{d\phi_{2n}^+}{dx} + (2n+2)\frac{d\phi_{2n+2}^+}{dx}\right].$$

Hence

$$\phi^-(x,\mu) = \frac{-\mu}{4\pi\sigma_T}\sum_n(4n+1)\frac{d\phi_{2n}^+}{dx}P_{2n}(\mu) - \sum_n P_{2n+1}(\mu)\Lambda_{s(2n+1)}\left[(2n+1)\frac{d\phi_{2n}^+}{dx} + (2n+2)\frac{d\phi_{2n+2}^+}{dx}\right]. \qquad (4.6\text{-}3)$$

Expanding $\phi^-(x,\mu)$ as

$$\phi^-(x,\mu) = \sum_k \left(\frac{4k+3}{4\pi}\right) \phi^-_{2k+1}(x)\, P_{2k+1}(\mu) \qquad (4.6\text{-}4)$$

the coefficients ϕ^-_{2k+1} can be obtained readily using (4.6-3). This gives

$$\phi^-_{2k+1}(x) = \frac{-1}{(4k+3)(\sigma_T - \sigma_{s(2k+1)})}\left[(2k+1)\frac{d\phi^+_{2k}}{dx} + (2k+2)\frac{d\phi^+_{2k+2}}{dx}\right]. \qquad (4.6\text{-}5)$$

Expression of the form on the right hand side of (4.6-5) involving $\frac{d\phi^+_i}{dx}$ will be required in the downscatter sources for the multigroup anisotropic scattering formulation. The coupling between the moments $\phi^-_i(x)$ and $\frac{d\phi^+_i}{dx}$ is illustrated below in Fig 4.8. For example, in a two moment expansion of $\phi^+(x,\mu)$, $\phi^-_1(x)$ couples $\frac{d\phi^+_0}{dx}$ and $\frac{d\phi^+_2}{dx}$ whereas $\phi^-_3(x)$ couples only $\frac{d\phi^+_2}{dx}$

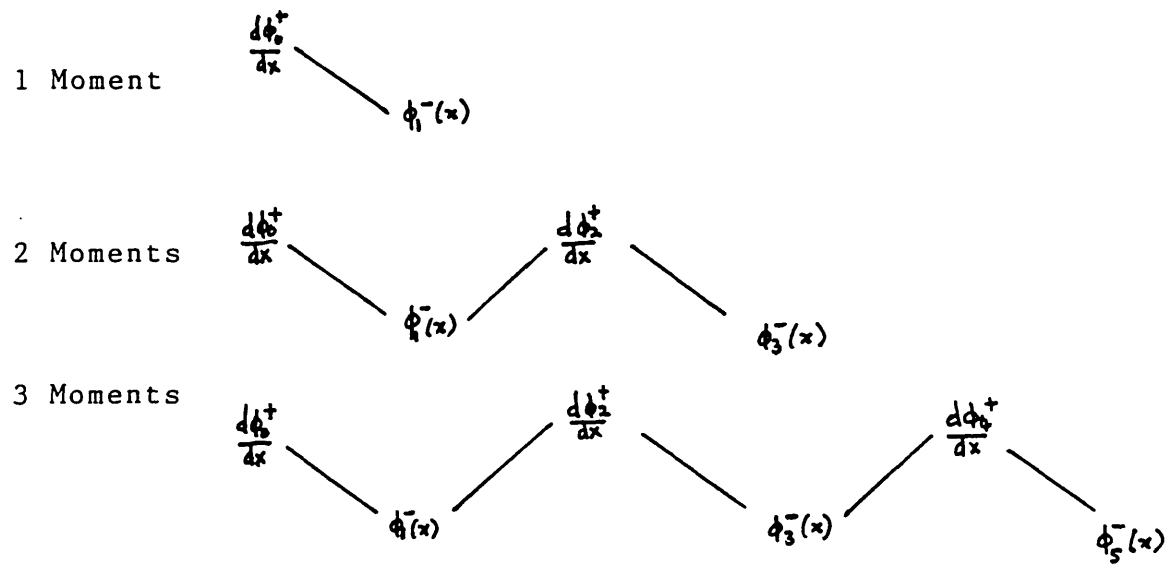


Fig. 4.8 Coupling of $\phi^-_i(x)$ and $\frac{d\phi^+_i}{dx}$

Since

$$\phi_1^-(x) = \phi_1(x) = \frac{-1}{3(\sigma_T - \sigma_{s1})}\left[\frac{d\phi_0^+}{dx} + 2\frac{d\phi_2^+}{dx}\right] \qquad (4.6\text{-}6)$$

and since the net neutron current at position x is

$$J = \int_{-1}^{1} \mu\,\phi(x,\mu)\,d\mu = \phi_1(x)/2\pi ,$$

then J can be calculated from (4.6-6).

In the case of the diffusion approximation

$$J = \frac{-1}{3(\sigma_T - \sigma_{s1})}\left(\frac{d\phi_0^+(x)}{dx}\right). \qquad (4.6\text{-}7)$$

See also Riyait [10].

4.7 The Multigroup Approximation

In order to solve practical problems of reactor physics over a large range of neutron energies, 10 MeV to $0.025 eV$, the energy dependent form of the transport equation is required, where the energy variable, E, is continuous. Solution of such a complex equation is extremely difficult. Hence, the multigroup approximation is introduced. See for instance Bell and Glasstone [11], or Duderstadt and Hamilton [12]. In this approximation the continuous energy range $E_{min} \leq E \leq E_{max}$ is divided into a finite number of intervals (say NG) separated by the energies E_g, where g=0,1,2.....NG. See Fig 4.9 below. E_0 represents the maximum energy E_{max} and E_{NG} the minimum energy with $E_g > E_{g+1}$.

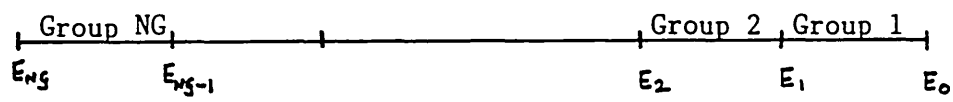


Fig. 4.9 Division of the Continuous Energy Range into NG Groups.

Each energy interval is termed a group and in determining neutron slowing down, the interactions e.g. energy dependent scattering, from group g' to g are required.

In order to include anisotropic scattering, within

the present finite element method, for multigroup problems, the $\int_V \langle \underline{\Omega}.\nabla\phi^+, \mathcal{S}S^- \rangle dV$ term has to be included in the functional, since it is now non-zero. Both even and odd parity downscatter sources have to be considered. It is assumed that there is no upscatter although this can be taken care of quite easily with the formulation given in Section 4.8 . Also it should be noted that in the multigroup case the functional $K^+(\phi^+)$ is approximate.

In solving the multigroup equations, we adopt the following procedure. Solve each group equation assuming the source is known. The source has three terms:

(i) The given extraneous source for that group.

(ii) The source arising from fission within all the groups.

(iii) The sources due to downscatter from higher energy groups.

The two cases considered are (a) Source Problems, (b) Eigenvalue Problems.

4.7.1 The Multigroup Equation

The one dimensional slab geometry version of the transport equation in energy group g may be written as

$$\mu \frac{d\phi_g}{dx} + \sigma_T \phi_g(x,\mu) = \sum_{g'=1}^{NG} \int_{\Omega'} \sigma_{Sg'\to g}(x,\mu\cdot\mu') \phi_{g'}(x,\mu') d\Omega' + Q_g(x,\mu) \qquad (4.7\text{-}1)$$

The overall approximate solution can be obtained by solving a series of one group equations with an effective source term, viz.,

$$\mu \frac{d\phi_g}{dx} + \sigma_{T_g} \phi_g = \int_{\Omega'} \sigma_{s_{gg}}(x,\mu_o)\, \phi_g(x,\mu')\, d\Omega' + S_g^{eff}(x,\mu) \tag{4.7-2}$$

where

$$S_g^{eff}(x,\mu) = \sum_{g'=1}^{g-1} \int_{\Omega'} \sigma_{s_{g'\to g}}(x,\mu_o)\, \phi_{g'}(x,\mu')\, d\Omega' + Q_g(x,\mu) \tag{4.7-3}$$

is an effective source term in group g, composed of downscatter sources from higher energy groups and an extraneous source term $Q_g(x,\mu)$. The even parity equation in group g becomes

$$-\mu \frac{d}{dx}\left[\frac{1}{\Sigma}\left(\mu \frac{d\phi_{o_g}^+}{dx}\right)\right] + c\,\phi_{o_g}^+ = S_g^{+eff} - \mu \frac{d}{dx}\left[\frac{1}{\Sigma} S_g^{-eff}\right] \tag{4.7-4}$$

where $\phi_{o_g}^+ = \phi_{o_g}^+(x,\mu)$ is the exact even parity angular flux in group g. The even and odd parity effective sources are

$$\begin{aligned} S_g^{+eff}(x,\mu) = & \sum_{g'=1}^{g-1} \int_{\Omega'} \sigma_{s_{g'\to g}}^{+}(x,\mu_o)\, \phi_{g'}^+(x,\mu')\, d\Omega' && \text{(Downscatter)} \\ & + \frac{\chi_g}{4\pi} \sum_{g'=1}^{NG} \nu\sigma_{f_{g'}} \int_{\Omega'} \phi_{g'}^+(x,\mu')\, d\Omega' && \text{(Fission)} \\ & + Q_g^+(x,\mu) && \text{(Extraneous Source)} \end{aligned} \tag{4.7-5}$$

and

$$S_g^{-\,eff}(x,\mu) = \sum_{g'=1}^{g-1} \int_{4\pi'} \sigma^{-}_{sg'\to g}(x,\mu_0)\, \phi_{g'}^{-}(x,\mu')\, d\Omega' + Q_g^{-}(x,\mu). \tag{4.7-6}$$

Since it is assumed that the extraneous (fixed) source is isotropic, then $Q_g^{-}(x,\mu) = 0$. In multigroup eigenvalue problems only the fission and downscatter source terms are required.

The approximate functional for group g may be written as

$$K_g^{+}(\phi_g^{+}) = \int_x \{ 2\langle \phi_g^{+}, S_g^{+\,eff} \rangle + 2\langle \mu \frac{d\phi_g^{+}}{dx}, \Sigma S_g^{-\,eff} \rangle - \langle \mu \frac{d\phi_g^{+}}{dx}, \Sigma \left(\mu \frac{d\phi_g^{+}}{dx} \right) \rangle - \langle \phi_g^{+}, C \phi_g^{+} \rangle \}\, dx + B.T. \tag{4.7-7}$$

Now $S_g^{-\,eff}(x,\mu)$ involves the odd parity flux $\phi_{g'}^{-}(x,\mu)$ from the previous groups. $\phi_{g'}^{-}(x,\mu)$ may be calculated starting with $\phi_1^{-}(x,\mu)$ of group 1 and working downwards to the lower energy groups. This is shown in the following section.

4.8 Even and Odd Parity Downscatter Sources

In this Section the even and odd parity downscatter sources and the functional source terms are considered in detail. Let

$$S_d^+(x,\mu) = \sum_{g'=1}^{g-1} \int_{\Omega'} \sigma^+_{s_{g'\to g}}(x,\mu_0)\, \phi^+_{g'}(x,\mu')\, d\Omega' \qquad (4.8\text{-}1)$$

and

$$S_d^-(x,\mu) = \sum_{g'=1}^{g-1} \int_{\Omega'} \sigma^-_{s_{g'\to g}}(x,\mu_0)\, \phi^-_{g'}(x,\mu')\, d\Omega' \,. \qquad (4.8\text{-}2)$$

The terms in the functional that are affected are

$$\int_x 2 < \phi_g^+, S_g^{+\,eff} > dx$$

and

$$\int_x 2 < \mu \frac{d\phi_g^+}{dx}, S_g(S_g^{-\,eff}) > dx \,.$$

From (4.8-1) we have

$$S_d^+(x,\mu) = \sum_{g'=1}^{g-1} \int_0^{2\pi} \int_{-1}^{1} \sum_n \sum_k \left(\frac{4n+1}{4\pi}\right) \sigma^+_{s_{2ng'\to g}} P_{2n}(\mu_0) \left(\frac{4k+1}{4\pi}\right) P_{2k}(\mu')\, \phi^+_{2kg'}(x)\, d\mu' d\omega'$$

$$= \sum_{g'=1}^{g-1} \sum_{n=0}^{\infty} \left(\frac{4n+1}{4\pi}\right) \sigma^+_{s_{2ng'\to g}} P_{2n}(\mu)\, \phi^+_{2ng'}(x) \,. \qquad (4.8\text{-}3)$$

Hence, the term in the functional involving S_d^+ becomes

$$2\int_x \int_{-1}^{1} \sum_{g'=1}^{g-1} \sum_n \sum_k \left(\frac{4n+1}{4\pi}\right)\left(\frac{4k+1}{4\pi}\right) \sigma^+_{s_{2ng'\to g}} P_{2n}(\mu) P_{2k}(\mu)\, \phi^+_{2ng'}(x)\, \phi^+_{2kg}(x)\, d\mu dx$$

This gives

$$\sum_{g'=1}^{g-1}\sum_{n=0}^{\infty}\left(\frac{4n+1}{4\pi^2}\right)\sigma^{+}_{s2ng'\to g}\int_x \phi^{+}_{2ng'}(x)\,\phi^{+}_{2ng}(x)\,dx \qquad (4.8\text{-}4)$$

Note the similarity between this term and the removal term (4.3-5) in the functional. The other terms of $S_g^{+\,eff}(x,\mu)$ give

$$\frac{\chi_g}{4\pi^2}\sum_{g'=1}^{g-1}\nu\sigma_{fg'}\int_x \phi^{+}_{0g'}(x)\,\phi^{+}_{0g}(x)\,dx \;+\; \frac{Q^{+}_{0}}{4\pi^2}\int_x \phi^{+}_{0g}(x)\,dx \qquad (4.8\text{-}5)$$

The odd parity downscatter source is easily written as

$$S_d^{-}(x,\mu) = \sum_{g'=1}^{g-1}\sum_{n=0}^{\infty}\left(\frac{4n+3}{4\pi}\right)\sigma_{s(2n+1)g'\to g}P_{2n+1}(\mu)\,\phi^{-}_{(2n+1)g'}(x) \qquad (4.8\text{-}6)$$

and clearly

$$S_g^{-\,eff}(x,\mu) = \frac{S_g^{-\,eff}(x,\mu)}{\sigma_{Tg}} + \int_{4\pi'} g_g(x,\mu\cdot\Omega')\,S_g^{-\,eff}(x,\mu')\,d\mu'\,d\omega' \qquad (4.8\text{-}7)$$

The term in the functional involving $S_g^{-\,eff}$ can also be written as

$$-2\int_x \langle\langle \mu\frac{d\phi^{+}_g}{dx},\; S_g\sum_{g'=1}^{g-1}\langle\langle \sigma^{-}_{sg'g},\,\phi^{-}_{g'}\rangle\rangle\rangle\, dx \;.$$

The first term in (4.8-7) gives

$$\frac{1}{\sigma_{Tg}}\sum_{g'=1}^{g-1}\sum_{n=0}^{\infty}\left(\frac{4n+3}{4\pi}\right)\sigma_{s(2n+1)g'\to g}P_{2n+1}(\mu)\,\phi^{-}_{(2n+1)g'}(x)\,,$$

while the second term gives

$$\sum_{n=0}^{\infty}\left(\frac{4n+3}{4\pi}\right)P_{2n+1}(\mu)\,\Lambda_{s(2n+1)g}\sum_{g'=1}^{g-1}\sigma_{s(2n+1)g'\to g}\,\phi^{-}_{(2n+1)g'}(x).$$

Hence

$$\Sigma_g S_g^{-eff} = \sum_{n=0}^{\infty}\left(\frac{4n+3}{4\pi}\right)\frac{1}{(\sigma_T-\sigma_{s(2n+1)})_g}\sum_{g'=1}^{g-1}\sigma_{s(2n+1)g'\to g}\,\phi^{-}_{(2n+1)g'}(x) \qquad (4.8\text{-}8)$$

Substituting in the relevant term in the functional, we have

$$2\int_x\int_{-1}^{1}\mu\,\frac{d\phi^{+}_g(x,\mu)}{dx}\sum_{n=0}^{\infty}\left(\frac{4n+3}{4\pi}\right)\frac{P_{2n+1}(\mu)}{(\sigma_T-\sigma_{s(2n+1)})_g}\sum_{g'=1}^{g-1}\sigma_{s(2n+1)g'\to g}\,\phi^{-}_{(2n+1)g'}(x)\,d\mu\,dx \qquad (4.8\text{-}9)$$

Expanding $\phi^{+}_g(x,\mu)$ in Legendre series and using the recurrence and orthonormality relations for Legendre polynomials reduces (4.8-9) to

$$\frac{1}{4\pi^2}\int_x\sum_{n=0}^{\infty}\frac{1}{(\sigma_T-\sigma_{s(2n+1)})_g}\left[(2n+1)\frac{d\phi^{+}_{2n}}{dx}{}_g+(2n+2)\frac{d\phi^{+}_{(2n+2)g}}{dx}\right]\sum_{g'=1}^{g-1}\sigma_{s(2n+1)g'\to g}\,\phi^{-}_{(2n+1)g'}(x)\,dx \qquad (4.8\text{-}10)$$

Now $\phi^{-}_{g'}(x,\mu)$ for group g' may be written as

$$\phi^{-}_{g'}(x,\mu) = \Sigma_{g'}\left[S^{-eff}_{g'}(x,\mu)-\mu\frac{d\phi^{+}_{g'}(x,\mu)}{dx}\right]$$

The coefficients $\phi^{-}_{g'(2n+1)}(x)$ are easily calculated. They are

$$\phi^{-}_{(2n+1)g'}(x) = \sum_{g''=1}^{g'-1}\frac{\sigma_{s(2n+1)g''\to g'}}{(\sigma_T-\sigma_{s(2n+1)})_{g'}}\,\phi^{-}_{(2n+1)g''}(x) - \frac{1}{(4n+3)(\sigma_T-\sigma_{s(2n+1)})_{g'}}\left[(2n+1)\frac{d\phi^{+}_{2n}}{dx}{}_{g'}+(2n+2)\frac{d\phi^{+}_{(2n+2)g'}}{dx}\right] \qquad (4.8\text{-}11)$$

This means that $\bar{\phi}^{(x)}_{(2n+1)}$ for group g' depends on the fluxes of the previous groups, where of course $\bar{\phi}^{(x)}_{(2n+1)}$ are just the odd spatial coefficients in the expansion for the angular flux $\phi(x,\mu)$. A more compact way [13,14] of writing $\bar{\phi}^{(x)}_{(2n+1)g'}$ and which is well suited for computational purposes is as follows:

Let Γ^{-1} be a diagonal matrix with element $\frac{1}{(\sigma_T - \sigma_{s(2n+1)})}$ and let Σ_{sd_0} be a strictly lower triangular matrix of group transfer downscattering cross sections $\sigma^{(x)}_{s(2n+1)g'\to g}$, i.e.

$$\Gamma^{-1} = \begin{bmatrix} \frac{1}{(\sigma_T - \sigma_{s(2n+1)})_1} & & & \\ & \frac{1}{(\sigma_T - \sigma_{s(2n+1)})_2} & & \\ & & \ddots & \\ & & & \frac{1}{(\sigma_T - \sigma_{s(2n+1)})_{NS}} \end{bmatrix}$$

and

$$\Sigma_{sd_0} = \begin{bmatrix} 0 & 0 & 0 \cdots & 0 & 0 \\ \sigma_{s(2n+1)1\to 2} & 0 & 0 \cdots & 0 & 0 \\ \sigma_{s(2n+1)1\to 3} & \sigma_{s(2n+1)2\to 3} & 0 \cdots & 0 & 0 \\ \vdots & \vdots & \sigma_{s(2n+1)3\to 4} & & \\ \vdots & \vdots & \vdots & & \\ \sigma_{s(2n+1)1\to NS} & \sigma_{s(2n+1)2\to NS} & & \sigma_{s(2n+1)NS-1\to NS} & 0 \end{bmatrix}$$

Where NG is the total number of energy groups. Then $\phi^-_{(2n+1)g'}(x)$ becomes

$$[\Phi^-] = \sum_{k=0}^{NG-1} \frac{1}{(4n+3)} \left(\Gamma^{-1} \Sigma_{sdo}\right)^k \Gamma^{-1} [D\Phi^+] \qquad (4.8\text{-}12)$$

where $[\Phi^-]$ is a column vector with entries $\phi^-_{(2n+1)g'}(x)$ and $[D\Phi^+]$ is a column vector with entries

$$d_i = \left[(2n+1)\frac{d\phi^+_{2n}}{dx} + (2n+2)\frac{d\phi^+_{(2n+2)}}{dx}\right]_i \qquad i=1,2,3.....,NG.$$

With the expression given for $\phi^-_{(2n+1)g}$, the term in the functional involving $\phi^-(x,\mu)$, (4.8-10), becomes

$$\frac{1}{4\pi^2}\int_x \sum_{n=0}^{\infty} \frac{1}{(\sigma_T - \sigma_{s(2n+1)})_g} \left[(2n+1)\frac{d\phi^+_{2n}}{dx} + (2n+2)\frac{d\phi^+_{(2n+2)}}{dx}\right]_g$$

$$\times \sum_{g'=1}^{g-1} \sigma_{s(2n+1)g'\to g} \left\{ \sum_{g''=1}^{g'-1} \frac{\sigma_{s(2n+1)g''\to g'}\,\phi^-_{(2n+1)g''}}{(\sigma_T - \sigma_{s(2n+1)})_{g'}} \right.$$

$$\left. - \frac{1}{(\sigma_T - \sigma_{s(2n+1)})_{g'}} \left[(2n+1)\frac{d\phi^+_{2n}}{dx} + (2n+2)\frac{d\phi^+_{(2n+2)}}{dx}\right]_{g'} \right\} \qquad (4.8\text{-}13)$$

With the definition of $[D\Phi^+]$, Γ^{-1}, Σ_{sdo}, above, (4.8-13) becomes

$$\frac{1}{4\pi^2}\int_x \sum_{n=0}^{\infty} \sum_{k=1}^{NG-1} \frac{1}{(4n+3)} \left(\Gamma^{-1}\Sigma_{sdo}\right)^k \Gamma^{-1} [D\Phi^+]\, d_{NG} \qquad (4.8\text{-}14)$$

For example in a three group calculation, (NG=3) we have

$$\frac{1}{4\pi^2}\sum_{g'=1}^{2}\sum_{n}\frac{\sigma_{s(2n+1)g'\to g}}{\alpha_g}\int_x \bar{\phi}_{(2n+1)g'}\, d_{ng}\, dx$$

$$= \frac{1}{4\pi^2}\sum_{n=0}^{\infty}\left[\frac{\sigma_{s(2n+1)1\to 3}}{\alpha_3}\int_x \bar{\phi}_{(2n+1)1}\, d_3\, dx + \frac{\sigma_{s(2n+1)2\to 3}}{\alpha_3}\int_x \bar{\phi}_{(2n+1)2}\, d_3\, dx\right]$$

$$= \frac{1}{4\pi^2}\sum_{n=0}^{\infty}\left[\frac{\sigma_{s(2n+1)1\to 3}}{\alpha_1\alpha_3}\int_x d_1 d_3\, dx + \frac{\sigma_{s(2n+1)1\to 2}\,\sigma_{s(2n+1)2\to 3}}{\alpha_1\alpha_2\alpha_3}\int_x d_1 d_3\, dx\right.$$

$$\left. + \frac{\sigma_{s(2n+1)2\to 3}}{\alpha_2\alpha_3}\int_x d_2 d_3\, dx\right]\frac{1}{(4n+3)}$$

(4.8-15)

Here $\alpha_g = (\sigma_T - \sigma_{s(2n+1)g})$.

Eqn.(4.8-15) gives the contribution to the odd parity source term in group 3. Whereas, in the even parity source, downscatter to group 3 involves $1\mapsto 3$ and $2\mapsto 3$ contributions, in the odd parity case, the contributions $1\mapsto 3$ and $2\mapsto 3$ are required, but, in addition $1\mapsto 2\mapsto 3$ is also needed. In general for group NG all downscatter combinations to this group are required for the odd parity source term. All the contributions involve $\bar{\phi}_{g'}$ of the previous groups. Looking at (4.8-13) or (4.8-14), it is seen that these expressions are similar to the anisotropic leakage term in the functional for one group theory. In the multigroup case (spatially) we have a term for group g multiplied by one from group g'. This leads to a downscatter source matrix similar to that given in Section 4.5 for the

anisotropic leakage term. Similarly, the even parity downscatter source matrix is similar to the removal matrix of Section 4.5. These are discussed below.

4.8.1 Local Downscatter Source Matrices

Local source matrices for downscatter sources in the functional can be readily obtained by expanding $\phi^{+}_{2n}(x)$ in finite element basis functions and maximising the functional with respect to nodal parameters. Consider the even parity downscatter source with linear elements. For one moment we have

$$\frac{1}{4\pi^2}\int_0^h \sum_{g'=1}^{g-1} \sigma_{s0g'\to g}\Big[(1-x/h)^2 \bar{\phi}_{1g}\bar{\phi}_{1g'} + (1-x/h)(x/h)\bar{\phi}_{1g}\bar{\phi}_{2g'} + (1-x/h)(x/h)\bar{\phi}_{2g}\bar{\phi}_{1g'} + \frac{x^2}{h^2}\bar{\phi}_{2g}\bar{\phi}_{2g'}\Big]dx .$$

This leads to a local source matrix

$$\sum_{g'=1}^{g-1} \frac{h\,\sigma_{s0g'\to g}}{4\pi^2}\begin{bmatrix} 1/3\,\bar{\phi}_{1g'} & 1/6\,\bar{\phi}_{2g'} \\ 1/6\,\bar{\phi}_{1g'} & 1/3\,\bar{\phi}_{2g'}\end{bmatrix}$$

$$= \frac{1}{8\pi^2}\sum_{g'=1}^{g-1} \sigma_{s0g'\to g}\cdot 2h\begin{bmatrix} 1/3 & 1/6 \\ 1/6 & 1/3\end{bmatrix}\begin{bmatrix}\bar{\phi}_{1g'}\\ \bar{\phi}_{2g'}\end{bmatrix}. \qquad (4.8\text{-}16)$$

after maximising with respect to $\bar{\phi}_{1g}$ and $\bar{\phi}_{2g}$ nodal values (unknowns) of $\phi^{+}_{g}(x,\mu)$ in group g.

Hence, the finite element matrix is the same as for the removal term in the one group case. In general the angular matrix may be written as

$$\begin{bmatrix} \sum_{g'=1}^{g-1} \sigma_{s_0 g' \to g}/8\pi^2 & & & & \\ & \sum_{g'} 5\sigma_{s_2 g' \to g}/8\pi^2 & & 0 & \\ & & \sum_{g'} 9\sigma_{s_4 g' \to g}/8\pi^2 & & \\ & 0 & & & \\ & & & & \sum_{g'} (4M-3)\sigma_{s_{2(M-1)} g' \to g}/8\pi^2 \end{bmatrix} \tag{4.8-17}$$

Similar arguments may be applied to the odd parity down-scatter source term in the functional. In this case the finite element matrix is

$$\frac{2}{h}\begin{bmatrix} 1 & -1 \\ -1 & 1 \end{bmatrix}$$

while the angular matrix becomes

$$\begin{bmatrix} -\lambda_1' \delta_0'^2 & -\lambda_1' \delta_0' \epsilon_0' & 0 & 0 & \cdots \\ -\lambda_1' \delta_0' \epsilon_0' & -(\lambda_1' \epsilon_0'^2 + \lambda_3' \delta_2'^2) & -\lambda_3' \delta_2' \epsilon_2' & 0 & \cdots \\ 0 & -\lambda_3' \delta_2' \epsilon_2' & -(\lambda_3' \epsilon_2'^2 + \lambda_5' \delta_4'^2) & & \\ \vdots & 0 & \vdots & & \\ \vdots & \vdots & \vdots & & \end{bmatrix} \tag{4.8-18}$$

where

$$\delta'_{2n} = (2n+1)/4\pi$$

$$\epsilon_{2n'} = (2n+2)/4\pi \qquad (4.8\text{-}19)$$

and $$\lambda'_{(2n+1)} = \frac{1}{(4n+3)} \sum_{k=1}^{NG-1} \left(\Gamma^{-1}\Sigma_{sd_0}\right)^k \Gamma^{-1}$$

is an (NGxNG) square matrix.

4.9 Extension to Higher Dimensions

The basic ideas introduced for anisotropic scattering in one dimensional geometry can be equally applied to higher spatial dimensions. The main difficulty is the complexity of the anisotropic leakage, and the odd parity downscatter source terms. The difficulty here is in evaluating the angular integrals and subsequent derivation of angular matrices of the reduced functional. Quah [15], for instance, in implementing the multigroup scheme for isotropic scattering in X-Y geometry performed both the angular and spatial integration, numerically. Consider, for example, the one group functional in X-Y geometry. From Fig. 4.10 we have

$$\underline{\Omega} \equiv \{\Omega_x, \Omega_y\} \equiv \{\sin\theta\cos\omega, \sin\theta\sin\omega\}$$

and

$$\underline{r} \equiv \{x, y\}$$

Also in X-Y geometry

$$\underline{\Omega}\cdot\nabla\phi^+(r,\underline{\Omega}) = \left[\sin\theta\cos\omega\,\frac{\partial\phi^+(r,\underline{\Omega})}{\partial x} + \sin\theta\sin\omega\,\frac{\partial\phi^+(r,\underline{\Omega})}{\partial y}\right]$$

$$= (1-\mu^2)^{\frac{1}{2}}\left[\cos\omega\,\frac{\partial\phi^+}{\partial x} + \sin\omega\,\frac{\partial\phi^+}{\partial y}\right] \qquad (4.9\text{-}1)$$

where $\mu = \cos\theta$.

Then the functional becomes

$$K^+(\phi^+) = \int_x\int_y \Big\{ 2\langle\phi^+, S^+\rangle - 2\langle(1-\mu^2)^{\frac{1}{2}}\left[\cos\omega\,\frac{\partial\phi^+}{\partial x} + \sin\omega\,\frac{\partial\phi^+}{\partial y}\right], SS^-\rangle$$
$$- \langle(1-\mu^2)^{\frac{1}{2}}\left[\cos\omega\,\frac{\partial\phi^+}{\partial x} + \sin\omega\,\frac{\partial\phi^+}{\partial y}\right], S\left((1-\mu^2)^{\frac{1}{2}}\left[\cos\omega\,\frac{\partial\phi^+}{\partial x}\right.\right.$$
$$\left.\left. + \sin\omega\,\frac{\partial\phi^+}{\partial y}\right]\right)\rangle - \langle\phi^+, C\phi^+\rangle \Big\}\, dx\,dy$$
$$- \int_{S_b}\int_{\Omega} (\phi^+)^2\, |\underline{\Omega}\cdot\underline{n}|\, d\Omega\, ds \qquad (4.9\text{-}2)$$

Of course, in the one group case with an isotropic extraneous source, $S^- = 0$. Next the even parity angular flux is expanded in spherical harmonics. In X-Y geometry we have

$$\phi^+(x,y;\underline{\Omega}) = \sum_{lm} \frac{\gamma_m}{\sqrt{2\pi}} \textcircled{H}_l^m(\mu)\left[\phi_{lm}\cos m\omega + \psi_{lm}\sin m\omega\right] \quad (4.9\text{-}3)$$

where $\phi_{lm} = \phi_{lm}(x,y)$, $\psi_{lm} = \psi_{lm}(x,y)$ are the spatial coefficients of the expansion and $\gamma_m = (2-\delta_{m,0})$, δ being the Kronecker delta. The spherical harmonics $Y_{lm}(\underline{\Omega})$ are defined as

$$\begin{aligned} Y_{lm}(\underline{\Omega}) &= \sum_{lm} \frac{\gamma_m}{\sqrt{2\pi}} \textcircled{H}_l^m(\mu)\cos m\omega \qquad m \geq 0 \\ &= \sum_{lm} \frac{\gamma_m}{\sqrt{2\pi}} \textcircled{H}_l^m(\mu)\sin |m|\omega \qquad m < 0 \end{aligned} \quad (4.9\text{-}4)$$

$\textcircled{H}_l^m(\mu)$ are the normalised Associated Legendre polynomials, viz.,

$$\textcircled{H}_l^m(\mu) = \left[\frac{(2l+1)}{2}\frac{(l-m)!}{(l+m)!}\right]^{\frac{1}{2}} P_l^m(\mu) \quad (4.9\text{-}5)$$

In this case the addition theorem for the spherical harmonics then becomes

$$P_l(\mu_0) = \frac{2}{(2l+1)} \textcircled{H}_l^0(\mu)\,\textcircled{H}_l^0(\mu') + \frac{4}{(2l+1)} \sum_{m=1}^{l} \textcircled{H}_l^m(\mu)\,\textcircled{H}_l^m(\mu')\cos m(\omega-\omega') \quad (4.9\text{-}6)$$

and the orthonormality condition becomes

$$\int_{-1}^{1} \textcircled{H}_l^m(\mu)\,\textcircled{H}_{l'}^m(\mu)\,d\mu = \delta_{ll'} \quad (4.9\text{-}7)$$

The even parity nature of $\phi^+(x, \underline{\Omega})$ implies that the index l is even. Also in X-Y geometry $Y(\underline{\Omega}^*) = Y(\underline{\Omega})$ implies that m is even.

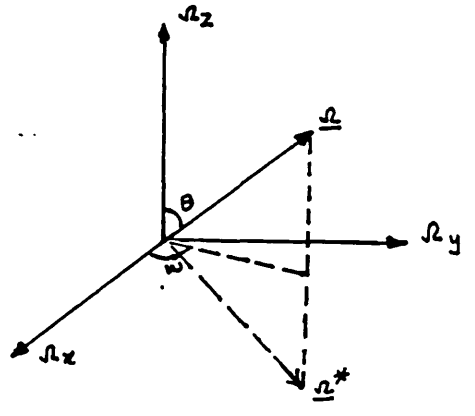


Fig. 4.10

$\underline{\Omega}^*$ is the reflection of $\underline{\Omega}$ in the x-y plane.

It can be seen that substitution of $\phi^+(x, \underline{\Omega})$ from (4.9-3) into $K^+(\phi^+)$ leads to integrals over w and θ involving products of sine and cosine terms. This integration can become tedious in higher dimensions, although, Williams [16] has done the angular integration analytically for R-Z cylindrical geometry. Riyait [17] has also done the same for X-Y geometry to obtain the reduced functional. Issa [18,19] has used a slightly different approach. He has converted the terms involving sine and cosine products to multiples of terms involving these trigonometric functions. Algorithms have been written to work out these integrals. Here the integration is exact and systematic. In this way the angular integration of the more complicated terms in the functional can be handled without too much difficulty.

4.10 One-Group Test Cases

In this, and the following Section, results of test problems, using the finite element method, are compared with those obtained from other methods. The comparison is with analytical and other numerical methods used in neutron transport calculations. Analytical solutions are available for simple one group problems and then again mostly for isotropic scattering. Only a few analytical solutions exist for anisotropic scattering. In calculations which are of a realistic nature with varied neutron energies, the multigroup approximation is introduced. In this case numerical techniques, e.g. discrete-ordinates finite-difference method, are used. In the following both source and eigenvalue problems are analysed.

4.10.1 Backward-Forward Isotropic Scattering Law Test Problem I

Recently, Ackroyd and Williams [20] have extended the variational principle so that it is applicable to an albedo type boundary condition. This condition arises with the use of the so called backward-forward-isotropic (BFI) scattering kernel and the subsequent transformation of the neutron transport equation to isotropic form. With the use of this kernel and the transformation, the existing finite element code, with a modified boundary condition, can be used to benchmark an anisotropic scattering finite

element code. Williams and Wood [16] have used this technique to test the one group version of the cylindrical geometry finite element code, FELICIT. We use this method to test the one group one dimensional anisotropic scattering equations and coding in FELTRAN.

The backward-forward-isotropic scattering kernel has the form

$$\sigma_s(\mu_0) = \frac{(1-\alpha-\beta)}{4\pi} + \frac{\alpha}{2\pi}\delta(\mu_0-1) + \frac{\beta}{2\pi}\delta(\mu_0+1) \qquad (4.10\text{-}1)$$

where α and β are parameters such that $\alpha \geq 0, \beta \leq 1$ and $\alpha+\beta \leq 1$. See Inonu [22]. As stated previously, the above kernel has the special property of enabling the resulting transport equation to be converted into an effective isotropic form with a modified boundary condition. Inserting $\sigma_s(\mu_0)$, from (4.10-1), into the transport equation gives

$$\mu \frac{d\phi_0(x,\mu)}{dx} + \phi_0(x,\mu) = \frac{(1-\alpha-\beta)c}{2\pi}\int_{\Omega'} \phi_0(x,\mu')\, d\Omega' + c\alpha\,\phi_0(x,\mu) + c\beta\,\phi_0(x,-\mu) + Q(x,\mu) \qquad (4.10\text{-}2)$$

Here $c = \frac{\sigma_s}{\sigma_T}$ and distances are measured in units of total mean free paths. The bare surface condition is

$$\phi_0(x,\mu) = 0 \qquad \text{for} \qquad -1 \leq \mu < 0 \qquad (4.10\text{-}3)$$

By writing

$$\phi_0(x,\mu) = A\,\tilde{\psi}(\xi,\mu) + B\,\tilde{\psi}(\xi,-\mu)$$

and

$$\hat{Q}(\xi,\mu) = \frac{1}{q(A-B)}\left[A\,Q(x,\mu) + BQ(x,-\mu)\right]$$

with

$$q = \left[(1-c\alpha)^2 - c^2\beta^2\right]^{\frac{1}{2}},$$

$$A = \frac{1}{2}\left\{1 + \left[\frac{1+c(\alpha+\beta)}{1-c(\alpha-\beta)}\right]^{\frac{1}{2}}\right\}, \quad B = 1-A$$

and $\xi = qx$,

then $\tilde{\psi}(\xi,\mu)$ satisfies the following equation

$$\mu\frac{d\tilde{\psi}}{d\xi} + \tilde{\psi}(\xi,\mu) + \frac{\hat{c}}{4\pi}\int_{4\pi'}\tilde{\psi}(\xi,\mu')\,d\Omega' + \tilde{Q}(\xi,\mu) \qquad (4.10\text{-}4)$$

where $\hat{c} = c(1-\alpha-\beta)/1-c(\alpha+\beta)$.

The bare surface boundary condition now becomes

$$\tilde{\psi}(\xi_b,\mu) = -B/A\,\tilde{\psi}(\xi_b,-\mu) \quad \text{for } -1\le\mu<0 \qquad (4.10\text{-}5)$$

Of course, the scalar fluxes associated with $\phi_0(x,\mu)$ and $\tilde{\psi}(\xi,\mu)$ are equal, i.e.

$$\phi_0(x) = \tilde{\psi}_0(\xi)$$

So the normal form of the transport equation with BFI scattering law is converted into an isotropic scattering form (4.10-4) with a backward reflective boundary condition (4.10-5). In the conventional anisotropic calculations, the scattering kernel is expanded as usual,

$$\sigma_s(\mu_0) = \sum_{l=0}^{\infty}\left(\frac{2l+1}{4\pi}\right)f_l\,P_l(\mu_0) \qquad (4.10\text{-}6)$$

where the coefficients f_L are given by

$$f_L = (1-\alpha-\beta)\delta_{L0} + \alpha + (-1)^L\beta \qquad (4.10\text{-}7)$$

$f_L = 1$ for forward only scattering. f_L's are used in the conventional anisotropic calculation.

Incorporation of the albedo boundary condition

$$\phi_0(r,\underline{\Omega}) = \rho\,\phi_0(r,-\underline{\Omega}) \qquad \rho<1,\ \underline{\Omega}\cdot\underline{n}<0 \qquad (4.10\text{-}8)$$

into $K^+(\phi^+)$ leads to an additional term

$$-\int_S\int_\Lambda |\underline{\Omega}\cdot\underline{n}|\,\frac{(1-\rho)}{(1+\rho)}(\phi^+)^2\,d\Lambda\,dS$$

in the functional, with $\rho = -B/A$. So in solving the isotropic scattering problem the boundary term over the bare surface is multiplied by a factor

$$Rc = \frac{(1-\rho)}{(1+\rho)} = \left[\frac{1-c(\alpha-\beta)}{1-c(\alpha+\beta)}\right]^{\frac{1}{2}}. \qquad (4.10\text{-}9)$$

In this first test problem, data provided by Williams and Wood [16] is used to check the one dimensional anisotropic scattering source calculation for slab geometry. The conventional anisotropic scattering calculation cross section data is given in Table 4.1 while the transformed isotropic scattering cross section data is shown in Table 4.2. This is a one region source problem with a perfect reflector condition at the left end point and a bare surface at the extreme right. The anisotropic scattering calculation was performed for P_1, P_3 and P_5 scattering using 120 linear elements, each of length 0.05cm. The result for the scalar flux at the end points and at a quarter, half and three quarters

x/cm	σ_T (cm^{-1})	σ_S (cm^{-1})	σ_{Sl} ($l>0$)	S ($ncm^{-1}s^{-1}$)
6.0	1.0	0.6	0.12(odd l) 0.36(even l)	1.0

Table 4.1 Anisotropic Scattering Calculation Cross Section Data for Problem 4.10.1.

x/cm	σ_T (cm^{-1})	σ_S (cm^{-1})	S ($ncm^{-1}s^{-1}$)
4.5027991	1.0	0.375	1.5625

Table 4.2 Isotropic Transformed Calculation Cross Section Data for Problem 4.10.1

of the distance in the slab are shown in Table 4.3. The number of even moments for the flux was increased simultaneously with the order of scattering.

The isotropic transformed calculation was performed for up to three moments expansion in $\phi^{+}(x,\mu)$. In addition the boundary term over the bare surface was modified by a factor R = 1.1726039. Again the results are at the end points and at quarter, half and three quarter of the distances in the slab. These scalar fluxes are shown in Table 4.4. Comparison of Tables 4.3 and 4.4 show that the two sets of results are almost identical, this indicating that the one group anisotropic scattering formulation is correctly incorporated in the code FELTRAN.

x/cm	Order of Scattering		
	P_1 NOM=1	P_3 NOM=2	P_5 NOM=3
0.1	2.49410	2.48690	2.48732
1.5	2.48559	2.47651	2.47681
3.0	2.43547	2.42751	2.42589
4.5	2.19912	2.23337	2.23015
6.0	1.09438	1.05477	1.03956

NOM = Number of Moments Used for Angular Flux

Table 4.3 Fluxes Calculated Directly for the Anisotropic Scattering Problem 4.10.1**

** In the direct calculation, there is an additional error due to the approximation for the scattering law in terms of a finite series. So in fact Table 4.4 gives the more accurate results against which the direct calculation results may be compared for any desired order of scattering.

x/cm	Number of Moments Used for Angular Flux		
	1	2	3
0.0	2.49410	2.48690	2.48732
1.1256997	4.85590	2.47652	2.47682
2.2513995	2.43549	2.42753	2.42591
3.3770992	2.19917	2.23343	2.23021
4.5027991	1.09444	1.05490	1.03975

Table 4.4 Fluxes Calculated for the Transformed Isotropic Problem 4.10.1*

* Errors made in transformed problems, apart from round-off errors, are due to the angular approximation for ϕ^+ and the spatial discretisation of ϕ^+.

4.10.2 Backward-Forward-Isotropic Scattering Law Test Problem II

This is a three region eigenvalue problem used by Williams and Wood [16] for checking anisotropic scattering in FELICIT. We consider the one dimensional analogue of this problem. The geometry of the problem is shown below in Fig. 4.11 and cross section data is given in Tables 4.5 and 4.6. Varying number of mesh intervals were considered for both the anisotropic and the transformed isotropic calculation. Results for keff shown in Table 4.7 for various order of scattering up to P_7 were obtained using sixty linear elements. The keff values were the same, for the decimal places shown, for both the anisotropic and transformed isotropic cases.

The variation in keff with $\left(\frac{Mmax}{M}\right)^2$ where Mmax is the maximum number of mesh intervals and M is the number of mesh intervals used, is shown in Fig. 4.12, for P_5 scattering. Both FELTRAN and ANISN(S6) show linear variation of keff with $\left(\frac{Mmax}{M}\right)^2$ However, the FELTRAN values converge closer to the reference value for keff of 1.5774. The reference value was obtained from an ANISN (S16), P_{15} scattering and 180 mesh-interval calculation.

Region	Distance (cm)	σ_T	σ_s	$\sigma_{s_L}(L>0)$	$\nu\sigma_f$
1	0 - 1.5	0.95	0.45	0.0	1.0
2	1.5 - 4.0	1.08	0.48	0.0	0.3
3	4.0 - 6.0	1.1375	0.6375	0.0	0.0

Table 4.5 Macroscopic cross section data for transformed isotropic method in Problem 4.10.2

Region	Distance (cm)	$\bar{\mu}_0$	σ_T	σ_s	$\sigma_{s_L}(L>0)$	$\nu\sigma_f$
1	0 - 1.5	0.1	1.0	0.5	0.05	1.0
2	1.5 - 4.0	0.2	1.2	0.6	0.12	0.3
3	4.0 - 6.0	0.15	1.25	0.75	0.1125	0.0

Table 4.6 Macroscopic cross section data for anisotropic method for Problem 4.10.2

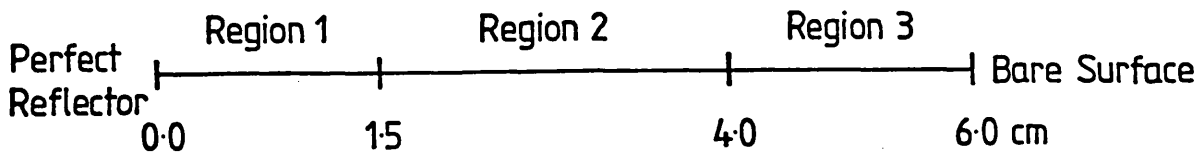
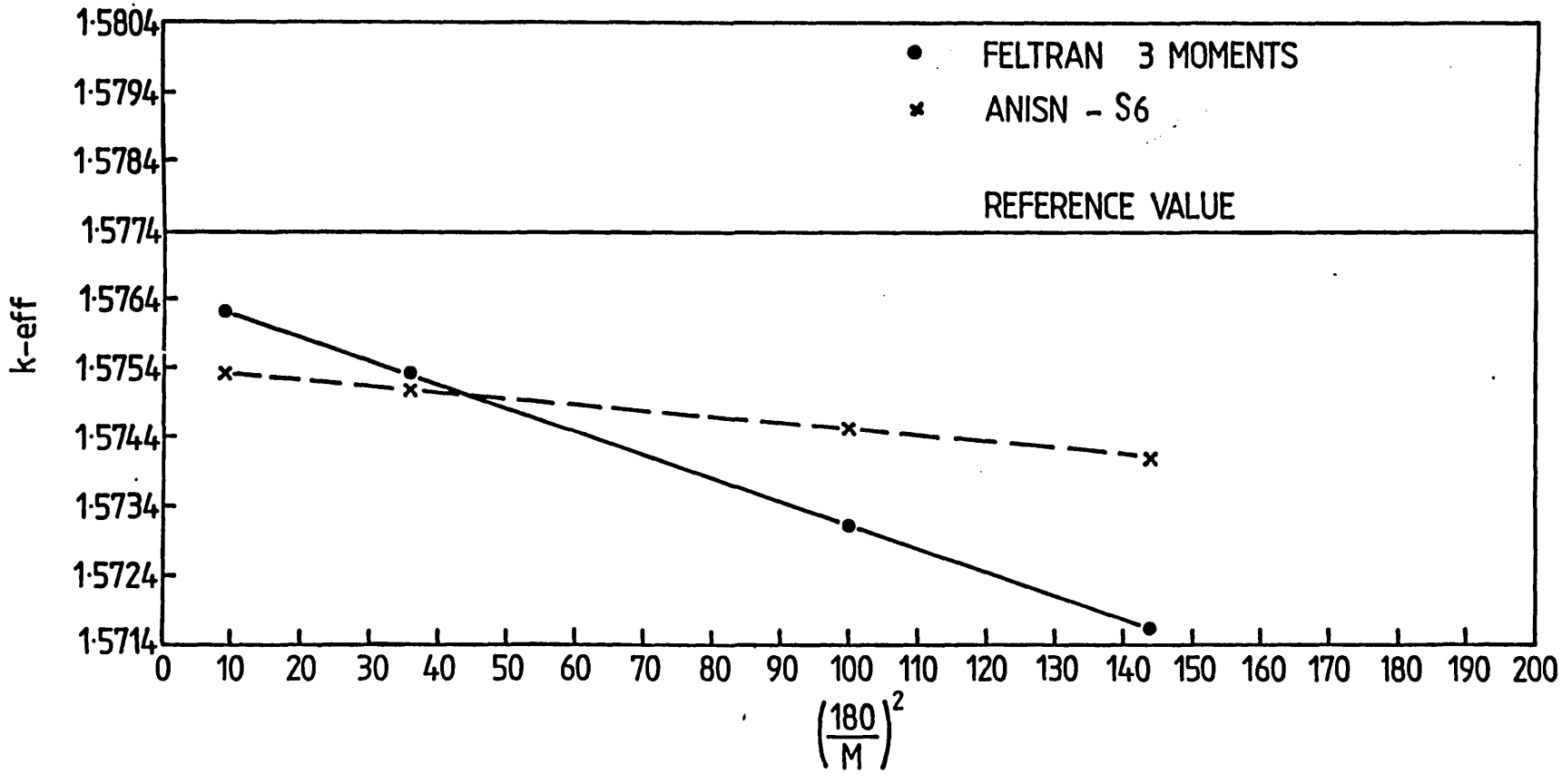


Fig. 4.11 Geometry for the three region eigenvalue problem with backward-forward-isotropic scattering law.

Scattering order	P_1	P_3	P_5	P_7
k-eff	1.531292	1.572843	1.576205	1.576880

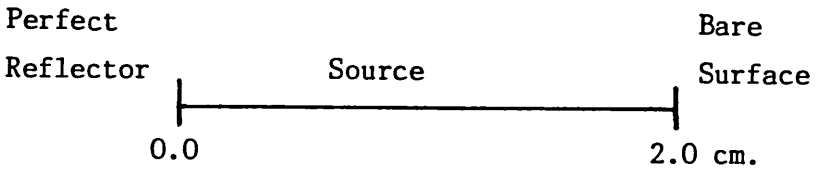
Table 4.7 Multiplication Factor for Problem 4.10.2 with various orders of anisotropic scattering.

Figure 4.12 Variation of the Multiplication Factor k-eff with $\left(\frac{M_{max}}{M}\right)^2$ for the One Group Backward-Forward-Isotropic Scattering Problem



4.10.3 Forward Scattering Source Problem

This is a one region source problem with anisotropic scattering for which an analytical solution exists [9,23]. The geometry and cross section data are given below.



σ_T =1.0 cm^{-1}, σ_S =0.8cm^{-1}, S=1.0, a(slab half-thickness)=2.0cm.

This problem has been investigated by Galliara [9] using the present finite element formulation. He presented the results in graphical form with error graphs. Since there is an analytical solution, the accuracy of the finite element method may be checked. Writing $\sigma_S(x,\mu_0)$ as

$$\sigma_S(x,\mu_0) = \sum_{l=0}^{\infty} \left(\frac{2l+1}{4\pi}\right) f_l \, \sigma_S(x) \, P_l(\mu_0)$$

then f_l =1 for forward scattering.
The analytical solution for the angular flux $\phi_0(x,\mu)$ for the above problem is given by [9]

$$\phi_0(x,\mu) = \frac{S}{2(1-c)}\left[1 - \exp\left[-(1-c)(a+x)/\mu\right]\right] \qquad (4.10\text{-}10)$$

for $0 < \mu \leq 1$

and

$$\phi_0(x,\mu) = \frac{S}{2(1-c)}\left[1 - \exp\left[-(1-c)(a-x)/\mu\right]\right] \qquad (4.10\text{-}11)$$

for $-1 \leq \mu < 0$.

where $c = \frac{\sigma_s}{\sigma_T}$.

The scalar flux is then

$$\Phi_0(x) = \int_{-1}^{1} \phi_0(x,\mu)\, d\mu$$

$$= \frac{S}{(1-c)}\left\{1 - \tfrac{1}{2} E_2\left[(1-c)(a+x)\right] - \tfrac{1}{2} E_2\left[(1-c)(a-x)\right]\right\} \qquad (4.10\text{-}12)$$

where

$$E_n(x) = \int_0^{\infty} \frac{e^{-xt}}{t^n}\, dt \qquad (4.10\text{-}13)$$

$n = 0, 1, 2, \ldots\ldots$

is the exponential function. See for instance [4,5].

For x=0, $E_n(0) = \frac{1}{(n-1)}$ $(n>1)$.

The results of twenty element calculations for increasing even moments in the even parity flux expansion are compared with analytical results in Table 4.8. Up to an equivalent of a P_{17} spherical harmonics expansion of the even parity flux was considered. The errors for the nine even moments calculation are less than 1%.

x/cm	'Exact'	NOM=1 (P1)	NOM=2 (P3)	NOM=3 (P5)	NOM=4 (P7)	NOM=5 (P9)	NOM=6 (P11)	NOM=7 (P13)	NOM=8 (P15)	NOM=9 (P17)
0.0	3.0532	2.6364	2.9604	3.0418	3.0637	3.0672	3.0651	3.0619	3.0589	3.0567
0.2	3.0465	2.6307	2.9527	3.0338	3.0559	3.0598	3.0580	3.0550	3.0523	3.0501
0.4	3.0261	2.6137	2.9297	3.0096	3.0323	3.0372	3.0365	3.0342	3.0319	3.0301
0.6	2.9915	2.5852	2.8910	2.9686	2.9922	2.9987	2.9996	2.9986	2.9972	2.9958
0.8	2.9414	2.5451	2.8363	2.9101	2.9343	2.9429	2.9458	2.9465	2.9463	2.9457
1.0	2.8741	2.4932	2.7647	2.8328	2.8569	2.8675	2.8727	2.8755	2.8769	2.8775
1.2	2.7866	2.4292	2.6755	2.7351	2.7577	2.7696	2.7796	2.7818	2.7851	2.7872
1.4	2.6742	2.3529	2.5675	2.6148	2.6335	2.6450	2.6536	2.6602	2.6652	2.6689
1.6	2.5286	2.2639	2.4396	2.4693	2.4802	2.4885	2.4961	2.5029	2.5087	2.5134
1.8	2.3319	2.1618	2.2900	2.2955	2.2928	2.2929	2.2954	2.2989	2.3027	2.3063
2.0	1.9979	2.0460	2.1170	2.0894	2.0648	2.0489	2.0391	2.0327	2.0283	2.0250

Table 4.8 Scalar Flux for the Forward Scattering Source Problem

Pn represents scattering order.

NOM is the number of even moments expansion in the even parity flux.

4.11 Multigroup Test Cases

4.11.1 Benchmark Problem with BFI Scattering Law

The energy dependent backward-forward isotropic scattering law model has been developed recently by Williams [24], who has reported some two group exact solutions for slab and spherical geometry. These results can be used in benchmarking multigroup anisotropic scattering calculations. The energy dependent scattering kernel can be written as

$$\sigma_s(E' \to E; \mu_0) = \sum_{l=0}^{\infty} \left(\frac{2l+1}{4\pi}\right) \sigma_{sl}(E' \to E) P_l(\mu_0) \,. \qquad (4.11\text{-}1)$$

The coefficients $\sigma_{sl}(E' \to E)$ are given by

$$\sigma_{sl}(E' \to E) = 2\pi \int_{-1}^{1} \sigma_s(E' \to E; \mu_0) P_l(\mu_0) \, d\mu_0 \,. \qquad (4.11\text{-}2)$$

The BFI scattering model is

$$\sigma_s(E' \to E; \mu_0) = \frac{1}{4\pi} \gamma(E' \to E) + \frac{1}{2\pi} \alpha(E' \to E) \delta(\mu_0 - 1) + \frac{1}{2\pi} \beta(E' \to E) \delta(\mu_0 + 1) \qquad (4.11\text{-}3)$$

and is an approximation to $\sigma_s(E' \to E; \mu_0)$. The coefficients α, β, γ can be obtained in terms of σ_{sl}.

$$\alpha = \frac{1}{2}(\sigma_{s1} + \sigma_{s2})$$

$$\beta = \frac{1}{2}(\sigma_{s2} - \sigma_{s1}) \qquad (4.11\text{-}4)$$

and $$\gamma = \sigma_{s0} - \sigma_{s2} \,.$$

For backward and forward scattering only, $\gamma = 0$ and

$$\alpha = \frac{1}{2}(\sigma_{s0} + \sigma_{s1})$$

and $$\beta = \frac{1}{2}(\sigma_{s0} - \sigma_{s1}) \,. \qquad (4.11\text{-}5)$$

Williams [24], has obtained exact solution for a two group bare slab problem containing a uniform source of unit strength in group one and zero in group two. The parameters for the exact solutions are as follows:

$$\sigma_{s_0}(1\to1) = 0.1 \qquad \sigma_{s_0}(2\to2) = 2.0 \qquad \sigma_{s_0}(1\to2) = 0.2$$

$$\sigma_{s_1}(1\to1) = 0.02 \qquad \sigma_{s_1}(2\to2) = 0.2 \qquad \sigma_{s_1}(1\to2) = 0.1$$

In the case of the conventional anisotropic scattering calculation, the scattering kernel for BFI model

$$\sigma_s(E'\to E;\mu_0) = \frac{1}{4\pi}\left[\sigma_{s_0}(E'\to E)+\sigma_{s_1}(E'\to E)\right]\delta(\mu_0-1) + \frac{1}{4\pi}\left[\sigma_{s_0}(E'\to E)+\sigma_{s_1}(E'\to E)\right]\delta(\mu_0+1) \qquad (4.11\text{-}5)$$

may be expanded as

$$\sigma_s(E'\to E;\mu_0) = \sum_{l=0}^{\infty}\left(\frac{2l+1}{4\pi}\right)\hat{\sigma}_{sl}(E'\to E)P_l(\mu_0) \qquad (4.11\text{-}6)$$

Hence, the coefficients $\hat{\sigma}_{sl}$ are given by

$$\hat{\sigma}_{sl}(E'\to E) = \frac{1}{2}\left\{1+(-1)^l\right\}\sigma_{s_0}(E'\to E) + \frac{1}{2}\left\{1-(-1)^l\right\}\sigma_{s_1}(E'\to E) \qquad (4.11\text{-}7)$$

i.e.

$$\hat{\sigma}_{sl}(E'\to E) = \sigma_{s_0}(E'\to E) \quad l \text{ even} \qquad (4.11\text{-}8)$$

and

$$\hat{\sigma}_{sl}(E'\to E) = \sigma_{s_1}(E'\to E) \quad l \text{ odd}.$$

Hence the multigroup anisotropic scattering cross sections to be used for the finite element calculations are

ℓ even		ℓ odd	
$\hat{\sigma}_{s\ell}(1 \rightarrow 1)$	= 0.1	$\hat{\sigma}_{s\ell}(1 \rightarrow 1)$	= 0.02
$\hat{\sigma}_{s\ell}(1 \rightarrow 2)$	= 0.2	$\hat{\sigma}_{s\ell}(1 \rightarrow 2)$	= 0.1
$\hat{\sigma}_{s\ell}(2 \rightarrow 1)$	= 0.0	$\hat{\sigma}_{s\ell}(2 \rightarrow 1)$	= 0.0
$\hat{\sigma}_{s\ell}(2 \rightarrow 2)$	= 2.0	$\hat{\sigma}_{s\ell}(2 \rightarrow 2)$	= 0.2 .

Calculations were performed for slab half thickness a = 1.0 cm and 5.0 cm. Ten linear elements were used for the first case and fifty for the second. The exact solutions [24] and the finite element results (for groups 1 and 2) are given in Tables 4.9 to 4.12. The finite element calculation was done for upto P_{17} scattering (nine moments) for a = 1.0 cm and upto P_{13} scattering (seven moments) for a = 5·0 cm. Although the Legendre series expansion for the scattering cross section shows slow convergence as more terms are included in the expansion, the results are in good agreement with analytical solutions for both groups. In the case $a \rightarrow \infty$, Williams's analytical results for group 1 and 2 are:

$$\Phi(x) = \begin{matrix}(4\cdot7620)\\(9\cdot5241).\end{matrix}$$

In this case the finite element calculations with a perfect reflector at both ends of the system gave the following scalar fluxes in groups 1 and 2.

$$\Phi(x) = \begin{matrix}(4\cdot7620)\\(9\cdot5238).\end{matrix}$$

Results for the 5 cm. slab half thickness case also agree with those obtained independently by de Oliveira [25].

x/cm	Analytical	P_1	P_5	P_9	P_{13}	P_{17}
0	2.169	1.6409	2.0839	2.1613	2.1769	2.1777
0.2	2.149	1.6294	2.0627	2.1382	2.1546	2.1566
0.4	2.088	1.5951	1.9981	2.0674	2.0852	2.0903
0.6	1.977	1.5376	1.8879	1.9433	1.9506	1.9688
0.8	1.795	1.4566	1.7284	1.7566	1.7654	1.7722
1.0	1.436	1.3513	1.5137	1.4923	1.4741	1.4639

Table 4.9 Group One Scalar Flux for the BFI Scattering Model Source Problem.

x/cm	Analytical	P_1	P_5	P_9	P_{13}	P_{17}
0	2.608	1.0026	2.2724	2.5818	2.6371	2.6375
0.2	2.557	0.9806	2.2129	2.5180	2.5774	2.5824
0.4	2.398	0.9145	2.0324	2.3205	2.3899	2.4071
0.6	2.107	0.8045	1.7235	1.9700	2.0465	2.0789
0.8	1.618	0.6509	1.2742	1.4315	1.4915	1.5274
1.0	0.578	0.4541	0.6664	0.6480	0.6256	0.6127

Table 4.10 Group Two Scalar Flux for the BFI Scattering Model Source Problem.

a=1.0 cm

Pn represents scattering order.

x/cm	Analytical	P_1	P_5	P_9	P_{13}
0	4.219	4.1953	4.2266	4.2179	4.2187
0.5	4.210	4.1823	4.2177	4.2089	4.2094
1.0	4.181	4.1428	4.1905	4.1810	4.1810
1.5	4.132	4.0748	4.1427	4.1328	4.1318
2.0	4.059	3.9753	4.0701	4.0611	4.0587
2.5	3.956	3.8398	3.9657	3.9606	3.9568
3.0	3.815	3.6619	3.8182	3.8221	3.8178
3.5	3.622	3.4337	3.6093	3.6288	3.6274
4.0	3.352	3.1445	3.3092	3.3482	3.3563
4.5	2.949	2.7812	2.8696	2.9142	2.9345
5.0	2.141	2.3270	2.2115	2.1857	2.1739

a=5.0 cm

Table 4.11 Group One Scalar Flux for the Two Group BFI Scattering Source Problem.

Pn represents scattering order.

x/cm	Analytical	P_1	P_5	P_9	P_{13}
0	7.836	7.7373	7.8581	7.8308	7.8330
0.5	7.807	7.6950	7.8304	7.8022	7.8039
1.0	7.716	7.5661	7.7452	7.7148	7.7148
1.5	7.563	7.3439	7.5954	7.5635	7.5602
2.0	7.332	7.0174	7.3677	7.3382	7.3304
2.5	7.008	6.5696	7.0396	7.0218	7.0093
3.0	6.563	5.9776	6.5738	6.5848	6.5706
3.5	5.925	5.2101	5.9088	5.9729	5.9678
4.0	5.092	4.2264	4.9415	5.0787	5.1054
4.5	3.799	2.9728	3.4951	3.6739	3.7494
5.0	1.175	1.3796	1.2579	1.2282	1.2147

a = 5.0 cm

Table 4.12 Group Two Scalar Flux for the Two Group BFI Scattering Source Problem.

Pn represents scattering order.

4.11.2 P1 and P3 Scattering Source Problems

A two region two group source problem with first P_1 and then P_3 anisotropic scattering was investigated. It was used to compare the finite element multigroup anisotropic scattering calculatinn with other numerical techniques.

Solutions were also obtained from the spherical-harmonics finite-difference code MARC/PN [14], which solves the even parity equation with a finite difference scheme in position space while using spherical harmonics expansion for the angular variable. In addition, the finite-difference discrete-ordinates code ANISN [26], was also used. The aim was to compare the nodal scalar flux for variation in mesh size and angular flux expansion.

(a) The P1 Scattering Case

The cross section data for the P1 scattering calculation is given in Table 4.13. Scalar fluxes obtained from an ANISN S16, 160 mesh calculation were used as reference. The geometry for this problem is shown in Fig. 4.13.

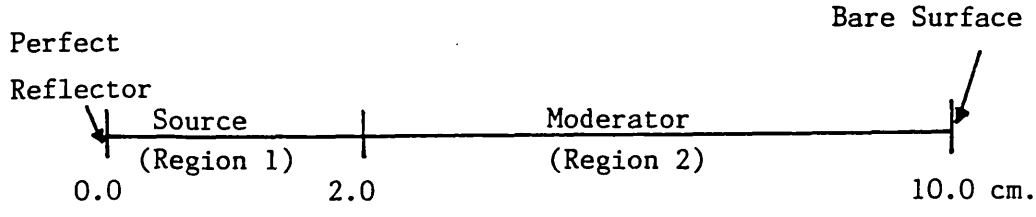


Fig. 4.13 Geometry for the P_1 Scattering Problem

	Source	σ_T	σ_{s0}	σ_{s1}	σ_{s0} $(1\to2)$	σ_{s1} $(1\to2)$
Group 1	1·0	1·0	0·5	0·5		
					0·1	0·05
Group 2	1·0	1·0	0·5	0·5		

Table 4.13 Cross Section Data for Regions One and Two.

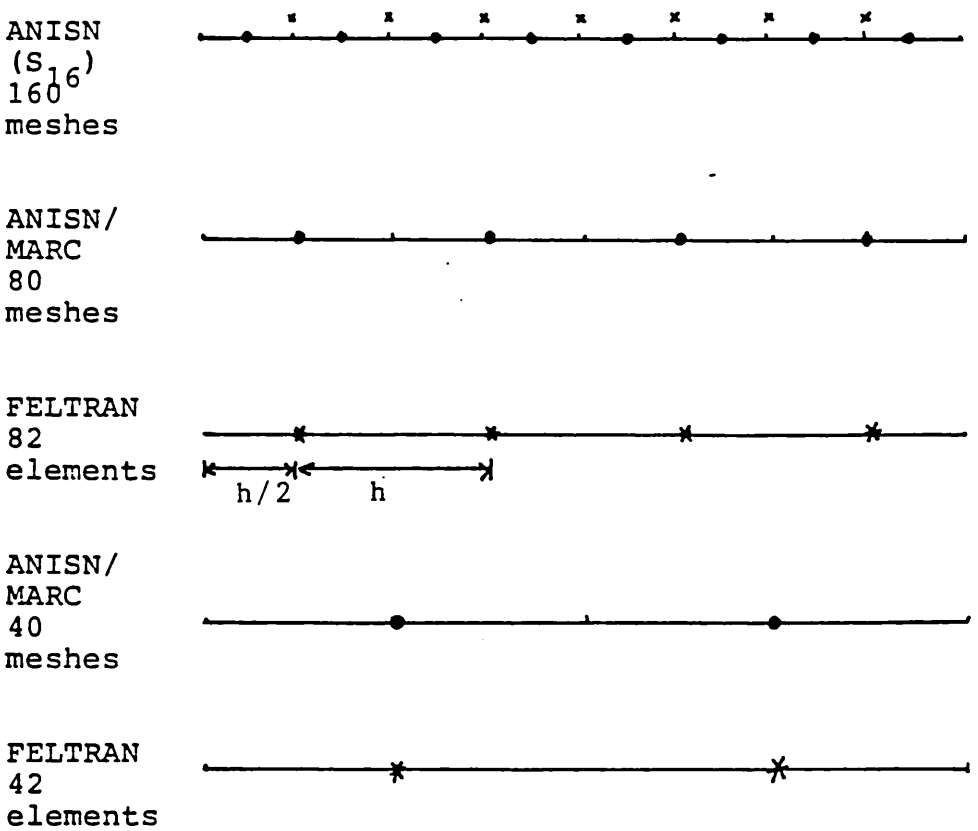
	S	σ_T	σ_{s0}	σ_{s1}	σ_{s2}	σ_{s3}	σ_{s0} $(1\to2)$	σ_{s1} $(1\to2)$	σ_{s2} $(1\to2)$	σ_{s3} $(1\to2)$
Group 1	1·0	1·0	1/2	3/10	1/5	3/35				
							1/2	3/10	1/5	3/35
Group 2	1·0	1·0	1/2	3/10	1/5	3/35				

Table 4.14 Cross Section Data for Regions 1 and 2 for Problem 4.11.2(b)

Calculations were performed for 40 and 80 mesh intervals and for one, two, three and four moment expansion of the even parity angular flux. Because, ANISN and MARC/PN use mesh centered nodes and FELTRAN uses element end nodes, a few additional elements were introduced in the finite element calculation to align the nodes. In the ANISN reference calculation, the scalar flux was linearly interpolated at the end of the mesh interval in order to align them with nodes of all FELTRAN, ANISN and MARC./PN calculations. This is illustrated below in Fig. 4.14.

The difference between FELTRAN scalar fluxes for isotropic and anisotropic scattering is graphically illustrated in Figs. 4.15 and 4.16. Effects of anisotropic scattering are more noticable away from the source region, as expected. Percentage errors (or deviations) were calculated relative to ANISN-S16 mesh values. Figs. 4.17 and 4.18 show the errors for 2 moments, 80 element calculations. Errors from all three codes follow each other closely. At the source moderator interface ANISN, MARC/PN and FELTRAN all give oscillations in percentage error.

If on the other hand, only 40 elements are used in the calculations, but, the number of moments is increased to four, then there is a reduction in percentage error as can be seen in Figs. 4.19 and 4.20. With four moments and 80



● - Mesh centre nodes

x - Linear interpolation

* - Element end nodes

Fig. 4.14 Alignment of Nodes

elements, FELTRAN shows good agreement with the reference fluxes. The error through the moderator region is small and nearly constant for FELTRAN. See Figs. 4.19 and 4.20. Percentage errors for MARC/PN and ANISN are also shown here. It can be seen that FELTRAN scalar flux is bounded below (above) by MARC/PN (ANISN) or 'vice-versa' except near the bare surface boundary.

Subsequently the dimension of the moderation region was extended in order to increase the attenuation in the former to 18 cm, giving an overall system of 20.0 cms. In addition the following scattering law was used for P_1 scattering.

$$\sigma_s(x,\mu_0) = \sigma_s(1+\mu_0)/2 .$$

Here $\sigma_{s0} = 1/2$, $\sigma_{s1} = 1/6$ in both regions and both groups. $\sigma_{s0}_{(1\to2)} = 1/2$ and $\sigma_{s1}_{(1\to2)} = 1/6$, again for both regions. In the above scattering law, the backward component is zero and the forward component unity, hence, providing a more severe test than the previous problem. Scalar fluxes in groups one and two are shown in Figs. 4.21 and 4.22

The percentage errors for the scalar flux relative to ANISN reference values is shown in Figs. 4.23 and 4.24. FELTRAN percentage errors are relatively small for both groups one and two for this deep penetration shield problem with P_1 scattering.

(b) P3 Scattering Case

In the P_3 scattering calculation the moderator region was also extended to 18 cms in order to obtain realistic flux attenuation for the problem. The following scattering function was derived for the P_3 scattering case.

$$\sigma_s(x,\mu_0) = \sigma_s \frac{\mu_0^2}{2}(1+\mu_0) \qquad (4.11\text{-}9)$$

The coefficients σ_{sl} of the Legendre series expansion for $\sigma_s(x,\mu_0)$ can be calculated from

$$\sigma_{sl} = 2\pi \int_{-1}^{1} \sigma_s(x,\mu_0) P_l(\mu_0)\, d\mu_0$$

The scattering law $f(\mu_0) = \frac{\mu_0^2}{2}(1+\mu_0)$ is shown graphically in Fig. 4.25. It is seen that the scattering is predominately forward with no back scattering (i.e. $f(\mu_0) = 0$ for $\mu_0 = -1$) and unit forward scattering. Hence, this provides a good test for the two group anisotropic scattering calculation. Cross section data for this problem is given in Table. 4.14

The isotropic and anisotropic (P3) FELTRAN scalar fluxes are shown in Figs. 4.26 and 4.27. Clearly there is a significant difference in the scalar fluxes at the boundary. In group 1 , the P_3 scattering flux is a factor 28 higher than the isotropic case (with $\sigma_{s_0} = \frac{1}{2}$) and in group 2 a factor 39 higher. This problem then represents a more reasonable test for the multigroup anisotropic scattering calculation in FELTRAN. In this case a four moment , 80 element calculation was done. The reference values were obtained from

an ANISN -S16 (320 mesh intervals) calculation. Percentage errors for FELTRAN, MARC/PN and ANISN are shown in Figs. 4.28 and 4.29. Again all three codes give oscillations at the source moderator interface. Through the moderator region FELTRAN errors are small (less than 2%) while MARC/PN and ANISN deviate towards the bare surface boundary. It may be noted that in the finite element calculation the errors introduced are due to spatial discretisation and truncation of the Legendre series, whereas in ANISN, additional error is introduced in the discretisation of the continuous angular variable. In MARC/PN the large errors near the bare surface may be due to the approximate way the bare surface boundary condition is satisfied in the spherical harmonics method.

In Tables 4.15 and 4.16 FELTRAN (4 moments, 80 elements) and ANISN reference results are given at various positions in the system for both groups. The attenuation through the moderator is approximately 10^{-7} in group 1 and 10^{-6} in group 2.

Group 1

x/cm	FELTRAN *	ANISN REF **
0.125	1.76036	1.75949
0.375	1.74811	1.74706
1.875	1.16774	1.16971
2.125	0.78757	0.78535
2.375	0.55389	0.55585
2.625	0.41592	0.41958
18.875	7.64580E-7	7.77495E-7
19.125	6.25003E-7	6.35673E-7
19.375	5.09395E-7	5.18211E-7
19.625	4.12576E-7	4.19663E-7
19.875	3.28674E-7	3.33956E-7
20.00	2.88921E-7	-

Table 4.15 Group One Scalar Fluxes for Problem 4.11.2(b).

* FELTRAN 82 elements, 4 moments (S8) results.

** ANISN 320 meshes, S16 results.

Group 2

x/cm	FELTRAN *	ANISN REF **
0.125	3.20628	3.20460
0.375	3.17957	3.17762
1.875	2.15892	2.16312
2.125	1.65155	1.64672
2.375	1.29099	1.29081
2.625	1.04268	1.04638
18.875	7.10429E-6	7.21376E-6
19.125	5.86106E-6	5.95205E-6
19.375	4.81770E-6	4.89303E-6
19.625	3.93055E-6	3.99218E-6
19.875	3.14589E-6	3.19123E-6
20.00	2.76610E-6	-

Table 4.16 Group Two Scalar Fluxes for Problem 4.11.2(b).

* FELTRAN 82 elements, 4 moments (S8) results.

** ANISN 320 meshes, S16 results.

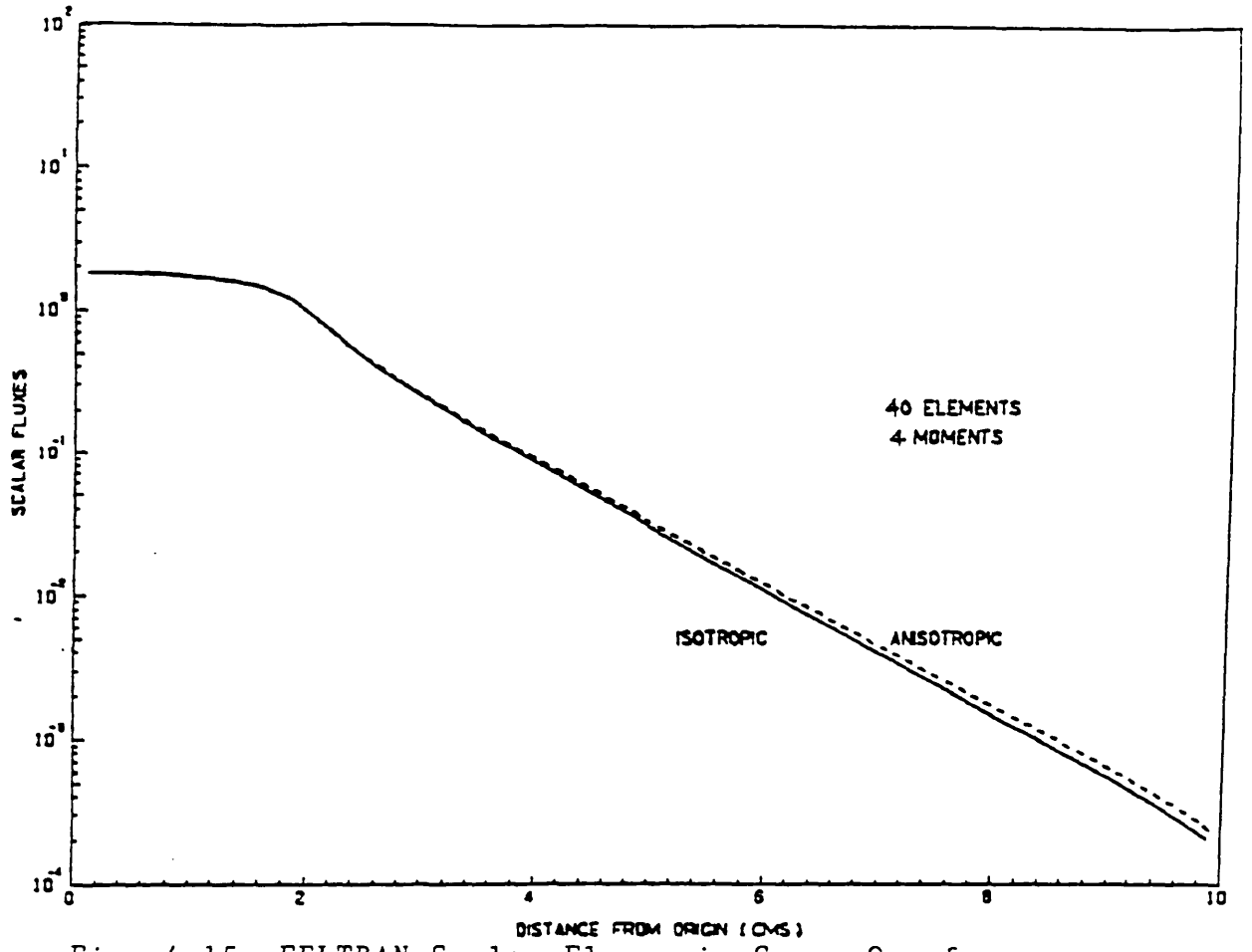


Fig. 4.15 FELTRAN Scalar Fluxes in Group One for Isotropic and Anisotropic (P1) Scattering.

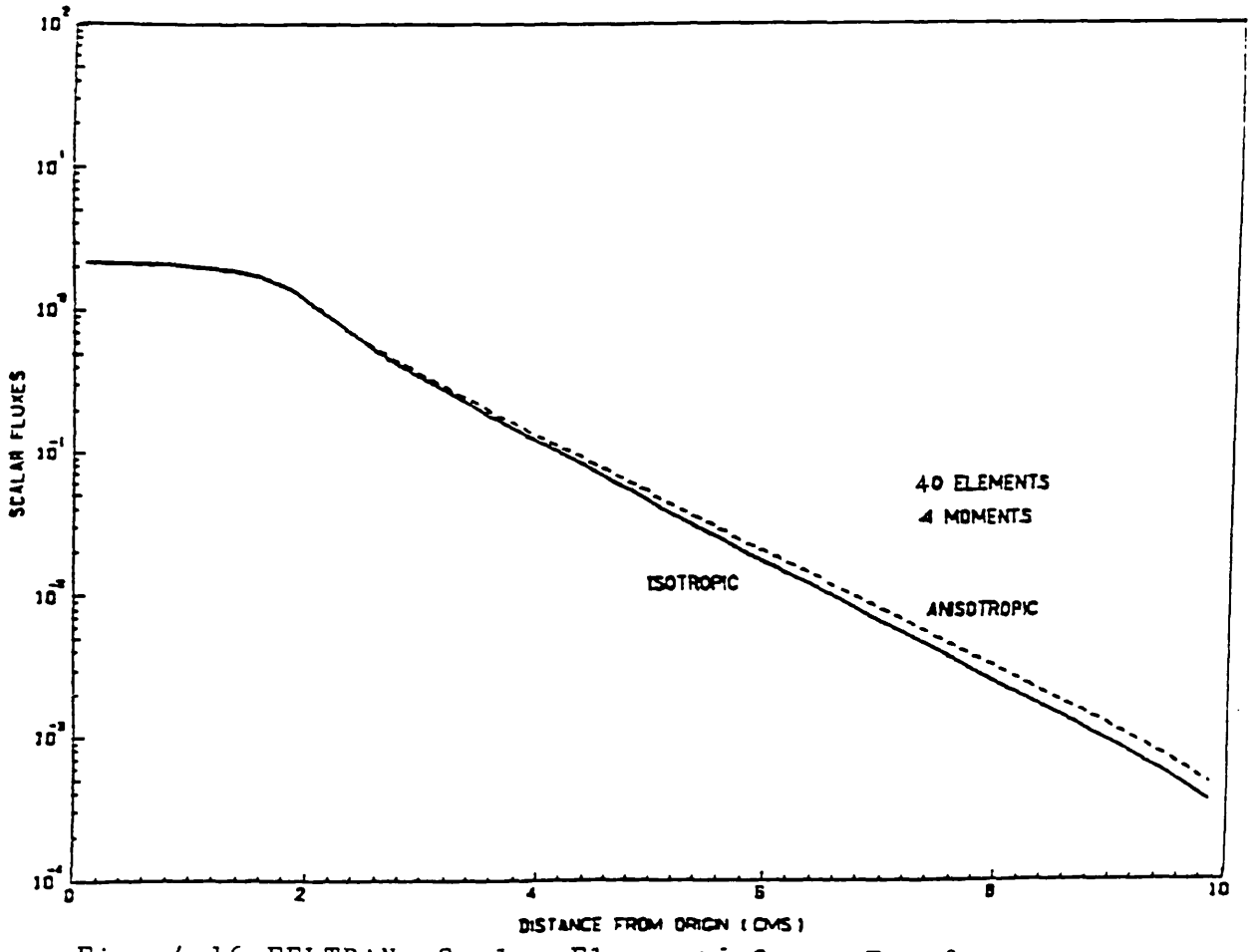


Fig. 4.16 FELTRAN Scalar Fluxes in Group Two for Isotropic and Anisotropic (P1) Scattering.

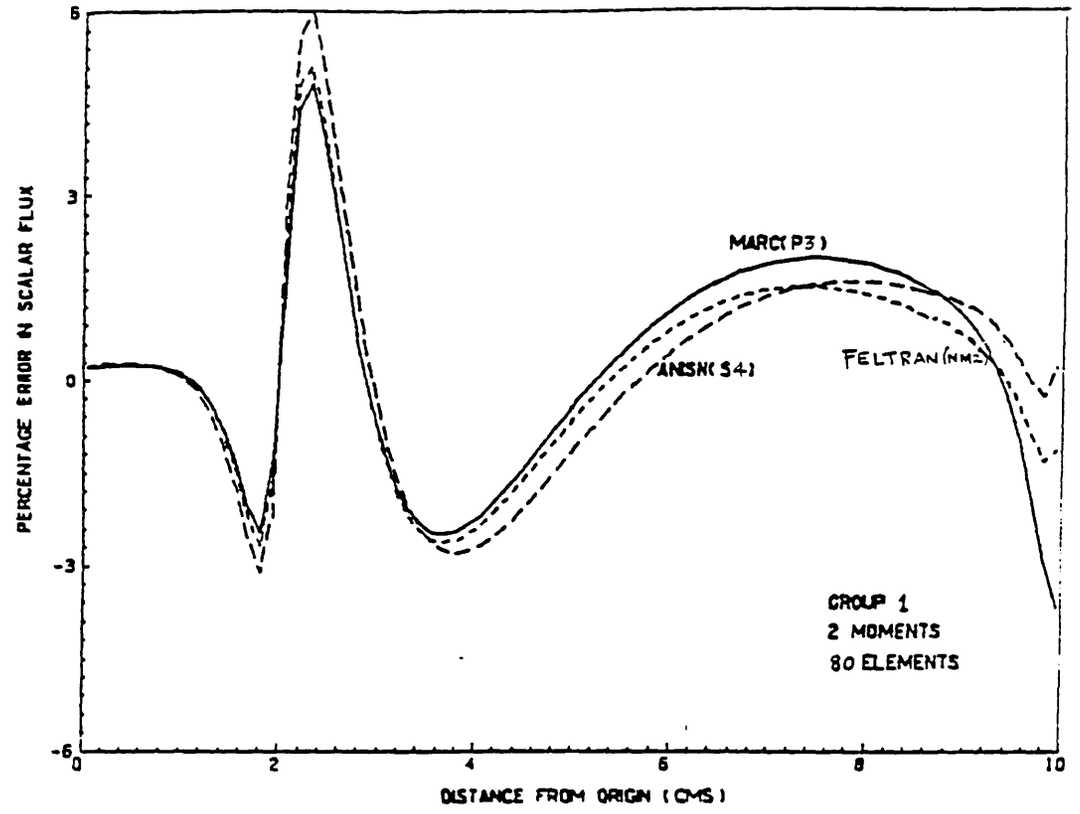


Fig. 4.17 Percentage Errors in Scalar Fluxes (Group 1) for Anisotropic (P1) Scattering.

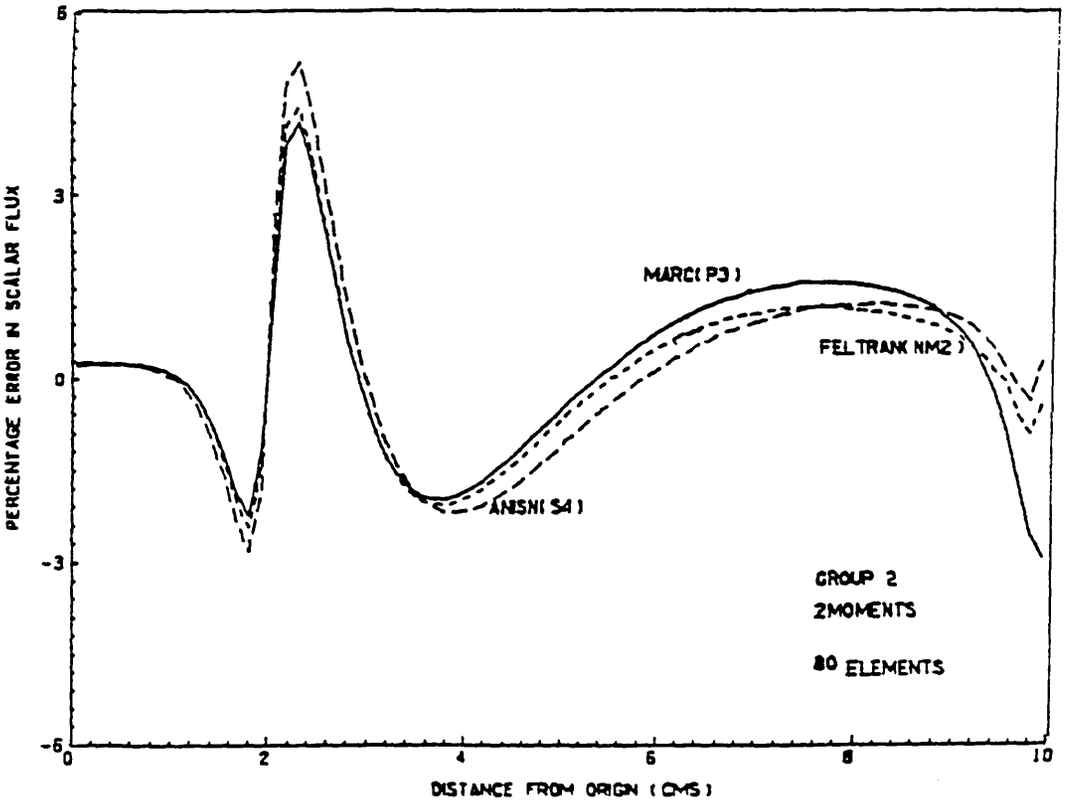


Fig. 4.18 Percentage Errors in Scalar Fluxes (Group 2) for Anisotropic (P1) Scattering.

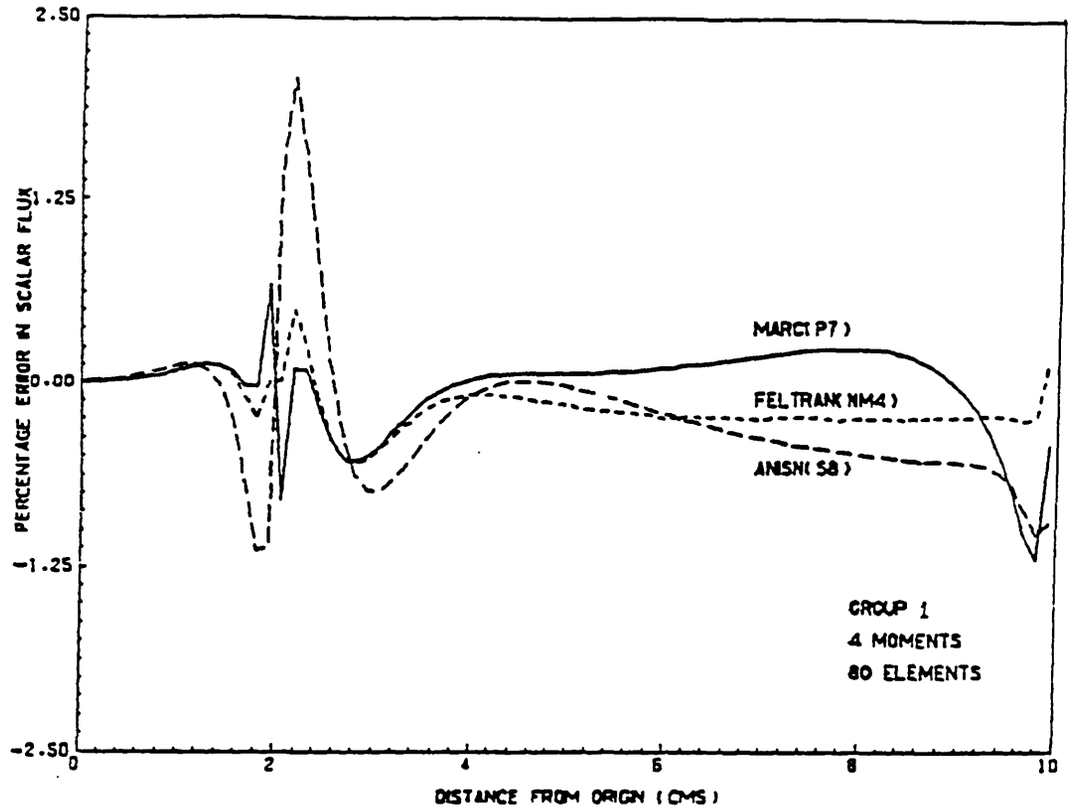


Fig. 4.19 Percentage Errors in Scalar Fluxes (Group 1) for Anisotropic (P1) Scattering Problem.

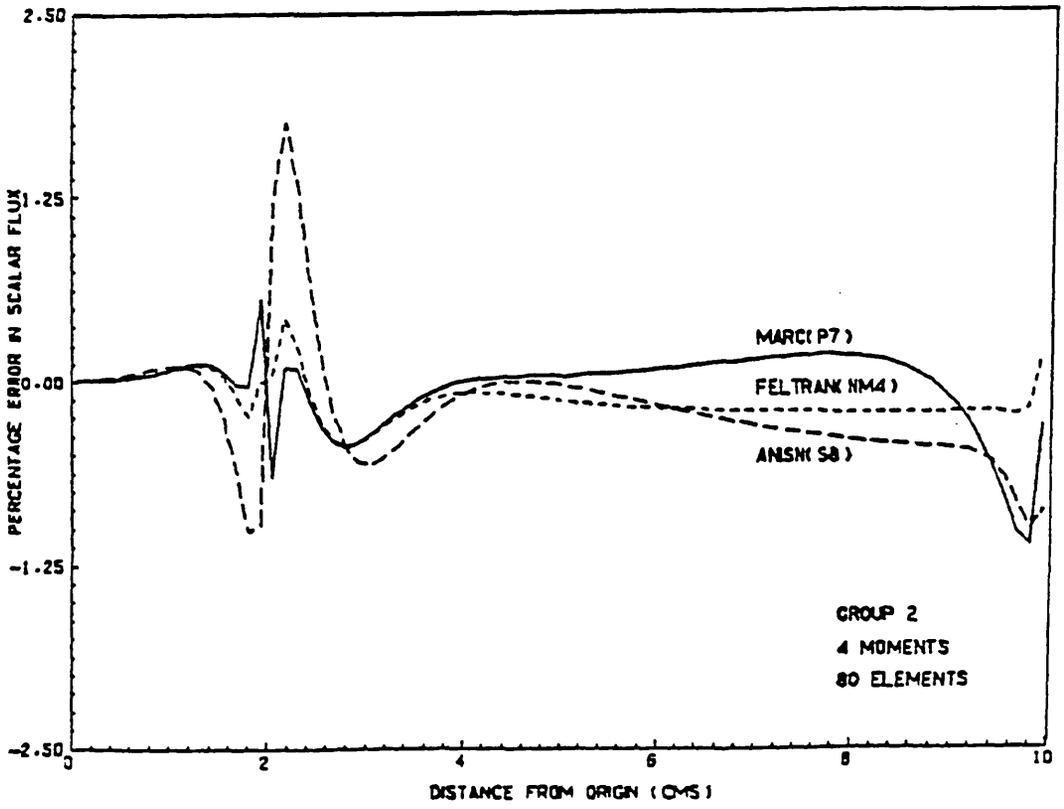


Fig. 4.20 Percentage Errors in Scalar Fluxes (Group 2) for Anisotropic (P1) Scattering Problem.

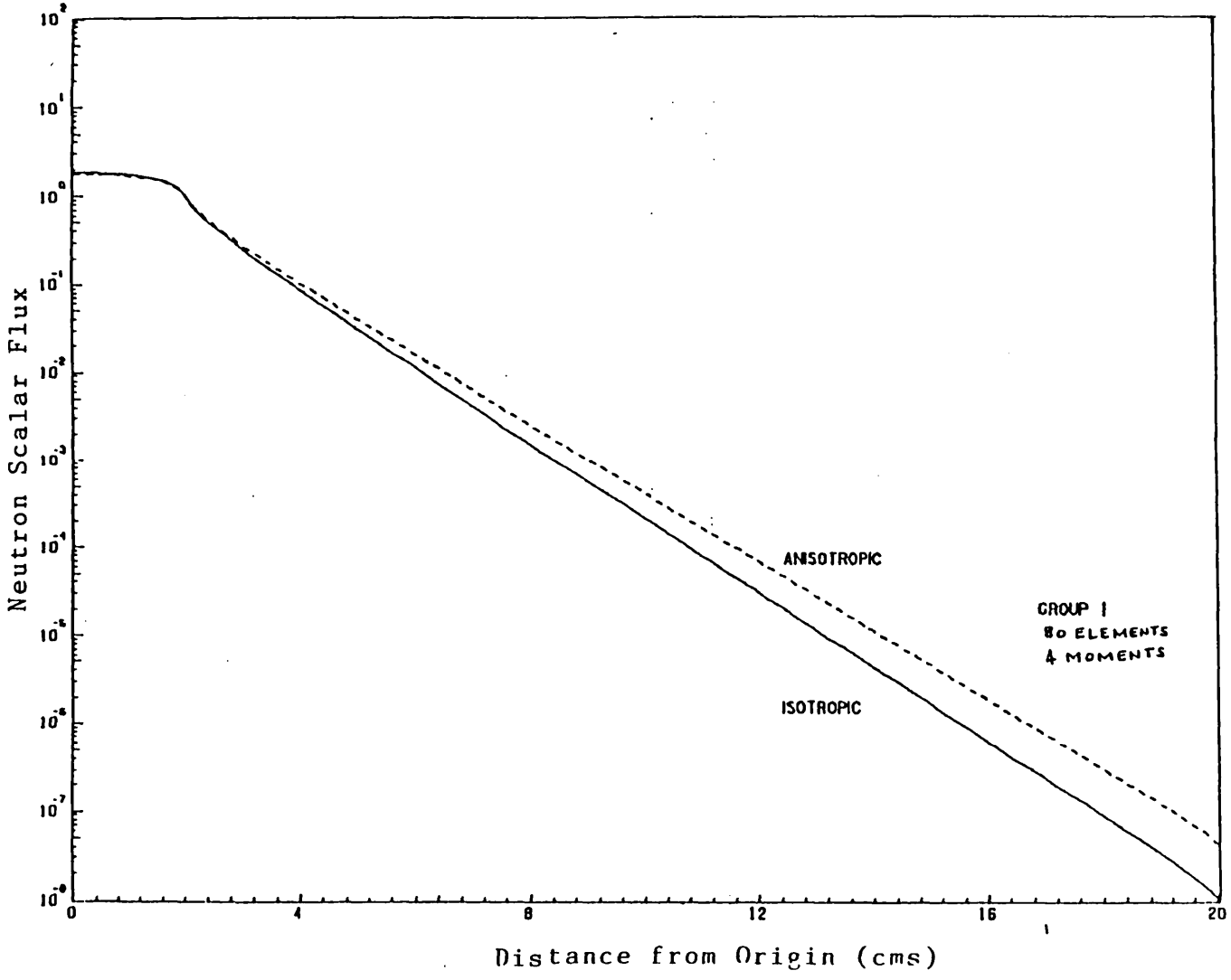


Fig. 4.21 FELTRAN Scalar Fluxes for Isotropic and Anisotropic (P1) Scattering

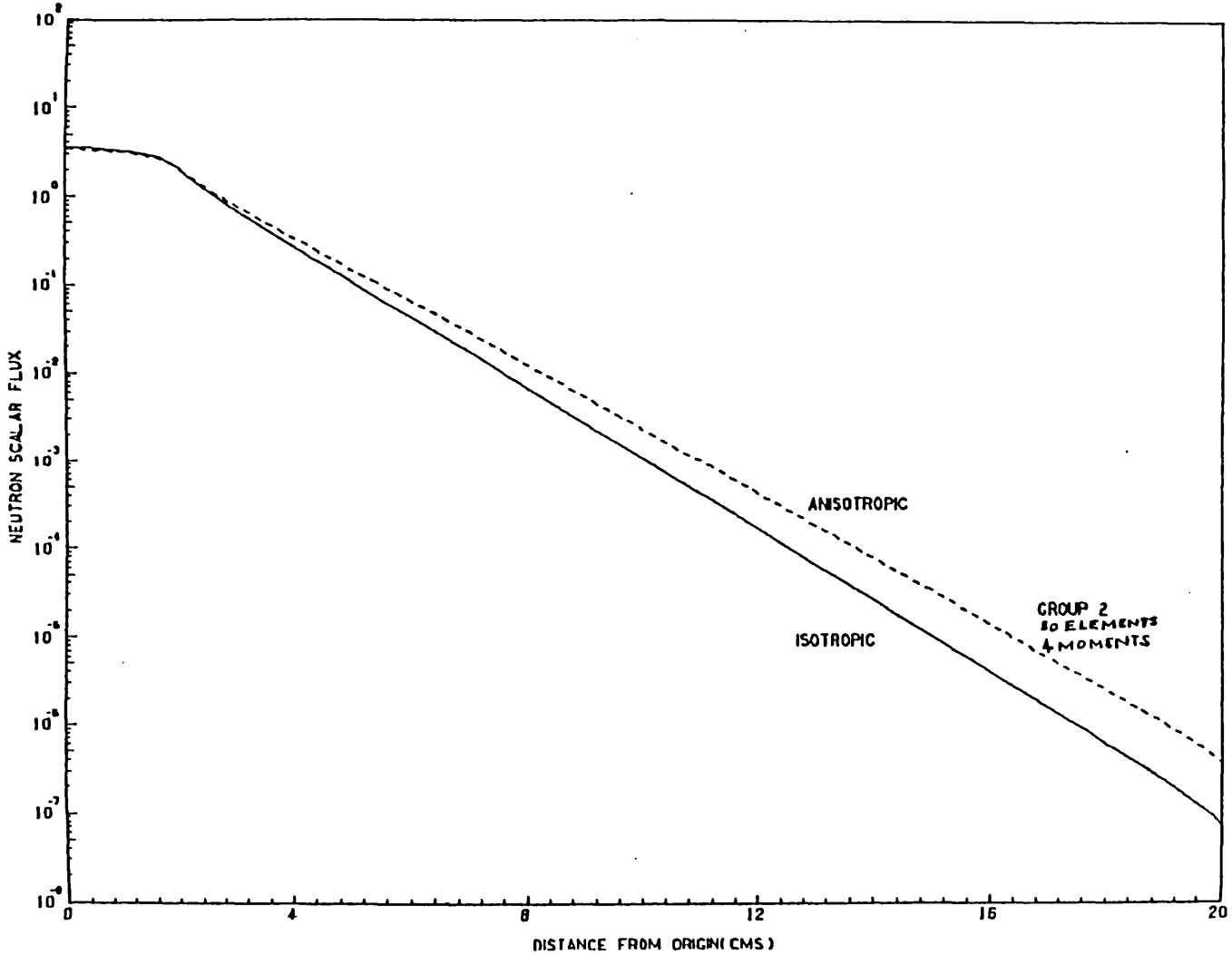


Fig. 4.22 FELTRAN Scalar Fluxes for Isotropic and Anisotropic (P1) Scattering.

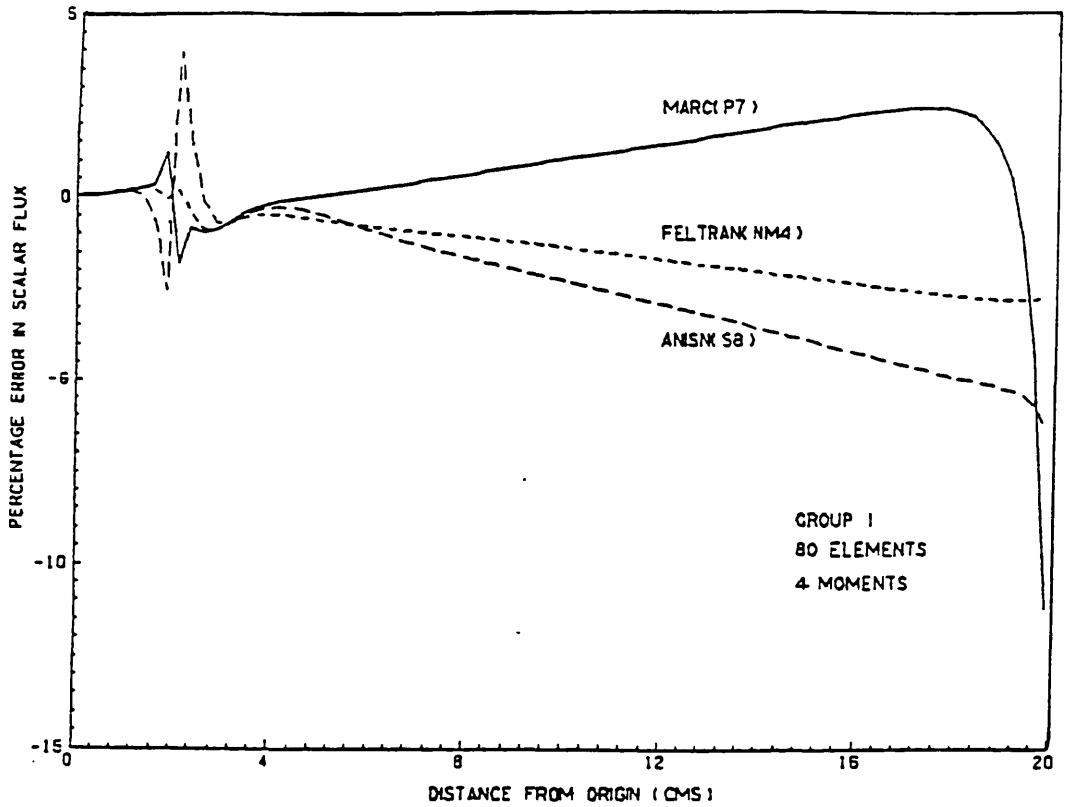


Fig. 4.23 Percentage Errors in Scalar Fluxes for Anisotropic (P1) Scattering.

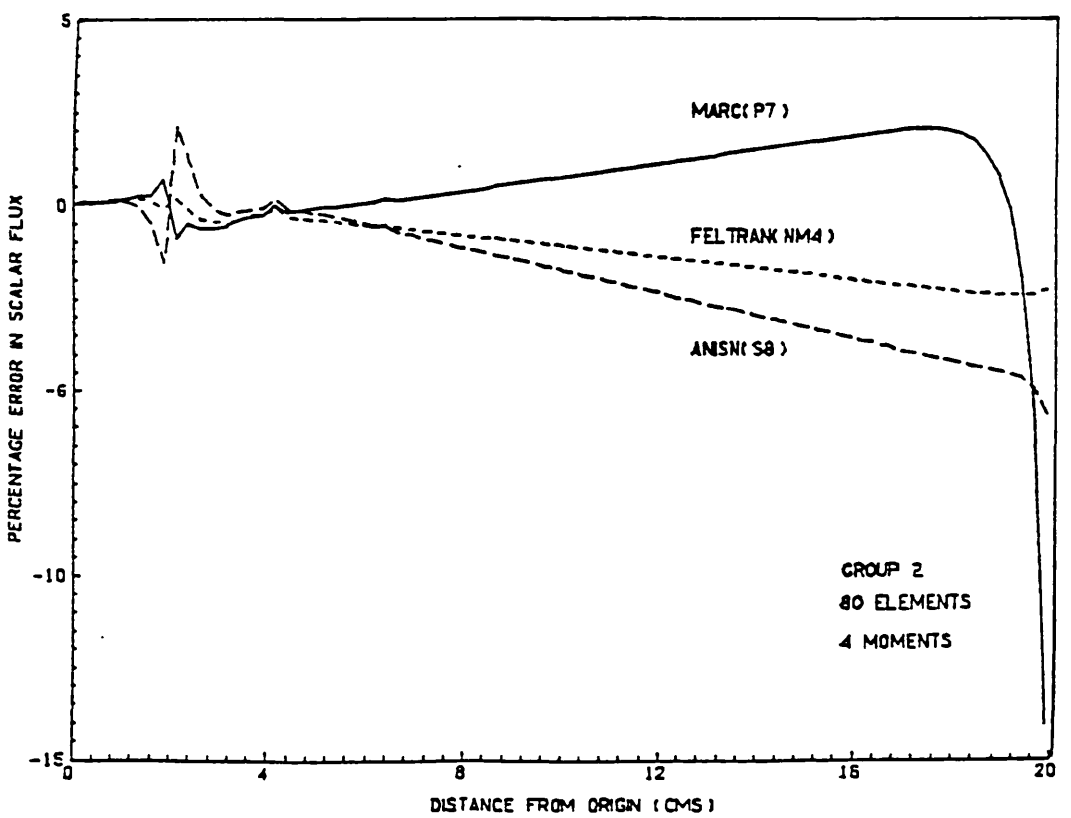


Fig. 4.24 Percentage Errors in Scalar Fluxes for Anisotropic (P1) Scattering.

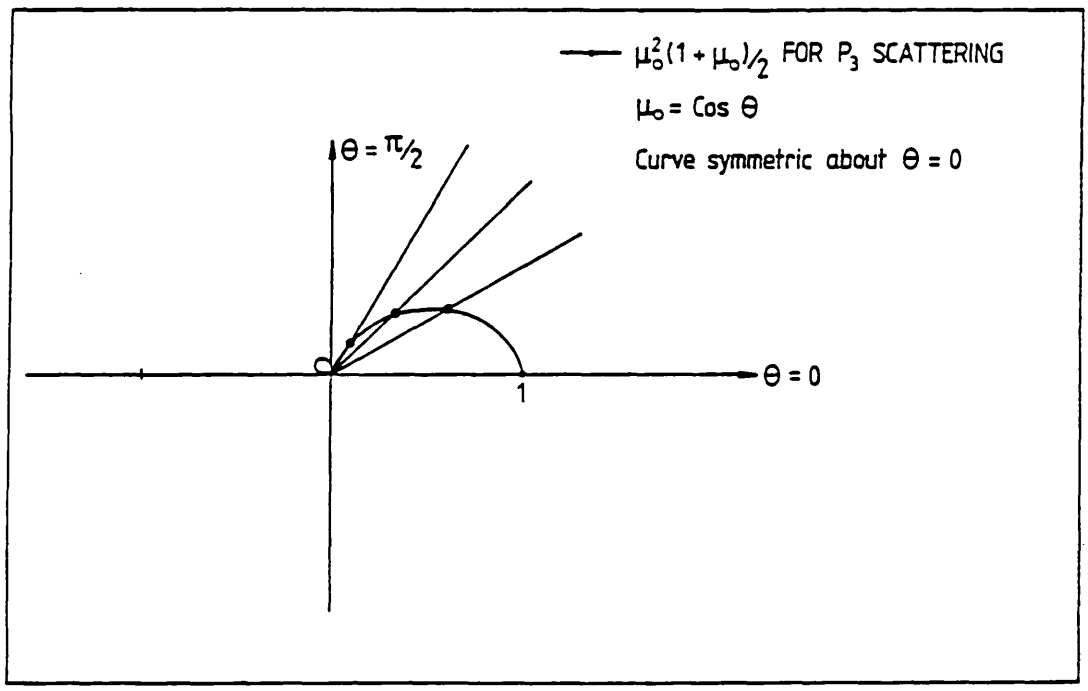


Fig. 4.25 Polar Plot of the Scattering Function used in Problem 4.11.2

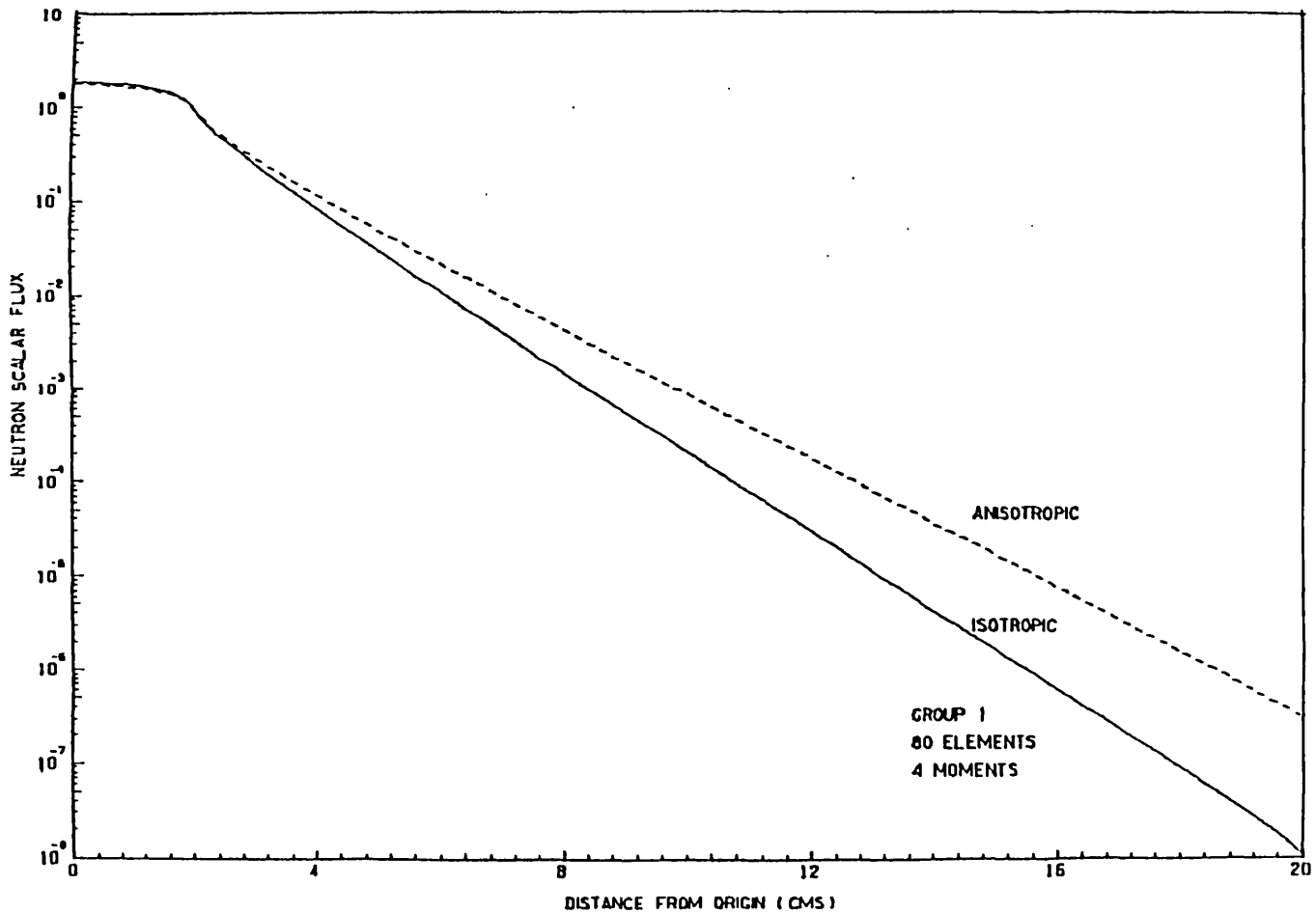


Fig. 4.26 FELTRAN Scalar Fluxes for Isotropic and Anisotropic (P3) Scattering.

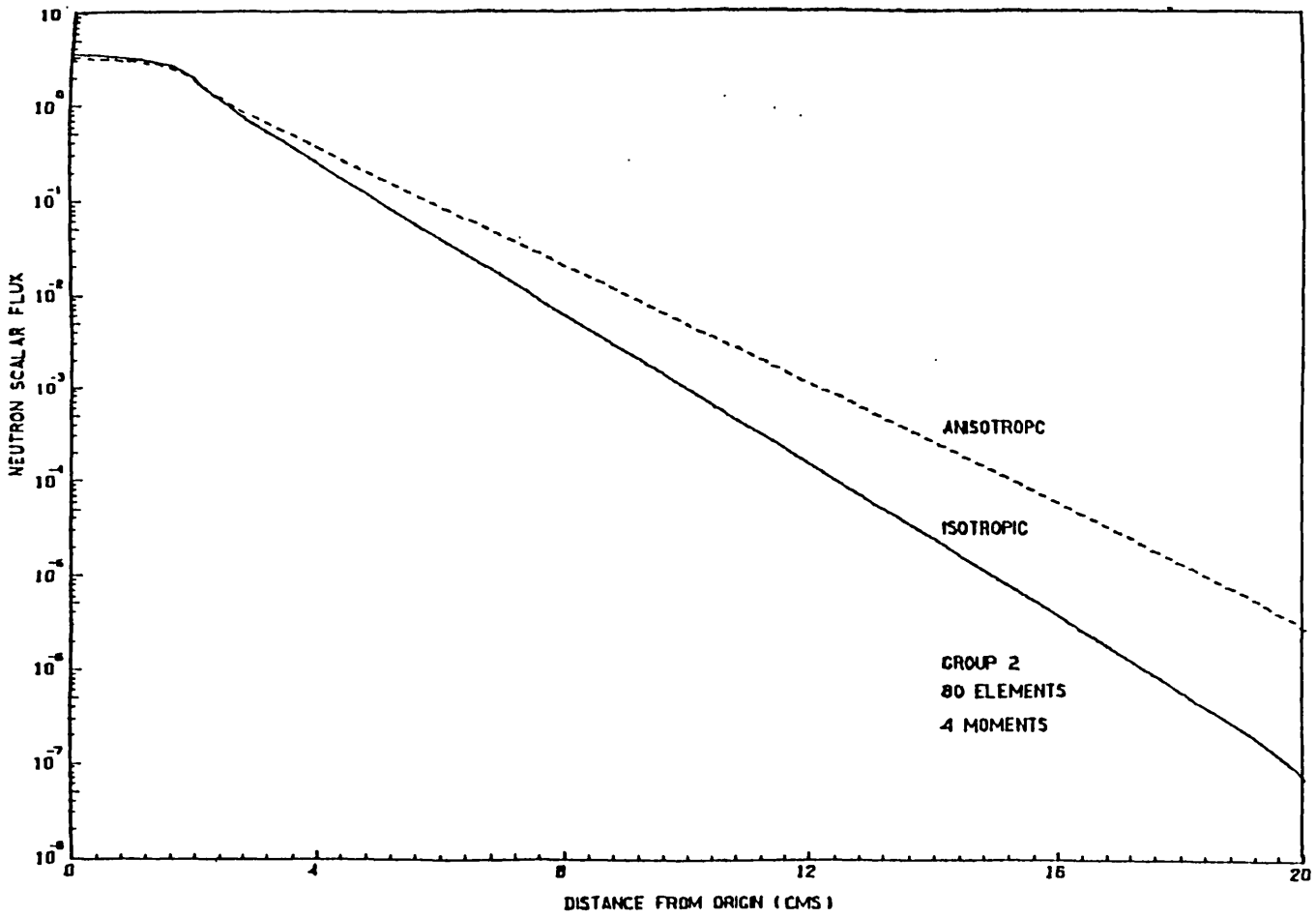


Fig. 4.27 FELTRAN Scalar Fluxes for Isotropic and Anisotropic (P3) Scattering.

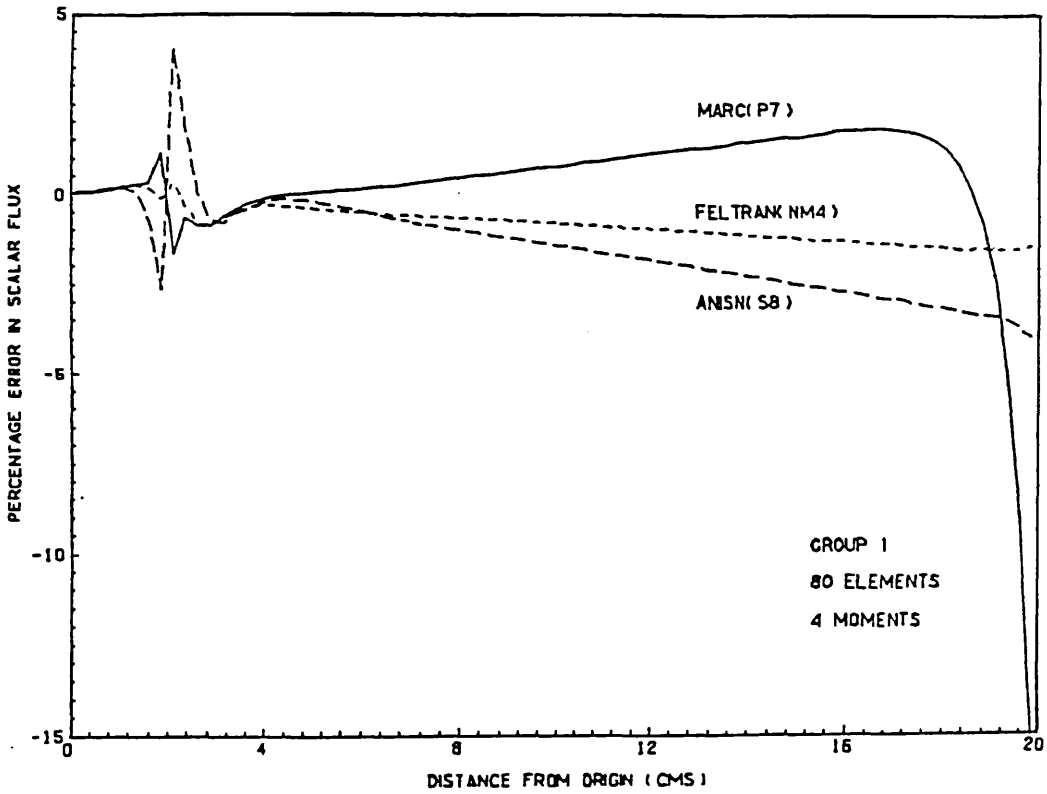


Fig. 4.28 Percentage Errors in Scalar Fluxes for Anisotropic (P3) Scattering.

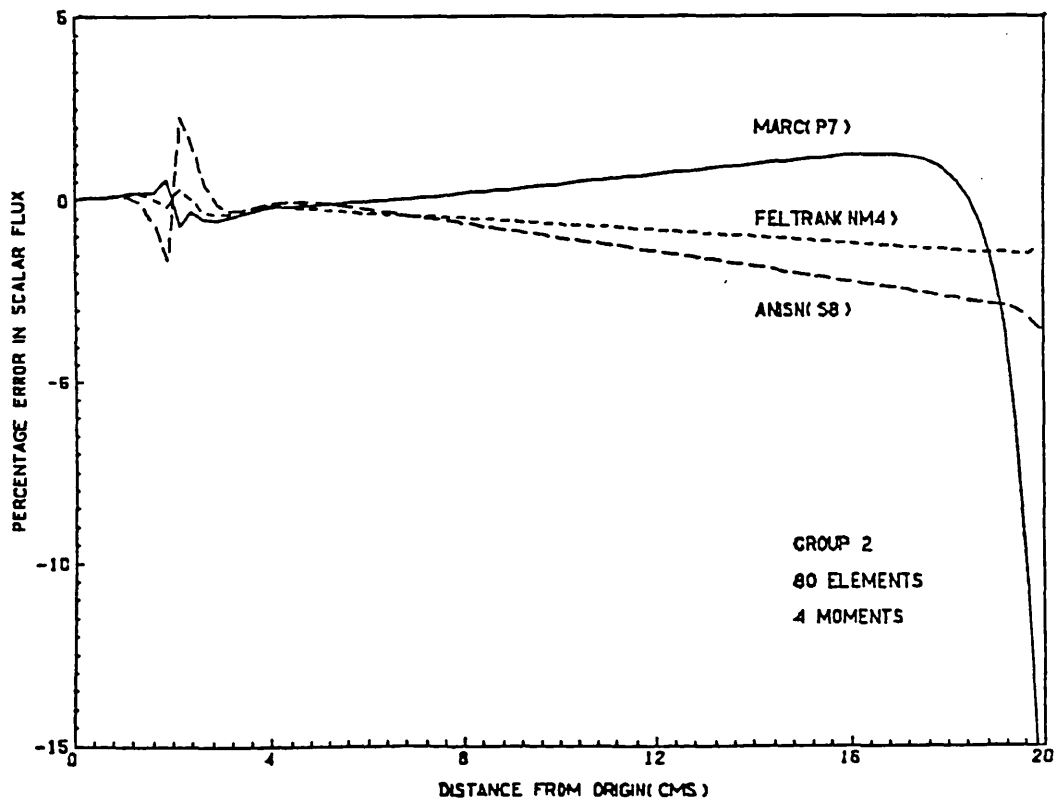


Fig. 4.29 Percentage Errors in Scalar Fluxes for Anisotropic (P3) Scattering.

4.11.3 P1 Scattering Multiregion Source Problem

This three group, P1 scattering, source problem is based on the two-dimensional (r,z) problem analysed by Asoaka et al [27]. The full geometry is shown in Fig. 4.30. Quah [28] also analysed this problem, but, along the line r=10 cm. for the one dimensional slab geometry analogue, with isotropic scattering. He carried out a systematic comparison of finite element calculations of FELTRAN with the discrete ordinates code ANISN. A similar scheme is followed here with linear anisotropic scattering. The geometry along x=10 cm is shown in Fig. 4.31. There is a perfect reflector condition at x=0.0 and a bare surface at x=130 cm. Multigroup cross section data is given in [27].

An ANISN S16 calculation was performed with 630 mesh intervals (ninety in each region). The average scalar flux per unit length $\bar{\phi}_R$ thus obtained, in each region was used as reference. Initially FELTRAN (2 moments) and ANISN (S4) calculations were done for various mesh intervals. In each case the number of mesh intervals were equal in each region. Execution times in CP seconds on the Amdahl 470 V/8 computed are quoted in Table 4.17. ANISN execution times are approximately twice the FELTRAN times. In Table 4.18 are shown the percentage deviations in $\bar{\phi}$ (the average scalar flux) for two moments and 560 elements. In groups 1 and 2, both ANISN and FELTRAN give similar errors upto region 5, which is the

first void. In this, and subsequent regions ANISN (S4) deviations are less than those of FELTRAN. It appears that the two moment flux expansion in FELTRAN is not sufficiently good here.

The convergence of $\bar{\phi}$ with $\left(\frac{M_{max}}{M}\right)^2$ is shown for regions 4 (iron) and 6 (water) in Figs. 4.32 and 4.33. FELTRAN shows an approximately linear variation in $\bar{\phi}$ with $\left(\frac{M_{max}}{M}\right)^2$ over the whole range of the latter. This means that with only the first two values of $\bar{\phi}$ from a coarse mesh calculation the results can be predicted to within a few percent with linear extrapolation.

Subsequently FELTRAN and ANISN were compared for varying number of moments and with 200 elements. In this case the number of elements in each region was different. The element scheme region-wise was (10,10,20,40,40,40,40). Percentage deviations for the four moment calculations are shown in Table 4.19. In Figs. 4.34 and 4.35 the scalar flux obtained for FELTRAN (4 moments and 200 elements) calculation are shown for groups one and two. It is seen that although the one and four moment cases give similar fluxes near the source region, there is a significant difference from x=80 cm onwards out to the bare surface boundary. Next the number of elements in regions 1,2and 3 were doubled while those in regions 4,5,6,7 were kept constant. A four

moment calculation was performed. Percentage errors are shown in Tables 4.20 (a,b,c), together with the average scalar flux values. Both FELTRAN and also ANISN errors are relatively small for an attenuation of approximately 10^{-6}. See also Riyait [29].

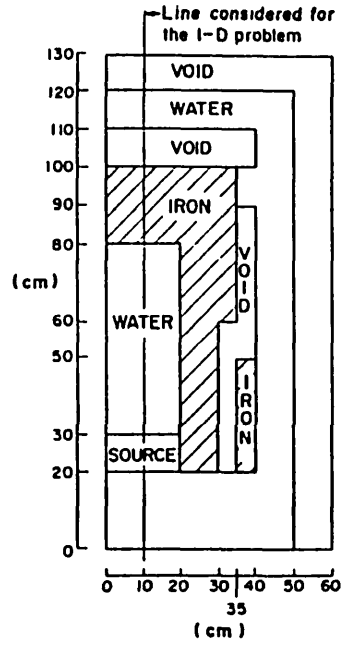


Fig. 4.30

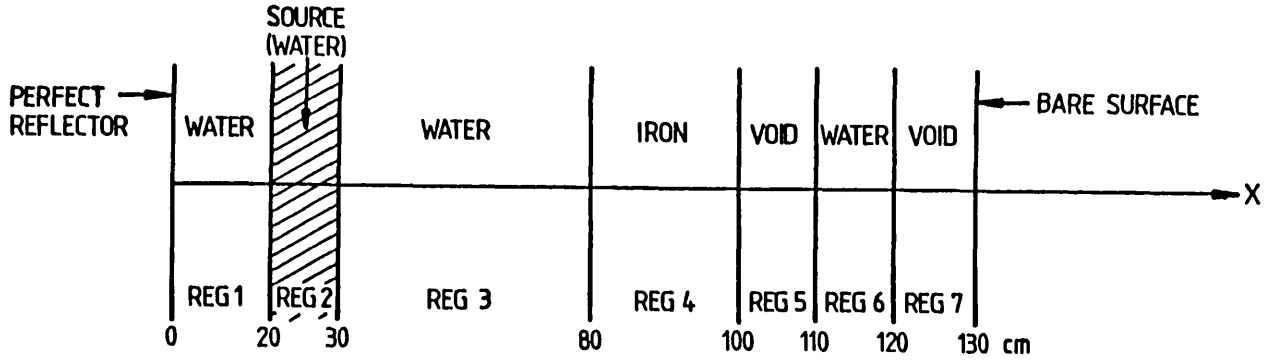


Fig. 4.31 Geometry for the Multiregion Source Problem.

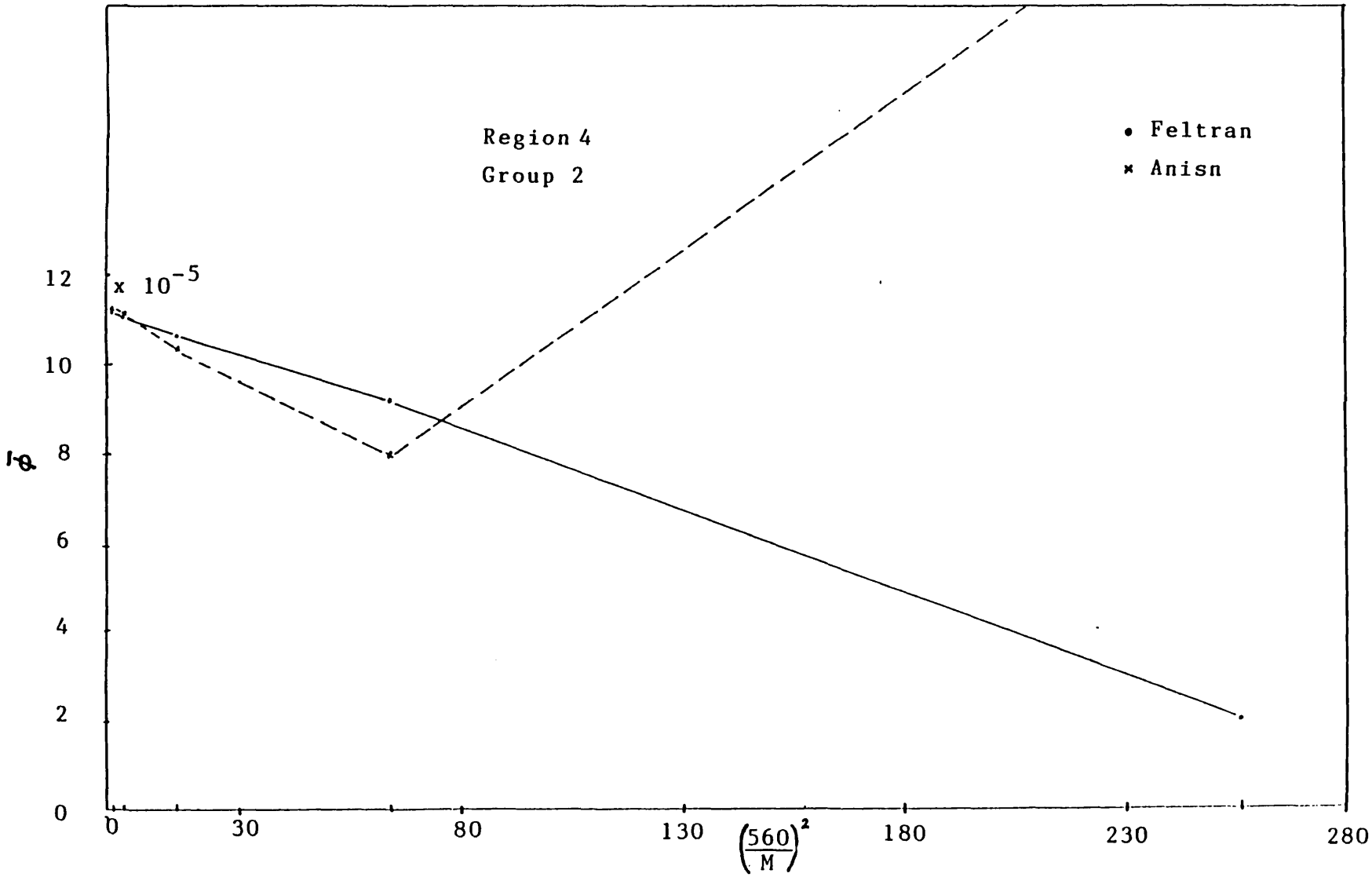


Fig. 4.32 Convergence of average scalar flux in region 4 with square of inverse mesh interval for problem 4.11.3

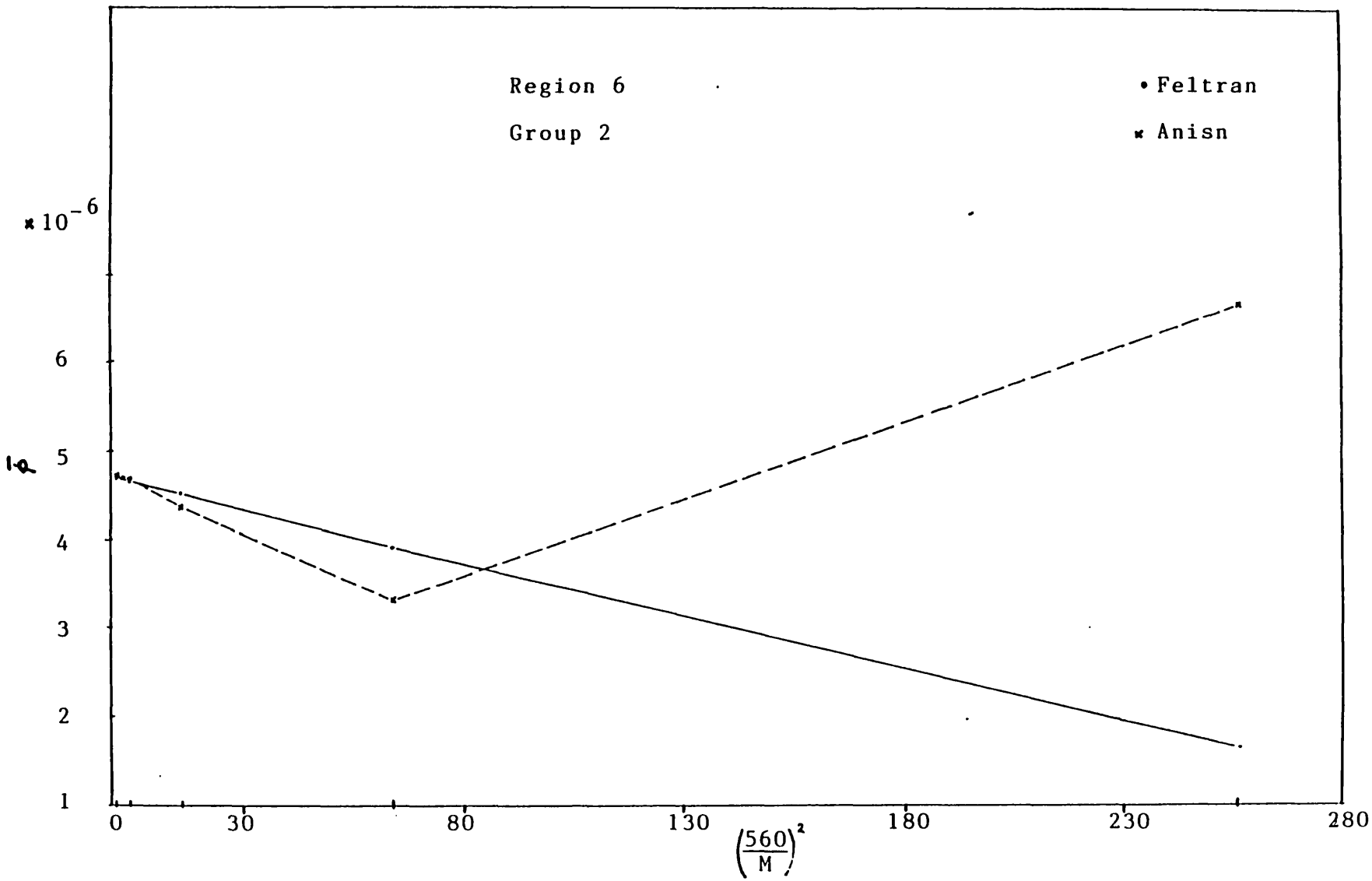


Fig. 4.33 Convergence of average scalar flux in region 6 with square of inverse mesh interval for problem 4.11.3

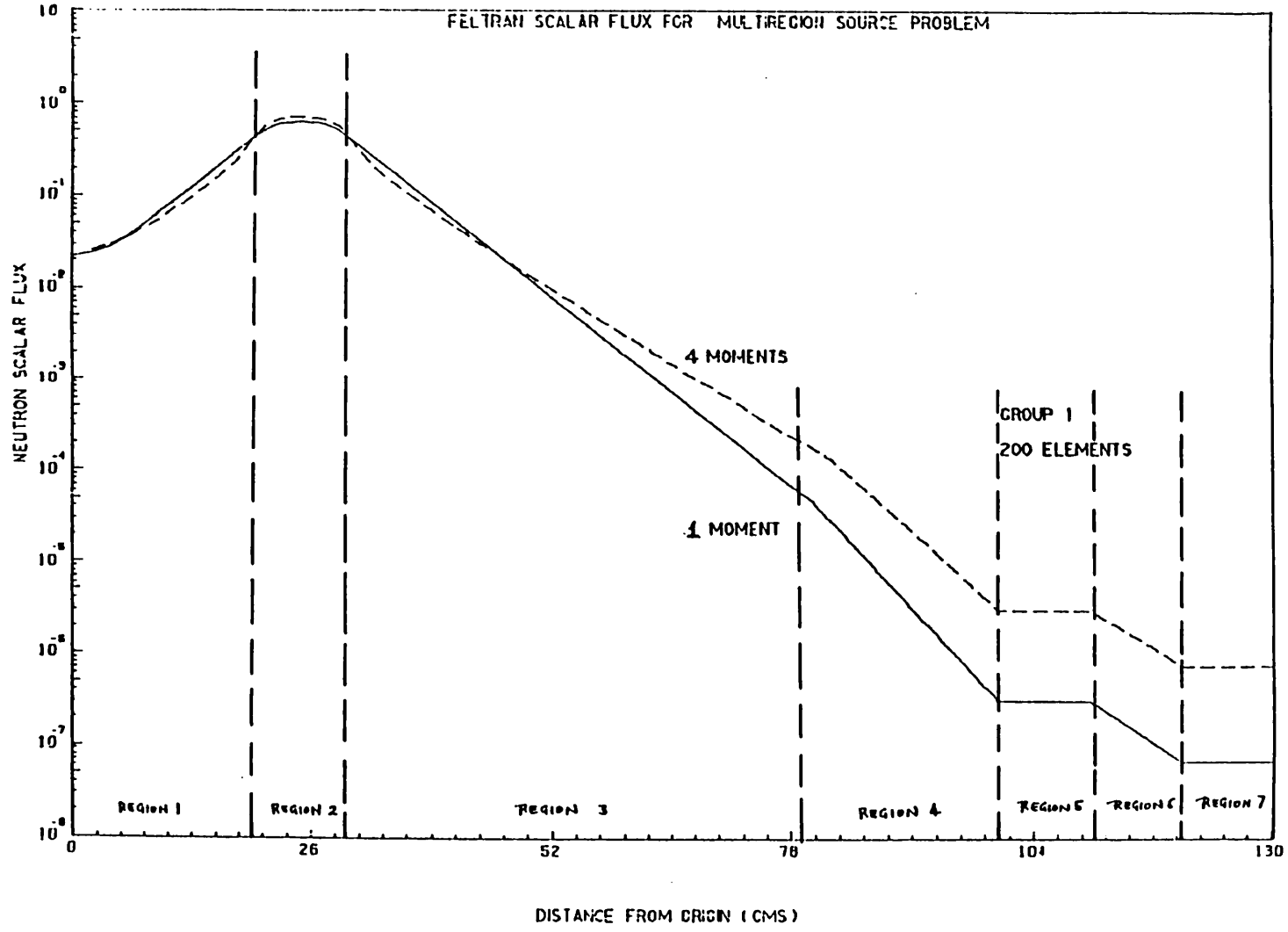


Fig. 4.34 Feltran group 1 scalar fluxes for multiregion source problem.

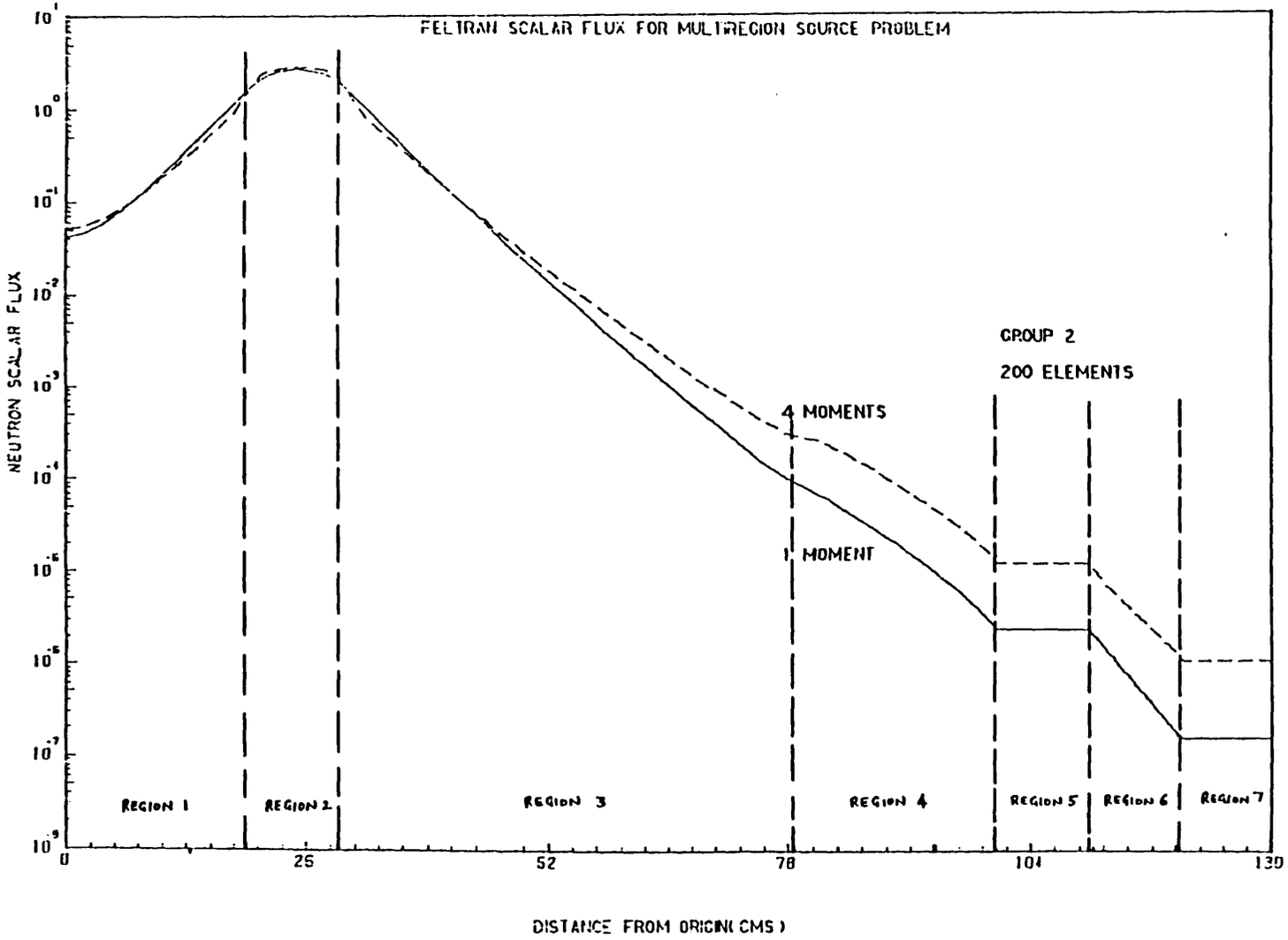


Fig. 4.35 Feltran group 2 scalar fluxes for multiregion source problem.

No. of Mesh Intervals	FELTRAN (NOM =2) (CP Seconds)*	ANISN(S4) (CP Seconds)*
35	0.36	0.70
70	0.49	0.80
140	0.77	1.31
280	1.32	2.27
560	2.44	5.49

Table 4.17 Execution times for FELTRAN and ANISN for various mesh intervals for Problem 4.11.3

No. of Mesh Intervals	Region	Group 1		Group 2	
		Δ% Feltran	Δ% Anisn	Δ% Feltran	Δ% Anisn
80	1	3.05	3.43	1.81	2.05
80	2	-1.96	-2.18	-0.95	-1.06
80	3	3.08	3.42	1.87	2.05
80	4	-0.23	0.74	-0.21	0.38
80	5	-3.25	-1.64	-0.51	0.45
80	6	-3.67	-1.98	-0.74	0.25
80	7	-4.19	-1.99	-1.04	0.06

Table 4.18 Percentage derivation in average scalar flux for 2 moments and 560 elements for Problem 4.11.3

4 Moments

No. of Mesh Intervals	Region	Group 1		Group 2	
		Δ% Feltran	Δ% Anisn	Δ% Feltran	Δ% Ansin
10	1	1.06	0.79	1.28	0.52
10	2	-0.78	-0.49	-0.78	0.27
20	3	1.38	0.77	1.72	0.51
40	4	-3.19	-6.69	-4.22	-8.21
40	5	-2.93	-6.69	-3.83	-7.84
40	6	-2.89	-6.75	-3.76	-7.79
40	7	-2.29	-6.60	-2.86	-7.53

Table 4.19 Percentage deviations in average scalar flux for the P_1 scattering multigroup source problem.

Group 1

Meshes	Region	$\bar{\phi}$(Feltran)	$\bar{\phi}$(Anisn)	Δ%Feltran	Δ%Anisn
20	1	1.0054E-1	1.0075E-1	0.50	0.72
20	2	6.1224E-1	6.1156E-1	-0.35	-0.46
40	3	4.0458E-2	4.0509E-2	0.59	0.71
40	4	4.8154E-5	4.7683E-5	-0.53	-1.50
40	5	3.0779E-6	3.0390E-6	-0.33	-1.59
40	6	1.6582E-6	1.6357E-6	-0.29	-1.65
40	7	7.5785E-7	7.4409E-7	0.33	-1.50

Table 4.20(a) Average scalar flux and percentage deviations in $\bar{\phi}$ for 240 elements and 4 moments.

Group 2

Region	$\bar{\phi}$ (Feltran)	$\bar{\phi}$ (Anisn)	Δ% Feltran	Δ% Anisn
1	3.5074E-1	3.5063E-1	0.47	0.44
2	2.6324	2.6337	-0.28	-0.23
3	1.4075E-1	1.4053E-1	0.59	0.44
4	1.1114E-4	1.0991E-4	-0.76	-1.86
5	1.3241E-5	1.3091E-5	-0.60	-1.73
6	4.7256E-6	4.6703E-6	-0.57	-1.73
7	1.1710E-6	1.1492E-6	0.27	-1.59

Table 4.20(b) Average scalar flux and percentage deviations in $\bar{\phi}$ for 240 elements and 4 moments for Problem 4.11.3

Group 3

Region	$\bar{\phi}$(Feltran)	$\bar{\phi}$(Anisn)
1	5.7175E2	5.7174E2
2	5.5737E2	5.5729E2
3	3.6346E2	3.6336E2
4	1.3529E2	1.3519E2
5	8.3070E1	8.3297E1
6	5.0792E1	5.0674E1
7	1.5744E1	1.5467E1

Table 4.20(c) Average scalar flux for 240 elements and 4 moments for Problem 4.11.3

4.11.4 P3 Scattering Eigenvalue Problem

This is a three region three group eigenvalue problem with P3 scattering which is presented in Reference [26]. There it is solved in one dimensional spherical geometry and is infact a critical sphere problem. We have used the data given in [26] to test FELTRAN for one dimensional keff calculation. The geometry for the problem is shown below in Fig. 4.36.

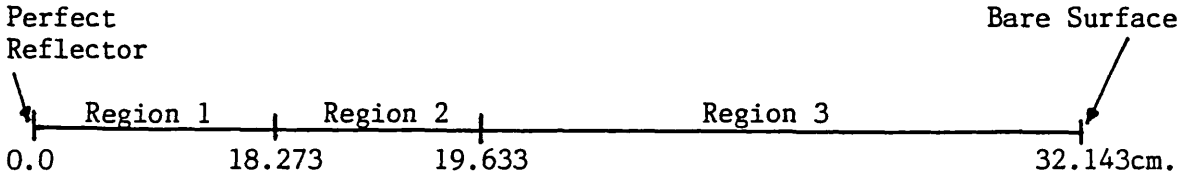


Fig. 4.36

The k-eff calculations were carried out for two and three moments with varying number of elements. Results from FELTRAN and ANISN are shown in Tables 4.21 and 4.22. Initially, five, one and three elements were used in Regions 1,2 and 3 respectively. These were subsequently increased by a factor of two each time.

Execution times on the Amdahl computer for FELTRAN and ANISN are given for three moments in Table 4.23. The k-eff values of both the finite element and finite difference calculations are in good agreement.

2 MOMENTS

Number of Elements	k-eff	
	FELTRAN	ANISN
9	1.43244	1.43036
18	1.43230	1.43202
36	1.43216	1.43236
72	1.43213	1.43242
144	1.43212	1.43244

Table 4.21

3 MOMENTS

Number of Elements	k-eff	
	FELTRAN	ANISN
9	1.43246	1.43047
18	1.43238	1.43211
36	1.43223	1.43244
72	1.43219	1.43249
144	1.43219	1.43252

Table 4.22

3 MOMENTS

Number of Elements	ANISN	FELTRAN
9	0.59	0.60
18	0.89	0.78
36	1.16	1.07
72	1.96	1.72
144	3.55	2.93

Table 4.23 Execution times in CP seconds on the Amdahl

REFERENCES TO CHAPTER 4

1. BROCKMANN, H.
"Treatment of Anisotropic Scattering in Numerical Transport Theory".
Nucl. Sci. Engng. 77, p377 (1981)

2. ACKROYD, R.T.
"A Finite Element Method for Neutron Transport - I. Some Theoretical Considerations".
Ann. Nucl. Energy. 5, p 75 (1978)

3. ACKROYD, R.T.
"The Finite Element Method for Neutron Transport I. The Even Parity Equation for Neutron Transport and its Maximum and Minimum Variational Principles".
UKAEA, TRG Report. 2705(R) (1975)

4. ABRAMOWITZ, M. and STEGUN, I
"Handbook of Mathematical Functions".
Dover Publications. (1965)

5. MAGNUS, W., OBERHETTINGER, F. and SONI, R.P.
"Formulas and Theorems for the Special Functions of Mathematical Physics".
Springer Verlag. (1966)

6. CAREY, G.F., and ODEN, J.T.
"The Texas Finite Element Series, Vol II, A Second Course".
Prentice-Hall (1983)

7. ZIENKIEWICZ, O.C.
"The Finite Element Method".
McGraw Hill Book Company Ltd. (1977)

17. RIYAIT, N.S.
" The Finite Element Method for Multigroup Neutron Transport With Anisotropic Scattering: The Reduced Functional in X-Y Geometry". Report SAF 078, Imperial College, London. (1985)

18. ISSA, J.G., RIYAIT, N.S., GODDARD, A.J.H. and STOTT, G.E.
"Multigroup Application of the Anisotropic FEM code FELTRAN to 1,2 and 3D Problems".
Prog. Nucl. Energy, 18, 1/2, p251 (1986)

19. ISSA, J.G.
"On the Exact Evaluation of the Spherical Harmonics Integrals Within the Finite Element Method in Various Geometries". Internal Report. Imperial College, London. (1984)

20. ACKROYD, R.T. and WILLIAMS, M.M.R.
"An Extended Variational Principle for an Albedo Boundary Condition".
Ann. Nucl. Energy, 11(6), p269 (1984)

21. INONU, E.
"Scaling and Time Inversion for the Linear Mono-Energetic Boltzmann Equation".
Phys. of Fluids, 19, 9, p1332 (1976)

22. LATHROP, K.D.
"Anisotropic Scattering Approximations in the Monoenergetic Boltzmann Equation".
Nucl. Sci. Engng. 21, p498 (1965)

23. GALLIARA, J.S. and WILLIAMS, M.M.R.
"A Finite Element Method for Neutron Transport. Part II: Some Practical Considerations".
Ann. Nucl. Energy, 6, p205 (1979)

24. WILLIAMS, M.M.R.
"The Energy Dependent Backward-Forward-Isotropic Scattering Model With Some Applications to the Neutron Transport Equation".
Ann. Nucl. Energy, 12(4), p167 (1985)

25. DE OLIVEIRA, C.R.E.
"An Arbitrary Geometry Finite Element Method for Multigroup Neutron Transport With Anisotropic Scattering".
Prog. Nucl. Energy, 18, 1/2, p227 (1986)

26. ENGLE, W.W.
"ANISN-ORNL, A One Dimensional Discrete Ordinates Transport Code".
CCC-254 Computer Technology Centre, Union Carbide Corporation, Oak Ridge. (1973)

27. ASOAKA, T., ASANO, N., NAKAMURA, H., MIZUTA, H., CHICHIWA, H.,OHNISHI, T., MIYASAKA, S., ZUKERAN, A., TSUTSUI, T., FUJIMURA, T. and KATSURAGI, S.
"Benchmark Tests of Radiation Transport Computer Codes for Reactor Core and Shield Calculations".
Jour. of Nucl. Sci. and Tech. 15(1), p56 (1978)

28. QUAH, C.S.
"A Comparison of Finite Elements and Discrete Ordinates Methods for One Dimensional Multigroup Problems".
Ann. Nucl. Energy, 8, p709 (1981)

29. RIYAIT, N. S.
"The Finite Element Method for Multigroup Neutron Transport: Few Group Test Problems With Anisotropic Scattering".
Report SAF 076. Imperial College, London. (1985)

CHAPTER 5

5. TREATMENT OF VOIDS

5.1 Introduction
5.2 Conventional FEM for Voids
5.3 Iteration Method for Voids
  5.3.1 Introduction
  5.3.2 Iteration for the First Order Equation
  5.3.3 Iteration for the Even Parity Equation
  5.3.4 Lower Bounds to the Exact Solution in Voids
5.4 Extrapolation Method for Voids
  5.4.1 Extrapolation Method Outlined
  5.4.2 Motivation for the Method
  5.4.3 Geometrical Interpretation
  5.4.4 Determination of Parameters
  5.4.5 Extrapolation for First Order Equation
  5.4.6 Improved Solution in Voids
  5.4.7 Sequential Extrapolation
  5.4.8 Multiparameter Extrapolation
  5.4.9 Choice of Trial Functions for Extrapolation
5.5 Void Test Problems
  5.5.1 Introduction
  5.5.2 Square Source Void Problem with Pure Absorber
  5.5.3 Straight Duct Source Problem with Pure Absorber
  5.5.4 Dog-Leg Duct Source Problem with Pure Absorber
  5.5.5 Square Source Void Problem with Scattering Media

References to Chapter 5

5. TREATMENT OF VOIDS

5.1 Introduction

Systems with voids/ducts have caused some difficulties for solutions of the even parity transport equation. This difficulty arises because of the total cross section, σ_T, appearing in the denominator of the leakage term in the even parity equation. Setting σ_T in the void to a very small number leads to a distorted and physically incorrect flux profile in the void. The flux in the latter becomes almost constant, which in turn gives inaccurate solutions in the neighbourhood of the void. In this chapter an explanation of this phenomena is presented. In addition, methods are developed, and tested, which give improved solutions for void problems. The methods are:

(a) Iteration

(b) Global or Elementary Extrapolation

(c) Nodal or Multiparameter Extrapolation.

The theory of all three methods is described and discussed. Subsequently, several void test problems are analysed using these methods.

5.2 Conventional Finite Element Method for Voids

In this section the conventional finite element method for the even parity equation for systems with voids is analysed. The treatment is restricted to voids surrounded by isotropic media. Extension to anisotropic scattering surrounding regions presents no problems. The physically incorrect flux profiles

produced by the conventional finite element method for voids are illustrated and discussed. Subsequently, an explanation for this phenomena is proposed. Consider the first order transport equation for a void region (V_v) without sources, viz.,

$$\underline{\Omega}\cdot\nabla\,\phi_o(\underline{r},\underline{\Omega}) = 0 \qquad (5.2\text{-}1)$$

The equivalent even parity form may be written as

$$\underline{\Omega}\cdot\nabla\left(\underline{\Omega}\cdot\nabla\,\phi_o^+(\underline{r},\underline{\Omega})\right) = 0 \qquad (5.2\text{-}2)$$

Here $\phi_o(\underline{r},\underline{\Omega})$ and $\phi_o^+(\underline{r},\underline{\Omega})$ are the exact angular and even parity angular fluxes respectively. In addition, the even parity equation for a source free absorbing medium can be written as

$$\frac{-\underline{\Omega}\cdot\nabla\,(\underline{\Omega}\cdot\nabla\phi^+)}{\sigma_a} + \sigma_a\,\phi_o^+ = 0 \qquad (5.2\text{-}3)$$

where σ_a is equal to σ_T for void problems.

A 'void' is defined as region of very low absorption cross section and zero scattering. If σ_v is the macroscopic absorption cross section in the void, then if $\sigma_v << \sigma_{T(surr)}$, where $\sigma_{T(surr)}$ is the total macroscopic cross section for the surrounding region, it is found that direct application of the finite element method to Eqn.(5.2-3), using K^+/ϕ^+, gives physically unsatisfactory results. In this case with $\sigma_v << \sigma_{T(surr)}$ the even parity flux $\phi(\underline{r},\underline{\Omega})$ is approximately constant in the void region. This distortion in the void flux influences the neutron flux in the

neighbourhood of the void. This is illustrated for a straight duct problem in Fig. 5.1, where various absorption cross sections, σ_v, have been chosen for the void region.

In order to explain this phenomena, consider the maximum principle functional $K^+(\phi^+)$ given in Section 4.2, i.e.

$$K^+(\phi^+) = \int_V \{ 2\langle \phi^+, s^+ \rangle + 2\langle \underline{\Omega}\cdot\nabla\phi^+, g s^- \rangle - \langle \underline{\Omega}\cdot\nabla\phi^+, g(\underline{\Omega}\cdot\nabla\phi^+)\rangle - \langle \phi^+, c\phi^+\rangle \} dV - \int_{S_b}\int_{\Omega} |\underline{\Omega}\cdot\underline{n}| (\phi^+)^2 d\Omega\, ds . \quad (5.2\text{-}4)$$

Then

$$K^+(\phi^+) \leq F^+(\phi_o^+, \phi_o^+) \quad (5.2\text{-}5)$$

where $F^+(\phi_o^+, \phi_o^+)$ is the functional associated with $\phi_o^+(r, \underline{\Omega})$ and is given by

$$F^+(\phi_o^+, \phi_o^+) = \int_V \{ \langle \underline{\Omega}\cdot\nabla\phi_o^+, g(\underline{\Omega}\cdot\nabla\phi_o^+)\rangle + \langle \phi_o^+, c\phi_o^+\rangle \} dV + \int_{S_b \cup S_s}\int_{\Omega} (\phi_o^+)^2 |\underline{\Omega}\cdot\underline{n}| d\Omega\, ds \quad (5.2\text{-}6)$$

When $K^+(\phi^+)$ is maximised, the quantity, $F^+(\phi^+ - \phi_o^+, \phi^+ - \phi_o^+)$, the global error in a generalised least squares sense, is minimised since

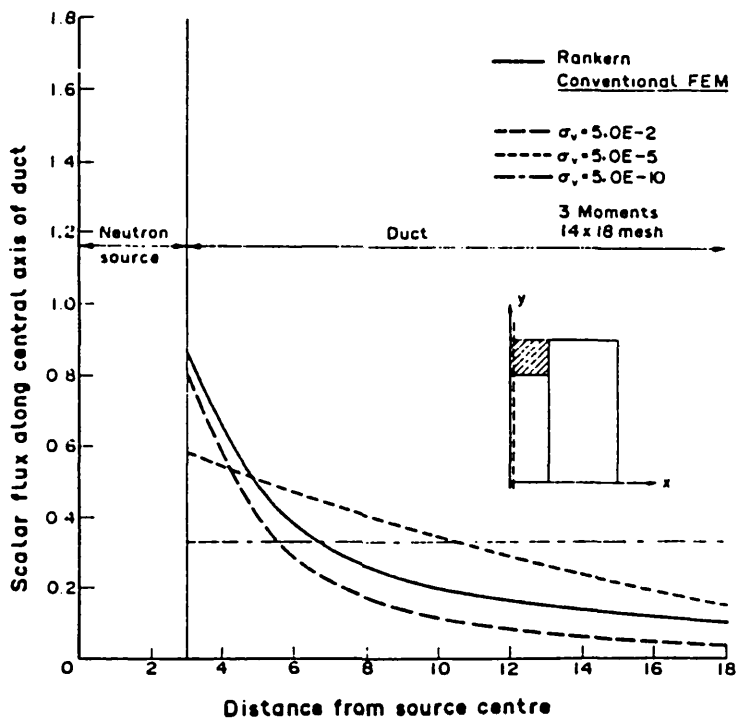


Fig. 5.1 Scalar Flux Distribution Along Central Axis of Duct.

$$K^+(\phi^+) + F^+(\phi^+ - \phi_o^+, \phi^+ - \phi_o^+) = F^+(\phi_o^+, \phi_o^+) \qquad (5.2\text{-}7)$$

for an arbitrary trial function. The quantity $F^+(\phi^+ - \phi_o^+, \phi^+ - \phi_o^+)$ is positive definite. See Ackroyd [1]. It is to be noted that the global error $F^+(\phi^+ - \phi_o^+, \phi^+ - \phi_o^+)$ can arise in many different ways. It can for example, be a uniformly distributed error, or on the other hand it may be localised as in void problems. Low values of the global error correspond to high values of $K^+(\phi^+)$ from (5.2-7), since $F^+(\phi^+ - \phi_o^+, \phi^+ - \phi_o^+)$ is positive definite. But high values of $K^+(\phi^+)$ may be obtained without $\phi^+(\underline{r}, \underline{\Omega})$ being a good approximation everwhere to $\phi_o^+(\underline{r}, \underline{\Omega})$, as in the case of voids. The void equation is of the kind (5.2-3) with σ_a replaced by σ_v . The contribution to $K^+(\phi^+)$ from the 'void' is

$$-\int_V \int_\Omega \left\{ \frac{[\underline{\Omega} \cdot \nabla \phi^+(\underline{r}, \underline{\Omega})]^2}{\sigma_v} + \sigma_v [\phi^+(\underline{r}, \underline{\Omega})]^2 \right\} d\Omega dV \qquad (5.2\text{-}8)$$

If $\underline{\Omega} \cdot \nabla \phi^+(\underline{r}, \underline{\Omega}) = 0$, then the contribution of the void to $K^+(\phi^+)$ becomes small for small σ_v as the second term in the integrand of equation (5.2-8) is then small. In practice the first term of the integrand of equation (5.2-8) is the ratio of two small positive quantities, which may be large if ϕ^+ is chosen inappropriately in some way.

When ϕ^+ is chosen by maximising $K^+(\phi^+)$ the contribution

to $K^+(\phi^+)$ from the void is made small, but, it can be made small for small σ_v without $(\phi^+ - \phi_o^+)$ becoming small. To see this consider the contribution of the void to the global error $F^+(\phi^+ - \phi_o^+, \phi^+ - \phi_o^+)$ viz.,

$$F_v^+(\phi^+ - \phi_o^+, \phi^+ - \phi_o^+) = \int_{V_v}\int_{\Omega} \left\{ \frac{[\underline{\Omega}\cdot\nabla(\phi^+ - \phi_o^+)]^2}{\sigma_v} + \sigma_v(\phi^+ - \phi_o^+)^2 \right\} d\Omega\, dV. \qquad (5.2\text{-}9)$$

If ϕ^+ is constant within the void, then

$$F_v^+(\phi^+ - \phi_o^+, \phi^+ - \phi_o^+) = \int_{V_v}\int_{\Omega} \left\{ \frac{(\underline{\Omega}\cdot\nabla\phi_o^+)^2}{\sigma_v} + \sigma_v(\phi^+ - \phi_o^+)^2 \right\} d\Omega\, dV \qquad (5.2\text{-}10)$$

The above quantity, (5.2-10), may also be written as

$$\int_{V_v}\int_{\Omega} \sigma_v \left\{ (\phi^+ - \phi_o^+)^2 + (\phi_o^-)^2 \right\} d\Omega\, dV \qquad (5.2\text{-}11)$$

since

$$\underline{\Omega}\cdot\nabla\phi_o^+ = -\sigma_v \phi_o^-$$

from the parity equations for a purely absorbing, source free medium. Now since

$$\phi_o = \phi_o^+ + \phi_o^- \qquad \text{and} \qquad \int_{\Omega} \phi_o^+ \phi_o^- \, d\Omega = 0$$

then

$$\int_{\Omega} \phi_o^2 \, d\Omega = \int_{\Omega} \left\{ (\phi_o^+)^2 + (\phi_o^-)^2 \right\} d\Omega > \int_{\Omega} (\phi_o^-)^2 \, d\underline{\Omega}$$

Hence, the contribution F_v^+ satisfies

$$F_v^+ < \sigma_v \int_{V_v}\int_{\Omega} \left\{ \phi_o^2 + (\phi^+ - \phi_o^+)^2 \right\} d\underline{\Omega}\, dV \qquad (5.2\text{-}12)$$

Since the integral on the right hand side above is finite,

then F_V^+ can be made indefinitely small by letting $\sigma_v \to 0$. The contribution from V_v to the global error vanishes as $\sigma_v \to 0$. This fact has to be taken into account in considering what may happen when $K^+(\phi^+)$ is maximised using a practical spherical harmonics expansion of P_5 (say). In the shield wall and source regions of the system, ϕ^+ can be made to approximate closely some solution of the transport equation, but not necessarily the solution ϕ_o^+.

Amongst the infinity of approximate solutions of the transport equation within the wall and source regions of the shield, there is one which is constant along the interface of the duct and the wall. This approximate solution and a constant approximation for the duct satisfy the continuity condition for trial functions admissible in the $K^+(\phi^+)$ principle. These two approximations define a trial function ϕ_f^+ (say) which makes the contributions of the wall/source region and the duct both small for small σ_v. Thus in maximising $K^+(\phi^+)$ for σ_v small and a low order expansion for ϕ^+, the function ϕ_f^+ may be selected.

5.3 Iteration Method for Voids

5.3.1 Introduction

As mentioned earlier, the basic idea behind the iteration scheme for source problems consists of absorbing and releasing neutrons in a void region filled with absorption cross section σ' (say). In other words, neutrons are stopped along their direction of travel in one iteration and are released along their original direction in the following iteration. In the first iteration or the initial solution the extraneous source $S(r,\Omega)$ is non-zero and the void is filled with material of absorption cross section σ' . It is assumed that the extraneous source is in the non-void region V_R . In the second and subsequent iterations $S(r,\underline{\Omega})$ is set to zero while the absorption sources in V_V are released. The iteration scheme may be continued until the absorption sources almost disappear. The macroscopic absorption cross section σ' is usually chosen to be less than the total macroscopic cross section of the surrounding region V_R . If $\sigma' = \sigma_T(V_R)$ then convergence of the iteration scheme will be slow, whereas on the other hand if $\sigma' \ll \sigma_T(V_R)$ then ϕ^+ will be approximately a constant in the void as in the conventional finite element method.

5.3.2 Iteration for the First Order Equation

The first order transport equation for the exact angular flux $\phi_0(r,\underline{\Omega})$ may be written as

$$\underline{\Omega} \cdot \nabla \phi_0 = 0 \qquad (5.3\text{-}1)$$

in a source free void region V_v , and

$$\underline{\Omega}.\nabla \phi_o + \Sigma \phi_o = S \qquad (5.3\text{-}2)$$

in a non-void region V_R .

Here Σ , the removal operator, is defined as

$$\Sigma \phi_o(r, \underline{\Omega}) = \sigma_T(r)\, \phi_o(r, \underline{\Omega}) - \int_{\Omega'} \sigma_s(r, \underline{\Omega}.\underline{\Omega}')\, \phi_o(r, \underline{\Omega}')\, d\Omega' \qquad (5.3\text{-}3)$$

The M^{th} iteration approximation to the exact flux $\phi_o(r,\Omega)$ is given by

$$\phi_M(r, \underline{\Omega}) = \sum_{m=1}^{M} \psi_m(r, \underline{\Omega}) \qquad (5.3\text{-}4)$$

where $\psi_m(r, \underline{\Omega})$ are the iteration component solutions. So for instance $\psi_1(r, \underline{\Omega})$ is obtained with cross section σ' in V_v and extraneous source $S(r,\Omega)$ in V_R . Each of the solutions ψ_m and also ϕ_M satisfy the boundary conditions on the bare surface, perfect reflector and are continuous at interfaces $S_i \cap S_j$ of adjacent regions V_i and V_j, for $\underline{\Omega}.\underline{n} \neq 0$.

The M^{th} iterative approximation to $\phi_o(r, \underline{\Omega})$ may be readily obtained by writing the first order equation for V_v, filled with an absorber, and V_R for each iteration and summing them.

In V_v

z-transform

$$
\begin{aligned}
&\text{I} \quad && \underline{\Omega}\cdot\nabla\psi_1 + \sigma^{-1}\psi_1 = 0 \\
&\text{II} \quad && \underline{\Omega}\cdot\nabla\psi_2 + \sigma^{-1}\psi_2 = \sigma^{-1}\psi_1 \\
&\text{III} \quad && \underline{\Omega}\cdot\nabla\psi_3 + \sigma^{-1}\psi_3 = \sigma^{-1}\psi_2 \\
&\quad \vdots \\
&\text{M} \quad && \underline{\Omega}\cdot\nabla\psi_M + \sigma^{-1}\psi_M = \sigma^{-1}\psi_{M-1}
\end{aligned}
\qquad (5.3\text{-}5)
$$

and in V_R

$$
\begin{aligned}
&\text{I} \quad && \underline{\Omega}\cdot\nabla\psi_1 + \Sigma\psi_1 = S \\
&\text{II} \quad && \underline{\Omega}\cdot\nabla\psi_2 + \Sigma\psi_2 = 0 \\
&\text{III} \quad && \underline{\Omega}\cdot\nabla\psi_3 + \Sigma\psi_3 = 0 \\
&\quad \vdots \\
&\text{M} \quad && \underline{\Omega}\cdot\nabla\psi_M + \Sigma\psi_M = 0
\end{aligned}
\qquad (5.3\text{-}6)
$$

Note that each ψ_m is positive, as ~~it~~ is the angular flux induced by a positive source. Positivity is established for ψ_1 and hence for ψ_2, etc.

Adding equations in (5.3-5) and then in (5.3-6) gives

$$
\underline{\Omega}\cdot\nabla\left(\sum_{m=1}^{M}\psi_m\right) + \sigma^{-1}\psi_M = 0 \qquad \text{in} \quad V_V \qquad (5.3\text{-}7)
$$

and

$$\underline{\Omega}\cdot\nabla\left(\sum_{m=1}^{M}\psi_m\right) + \Sigma\left(\sum_{m=1}^{M}\psi_m\right) = S \quad \text{in} \quad V_R \tag{5.3-8}$$

Equation (5.3-7) represents an approximation for the void, V_V. The ψ_M angular flux is due to extraneous source S in V_R and an imposed sink $\sigma'\psi_M$ in V_V. The effect of the sink in V_V is to make ψ_M less than ϕ_o everywhere. Note that each of the iteration component solution $\psi_m(\underline{r},\underline{\Omega})$ is an exact solution for that problem. In practice, however, each ψ_m will be approximate when spatial and angular approximations are introduced. Now, from (5.3-4), $\phi_M(\underline{r},\underline{\Omega})$ is the exact solution for the problem generated by filling the void with material of absorption cross section σ' and having a sink $\sigma'\psi_M$ in V_V. Also ϕ_M satisfies the same boundary conditions as the ψ_m. In addition, $\phi_M(\underline{r},\underline{\Omega})$ is positive within $V_V \cup V_R$, as each of the $\psi_m(\underline{r},\underline{\Omega})$ are positive.

If we let

$$X_M = \phi_o - \phi_M \tag{5.3-9}$$

then the specification for ϕ_o and ϕ_M give

$$\underline{\Omega}\cdot\nabla X_M = \sigma'\psi_M \quad \text{in} \quad V_V \tag{5.3-10}$$

and

$$\underline{\Omega}\cdot\nabla X_M + \Sigma X_M = 0 \text{ in} \quad V_R \tag{5.3-11}$$

So $X_M(\underline{r},\underline{\Omega})$ is the angular flux due to a source $\sigma'\psi_M$ in V_V

since $\psi_M > 0$, in V_V , with no sources in V_R.
This means that

$$\chi_M > 0 \text{ within } V_V \cup V_R ,$$

and so $\phi_0 - \phi_M > 0$ from (5.3-9)

i.e. $$\phi_M < \phi_0 . \qquad (5.3\text{-}12)$$

Now the sequence $\{\phi_m\}$ is monotonically increasing with m since ϕ_m is the sum of positive angular fluxes ψ_m. Since, ϕ_M is bounded above by ϕ_0, from (5.3-12), and $\{\phi_m\}$ is an increasing sequence, then $\{\phi_m\}$ converges. Thus ϕ_M approaches ϕ_0 from below. Since ψ_2 is the angular flux induced by the source $\sigma'\psi_1$ in a non-multiplying system, $\psi_2 < \psi_1$. Similarly $\psi_3 < \psi_2$. The sequence of sources $\sigma'\psi_m$ is consequently a monotonically decreasing sequence. In practice this sequence converges to practically zero in a few iterations. Consequently ϕ_M for a few iterations, M, converges practically to ϕ_0.

5.3.3 Iteration for the Even Parity Equation

Ideas similar to those described in the previous section may be used to obtain approximate solutions to void problems using the even parity equation. The even parity iterative solutions for the even parity flux $\psi_m^+(r, \mu)$ are derived from the first order transport equation in Appendix A. Taking even and odd parity components of the first order equation (5.3-5) and (5.3-6) gives the even parity equations for the iteration scheme.

In V_V

$$\begin{aligned}
&\text{I} && \frac{-\underline{\Omega}\cdot\nabla(\underline{\Omega}\cdot\nabla\psi_1^+)}{\sigma'} + \sigma'\psi_1^+ = 0 \\
&\text{II} && \frac{-\underline{\Omega}\cdot\nabla(\underline{\Omega}\cdot\nabla\psi_2^+)}{\sigma'} + \sigma'\psi_2^+ = 2\sigma'\psi_1^+ \\
&\text{III} && \frac{-\underline{\Omega}\cdot\nabla(\underline{\Omega}\cdot\nabla\psi_3^+)}{\sigma'} + \sigma'\psi_3^+ = 2\sigma'\psi_2^+ - \sigma'\psi_1^+ \qquad (5.3\text{-}13) \\
&\vdots \\
&\text{M} && \frac{-\underline{\Omega}\cdot\nabla(\underline{\Omega}\cdot\nabla\psi_M^+)}{\sigma'} + \sigma'\psi_M^+ = 2\sigma'\psi_{M-1}^+ - \sigma'\psi_{M-2}^+
\end{aligned}$$

and in V_R the even parity equations are

$$\begin{aligned}
&\text{I} && -\underline{\Omega}\cdot\nabla[S(\underline{\Omega}\cdot\nabla\psi_1^+)] + c\psi_1^+ = S^+ \\
&\text{II} && -\underline{\Omega}\cdot\nabla[S(\underline{\Omega}\cdot\nabla\psi_2^+)] + c\psi_2^+ = 0 \\
&\text{III} && -\underline{\Omega}\cdot\nabla[S(\underline{\Omega}\cdot\nabla\psi_3^+)] + c\psi_3^+ = 0 \qquad (5.3\text{-}14) \\
&\vdots \\
&\text{M} && -\underline{\Omega}\cdot\nabla[S(\underline{\Omega}\cdot\nabla\psi_M^+)] + c\psi_M^+ = 0
\end{aligned}$$

for an isotropic extraneous source $S^+(x, \underline{\Omega})$. The component solutions $\psi_m^+(x, \underline{\Omega})$ satisfy the bare surface, perfect reflector and continuity conditions given in Section 5.3.2. Since the ψ_m are positive, then so are the ψ_m^+. Thus, the sum of sources and sinks should be positive. I.e.,

$$(2\psi_{m-1}^+ - \psi_{m-2}^+) > 0 \qquad (5.3\text{-}15)$$

for $m \geq 3$.

Adding the equations in (5.3-13) gives for V_V

$$\frac{-\underline{\Omega}\cdot\nabla\left(\underline{\Omega}\cdot\nabla\,\phi_M^+\right)}{\sigma'} + \sigma'\,\frac{\psi_M^+}{M} = 0 \qquad (5.3\text{-}16)$$

where

$$\phi_M^+ = \left(\psi_1^+ + \frac{M-1}{M}\psi_2^+ + \cdots + \frac{(M-k+1)}{M}\psi_k^+ + \cdots + \frac{\psi_M^+}{M}\right) \qquad (5.3\text{-}17)$$

Also for V_R, we get

$$-\underline{\Omega}\cdot\nabla\left[S\left(\underline{\Omega}\cdot\nabla\phi_M^+\right)\right] + C\,\phi_M^+ = S^+ \qquad (5.3\text{-}18)$$

In theory the solution $\phi_M^+(r, \underline{\Omega})$ in V_V provides a lower bound to $\phi_o^+(r, \underline{\Omega})$, the exact even parity flux. Other lower bounds to ϕ_o^+ can also be obtained as will be seen in the following Section and in Appendix B.

5.3.4 Lower Bounds to the Exact Solution in Voids

The even parity iterative approximation $\phi_M^+(r, \underline{\Omega})$ given above, is a theoretical lower bound to the exact solution in the void, $\phi_o^+(r, \underline{\Omega})$, as is shown below. From (5.2-2), and (5.3-16), we have

$$\frac{-\underline{\Omega}\cdot\nabla\left(\underline{\Omega}\cdot\nabla\right)\left[\phi_o^+ - \phi_M^+\right]}{\sigma'} = \sigma'\,\frac{\psi_M^+}{M} \quad \text{in } V_V \qquad (5.3\text{-}19)$$

and

$$-\underline{\Omega}\cdot\nabla\left[S\left(\underline{\Omega}\cdot\nabla\right)\right]\left[\phi_o^+ - \phi_M^+\right] + C\left[\phi_o^+ - \phi_M^+\right] = 0 \quad \text{in } V_R \qquad (5.3\text{-}20)$$

Since, $\psi_M^+ > 0$, the effective source inducing $[\phi_o^+ - \phi_M^+]$ is non-negative everywhere, hence, $\phi_o^+ > \phi_M^+$, i.e. ϕ_M^+ is

a lower bound to ϕ_0^+. The equations (5.3-13) and (5.3-14) can be re-written, for practical convenience, to give the following modified scheme (for three iterations). In V_V

$$\text{I} \quad \frac{-\underline{\Omega}\cdot\nabla(\underline{\Omega}\cdot\nabla\bar{\psi}_1^+)}{\sigma'} + \sigma'\bar{\psi}_1^+ = 0 \,, \quad \text{with} \quad \bar{\psi}_1^+ = \psi_1^+$$

$$\text{II} \quad \frac{-\underline{\Omega}\cdot\nabla(\underline{\Omega}\cdot\nabla\bar{\psi}_2^+)}{\sigma'} + \sigma'\bar{\psi}_2^+ = \sigma'\bar{\psi}_1^+, \quad \bar{\psi}_2^+ = \psi_2^+/2 \qquad (5.3\text{-}21)$$

$$\text{III} \quad \frac{-\underline{\Omega}\cdot\nabla(\underline{\Omega}\cdot\nabla\bar{\psi}_3^+)}{\sigma'} + \sigma'\bar{\psi}_3^+ = \sigma'\bar{\psi}_2^+ \,, \quad \bar{\psi}_3^+ = \psi_3^+/4 + \psi_2^+/8$$

and in V_R

$$\text{I} \quad -\underline{\Omega}\cdot\nabla[S(\underline{\Omega}\cdot\nabla)\bar{\psi}_1^+] + c\bar{\psi}_1^+ = s^+$$

$$\text{II} \quad -\underline{\Omega}\cdot\nabla[S(\underline{\Omega}\cdot\nabla)\bar{\psi}_2^+] + c\bar{\psi}_2^+ = 0 \qquad (5.3\text{-}22)$$

$$\text{III} \quad -\underline{\Omega}\cdot\nabla[S(\underline{\Omega}\cdot\nabla)\bar{\psi}_3^+] + c\bar{\psi}_3^+ = 0 \,.$$

Thus the modified iteration scheme gives

$$\frac{-\underline{\Omega}\cdot\nabla(\underline{\Omega}\cdot\nabla\bar{\phi}_3^+)}{\sigma'} + \sigma'\bar{\phi}_3^+ = 0 \quad \text{in} \quad V_V \qquad (5.3\text{-}23)$$

$$\text{and} \quad -\underline{\Omega}\cdot\nabla[S(\underline{\Omega}\cdot\nabla\bar{\phi}_3^+)] + c\bar{\phi}_3^+ = s^+ \quad \text{in} \quad V_R \qquad (5.3\text{-}24)$$

$$\text{where} \quad \bar{\phi}_3^+ = \bar{\psi}_1^+ + \bar{\psi}_2^+ + \bar{\psi}_3^+ \,. \qquad (5.3\text{-}25)$$

Letting $\bar{x}_3 = \phi_0^+ - \bar{\phi}_3^+$ then we have

$$\frac{-\underline{\Omega}\cdot\nabla(\underline{\Omega}\cdot\nabla)[\phi_0^+ - \bar{\phi}_3^+]}{\sigma'} = \sigma'\bar{\phi}_3^+ \quad \text{in} \quad V_V \qquad (5.3\text{-}26)$$

and

$$-\underline{\Omega}\cdot\nabla[S(\underline{\Omega}\cdot\nabla)(\phi_0^+ - \bar{\phi}_3^+)] + c\bar{\phi}_3^+ = s^+ \quad \text{in} \quad V_R \qquad (5.3\text{-}27)$$

Since the effective source $\sigma' \bar{\phi}_2^+$ is positive everywhere, $\phi_0^+ > \bar{\phi}_3^+$, i.e. $\bar{\phi}_2^+$ is a lower bound to ϕ_0^+. The lower bound for the modified scheme with three iterations is, in terms of the ψ_m of the original scheme,

$$\bar{\phi}_3^+ = \psi_1^+ + \frac{15}{24}\psi_2^+ + \frac{\psi_3^+}{4} \qquad (5.3\text{-}28)$$

whereas the corresponding lower bound for the original iteration scheme is slightly better, viz.,

$$\phi_3^+ = \psi_1^+ + \frac{16}{24}\psi_2^+ + \frac{\psi_3^+}{3} \qquad (5.3\text{-}29)$$

The reason for adopting the modified iteration scheme for practical calculation is as follows:

Looking at the original iteration scheme equations in V_v as given by (5.3-13), it is seen that the inducing source after the second iteration is of the form $2\sigma' \psi_{m-1}^+ - \sigma' \psi_{m-2}^+$. If the source is positive everywhere so is the induced angular flux.

The angular flux can be positive everywhere in a system with sources and sinks, The component of the angular flux induced by the source being greater than the component induced in the sink. In practice it is necessary to use approximations for $2\sigma' \psi_{m-1}^+$ and $\sigma' \psi_{m-2}^+$ for calculating ψ_m^+ and, in subtracting these equations to obtain the right hand sides of (5.3-13), errors

can be incurred. In order to maintain positive inducing sources, the modified iteration scheme is introduced.

5.4 Extrapolation Method for Voids

5.4.1 Extrapolation Method Outlined

The method of extrapolation is based on the idea of best approximation in a Hilbert space from functional analysis. If $\mathcal{P}$ is a projection operator and $\psi_1^+, \psi_2^+, \psi_3^+ \ldots\ldots$ are independent functions spanning a Hilbert space H, then $\mathcal{P}\underline{\phi}_0$ is a best approximation to $\underline{\phi}_0$ when $\mathcal{P}$ projects orthogonally onto H. See Fig. 5.2 below.

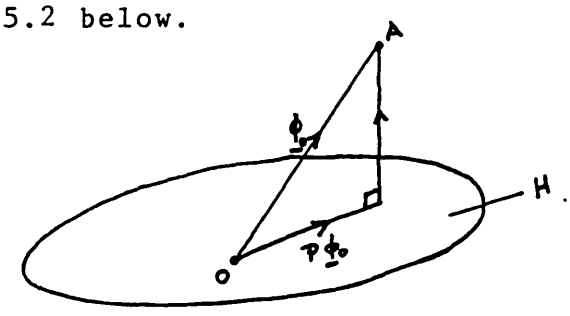


Fig. 5.2 Orthogonal projection of a vector $\underline{\phi}_0$ onto a space H.

The orthogonal projection or best approximation then minimises the distance from A to the space H. See for instance Kreyzig [2] and Prenter [3]. Independent solutions $\psi_1^+, \psi_2^+, \psi_3^+, \ldots$ can be obtained for a sequence of problems by filling the void with absorbing media of macroscopic absorption cross sections $\sigma_{v1}, \sigma_{v2}, \ldots\ldots$ with $\sigma_{v1} > \sigma_{v2} > \sigma_{v3} \ldots\ldots\ldots$ The $\psi_1^+, \psi_2^+, \psi_3^+, \ldots$ etc. above, should not be confused with the ψ_m^+ of the

iteration scheme. The extrapolated solution is then taken to be

$$\psi_\varepsilon^+(\underline{r},\underline{\Omega}) = \sum_{i=1}^{N} \alpha_i \psi_i^+(\underline{r},\underline{\Omega}) \qquad (5.4\text{-}1)$$

with the α_i chosen by making $\psi_\varepsilon^+(\underline{r},\underline{\Omega})$ an optimised approximation solution for the problem with a void. To ensure that the same source is used for ψ_ε^+ and ψ_i^+ the following constraint on the α_i is imposed.

$$\sum_{i=1}^{N} \alpha_i = 1 \qquad (5.4\text{-}2)$$

where N is the number of trial functions used in the extrapolation scheme. So for instance, with two trial function extrapolation, with ψ_1^+ and ψ_2^+, we have

$$\alpha_1 + \alpha_2 = 1$$

and

$$\psi_\varepsilon^+(\underline{r},\underline{\Omega}) = \alpha_1 \psi_1^+(\underline{r},\underline{\Omega}) + (1-\alpha_1)\psi_2^+(\underline{r},\underline{\Omega}) \qquad (5.4\text{-}3)$$

This combined approximation can be optimised with respect to the coefficients α_i in the linear combination. The error between the exact solution of the given problem and the combined approximation is minimised in a generalised least squares sense by the optimisation. In the void region, V_V, the coefficients α_i are expanded in a power series in σ_V and the limit taken for ψ_ε^+ as $\sigma_V \to 0$. The trial function given in (5.4-1) together with constraints (5.4-2) have similarity with simplex elements in finite element theory. See for instance Carey and

Oden [4]. In the global version of the extrapolation method the parameters α_i do not change across the system, i.e. α_i is the same at each node of V_V and V_R. In the nodal extrapolation method α_i are allowed to vary from one node to the next, spatially, in the system. In the case of sequential or regional extrapolation the α_i remain constant within a region but, are allowed to vary from region to region. Sequential extrapolation is intermediate to global and nodal or multi-parameter extrapolation. Approximation of the type given in (5.4-1) are used in both the void and non-void regions. Calculations of the coefficients α_i is discussed in Section 5.4.3.

5.4.2 Motivation for the Method

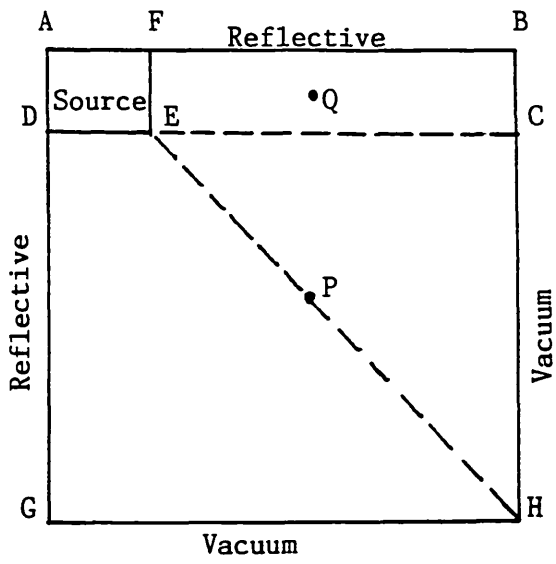
Initial motivation for the extrapolation method came by looking at scalar flux profiles in a void region with the void filled with a range of macroscopic absorption cross sections σ_V. Flux profiles were generated using the conventional finite element method. It was observed that for relatively high values of σ_V ($< \sigma_{T(SUPP)}$), the flux profiles were reasonable and had an overall 'correct' shape, but, were lower than the exact solution whereas for $\sigma_V << \sigma_{T(SUPP)}$, an almost flat flux profile was obtained in the void which distorted the solution in V_R, in the neighbourhood of the void. It then became apparent that linear combinations of 'correct' profiles might generate a good approximation to the exact

solution in a void region. This was subsequently investigated. It may happen that if the mesh and directional approximation in the finite element representation for $\phi^+(x, \Omega)$ is coarse, that relatively high values of $K^+(\phi^+)$ can be obtained for ϕ^+ constant in the void region. The $K^+(\phi^+)$ calculation takes account of absorption in the void and also the spreading of neutron beams streaming for the source. By combining ψ_1^+ and ψ_2^+ in the way described above, the aim is to provide a combination ψ_ε^+, in which the absorption effects are minimised as far as possible without upsetting the streaming effects.

In the conventional finite element method or direct application of the $K^+(\phi^+)$ principle the trial function used has complete flexibility in the specification at a node of the nodal values of an element for the spherical harmonics expansion. This leads to $\phi^+(x,\Omega)$ being approximately constant in the void. The extrapolation method uses biased trial functions instead of the unbiased trial functions of the conventional method and thus avoids the almost flat flux profile in the void regions.

Further motivation for the extrapolation technique is given below by considering a straight duct problem with purely absorbing walls [5].

Problem I Shield Without Duct



Even-parity angular flux ϕ_{01}^{+}. ABGH a square absorbing region with a square source region. Uniform isotropic source in AFED.

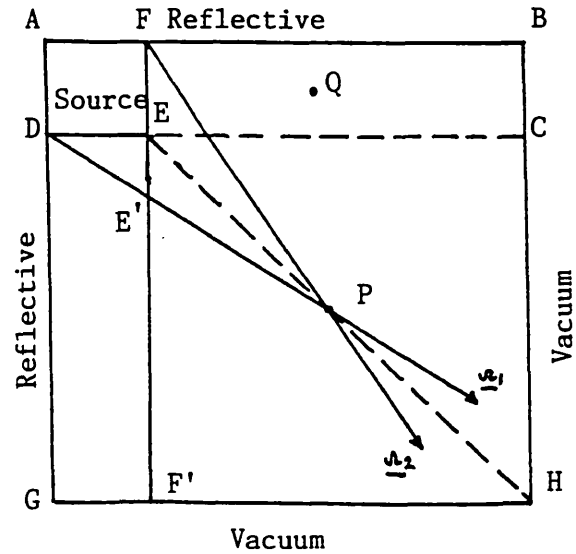
Fig. 5.3

With a mesh pitch of the order of a mean free path and a P_5 spherical harmonics expansion for the trial function ϕ_1^+, a fairly accurate approximation for ϕ_{01}^{+} can be obtained. The even parity equation

$$-\frac{1}{\sigma_a}\,\underline{\Omega}\cdot\nabla\left(\underline{\Omega}\cdot\nabla\phi_{01}^{+}\right)+\sigma_a\,\phi_{01}^{+}=0$$

is nearly satisfied in the source free region, if a fine mesh and a P_4 approximation are used.

Problem 2. Shield with Duct



Even parity angular flux ϕ_{02}^{+}. Duct absorption cross section $\sigma_v \ll \sigma_a$. Duct - DEFG.

Fig. 5.4

Although fairly accurate approximate solutions of the wall equation

$$-\frac{1}{\sigma_a}\,\underline{\Omega}\cdot\nabla\left(\underline{\Omega}\cdot\nabla\psi^{+}\right)+\sigma_a\,\psi^{+}=0$$

can be obtained, they will not necessarily be good approximations for ϕ_{o2}^{+}, because the angular flux ϕ_{o2}^{+} varies with direction $\underline{\Omega}$ in a more complicated way than the angular flux ϕ_{o1}^{+}. At a position P on the diagonal AEH of Fig. 5.3 the distribution of ϕ_{o1}^{+} is by symmetry of the problem, symmetrical about the diagonal. For the corresponding point P of Fig. 5.4, $\phi_{o2}^{+}(P,\underline{\Omega}_1) > \phi_{o2}^{+}(P,\underline{\Omega}_2)$ because the path DEP is less absorbing than the path FP. In both cases, the angular flux is confined to the wedge of directions lying between $\underline{\Omega}_1$ and $\underline{\Omega}_2$. On the otherhand, for a point Q lying in BCEF

$$\phi_{o1}^{+}(Q,\underline{\Omega}) = \phi_{o2}^{+}(Q,\underline{\Omega})$$

because, neutrons reaching Q from the source do not see the duct.

Since ϕ_{o2}^{+} varies in a more complex way than ϕ_{o1}^{+} a higher expansion in spherical harmonics for ϕ_2^{+}, than ϕ_1^{+}, seems necessary. Practical considerations may restrict computation to P_4 (say) expansion for ϕ_2^{+}.

Consider two auxilliary problems differing from Problem 2 in one respect only. The duct filling σ_V is replaced by

duct fillings σ_{v1} and σ_{v2}, with $\sigma_v < \sigma_{v2} < \sigma_{v1} << \sigma_a$. The cross section σ_{v2} is chosen to be not more than two orders of magnitude less than σ_a so that the flux flattening in the duct does not occur significantly for these auxilliary problems. Let $\phi_o^{+\prime}$ and $\phi_o^{+\prime\prime}$ be the angular fluxes for the problems with duct fillings σ_{v1} and σ_{v2} respectively. Consider the angular fluxes at P for Problem 2 and the auxilliary problems. Since the beams with directions $\underline{\Omega}_2$ do not intersect the duct

$$\phi_{o2}(P, \underline{\Omega}_2) = \phi_o^{+\prime}(P, \underline{\Omega}_2) = \phi_o^{+\prime\prime}(P, \underline{\Omega}_2)$$

Let the parameter α be given by

$$\alpha\, \phi_o^{+\prime}(P, \underline{\Omega}_1) + (1-\alpha)\, \phi_o^{+\prime\prime}(P, \underline{\Omega}_1) = \phi_{o2}^{+}(P, \underline{\Omega}_1)$$

then, for directions $\underline{\Omega}$ lying between $\underline{\Omega}_1$ and $\underline{\Omega}_2$ the approximation

$$\alpha\, \phi_o^{+\prime}(P, \underline{\Omega}) + (1-\alpha)\, \phi_o^{+\prime\prime}(P, \underline{\Omega}) \approx \phi_2^{+}(P, \underline{\Omega})$$

suggests the interpolation formula,

$$\alpha\, \phi^{+\prime}(P, \underline{\Omega}) + (1-\alpha)\, \phi^{+\prime\prime}(P, \underline{\Omega}) = \phi_2^{+}(P, \underline{\Omega})$$

where $\phi^{+\prime}(P, \underline{\Omega})$ is the optimised trial function for $\phi_o^{+\prime}$ and $\phi^{+\prime\prime}(P, \underline{\Omega})$, the optimised trial function for $\phi_o^{+\prime\prime}$. The parameter α has to be determined. Strictly it should vary from point to point in the system. Methods for determining α are given subsequently. They are based on the K^+ principle and the motivation for the method used is suggested by a study of the

phenomena arising in the duct regions where a similar extrapolation procedure is used. Two extrapolation procedures, global and nodal, are considered. For the former α is a constant, and for the latter α varies from node to node of the mesh.

5.4.3 Geometrical Interpretation

In this section a simple geometrical interpretation of the extrapolation method is given, using two trial functions. Let ϕ_0^+ be the exact solution of the void problem and let ψ_1^+ and ψ_2^+ be approximate solutions with void filled with σ_{v_1} and σ_{v_2} respectively. With each of the above solutions we can associate vectors $\underline{\Phi}_0^+$, $\underline{\Psi}_1^+$ and $\underline{\Psi}_2^+$ in a Hilbert space. The metric of the Hilbert space H is given in terms of nuclear data for the problem with solution ϕ_0^+ [1]. With the extrapolation solution

$$\psi_\varepsilon^+ = \alpha \psi_1^+ + (1-\alpha)\psi_2^+ \qquad (5.4\text{-}4)$$

where we have put $\alpha_1 = \alpha$, there is a corresponding vector

$$\underline{\Psi}_\varepsilon^+ = \alpha \underline{\Psi}_1^+ + (1-\alpha)\underline{\Psi}_2^+ \qquad (5.4\text{-}5)$$

$$= \alpha(\underline{\Psi}_1^+ - \underline{\Psi}_2^+) + \underline{\Psi}_2^+$$

See Fig. 5.5. As α varies the point C in Fig. 5.5, the extremity of the vector $\underline{\Psi}_\varepsilon^+$ describes a linear space or a straight line in this case. Maximisation of $K^+(\Psi_\varepsilon^+)$ with respect to the parameter α corresponds to minimisation of $(CD)^2$. Of course the distance CD is minimised when CD is perpendicular to BC,. If $\hat{\alpha}$ maximises $K^+(\Psi_\varepsilon^+)$ and

$$\hat{\Psi}_\varepsilon^+ = \hat{\alpha}\left(\Psi_1^+ - \Psi_2^+\right) + \Psi_2^+ \qquad (5.4\text{-}6)$$

then by the projection theorem

$$\left(\underline{\Phi}_0^+ - \hat{\underline{\Psi}}_\varepsilon^+\right).\left(\underline{\Psi}_1^+ - \underline{\Psi}_2^+\right) = 0 \qquad (5.4\text{-}7)$$

i.e. DC is orthogonal to the line BC. We may then write

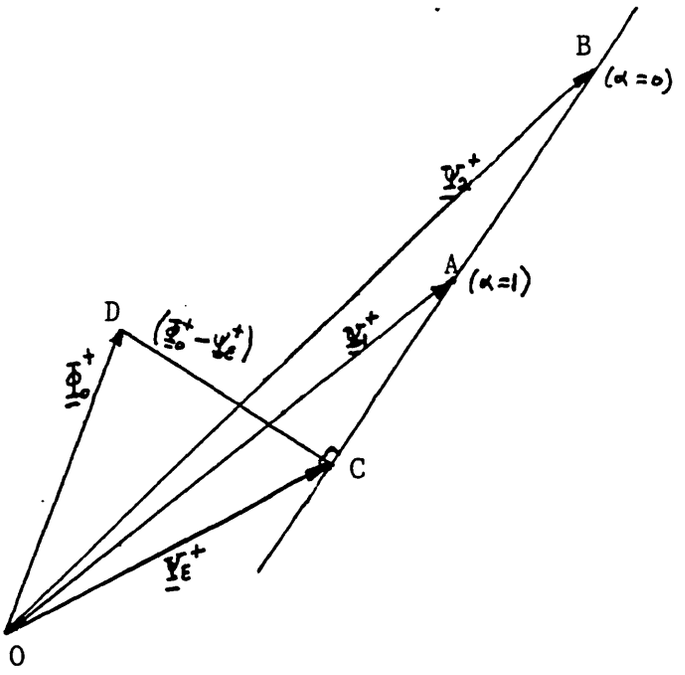
$$\mathcal{P}\,\underline{\Phi}_0^+ = \hat{\underline{\Psi}}_\varepsilon^+$$

where $\mathcal{P}$ is an orthogonal projection operator onto AB.
The above geometrical interpretation can be easily generalised when Ψ_ε^+ is a linear combination of N trial functions $\Psi_1^+, \Psi_2^+, \ldots\ldots, \Psi_N^+$. Corresponding to the extrapolation approximation (5.4-1) there is the vector

$$\underline{\Psi}_\varepsilon^+ = \sum_{i=1}^{N} \alpha_i \underline{\Psi}_i^+ \qquad (5.4\text{-}8)$$

with α_i satisfying the conditions given in (5.4-2). Hence,

$$\underline{\Psi}_\varepsilon^+ = \sum_{i=1}^{N-1} \alpha_i \left(\underline{\Psi}_i^+ - \underline{\Psi}_N^+\right) + \underline{\Psi}_N^+ \qquad (5.4\text{-}9)$$



$(\underline{\Phi}_o^+ - \underline{\Psi}_\epsilon^+)$ orthogonal to line AB produced.

Fig. 5.5 Hilbert Space Interpretation of Maximising $K^+(\Psi_\epsilon^+)$.

The extremity of the approximation vector $\underline{\Psi}_\epsilon^+$ lies on the linear $N-1$ space specified by (5.4-9). When $K^+(\Psi_\epsilon^+)$ is maximised with respect to the α_i then $(\underline{\Phi}_0^+ - \underline{\Psi}_\epsilon^+)^2$ is minimised and this leads to the orthogonality conditions

$$(\underline{\Phi}_0^+ - \hat{\underline{\Psi}}_\epsilon^+).(\underline{\Psi}_i^+ - \underline{\Psi}_N^+) = 0 \qquad (5.4\text{-}10)$$

for the optimised approximation vector $\hat{\underline{\Psi}}_\epsilon^+$. Hence

$$(\underline{\Phi}_0^+ - \hat{\underline{\Psi}}_\epsilon^+).(\underline{\Psi}_i^+ - \underline{\Psi}_j^+) = 0$$

i.e. $(\underline{\Phi}_0^+ - \hat{\underline{\Psi}}_\epsilon^+)$ is orthogonal to every vector lying in the linear $N-1$ space.

5.4.4 Determination of Parameters

In the elementary method of extrapolation with two trial functions Ψ_1^+ and Ψ_2^+ there is a single parameter $\alpha_1 (= \alpha)$ to be determined for the void and infact for the whole system. α is constant throughout the system. Maximising the functional

$$K^+(\Psi_\epsilon^+) = \int_{V_R}\int_{\Omega} \{ 2\Psi_\epsilon^+ s^+ - [\underline{\Omega}.\nabla\Psi_\epsilon^+ G(\underline{\Omega}.\nabla\Psi_\epsilon^+) + \Psi_\epsilon^+ c \Psi_\epsilon^+] \} d\Omega\, dV$$

$$- \int_{V_V}\int_{\Omega} \left[\frac{1}{\sigma_V} (\underline{\Omega}.\nabla\Psi_\epsilon^+)^2 + \sigma_V (\Psi_\epsilon^+)^2 \right] d\Omega\, dV$$

$$- \int_{S_b}\int_{\Omega} (\Psi_\epsilon^+)^2 \, |\underline{\Omega}.\underline{n}| \, d\Omega\, dS \qquad (5.4\text{-}11)$$

with respect to α gives

$$0 = \sigma_v \int_{V_R} \int_{\Omega} \{ [\psi_1^+ - \psi_2^+] S^+ - (\alpha \underline{\Omega}\cdot\nabla [\psi_1^+ - \psi_2^+] + \underline{\Omega}\cdot\nabla \psi_2^+) \frac{1}{\underline{\Omega}\cdot\nabla} (\psi_1^+ - \psi_2^+)$$
$$- (\alpha [\psi_1^+ - \psi_2^+] + \psi_2^+) C [\psi_1^+ - \psi_2^+] \} \, d\Omega \, dV$$

$$- \int_{V_v} \int_{\Omega} \{ (\alpha \underline{\Omega}\cdot\nabla [\psi_1^+ - \psi_2^+] + \underline{\Omega}\cdot\nabla \psi_2^+) \underline{\Omega}\cdot\nabla [\psi_1^+ - \psi_2^+] + \sigma_v^2 (\alpha [\psi_1^+ - \psi_2^+) + \psi_2^+) \cdot$$
$$C (\psi_1^+ - \psi_2^+) \} \, d\Omega \, dV$$

$$- \sigma_v \int_{S_b} \int_{\Omega} |\underline{\Omega}\cdot\underline{n}| (\alpha [\psi_1^+ - \psi_2^+] + \psi_2^+) [\psi_1^+ - \psi_2^+] \, d\Omega \, dS$$

(5.4-12)

If now α is expanded in a power series in σ_v as

$$\alpha = a_0 + a_1 \sigma_v + a_2 \sigma_v^2 + \ldots\ldots$$

(5.4-13)

and substituting into (5.4-12), taking the limit as $\sigma_v \to 0$ leads to the following simple formula for the optimised value of α .

$$\hat{a}_0 = \frac{-\int_{V_V}\int_{\Omega} \underline{\Omega}\cdot\nabla\psi_2^+ \, \underline{\Omega}\cdot\nabla(\psi_1^+ - \psi_2^+)\, d\Omega\, dV}{\int_{V_V}\int_{\Omega} [\underline{\Omega}\cdot\nabla(\psi_1^+ - \psi_2^+)]^2 \, d\Omega\, dV} \qquad (5.4\text{-}14)$$

The spatial integration here is over all the void elements. The single coefficient $\hat{a}_0$ is then used in combining ψ_1^+ and ψ_2^+ over the entire system. The non-void term in the functional disappears in the limiting process, $\sigma_V \to 0$. The derivation of $\hat{a}_0$ is given in Appendix C. Although $\hat{a}_0$ calculated above is used to combine ψ_1^+ and ψ_2^+ over the entire system, $V_V \cup V_R$, it is still possible to define a coefficient $\hat{a}_{0R}$ for the non-void region.

$$\hat{a}_{0R} = \frac{\int_{V_R}\int_{\Omega} [(\psi_1^+ - \psi_2^+) S^+ - \underline{\Omega}\cdot\nabla\psi_2^+ \, S(\underline{\Omega}\cdot\nabla(\psi_1^+ - \psi_2^+)) - \psi_2^+ C(\psi_1^+ - \psi_2^+)]\, d\Omega\, dV - \int_{S_b}\int_{\Omega} |\underline{\Omega}\cdot\underline{n}|\, \psi_2^+ (\psi_1^+ - \psi_2^+)\, d\Omega\, dS}{\int_{V_R}\int_{\Omega} [\underline{\Omega}\cdot\nabla(\psi_1^+ - \psi_2^+) S(\underline{\Omega}\cdot\nabla(\psi_1^+ - \psi_2^+)) + (\psi_1^+ - \psi_2^+) C(\psi_1^+ - \psi_2^+)]\, d\Omega\, dV + \int_{S_b}\int_{\Omega} |\underline{\Omega}\cdot\underline{n}|\, \psi_2^+ (\psi_1^+ - \psi_2^+)^2 \, d\Omega\, dS} \qquad (5.4\text{-}15)$$

In this case matching of solutions at the void/non-void interface is required. At the interface nodes either, $\hat{\psi}_{\varepsilon}^{+}$ using $\hat{a}_{\circ}$ or $\hat{\psi}_{\varepsilon}^{+}$ using $\hat{a}_{\circ R}$, may be defined or, a mean value of the two solutions. Later it is shown that the idea of extrapolation can be extended such that the value of varies node by node in the system.

In the case of three trial function extrapolation. using ψ_1^{+}, ψ_2^{+} and ψ_3^{+}, the condition (5.4-2) becomes

$$\alpha_1 + \alpha_2 + \alpha_3 = 1 \tag{5.4-16}$$

If $\alpha_1 = \alpha$ and $\alpha_2 = \beta$ then the extrapolated solution becomes

$$\psi_{\varepsilon}^{+} = \alpha \phi_1^{+} + \beta \phi_2^{+} + (1-\alpha-\beta)\phi_3^{+} \tag{5.4-17}$$

In this case two parameters, α and β need to be calculated. Derivation of the optimised coefficients $\hat{a}_{\circ}$ and $\hat{b}_{\circ}$ is given in Appendix C. The following result is obtained for $\hat{a}_{\circ}$ and $\hat{b}_{\circ}$.

$$\hat{a}_{\circ} = \frac{c_1 d_{22} - c_2 d_{12}}{(d_{11} d_{22} - d_{12} d_{21})} \tag{5.4-18}$$

and

$$\hat{b}_{\circ} = \frac{c_2 d_{11} - c_1 d_{21}}{(d_{11} d_{22} - d_{12} d_{21})} \tag{5.4-19}$$

where

$$\begin{aligned}
d_{11} &= \int_V \int_{\Omega} [\underline{\Omega}.\nabla (\psi_1^{+} - \psi_3^{+})]^2 \, d\Omega \, dV \\
d_{12} = d_{21} &= \int_V \int_{\Omega} \underline{\Omega}.\nabla (\psi_1^{+} - \psi_3^{+}) \, \underline{\Omega}.\nabla (\psi_2^{+} - \psi_3^{+}) \, d\Omega \, dV \\
d_{22} &= \int_V \int_{\Omega} [\underline{\Omega}.\nabla (\psi_2^{+} - \psi_3^{+})^2] \, d\Omega \, dV \\
c_1 &= -\int_V \int_{\Omega} \underline{\Omega}.\nabla \psi_3^{+} \, \underline{\Omega}.\nabla (\psi_1^{+} - \psi_3^{+}) \, d\Omega \, dV \\
c_2 &= -\int_V \int_{\Omega} \underline{\Omega}.\nabla \psi_3^{+} \, \underline{\Omega}.\nabla (\psi_2^{+} - \psi_3^{+}) \, d\Omega \, dV
\end{aligned} \tag{5.4-20}$$

The coefficients for four trial functions case are given in Appendix C. In the case of N trial functions extrapolation (N-1) parameters α_i are required to be calculated.

Going back to the optimised coefficient $\hat{a}_0$ for two trial functions extrapolation in(5.4-14),it is illustrated below as to how this may be evaluated. Consider a linear element in one dimensional slab geometry with two moment expansions for ψ_1^+ and ψ_2^+.

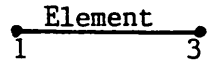


Fig. 5.6

The local node numbering is shown above. The quantity to be evaluated is

$$\hat{a}_0 = \frac{-\int_0^h \int_\mu \mu^2 \frac{d\psi_2^+}{dx} \frac{d\chi_{12}}{dx} d\mu dx}{\int_0^h \int_\mu \mu^2 \left(\frac{d\chi_{12}}{dx}\right)^2 d\mu dx} \qquad (5.4\text{-}21)$$

Consider the denominator. This may be written as

$$\frac{\alpha_0}{h}\left(\bar{\chi}_1^2 - 2\bar{\chi}_1\bar{\chi}_3 + \bar{\chi}_3^2\right)_{12} + \frac{\beta_0}{h}\left(\bar{\chi}_1\bar{\chi}_2 - \bar{\chi}_1\bar{\chi}_4 - \bar{\chi}_2\bar{\chi}_3 + \bar{\chi}_3\bar{\chi}_4\right)_{12}$$

$$+ \frac{\gamma_2}{h}\left(\bar{\chi}_1\bar{\chi}_2 - \bar{\chi}_2\bar{\chi}_3 - \bar{\chi}_4\bar{\chi}_1 + \bar{\chi}_4\bar{\chi}_3\right)_{12} + \frac{\alpha_2}{h}\left(\bar{\chi}_2^2 - 2\bar{\chi}_2\bar{\chi}_4 + \bar{\chi}_4^2\right)_{12}$$

(5.4-22)

where α_0, β_0, γ_2, α_2 are defined in Section 4.5 and

with the node numbering given in Fig. 5.6. The $(\bar{\chi}_i)_{12}$ are nodal values of $\psi_1^+(x,\mu) - \psi_2^+(x,\mu)$ after Legendre polynomial expansion and linear finite element shape function substitution. The quantity in (5.4-22) may also be expressed as

$$\left[\bar{\chi}_1\ \bar{\chi}_2\ \bar{\chi}_3\ \bar{\chi}_4\right]_{12}\begin{bmatrix} A/h & -A/h \\ -A/h & A/h \end{bmatrix}\begin{bmatrix}\bar{\chi}_1\\ \bar{\chi}_2\\ \bar{\chi}_3\\ \bar{\chi}_4\end{bmatrix} \qquad (5.4\text{-}23)$$

or

$$\bar{\underline{\chi}}_{12}^T\, S_A\, \bar{\underline{\chi}}_{12} \qquad (5.4\text{-}24)$$

where S_A is the full local matrix consisting of angular and spatial matrices A and $\frac{2}{h}\begin{bmatrix}1 & -1\\ -1 & 1\end{bmatrix}$. Here $\bar{\underline{\chi}}_{12}^T$ is a row vector of nodal values of χ_{12} and $\bar{\underline{\chi}}_{12}$ is a column vector of nodal values. So existing spatial and angular matrices, together with nodal values of ψ_1^+ and ψ_2^+, can be used to evaluate $\hat{a}_0$. This also applies to two and three dimensional geometry. The $\int_0^h\int_\mu \mu^2 \frac{d\psi_2^+}{dx}\frac{d\chi_{12}}{dx}\,d\mu\,dx$ term is evaluated as

$$\bar{\underline{\psi}}_2^T\, S_A\, \bar{\underline{\chi}}_{12} \qquad (5.4\text{-}25)$$

where $\bar{\underline{\chi}}_{12}$ and S_A are defined as before and $\bar{\underline{\psi}}_2^T$ is a row vector of the nodal values of ψ_2^+. An alternative way of writing (5.4-24) is

$$\int_0^h \sum_{i=1}^{2}\sum_{k=1}^{2}\sum_{j=1}^{2}\sum_{l=1}^{2} \left(\frac{d\psi_k}{dx}\right)\left(\frac{d\psi_l}{dx}\right)(\bar{\chi}_{ik})\,(\bar{\chi}_{jl})\,a_{ij}\,dx \qquad (5.4\text{-}26)$$

where Ψ_k are element shape functions a_{ij} are angular constants, $(\bar{\chi}_{ik})_{12}$ are nodal values of $\chi^+(r, \Omega)$. The quantity in (5.4-26) is a polynomial in the nodal values of $\chi^+(r, \Omega)$.

5.4-5 Extrapolation Method for the First Order Equation

The elementary extrapolation method described earlier can be used for the first order equation. Ackroyd [6] has obtained boundary tied and boundary free maximum principles $\hat{K}(\phi)$ and $\bar{K}(\phi)$ respectively for the first order transport equation. The $\bar{K}(\phi)$ is the more general principle. Extrapolation methods can be defined for both of these principles. Consider for instance, the $\bar{K}(\phi)$ functional given below

$$\begin{aligned}\hat{K}(\phi) = & \; 2\int_V \left[\langle \phi, s \rangle + \langle \Omega \cdot \nabla \phi \, \Sigma^{-1} s \rangle \right] dv \\ & - \int_V \left[\langle \Omega \cdot \nabla \phi, \Sigma^{-1} \Omega \cdot \nabla \phi \rangle + \langle \phi, \Sigma \phi \rangle \right] dv \\ & - \int_{S_b} \int_{\Omega} |\Omega \cdot n| \, (\phi)^2 \, d\Omega \, ds\end{aligned} \tag{5.4-27}$$

where the self-adjoint positive operators Σ and Σ^{-1} are defined as

$$\Sigma \phi = \sigma_T \phi - \int_{\Omega'} \sigma_s (r, \Omega \cdot \Omega') \, \phi(r, \Omega') \, d\Omega' \tag{5.4-28}$$

and

$$\Sigma^{-1} \phi = \phi / \sigma_T + \int_{\Omega'} f(r, \Omega \cdot \Omega') \, \phi(r, \Omega') \, d\Omega' \tag{5.4-29}$$

with $f(r, \Omega \cdot \Omega')$ defined by

$$f(r, \Omega \cdot \Omega') = \frac{\sigma_s(r, \Omega \cdot \Omega')}{\sigma_T^2} + \int_{\Omega''} f(r, \Omega'' \cdot \Omega') \frac{\sigma_s (r, \Omega \cdot \Omega'')}{\sigma_T} \, d\Omega'' \tag{5.4-30}$$

The trial function ϕ in the $\tilde{K}(\phi)$ principle has to satisfy the perfect reflector boundary condition and has to be continuous at interfaces for all directions $\underline{\Omega}$ crossing interfaces. The Euler-Lagrange equation for $\tilde{K}(\phi)$ is a differential equation of the type

$$\underline{\Omega}.\nabla \left[\Sigma^{-1} (s - \underline{\Omega}.\nabla\phi_0)\right] + \Sigma\phi_0 = s \qquad (5.4\text{-}31)$$

with the boundary conditions

$$\begin{aligned} |\underline{\Omega}.\underline{n}| (2T - \phi_0) + \underline{\Omega}.\underline{n}\, \Sigma^{-1} (s - \underline{\Omega}.\nabla\phi_0) &= 0 \qquad S_s \\ |\underline{\Omega}.\underline{n}|\, \phi_0 - \underline{\Omega}.\underline{n}\, \Sigma^{-1} (s - \underline{\Omega}.\nabla\phi_0) &= 0 \qquad S_b \end{aligned} \qquad (5.4\text{-}32)$$

where $T(r,\underline{\Omega})$ is an inward surface source.

Equation (5.4-31) can be transformed into even or odd parity second order transport equations or the first order Boltzmann equation [6]. In the case of the $\tilde{K}(\phi)$ functional the optimised coefficient $\hat{a}_0$ for V_V for two trial function extrapolation is

$$\hat{a}_0 = \frac{-\int_V \int_\Omega \underline{\Omega}.\nabla\psi_2\, \underline{\Omega}.\nabla(\psi_1 - \psi_2)\, d\Omega\, dV}{\int_V \int_\Omega \left[\underline{\Omega}.\nabla(\psi_1 - \psi_2)\right]^2 d\Omega\, dV} \qquad (5.4\text{-}33)$$

where $\psi_i(r,\underline{\Omega})$ are of course the angular fluxes obtained by filling the void with absorbers of cross section σ_{V_i}, $i = 1, 2, \ldots, N$.

Then

$$\hat{\psi}_E(r,\underline{\Omega}) = \hat{a}_0 \psi_1(r,\underline{\Omega}) + (1-\hat{a}_0)\psi_2(r,\underline{\Omega}) \qquad (5.4\text{-}34)$$

is the extrapolated solution.

5.4.6 Improved Solution in the Void

A way of improving the flux profile obtained in the void, from elementary extrapolation, suggested by Ackroyd [5], is described below. Having already obtained a two trial function extrapolation solution, viz.,

$$\hat{\psi}_E^+ = \hat{a}_0 \psi_1^+ + (1-\hat{a}_0)\psi_2^+$$

for the whole system, the main aim is to use $\hat{\psi}_E^+$ as a foundation for an improved solution in the void, V_V.

Let $\bar{\psi}_E^+ = \hat{\psi}_E^+$ in the nonvoid region

and $\bar{\psi}_E^+ = \hat{\psi}_E^+ + \phi_V^+$ in the void region (5.4-35)

where $$\phi_V^+ = \sum_{n=1}^{N} a_n \phi_{Vn}^+ .$$

The finite element approximation $\phi_V^+(r,\underline{\Omega})$ vanishes on the boundary of the void region since $\bar{\psi}_E^+$ has to be continuous at interfaces. If σ_V is the macroscopic absorption cross section in V_V, then we can write

$$K(\bar{\psi}_E^+) = \int_{V_R}\int_{\Omega} \{ 2\bar{\psi}_E^+ S^+ - [\underline{\Omega}.\nabla\bar{\psi}_E^+ g(\underline{\Omega}.\nabla\bar{\psi}_E^+) + \bar{\psi}_E^+ c\,\bar{\psi}_E^+] \} d\underline{\Omega}\,dV$$

$$-\int_{V_V}\int_{\Omega} [\frac{(\underline{\Omega}.\nabla\bar{\psi}_E^+)^2}{\sigma_v} + \sigma_v (\bar{\psi}_E^+)^2] d\Omega\,dV$$

$$-\int_{S_b}\int_{\Omega} (\bar{\psi}_E^+)^2 |\underline{\Omega}.\underline{n}|\, d\Omega\,ds$$

Maximising $K(\bar{\psi}_E^+)$ with respect to the coefficients a_n gives

$$\int_{V_V}\int_{\Omega} \{ (\underline{\Omega}.\nabla\bar{\psi}_E^+)\underline{\Omega}.\nabla\phi_{Vn}^+ + \sigma_v^2 \bar{\psi}_E^+ \phi_{Vn}^+ \} d\Omega\,dV = 0 \qquad (5.4\text{-}36)$$

where $\bar{\psi}_E^+ = \hat{\psi}_E^+ + \sum_{n=1}^{N} \hat{a}_n \phi_{Vn}^+$ and $\hat{a}_n$ are the optimised coefficients. Equation (5.4-36) may be written as:

$$\int_{V_V}\int_{\Omega} \{ \underline{\Omega}.\nabla(\hat{\psi}_E^+ + \sum_n \hat{a}_n \phi_{Vn}^+)\underline{\Omega}.\nabla\phi_{Vm}^+ + \sigma_v^2(\hat{\psi}_E^+ + \sum_n \hat{a}_n \phi_{Vn}^+)\phi_{Vm}^+ \} d\Omega\,dV$$

where $n,m = 1,2,\ldots,N$,

or

$$\sum_{n=1}^{N} \hat{a}_n \int_{V_V}\int_{\Omega} [\underline{\Omega}.\nabla\phi_{Vn}^+ \underline{\Omega}.\nabla\phi_{Vm}^+ + \sigma_v^2 \phi_{Vm}^+ \phi_{Vm}^+] d\Omega\,dV$$

$$= -\int_{V_V}\int_{\Omega} [\underline{\Omega}.\nabla\hat{\psi}_E^+ \underline{\Omega}.\nabla\phi_{Vm}^+ - \sigma_v^2 \hat{\psi}_E^+ \phi_{Vm}^+] d\Omega\,dV \qquad (5.4\text{-}37)$$

This may be written in matrix form as

$$B\underline{a} = \underline{c} \qquad (5.4\text{-}38)$$

where $\mathcal{B}$ is a symmetric square matrix with elements

$$b_{mn} = \int_{V_V}\int_{\Omega} [\underline{\Omega}.\nabla \phi^+_{Vn}\, \underline{\Omega}.\nabla \phi^+_{Vm} + \sigma_V^2\, \phi^+_{Vn}\, \phi^+_{Vm}]\, d\Omega\, dV \ .$$

$\underline{a}$ is vector of unknowns $\hat{a}_n$, $\underline{c}$ is a vector of known quantities

$$-\int_{V_V}\int_{\Omega} [\underline{\Omega}.\nabla \hat{\psi}^+_{\epsilon}\, \underline{\Omega}.\nabla \phi^+_{Vm} - \sigma_V^2\, \hat{\psi}^+_{\epsilon}\, \phi^+_{Vm}]\, d\Omega\, dV \ .$$

The solutions ϕ^+_{Vn} can be obtained with void filled with absorbers σ_{Vn} and with the condition that ϕ^+_{Vn} vanish at V_V/V_R interface nodes. The $\hat{a}_n$ are then obtained from the matrix equation (5.4-38).

5.4.7 Sequential Extrapolation

In Section 5.4.1, the method of elementary extrapolation for void problems was described where a single parameter α was used for the whole system. Below, we illustrate the idea of sequential extrapolation in which the parameter α varies in a way to be described. A generalisation is of course nodal extrapolation which is discussed in Section 5.4.8.

Sequential extrapolation is based on a sequence of increasing large systems. Consider the void problem shown in Fig. 5.7, that of the straight duct. Approximation ψ_ϵ^+ for this problem can be obtained in the elementary version of the extrapolation method by maximising the functional $K^+(\psi_\epsilon^+)$, defined for the whole of the duct region in terms of a single parameter α . The elementary method cannot be expected to

be a good approximation everywhere in the duct. The original duct problem can be considered to be a sequence of duct problems as shown in Fig. 5.8. In the first system, parameters α_I can be found for $x \in [a_1, a_2]$, which gives an optimised solution

$$\hat{\psi}^+_{I\epsilon} = \hat{\alpha}_I \psi_1^+ + (1 - \hat{\alpha}_I)\, \psi_2^+ \qquad (5.4\text{-}39)$$

by minimising the duct functional $K^+(\psi^+_{I\epsilon})$ for $x \in [a_1, a_2]$. The calculation of $\hat{\alpha}_I$ being as in (5.4-14) with the spatial integration performed over a single element. With system II of the duct, the optimised solution is taken to be

$$\hat{\psi}^+_{\epsilon II} = \hat{\alpha}_I \psi_1^+ + (1 - \hat{\alpha}_I)\, \psi_2^+ \quad \text{for} \quad x \in [a_1, a_2] \qquad (5.4\text{-}40)$$

and

$$\hat{\psi}^+_{\epsilon II} = \hat{\alpha}_{II} \psi_1^+ + (1 - \hat{\alpha}_{II})\, \psi_2^+ \quad \text{for} \quad x \in [a_3, a_4] \qquad (5.4\text{-}41)$$

The parameter $\hat{\alpha}_{II}$ is found by optimising the duct functional for $x \in [a_3, a_4]$. Along AB and CD the nodal values are determined by (5.4-40) and (5.4-41). See Fig. 5.8. If the nodes of the shaded elements lie on AB and CD only then $\psi^+_{\epsilon II}$ is defined over these elements. If on the other hand, the nodes of the shaded elements do not lie on AB or CD the value of $\hat{\alpha}$ can be obtained by linear interpolation of $\hat{\alpha}_I$ and $\hat{\alpha}_{II}$. The above process then defines $\hat{\psi}^+_{\epsilon II}$ for $x \epsilon [a_0, a_4]$. For system III we have

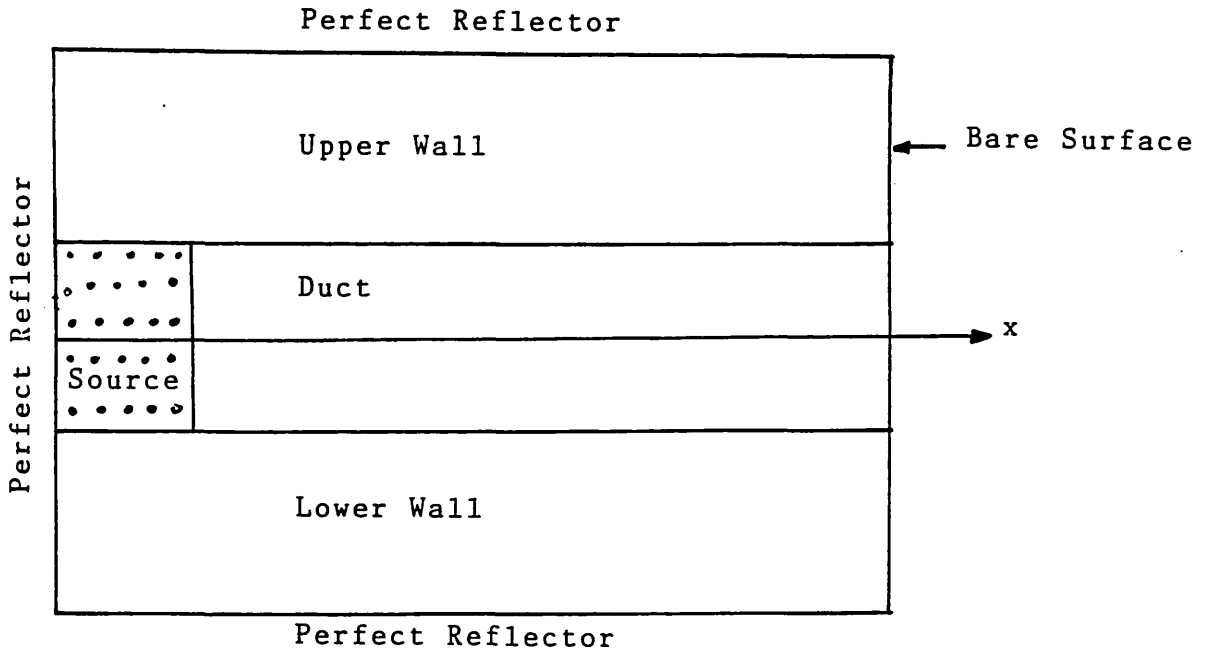


Fig. 5.7 Duct Problem for Sequential Extrapolation Example

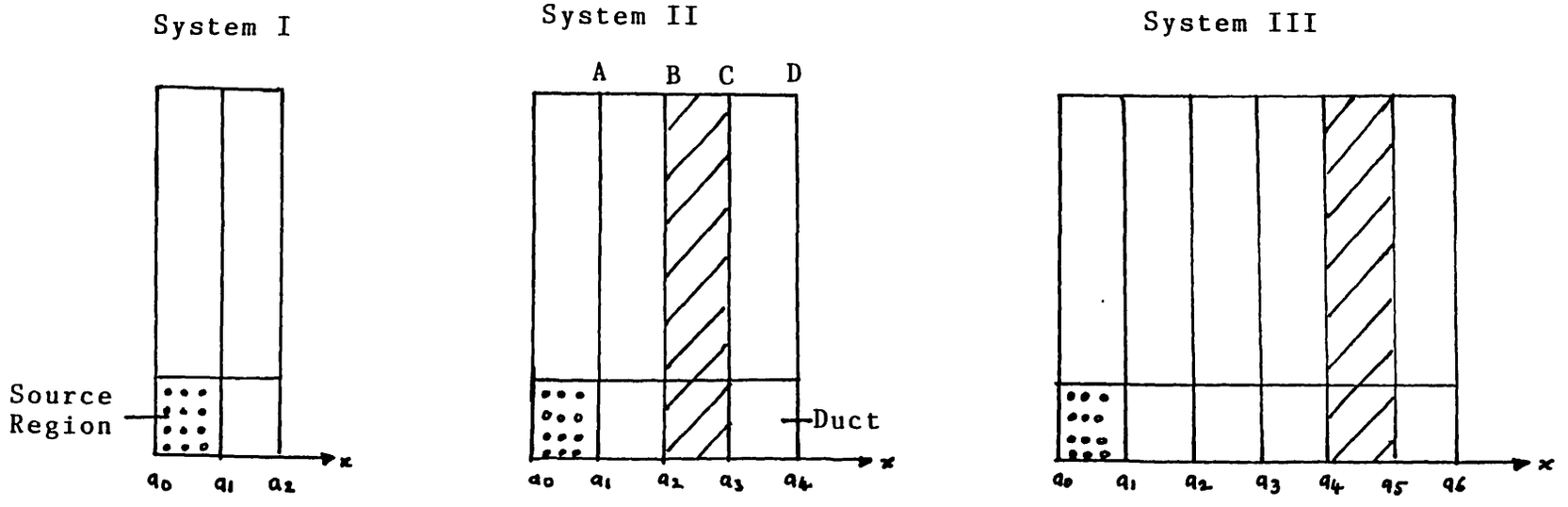


Fig. 5.8 Sequence of Duct Problems

$$\hat{\psi}^{+}_{E\,III} = \hat{\alpha}_{I}\,\psi_1^{+} + (1-\hat{\alpha}_{I})\,\psi_2^{+} \qquad x \in [a_0, a_2]$$

$$\hat{\psi}^{+}_{E\,III} = \hat{\psi}^{+}_{E\,II} \qquad x \in [a_2, a_3] \qquad (5.4\text{-}42)$$

and $$\hat{\psi}^{+}_{E\,III} = \hat{\alpha}_{II}\,\psi_1^{+} + (1-\hat{\alpha}_{II})\,\hat{\psi}_2^{+} \qquad x \in [a_3, a_4]$$

from the previous calculations. For the interval $[\,a_5, a_6\,]$

$$\hat{\psi}^{+}_{E\,III} = \hat{\alpha}_{III}\,\psi_1^{+} + (1-\hat{\alpha}_{III})\,\psi_2^{+} \qquad (5.4\text{-}43)$$

where $\hat{\alpha}_{III}$ minimises the duct functional for $x \in [\,a_5, a_6\,]$. For $x \in [\,a_4, a_5\,]$, $\hat{\psi}^{+}_{E\,III}$ is defined by interpolation as before. The above sequential extrapolation may give appropriate values of α since the duct functional is minimised for segments of the duct. Strictly, the duct functional should be minimised for the whole duct as in the nodal (or multiparameter) extrapolation method.

A Correction Procedure.

If the extrapolated solution ψ_E^{+} is equated to the exact solution $\phi_0^{+}(x,\underline{\Omega})$ in the void, i.e.

$$\phi_0^{+}(x,\underline{\Omega}) = \alpha\,(\psi_1^{+} - \psi_2^{+}) + \psi_2^{+}$$

we have

$$\alpha = \left(\frac{\phi_0^{+} - \psi_2^{+}}{\psi_1^{+} - \psi_2^{+}}\right) . \qquad (5.4\text{-}44)$$

Since $\sigma_{V1} > \sigma_{V2}$, then in theory $\psi_2^{+} > \psi_1^{+}$ in the void. Also $\phi_0^{+} > \psi_2^{+}$

because there is no absorption in the duct for the exact solution ϕ_0^+ . The more closely ψ_E^+ approaches ϕ_0^+ the better is the approximation ψ_E^+ . A necessary condition on ψ_E^+ is that

$$\psi_E^+ > \psi_2^+ .$$

i.e. $\alpha < 0$. When the above process of sequential extrapolation gives $\alpha \geq 0$, the value should be ignored and a value of α for the previous system in the sequence should be used. An alternative is to use the global α , which generally is negative everywhere, when sequential extrapolation gives $\alpha \geq 0$.

Fig. 5.9 illustrates the behaviour of ψ_E^+ with α for two trial function global extrapolation.

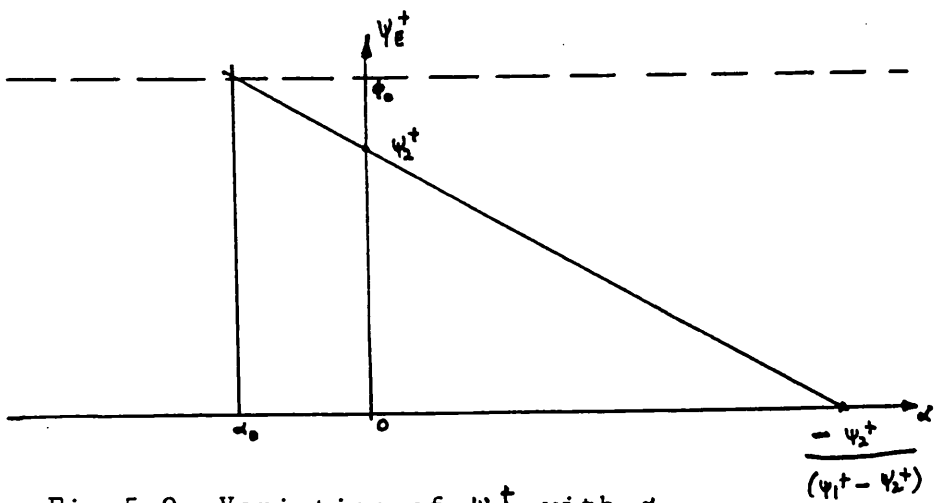


Fig 5.9 Variation of ψ_E^+ with α .

In theory we will have $\phi_0^+ > \psi_E^+ > \psi_2^+ > \psi_1^+$ everywhere in a system since ψ_1^+, ψ_2^+ are obtained with absorption cross-sections σ_{v1} and σ_{v2} in the void with $\sigma_{v2} < \sigma_{v1}$. In this case α will lie in the range $(\alpha_0, 0)$ and will be negative. If $\alpha = 0$ then the second solution ψ_2^+ is recovered.

5.4.8 Multiparameter Extrapolation

One reason for obtaining high values of $K^+(\phi^+)$ with a trial function which is not a good approximation to the exact solution may lie in the flexibility of the trial function. In the direct application of the $K^+(\phi^+)$ principle or the conventional finite elements for voids the trial function has complete flexibility in the specification, at a node, of the nodal values of an element, for the spherical harmonics expansion; i.e. flexibility in all the nodes, the first moment and higher moment nodes. In the elementary method of extrapolation the complete flexibility was restricted in such a way that the nodal values at a node (and in fact for the whole system) for all the spherical harmonics are weighted in the same way, whereas in the conventional method they are not constrained. So the extrapolation method uses biased trial functions in place of the unbiased trial functions of the conventional method. The generalised (or multiparameter) extrapolation method also uses biased trial functions. Here the parameter α can be varied and specified independently at each node but, for each node the values for all the spherical harmonics for that node are weighted in the same way. This is illustrated below for a rectangular element with two moments expansion of the even parity flux. At spatial node 1 there are four unknowns corresponding to the two moments spherical harmonics expansion. The weight at node 1 is α_1 for all the four unknowns. Similarly α_5, α_9 and α_{13} are the weights at the other

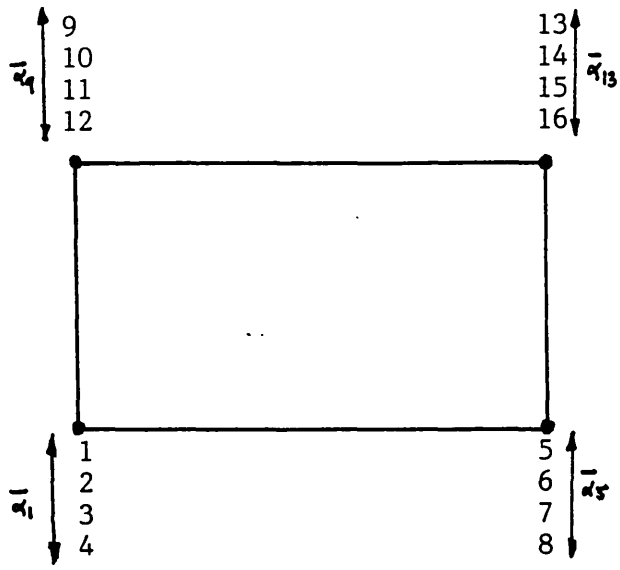


Fig. 5.10 Rectangular Element with Varying α.

nodes of the element. This means that the calculation of nodal α is simply a diffusion theory type calculation, i.e. it is effectively a one moment calculation, involving one unknown per node. Since the elementary extrapolation method is a special case of the generalised extrapolation method, and since in both cases the parameter (or parameters) α (α_i) are found by maximising a void functional, the generalised method should give more accurate results than the elementary technique.

In the case of two trial functions, ψ_1^+ and ψ_2^+, the extrapolated solution $\psi_e^+(\underline{r},\underline{\Omega})$ takes the form

$$\psi_e^+(\underline{r},\underline{\Omega}) = \sum_j \sum_i \left(\alpha_j \bar{\psi}_{1ij}^+ + (1-\alpha_j)\bar{\psi}_{2ij}^+\right) a_i(\underline{\Omega})\, \bar{\psi}_j(\underline{r}) \qquad (5.4\text{-}45)$$

for an element. Here i represents the angular expansion index and j the spatial expansion index. $\Omega_i(\underline{\Omega})$ are the even spherical harmonics and $\Psi_j(\underline{r})$ are the shape functions for element e. The bar on ψ^+_{ij} indicates nodal values of the flux. We obtain the following set of linear equations after maximisation of $K^+(\psi_e{}^+)$ with respect to α_i s. For a void element

$$\int_{V_v}\int_{\Omega} \underline{\Omega}.\nabla\Big[\sum_j \alpha_j\Big(\sum_i \bar{X}^+_{ij}\,\Omega_i(\underline{\Omega})\Big)\Psi_j(\underline{r})\Big]\,\underline{\Omega}.\nabla\Big[\sum_l \bar{X}^+_{lk}\,\Omega_l\,\Psi_k\Big]\,d\Omega\,dV$$

$$= -\int_{V_v}\int_{\Omega}\Big[\underline{\Omega}.\nabla\sum_{ij}\Big(\bar{\psi}^+_{2ij}\,\Omega_i(\underline{\Omega})\,\Psi_j(\underline{r})\Big)\Big]\,\underline{\Omega}.\nabla\Big[\sum_l \bar{X}^+_{lk}\,\Omega_l\,\Psi_k\Big]\,d\Omega\,dV \qquad (5.4\text{-}46)$$

where $$\bar{X}^+_{ij} = \left(\bar{\psi}^+_{1ij} - \bar{\psi}^+_{2ij}\right) \qquad (5.4\text{-}47)$$

is difference of nodal values. Going over all elements of the void leads to a matrix equation for the α_i,

$$A\,\underline{\alpha} = \underline{b} \qquad (5.4\text{-}48)$$

where A is a symmetric banded global matrix.

For a non-void element we have

$$\int_{V_R}\int_{\Omega}\left[\underline{\Omega}\cdot\nabla\left(\sum_{ij}\alpha_j\,\bar{X}^{+}_{ij}\,a_i\psi_j\right)G\,\underline{\Omega}\cdot\nabla\left(\sum_{l}\bar{X}^{+}_{lk}\,a_l\psi_k\right)+\left(\sum_{ij}\alpha_j\,\bar{X}^{+}_{ij}\,a_i\psi_j\right)C\left(\sum_{l}\bar{X}^{+}_{lk}\,a_l\psi_k\right)\right]d\Omega\,dV$$

$$+\int_{S_b}\int_{\Omega}|\underline{\Omega}\cdot\underline{n}|\left(\sum_{ij}\alpha_j\,\bar{X}^{+}_{ij}\,a_i\psi_j\right)\left(\sum_{l}\bar{X}^{+}_{lk}\,a_l\psi_k\right)d\Omega\,dS$$

$$=\int_{V_R}\int_{\Omega}\left[\left(\sum_{ij}s^{+}_{ij}\,a_i\psi_j\right)\left(\sum_{l}\bar{X}^{+}_{lk}\,a_l\psi_k\right)-\underline{\Omega}\cdot\nabla\left(\sum_{ij}\bar{\Psi}^{+}_{2ij}\,a_i\psi_j\right)G\,\underline{\Omega}\cdot\nabla\left(\sum_{l}\bar{X}^{+}_{lk}\,a_l\psi_k\right)\right.$$

$$\left.-\left(\sum_{ij}\bar{\Psi}^{+}_{2ij}\,a_i\psi_j\right)C\left(\sum_{l}\bar{X}^{+}_{lk}\,a_l\psi_k\right)\right]d\Omega\,dV$$

$$-\int_{S_b}\int_{\Omega}|\underline{\Omega}\cdot\underline{n}|\left(\sum_{ij}\bar{\Psi}^{+}_{2ij}\,a_i\psi_j\right)\left(\sum_{l}\bar{X}^{+}_{lk}\,a_l\psi_k\right)d\Omega\,dS$$

(5.4-49)

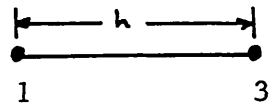
A similar matrix equation to (5.4-48) can be set up for the non-void region. At the interface between a void and non-void region either the void solution can be chosen or the non-void or a mean value of void and non-void fluxes. If two or more void (non-void) regions are non-intersecting then separate calculations are required for each void (non-void) region. How the nodal parameter calculation can be performed with existing spatial and angular matrices is described below.

Consider a line element in one dimensional slab geometry with a two moments expansion for $\psi_1^{+}(x,\mu)$ and $\psi_2^{+}(x,\mu)$. The extrapolated solution may be written as

$$\psi_E^+(x,\mu) = \bar{\alpha}_1 \left(\sum_i \bar{\chi}_i a_i \right) \psi_1(x) + \bar{\alpha}_3 \left(\sum_i \bar{\chi}_i a_i \right) \psi_3(x)$$

$$+ \left(\sum_i \bar{\psi}_{2i}^+ a_i \right) \psi_1(x) + \left(\sum_i \bar{\psi}_{2i}^+ a_i \right) \psi_3(x)$$

(5.4-50)



Element e

where $\bar{\chi}_i = \left(\bar{\psi}_{1i}^+ - \bar{\psi}_{2i}^+ \right)$ is the difference in nodal values of $\psi_1^+(x,\mu)$ and $\psi_2^+(x,\mu)$. The left hand side of the local matrix equation for the parameters $\bar{\alpha}_i$ comes from the $(\bar{\alpha}_i)^2$ term in the functional $K^+(\psi_E^+)$. We have, using the notation of Section 4.5.

$$\frac{\alpha_0}{h}\left[\bar{\alpha}_1^2\bar{\chi}_1^2 - 2\bar{\alpha}_1\bar{\alpha}_3\bar{\chi}_1\bar{\chi}_3 + \bar{\alpha}_3^2\bar{\chi}_3^2\right] + \frac{\beta_0}{h}\left[\bar{\alpha}_1^2\bar{\chi}_1\bar{\chi}_2 - \bar{\alpha}_1\bar{\alpha}_3\bar{\chi}_1\bar{\chi}_4\right.$$

$$\left. - \bar{\alpha}_1\bar{\alpha}_3\bar{\chi}_2\bar{\chi}_3 + \bar{\alpha}_3^2\bar{\chi}_3\bar{\chi}_4\right] + \frac{\alpha_2}{h}\left[\bar{\alpha}_1^2\bar{\chi}_1\bar{\chi}_2 - \bar{\alpha}_1\bar{\alpha}_3\bar{\chi}_2\bar{\chi}_3 - \bar{\alpha}_1\bar{\alpha}_3\bar{\chi}_1\bar{\chi}_4\right.$$

$$\left. + \bar{\alpha}_3^2\bar{\chi}_3\bar{\chi}_4\right] + \frac{\alpha_2}{h}\left[\bar{\alpha}_1^2\bar{\chi}_2^2 - 2\bar{\alpha}_1\bar{\alpha}_3\bar{\chi}_2\bar{\chi}_4 + \bar{\alpha}_3^2\bar{\chi}_4^2\right]$$

(5.4-51)

Taking derivatives with respect to $\bar{\alpha}_1$ and $\bar{\alpha}_3$ of (5.4-51) gives

$$\frac{\alpha_0}{h}\left[2\bar{\alpha}_1 \bar{X}_1^2 - 2\bar{\alpha}_3 \bar{X}_1 \bar{X}_3 \right] + \beta_0 \left[2\bar{\alpha}_1 \bar{X}_1 \bar{X}_2 - \bar{\alpha}_3 \bar{X}_1 \bar{Y}_4 - \bar{\alpha}_3 \bar{X}_2 \bar{Y}_3 \right]$$

$$+ \frac{\gamma_2}{h}\left[2\bar{\alpha}_1 \bar{X}_1 \bar{X}_2 - \bar{\alpha}_3 \bar{X}_2 \bar{Y}_3 - \bar{\alpha}_3 \bar{X}_1 \bar{Y}_4 \right]$$

$$+ \frac{\alpha_2}{h}\left[2\bar{\alpha}_1 \bar{X}_2^2 - 2\bar{\alpha}_3 \bar{X}_2 \bar{X}_4 \right]$$

and

$$\frac{\alpha_0}{h}\left[-2\bar{\alpha}_1 \bar{X}_1 \bar{X}_3 + 2\bar{\alpha}_3 \bar{X}_3^2 \right] + \frac{\beta_0}{h}\left[-\bar{\alpha}_1 \bar{X}_1 \bar{Y}_4 - \bar{\alpha}_1 \bar{X}_2 \bar{Y}_3 + 2\bar{\alpha}_3 \bar{X}_3 \bar{Y}_4 \right]$$

$$+ \frac{\gamma_2}{h}\left[-\bar{\alpha}_1 \bar{X}_2 \bar{X}_3 - \bar{\alpha}_1 \bar{X}_1 \bar{Y}_4 + 2\bar{\alpha}_3 \bar{X}_3 \bar{Y}_4 \right] + \frac{\alpha_2}{h}\left[-2\bar{\alpha}_1 \bar{X}_2 \bar{Y}_4 + 2\bar{\alpha}_3 \bar{X}_4^2 \right]$$

These may be written in matrix form as

$$\frac{2}{h}\begin{bmatrix} [\bar{X}_1\ \bar{X}_2]\begin{bmatrix} \alpha_0 & (\beta_0+\gamma_2)/2 \\ * & \alpha_2 \end{bmatrix}\begin{bmatrix} \bar{X}_1 \\ \bar{X}_2 \end{bmatrix} & -[\bar{X}_1\ \bar{X}_2]\begin{bmatrix} \alpha_0 & (\beta_0+\gamma_2)/2 \\ * & \alpha_2 \end{bmatrix}\begin{bmatrix} \bar{X}_3 \\ \bar{X}_4 \end{bmatrix} \\ -[\bar{X}_3\ \bar{X}_4]\begin{bmatrix} \alpha_0 & (\beta_0+\gamma_2)/2 \\ * & \alpha_2 \end{bmatrix}\begin{bmatrix} \bar{X}_1 \\ \bar{X}_2 \end{bmatrix} & [\bar{X}_3\ \bar{X}_4]\begin{bmatrix} \alpha_0 & (\beta_0+\gamma_2)/2 \\ * & \alpha_2 \end{bmatrix}\begin{bmatrix} \bar{X}_3 \\ \bar{X}_4 \end{bmatrix} \end{bmatrix}\begin{bmatrix} \bar{\alpha}_1 \\ \bar{\alpha}_3 \end{bmatrix}$$

(5.4-52)

Hence this involves the angular matrix $A = \begin{bmatrix} \alpha_0 & (\beta_0+\beta_2)/2 \\ (\beta_0+\beta_2)/2 & \alpha_2 \end{bmatrix}$,

the spatial matrix $S = \frac{2}{h}\begin{bmatrix} 1 & -1 \\ -1 & 1 \end{bmatrix}$ and the known values $\bar{X}_1, \bar{X}_2, \bar{X}_3, \bar{X}_4$.

The right hand side term is of the form given in (5.4-46). This leads to the following local 'source' vector.

$$\frac{2}{h}\begin{bmatrix} [\bar{X}_1\ \bar{X}_2]\, A \begin{bmatrix} \bar{\psi}_1^+ \\ \bar{\psi}_2^+ \end{bmatrix} - [\bar{X}_1\ \bar{X}_2]\, A \begin{bmatrix} \bar{\psi}_3^+ \\ \bar{\psi}_4^+ \end{bmatrix} & \leftarrow \text{At first spatial node} \\ -[\bar{X}_3\ \bar{X}_4]\, A \begin{bmatrix} \bar{\psi}_1^+ \\ \bar{\psi}_2^+ \end{bmatrix} + [\bar{X}_3\ \bar{X}_4]\, A \begin{bmatrix} \bar{\psi}_3^+ \\ \bar{\psi}_4^+ \end{bmatrix} & \leftarrow \text{At second spatial node} \end{bmatrix}$$

(5.4-53)

Extending the example to a bilinear rectangular element (X-Y geometry), gives for the left hand side

matrix?

$$\begin{bmatrix} [\bar{X}_1\ \bar{X}_2\ \bar{X}_3\ \bar{X}_4]\, S_{11} A \begin{bmatrix} \bar{X}_1 \\ \bar{X}_2 \\ \bar{X}_3 \\ \bar{X}_4 \end{bmatrix} & [\bar{X}_1 \dots \bar{X}_4]\, S_{12} A \begin{bmatrix} \bar{X}_5 \\ \vdots \\ \bar{X}_8 \end{bmatrix} & [\bar{X}_1 \dots \bar{X}_4]\, S_{13} A \begin{bmatrix} \bar{X}_9 \\ \vdots \\ \bar{X}_{12} \end{bmatrix} & \dots \\ [\bar{X}_5 \dots \bar{X}_8]\, S_{21} A \begin{bmatrix} \bar{X}_1 \\ \vdots \\ \bar{X}_4 \end{bmatrix} & [\bar{X}_5 \dots \bar{X}_8]\, S_{22} A \begin{bmatrix} \bar{X}_5 \\ \vdots \\ \bar{X}_8 \end{bmatrix} & \dots\dots & \\ [\bar{X}_9 \dots \bar{X}_{12}]\, S_{31} A \begin{bmatrix} \bar{X}_1 \\ \vdots \\ \bar{X}_4 \end{bmatrix} & [\bar{X}_9 \dots \bar{X}_{12}]\, S_{32} A \begin{bmatrix} \bar{X}_5 \\ \vdots \\ \bar{X}_8 \end{bmatrix} & \dots\dots & \\ [\bar{X}_{13} \dots \bar{X}_{16}]\, S_{41} A \begin{bmatrix} \bar{X}_1 \\ \vdots \\ \bar{X}_4 \end{bmatrix} & [\bar{X}_{13} \dots \bar{X}_{16}]\, S_{42} A \begin{bmatrix} \bar{X}_5 \\ \vdots \\ \bar{X}_8 \end{bmatrix} & \dots\dots & \end{bmatrix} \begin{bmatrix} \bar{a}_1 \\ \bar{a}_5 \\ \bar{a}_9 \\ \bar{a}_{13} \end{bmatrix}$$

(5.4-54)

Here S_{ij} are elements of the spatial matrix S. Similarly the right hand side gives

$$\begin{bmatrix} [\bar{\chi}_1 \ldots \bar{\chi}_4]\, S_{11}\, A \begin{bmatrix} \bar{\psi}_1^+ \\ \vdots \\ \bar{\psi}_4^+ \end{bmatrix} + [\bar{\chi}_1 \cdots \bar{\chi}_4]\, S_{12}\, A \begin{bmatrix} \bar{\psi}_5^+ \\ \vdots \\ \bar{\psi}_8^+ \end{bmatrix} + [\bar{\chi}_1 \cdots \bar{\chi}_4]\, S_{13}\, A \begin{bmatrix} \bar{\psi}_9^+ \\ \vdots \\ \bar{\psi}_{12}^+ \end{bmatrix} + \cdots & \leftarrow \text{At node 1} \\ [\bar{\chi}_5 \ldots \bar{\chi}_8]\, S_{21}\, A \begin{bmatrix} \bar{\psi}_1^+ \\ \vdots \\ \bar{\psi}_4^+ \end{bmatrix} + [\bar{\chi}_5 \cdots \bar{\chi}_8]\, S_{22}\, A \begin{bmatrix} \bar{\psi}_5^+ \\ \vdots \\ \bar{\psi}_8^+ \end{bmatrix} + \cdots & \leftarrow \text{At node 5} \\ [\bar{\chi}_9 \cdots \bar{\chi}_{12}]\, S_{31}\, A \begin{bmatrix} \bar{\psi}_1^+ \\ \vdots \\ \bar{\psi}_4^+ \end{bmatrix} + [\bar{\chi}_9 \cdots \bar{\chi}_{13}]\, S_{32}\, A \begin{bmatrix} \bar{\psi}_5^+ \\ \vdots \\ \bar{\psi}_8^+ \end{bmatrix} + \cdots & \leftarrow \text{At node 9} \\ [\bar{\chi}_{13} \ldots \bar{\chi}_{16}]\, S_{41}\, A \begin{bmatrix} \bar{\psi}_1^+ \\ \vdots \\ \bar{\psi}_4^+ \end{bmatrix} + \cdots & \leftarrow \text{At node 13} \end{bmatrix}$$

(5.4-55)

In the process described above we are essentially summing all the flux moments at a spatial node with appropriate spherical harmonics weighting.

Similar ideas will apply when calculating $\bar{\varphi}_i$, in the nodal extrapolation method, in the non-void region. Here of course the material parameters will be included via the leakage and removal operators, G and C, respectively.

Summing the known nodal fluxes from ψ_1^+ and ψ_2^+ at a node with appropriate weights introduces a biased trial function ψ_ϵ^+, i.e. there is only one value of $\bar{\varphi}_i$ which

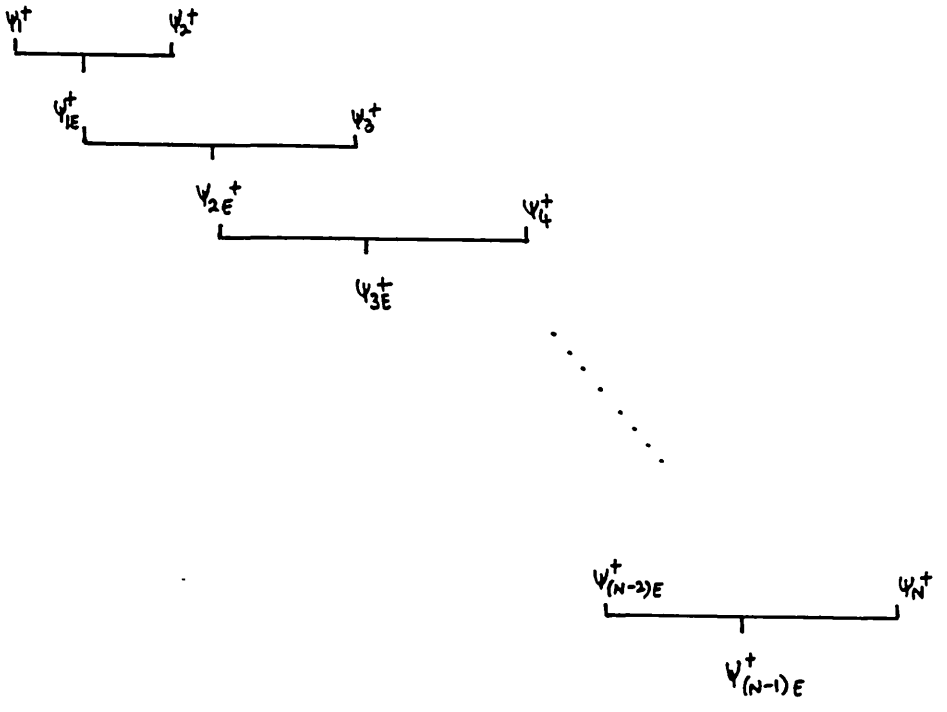
multiplies the first and higher moments at a spatial node. If the trial function is made more flexible by specifying a different $\bar{r}_i$ for each of the higher moments at a node, then the original deficiency of the conventional finite element method would be introduced thus producing ψ_e^+ approximately a constant. This of course, also applies to the case when only the scalar fluxes from $\psi_1^+(r,\Omega)$ and $\psi_2^+(r,\Omega)$ are used to calculate $\bar{r}_i$. The nodal extrapolation method simply requires a diffusion theory type (one moment) calculation. The quantities in (5.4-54) and (5.4-55) are local, i.e. for a single element. The global matrix and the right hand side for the $\bar{r}_i$ calculation over the entire system can be obtained by assembly of local matrices in the usual way.

Schemes for Nodal Extrapolation

The nodal extrapolation solution obtained using two trial functions ψ_1^+ and ψ_2^+ may be used to perform a series of extrapolation calculations. Two schemes are considered below.

Scheme A

Let $\psi_1^+, \psi_2^+, \psi_3^+, \ldots\ldots\ldots, \psi_N^+$ be N independent solutions of related problems obtained by filling the void with materials of absorption cross section $\sigma_{v1}, \sigma_{v2}, \sigma_{v3}, \ldots\ldots, \sigma_{vN}$. Then construct the extrapolated solution as shown below



where

$$\psi_{1E}^+ = \alpha\,\psi_1^+ + (1-\alpha)\,\psi_2^+ \qquad (5.4\text{-}56)$$

$$\psi_{2E}^+ = \alpha\,\psi_{1E}^+ + (1-\alpha)\,\psi_3^+$$

$$\vdots$$

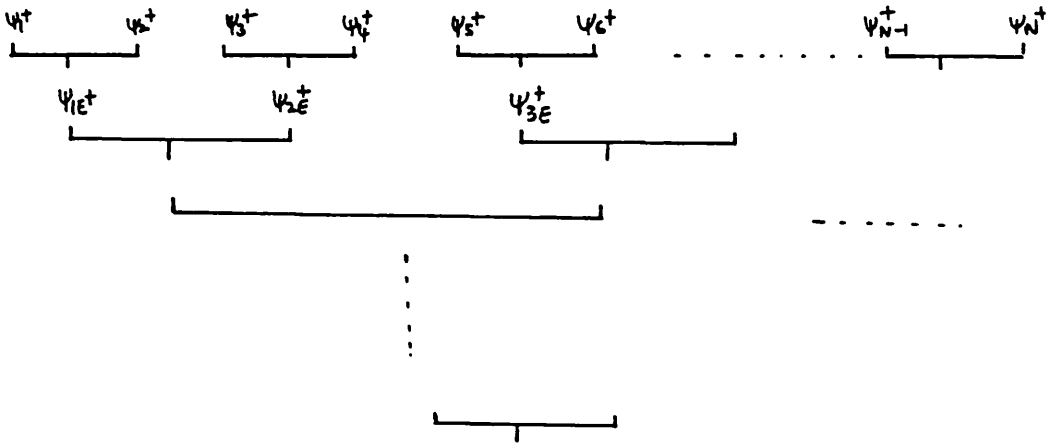
$$\psi_{(N-1)E}^+ = \alpha\,\psi_{(N-2)E}^+ + (1-\alpha)\,\psi_N^+$$

where the α^{j}s will be nodal parameters and $\bar{\alpha}_i$ for each of above equations will be a different set. With this scheme N parallel calculations may be performed to obtain $\psi_1^+, \psi_2^+, \ldots \psi_N^+$. These will be the full angular and spatial calculations. Subsequently only the $\bar{\alpha}_i$ are to be calculated at each stage and this involves only one unknown per node. These latter calculations will not require large execution times or computer memory. An advantage with this approach is that σ_{vi} can be made slowly varying,

and kept relatively high, thus avoiding any distortion in the flux profile. This way we may be more certain of obtaining lower bounds to the exact solution, $\phi_0^+(r, \underline{\Omega})$, even when the solutions $\psi_1^+, \psi_2^+, \ldots, \psi_N^+$ are not necessarily accurate approximations to the related problems. For instance σ_{v1} may be set to $\sigma_{T(surr)}$ with $\sigma_{v2} = \frac{1}{2}\sigma_{T(surr)}$, $\sigma_{v3} = \frac{1}{3}\sigma_{T(surr)}$, $\sigma_{v4} = \frac{1}{4}\sigma_{T(surr)}$.

Scheme B

Again in this scheme parallel calculations can be done to obtain ψ_i^+. Choose N such that there is an even number of solutions at each state of the scheme, until the last.



So combine ψ_1^+ and ψ_2^+ to get ψ_{1E}^+; ψ_3^+ and ψ_4^+ to get ψ_{2E}^+ etc. Then combine the extrapolated solutions using nodal extrapolation in subsequent stages. Another way would be to combine ψ_1^+ and ψ_2^+ to get ψ_{1E}^+, then ψ_2^+ with ψ_3^+ to get ψ_{2E}^+; ψ_3^+ and ψ_4^+ to get ψ_{3E}^+ etc..... Again relatively high values of σ_{vi} can be chosen. It remains to be seen how sensitive these schemes are to variation in σ_{vi}. Scheme A seems to be more promising in getting lower bounds to ϕ_0^+. why?

5.4.9 Choice of Trial Functions for Extrapolation Method

In the extrapolation method, as seen earlier, trial functions, i.e. independent solutions of related problems, are combined linearly to obtain a best approximation solution for the void problem. In order to get satisfactory results with this method, some guide lines as to the choice of trial functions is needed, since in theory there is an infinite choice. We need to restrict the space of admissible trial functions. The trial functions $\psi_1^+, \psi_2^+, \ldots, \psi_N^+$ which are solutions of related problems, are of course dependent on $\sigma_{v1}, \sigma_{v2}, \ldots, \sigma_{vN}$, the void-fill cross sections used in solving the related problems. Hence, some restriction on the choice of σ_{vi} is necessary. As we have seen, low values of σ_{vi} approximately 10^{-3} or less, in the void, produces an almost flat flux profile in the latter. In an N trial function extrapolation we may choose $\sigma_{v1} = \sigma_{T(surr)}$, the total macroscopic cross section for the surrounding region, and choose $\sigma_{vN} > 10^{-3}$. In fact, from test problems analysed it is seen that $\sigma_{vN} \approx \frac{1}{10}\sigma_{T(surr)}$ produces satisfactory results. σ_{vi} $(i = 1, 2, 3, \ldots, N-1)$ can then be chosen such that

$$\frac{1}{10}\sigma_{T(surr)} < \sigma_{vi} \leq \sigma_{T(surr)} \qquad (5.4\text{-}57)$$

We must avoid too low a value for σ_{vN} because it will lead to a flat flux component in the duct. Also, if a lower value of σ_{vN} is chosen, the component solution ψ_N^+ may not be a lower

bound to ϕ_0^+, which is required in theory. In this case the extrapolation method will further push the component solution above the exact solution. Now σ_{V1}, the first term of the sequence of void fill cross sections $\{\sigma_{Vi}\}_{i=1,N}$ may be selected such that they satisfy (5.4-57), i.e.

$$\sigma_{VN} < \sigma_{VN-1} < \cdots\cdots < \sigma_{V2} < \sigma_{V1} \leq \sigma_{T(SUM)}$$

Once σ_{V1} and σ_{VN} have been selected, other terms in the sequence $\{\sigma_{Vi}\}$ may be chosen such that $\{\sigma_{Vi}\}$ form a geometric progression. By keeping σ_{VN} fixed (say $\frac{1}{10}\sigma_{T(SUM)}$) and varying σ_{Vi} ($i<N$) for two trial functions does not significantly vary the extrapolated solution. This is discussed in Section 5.5.3.

5.5 Void Test Problems

5.5.1 Introduction

In the following sections, several one group problems involving voids are analysed in X-Y geometry. The material of the non-void regions has been kept purely absorbing in order to obtain point kernel integration solutions. These can be used as reference solutions against which the new methods can be compared. With a pure absorber the flux in the walls is strongly anisotropic and provides a more difficult problem for the finite element method. Point kernel solutions were obtained from the code RANKERN [7], which performs the integration stochastically. Hence, there is a standard deviation associated with these results. RANKERN results may be considered as 'almost exact' solutions. Comparison of finite element solutions is also made with the finite-difference discrete - ordinate code DOT 3.5 [8] and the Monte Carlo codes McBEND [9] and MORSE [10].

In the iteration method, the void fill cross section shouldn't be too small, since then an almost flat flux will be obtained in the first iteration and the absorption sources in the subsequent iterations will be negligible. On the other hand, if $\sigma_{Vi} = \sigma_{T(surr)}$, then the iteration scheme will have slow convergence. Hence for the iteration method the σ_{Vi} should be chosen such that

$$\frac{1}{100} < \sigma_{Vi} < \sigma_{T(surr)}.$$

The criteria for σ_{Vi} for the extrapolation method was given in the previous section. In addition, each of the trial functions of both the iteration and extrapolation method should be fairly accurate solutions for the specified related problems, with the void filled with an absorbing material. If this is not the case then the combined solutions may not always produce accurate results. In using the iteration and extrapolation methods, the above criteria for σ_{Vi} should be observed to obtain satisfactory results.

5.5.2 Square Source Void Problem with Pure Absorber

This X-Y source problem for an isotropic source has the same geometry as the one analysed by Watanabe and Maynard [11,12] in testing their discrete cones method. The source is surrounded by a void region which is then surrounded by a purely absorbing region. Because of the symmetric nature of the problem only one quarter of the problem is analysed. The source region is of the same material as the outer region. The geometry of this void problem is shown in Fig. 5.11 and the macroscopic cross section data is given in Table 5.1.

Source problems with highly absorbing media and voids problems can be difficult to solve accurately with numerical methods for transport theory, such as the finite-difference discrete-ordinates method. This method of course shows oscillations in the flux for low angular quadrature. On the

Region	S	σ_T (cm^{-1})	σ_S (cm^{-1})
1	6·4	0·8	0·0
2	0·0	· VOID	
3	0·0	0·8	0·0

Table 5.1 Cross Section Data for Square Source Void Problem

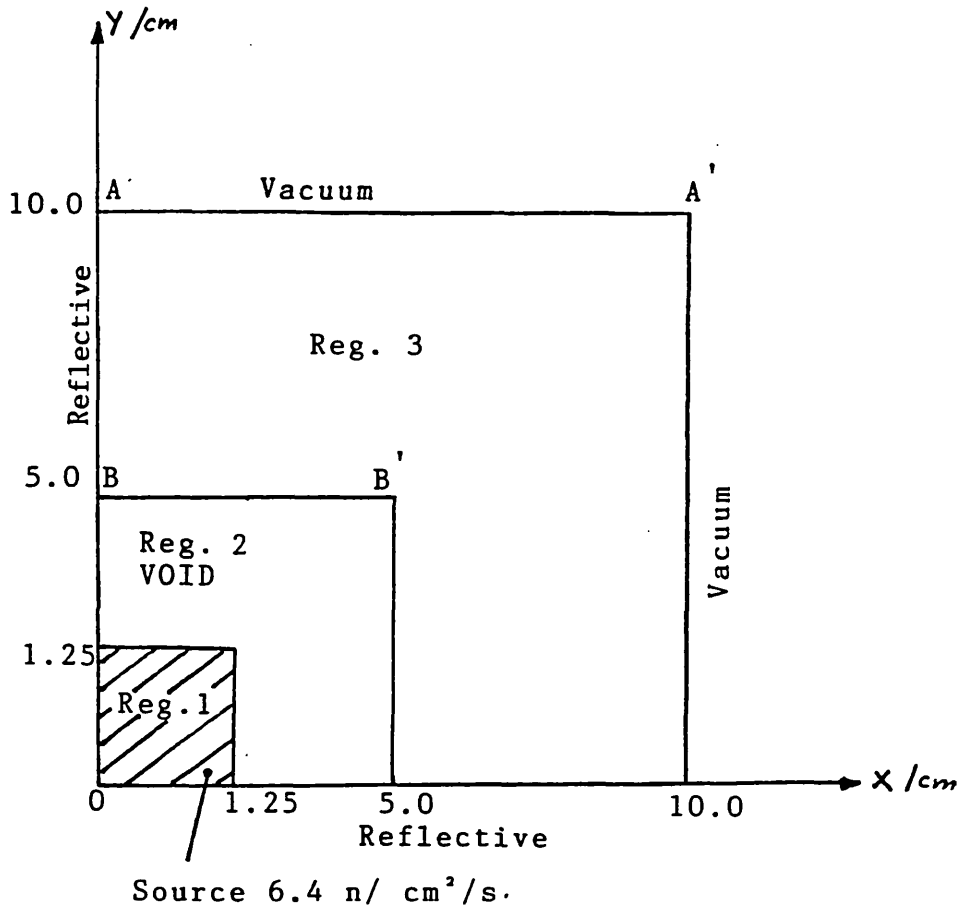


Fig. 5.11 Geometry for the Square Source Void Problem

other hand, point kernel methods, such as the one used in RANKERN [2], are only applicable for voids surrounded by purely absorbing media and not scattering regions.

Conventional finite element calculations were performed for this problem for σ_v = .08 cm^{-1} and σ_v = .008 cm^{-1} in the void region. Calculations are done for three (S6) and four (S8) moments expansion of the even parity flux with (8x8) and (16x16) linear element mesh. The four moments, (16x16) mesh results, along the diagonal are shown in Fig. 5.12. The σ_v = .08 cm^{-1} solution underestimates the flux along the diagonal, while the σ_v = .008 cm^{-1} solution gives fairly good results in the outer region. In fact for this problem difficulty was encountered in obtaining accurate results for component solutions at the source-void interface and the source upper right hand corner. If on the other hand we plot the scalar flux for σ_v = .008 cm^{-1} in V_v along x=0, the perfect reflector surface, we can see significant discrepency with the reference point kernel solution, in the void region. See Fig. 5.13. With further decrease in the void fill cross section, σ_v, the flatness in the void flux starts to appear as shown in Fig. 5.14, along the Y-axis, for σ_v = .0008 cm^{-1}. The global extrapolated solutions with three trial functions and with the following cross section sets $\{0.8, 0.319, 0.128\}$ and $\{0.8, 0.256, 0.08\}$ are shown along the diagonal in Fig 5.15. These are in good agreement with RANKERN values, although at the source-void interface, the solutions are still higher.

This is due to the fact that not all component solutions for 4 moments (16x16) mesh are below the RANKERN values, as they should be in theory. The iteration method was also investigated with various values of σ_v. In Fig. 5.16, results of the iteration scheme with 3 iterations and $\sigma_v = .08\ cm^{-1}$ are shown together with DOT 3.5 results. The iteration solution is not quite as good as the extrapolation results. DOT (S8) profile along the diagonal does not show severe oscillations. This may be due to the symmetry of the problem along the plane X=Y, since along this plane the problem is essentially one dimentional in nature.

The Monte Carlo McBEND results are shown in Fig. 5.17 . They are also in fairly good agreement with RANKERN values along the diagonal. The Monte Carlo calculation, performed by Watmough [13], was for 8x8 mesh.

Results along the outer boundary (bare surface) AA' are shown for conventional finite element method in Fig. 5.18 . Global extrapolation and iteration scalar fluxes are shown graphically in Figs. 5.19 and 5.20 . It is seen that the elementary extrapolation results are in good agreement with RANKERN values. The discrete ordinates calculation (S8) shows oscillations, as expected. Again the three iterations solution is not quite as good as the three trial function global extrapolation solutions. In Fig. 5.21 . McBEND results along $y = 9.5$ cm and the global extrapolated solution along $y = 9.375$ cm are compared. Both are in reasonable agreement with each other

and are above the RANKERN reference solution at y = 10.0 cm., which is physically correct. Next, results along the void boundary BB' are compared. Here nodal or multiparameter results are also generated. Iteration, conventional finite element and elementary extrapolation solutions along the void boundary (BB') are shown in Fig. 5.22 . Elementary extrapolation is in good agreement with reference scalar flux. In the case of two trial functions, elementary extrapolation is compared with nodal extrapolation along BB', since the latter is coded for void regions. Here it is seen that nodal extrapolation provides better results than the other methods, as expected. See Fig. 5.23.These fluxes are for a 3 moment (16x16) mesh and two trial functions nodal extrapolation calculation. Solutions along the diagonal are shown in Figs. 5.24 and 5.25 . Overall the nodal extrapolation results are in better agreement with RANKERN than any of the other methods..

This square source void problem shows that both the extrapolation and iteration methods give satisfactory results even for the case of highly absorbing surrounding regions. Nodal extrapolation gives better results than either of the other two methods. When the region surrounding the void has scattering, the results from the above methods should be even better for low angular expansion of the even parity flux. RANKERN point solutions and some global extrapolation method point scalar fluxes are given in Appendix D.

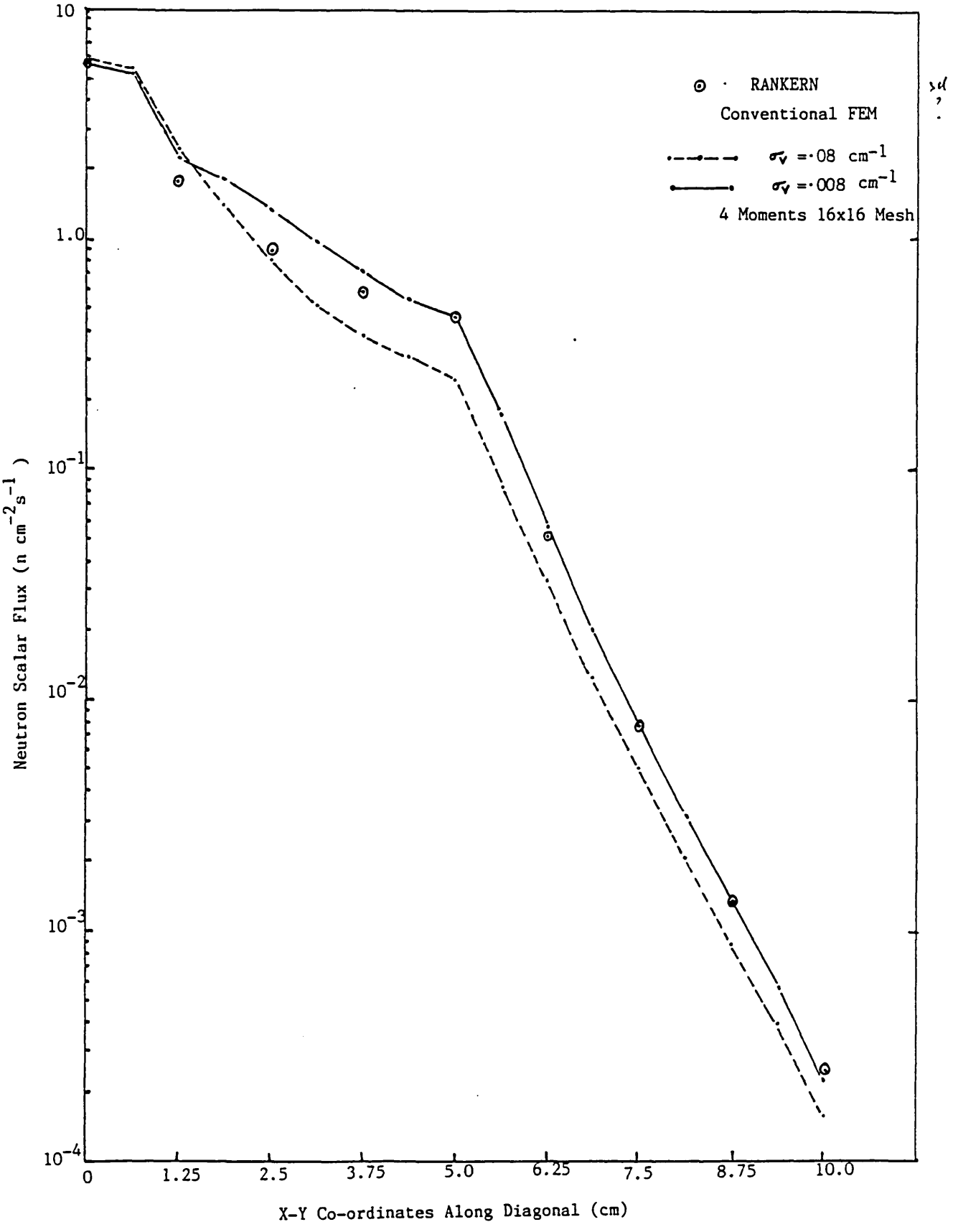


Fig. 5.12 RANKERN and Conventional Finite Element Solutions Along Diagonal OA'.

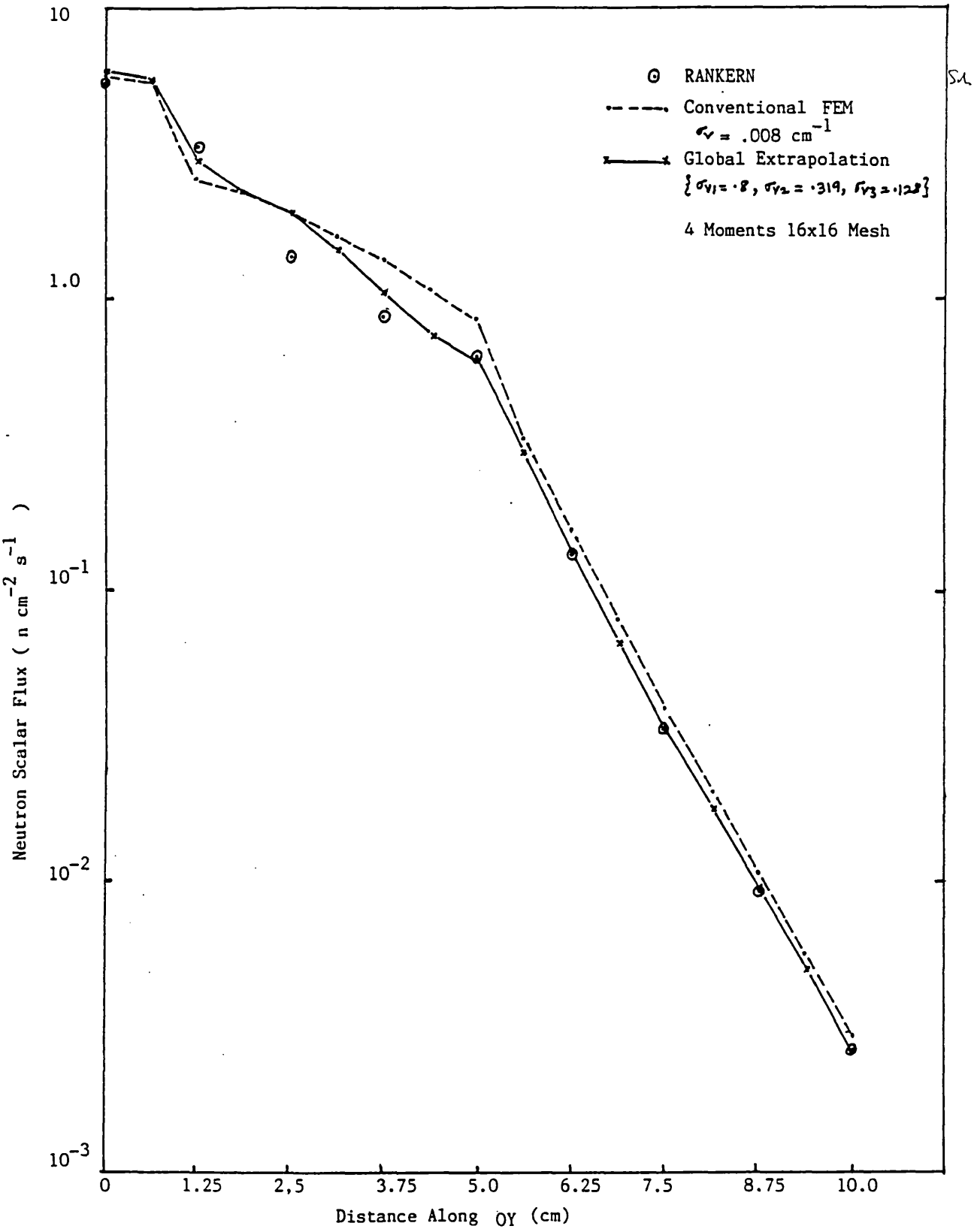


Fig. 5.13 RANKERN, Conventional Finite Element and Global Extrapolation Solutions Along Y Axis.

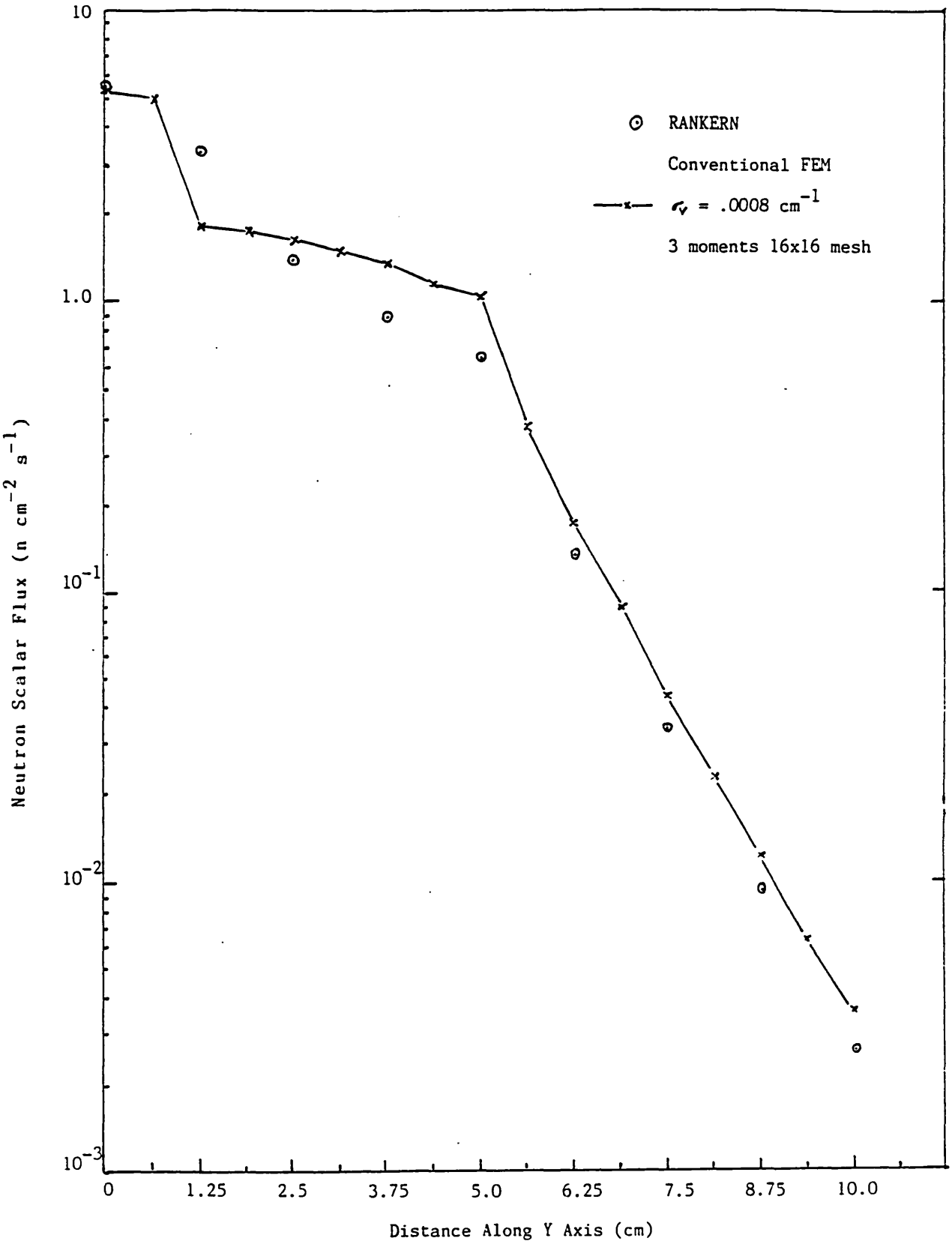


Fig. 5.14 RANKERN and Conventional Finite Element Solutions Along Y Axis.

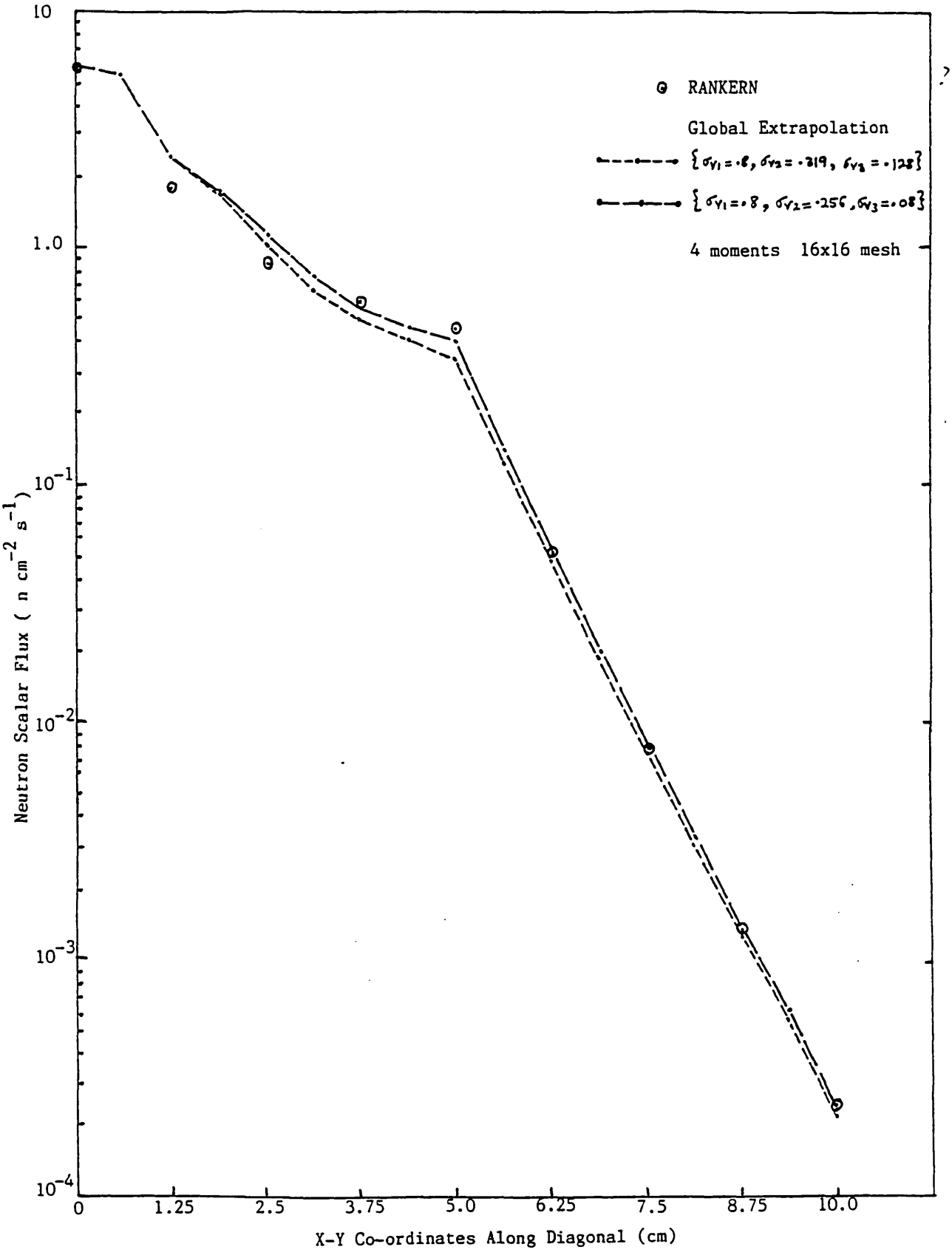


Fig. 5.15 RANKERN and Global Extrapolation Solutions Along Diagonal OA'.

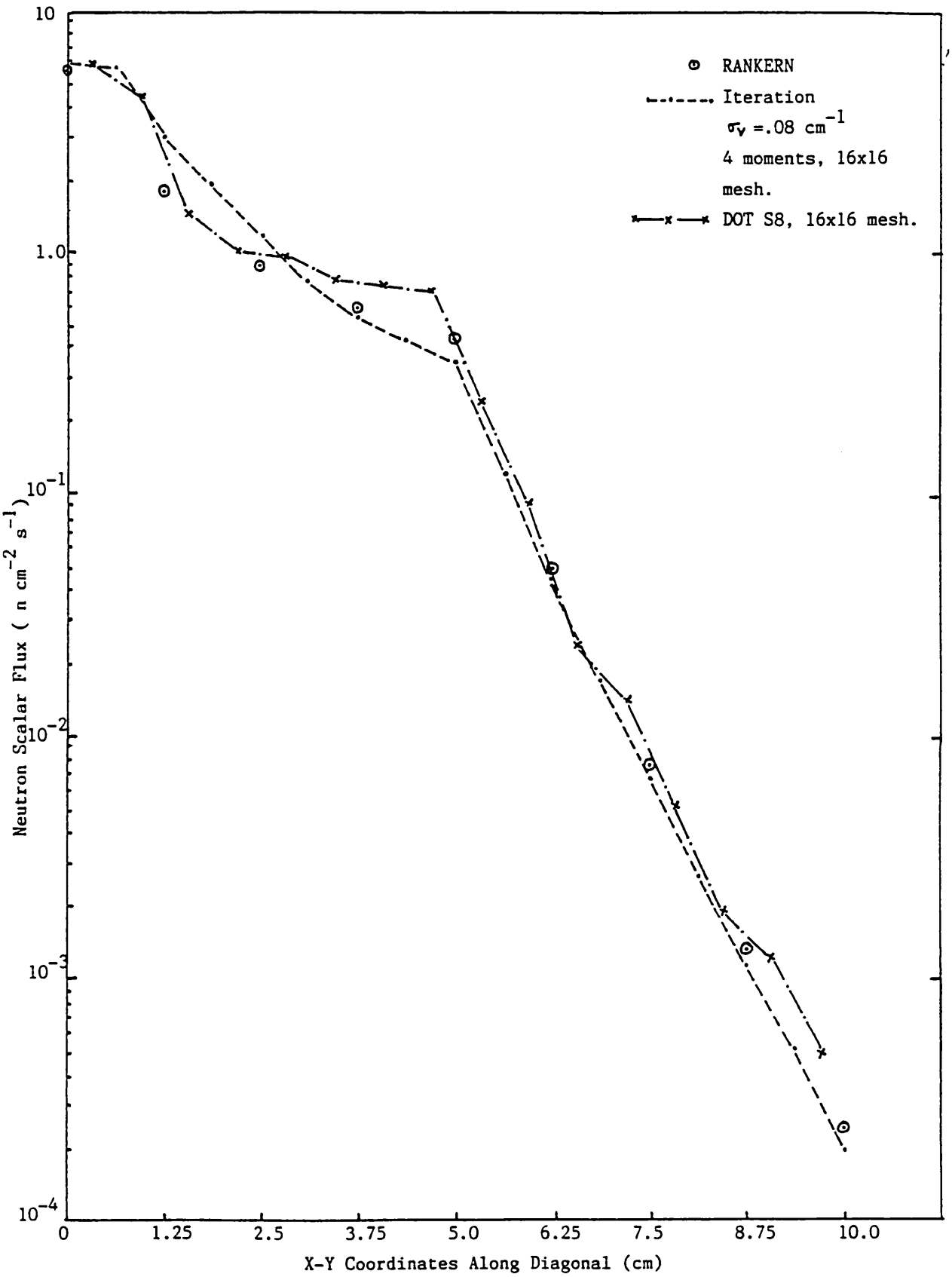


Fig. 5.16 RANKERN, Iteration and DOT Solutions Along Diagonal OA'.

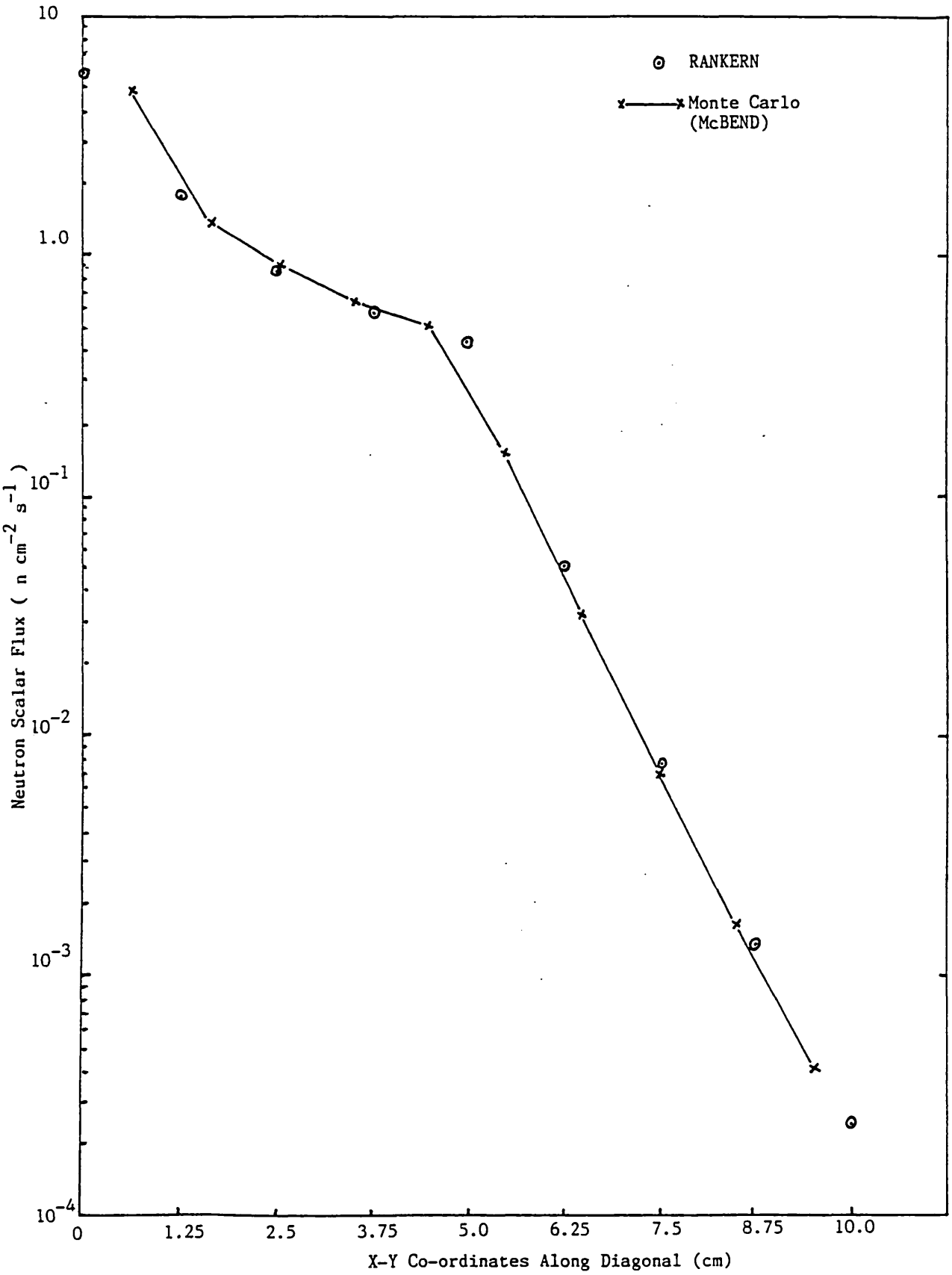


Fig. 5.17 RANKERN, and McBEND (Monte Carlo) Solutions Along Diagonal OA'.

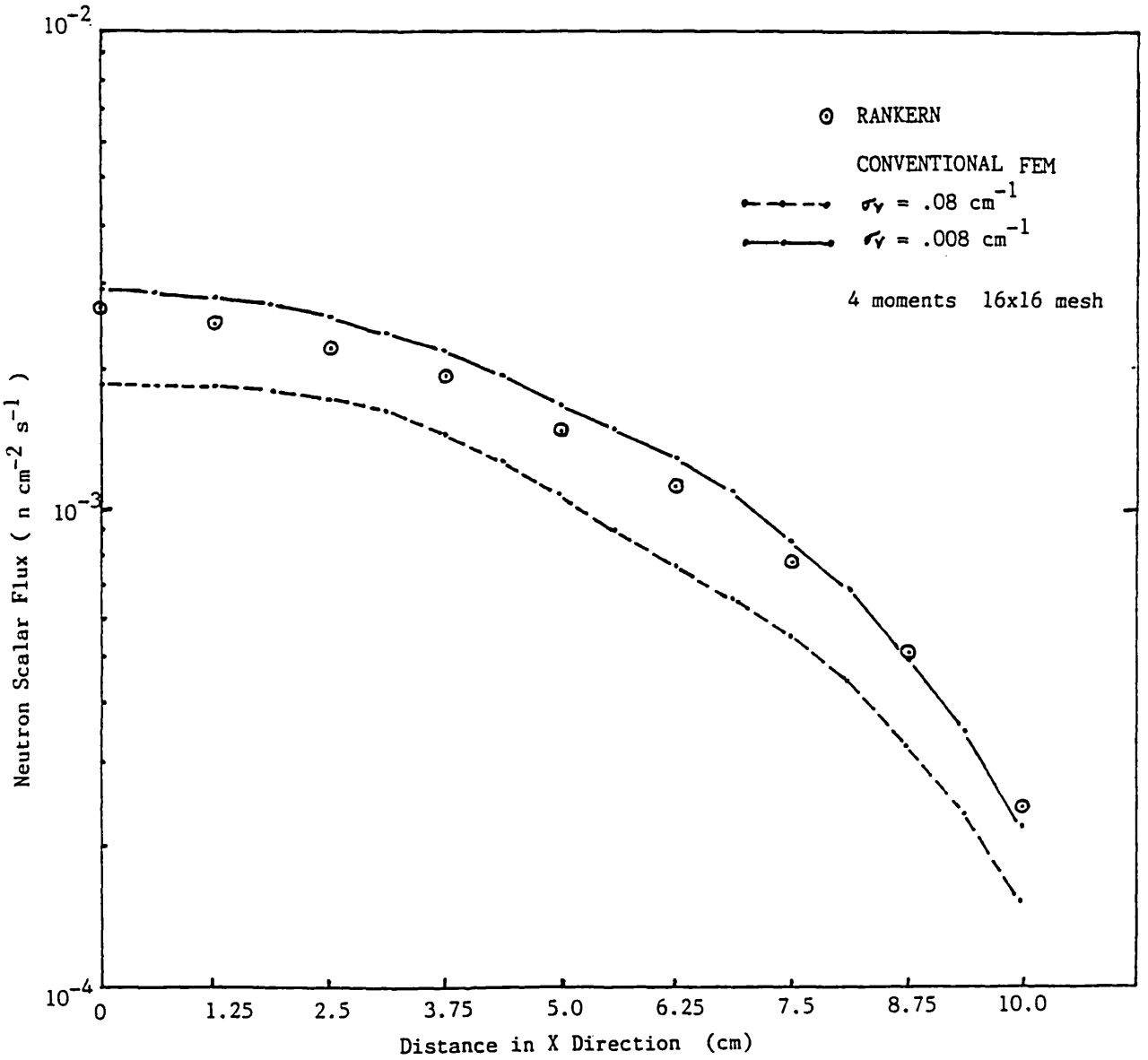


Fig. 5.18 RANKERN and Conventional Finite Element Solution Along the Outer Boundary AA'.

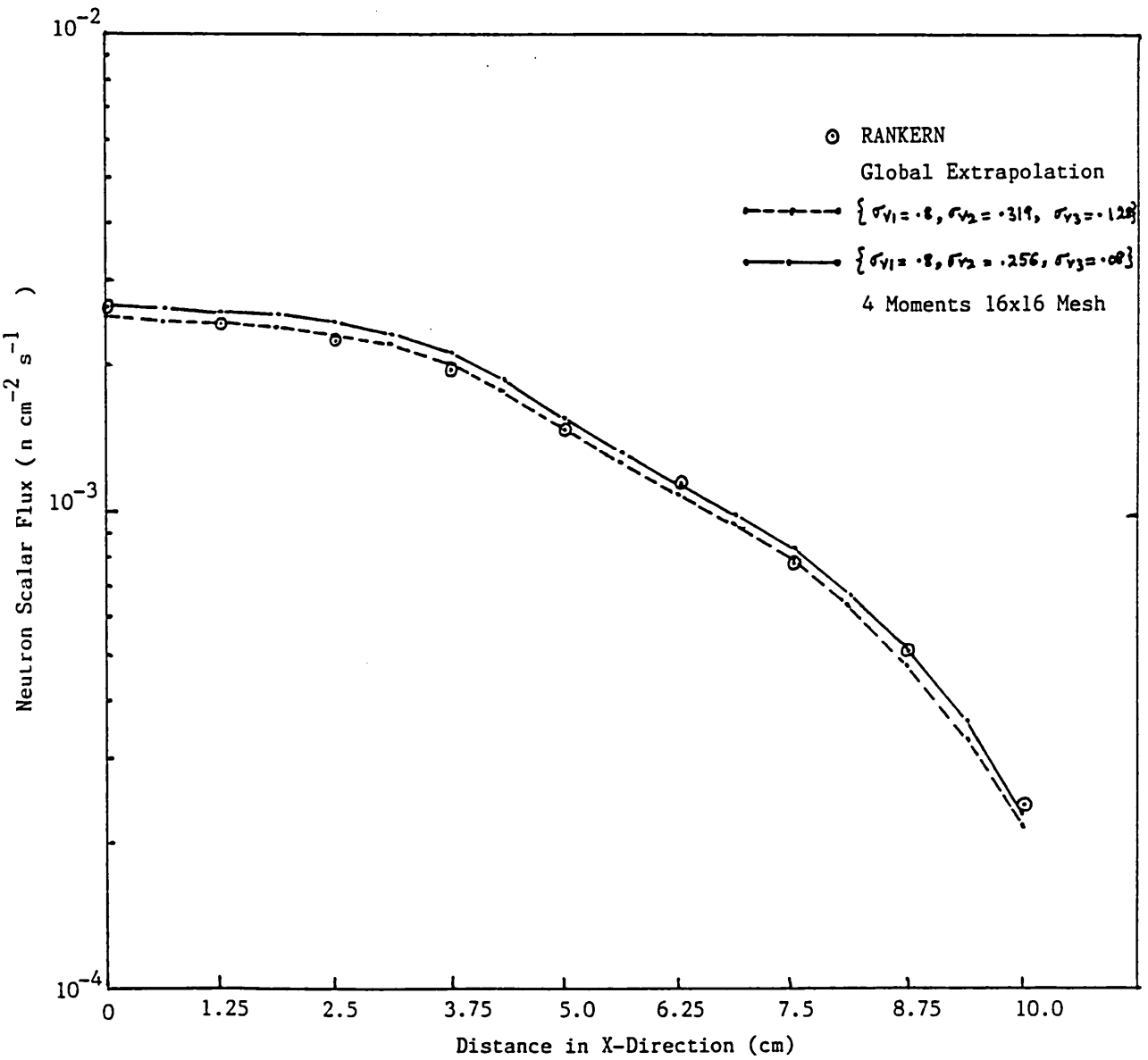


Fig. 5.19 RANKERN and Global Extrapolation Solution Along the Outer Boundary AA'.

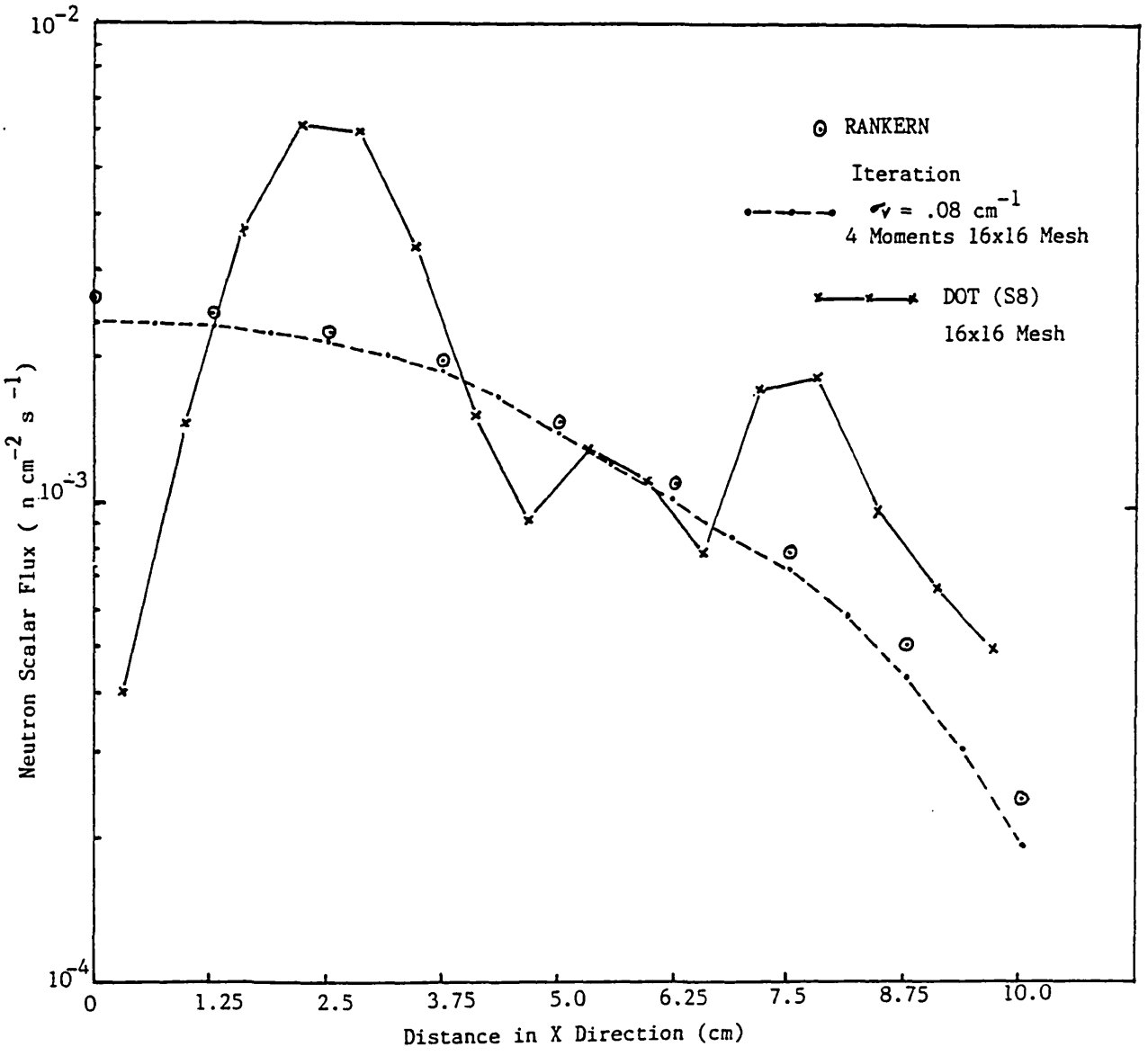


Fig. 5.20 RANKERN, Iteration and DOT Solutions Along the Outer Boundary AA'.

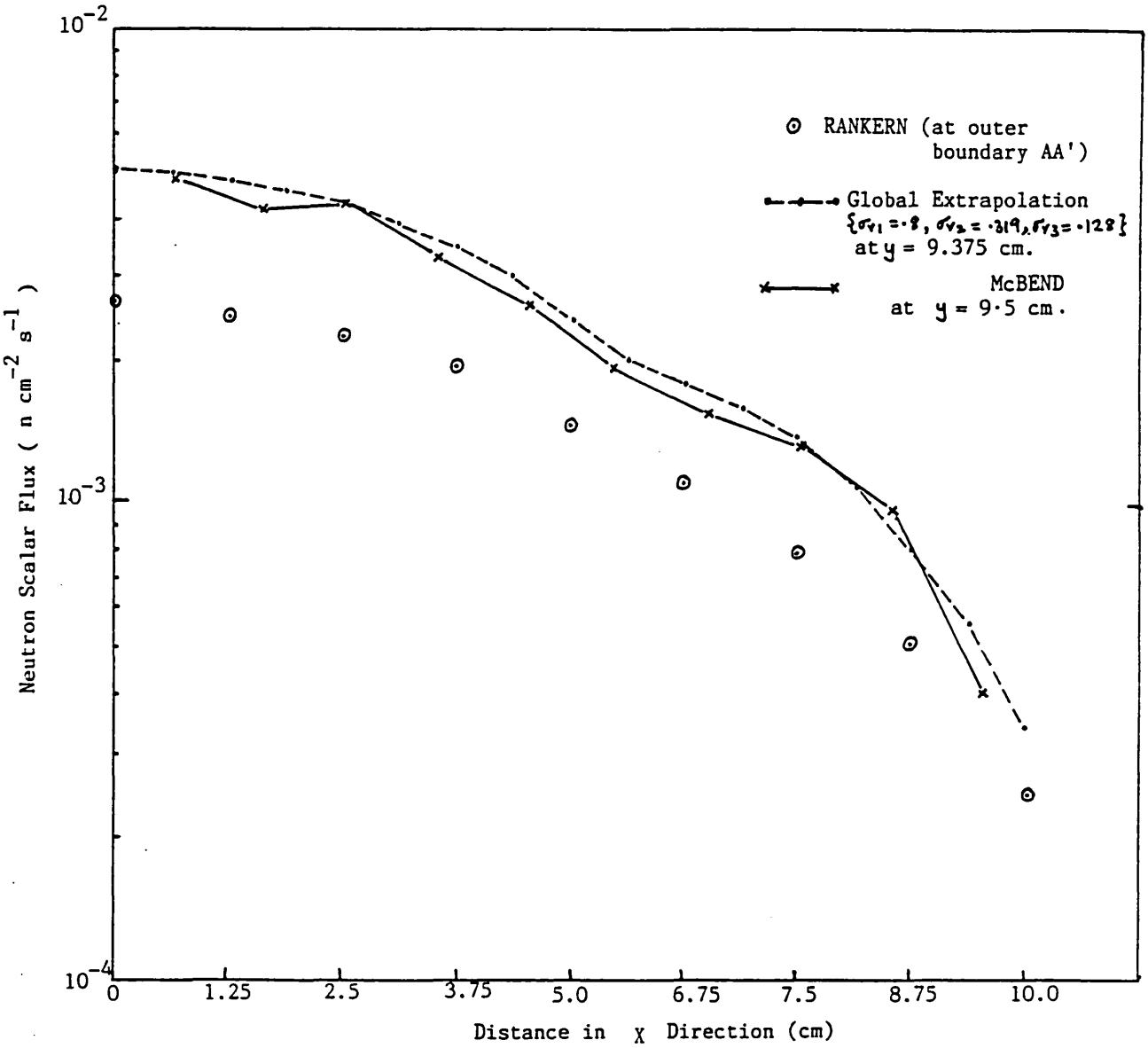
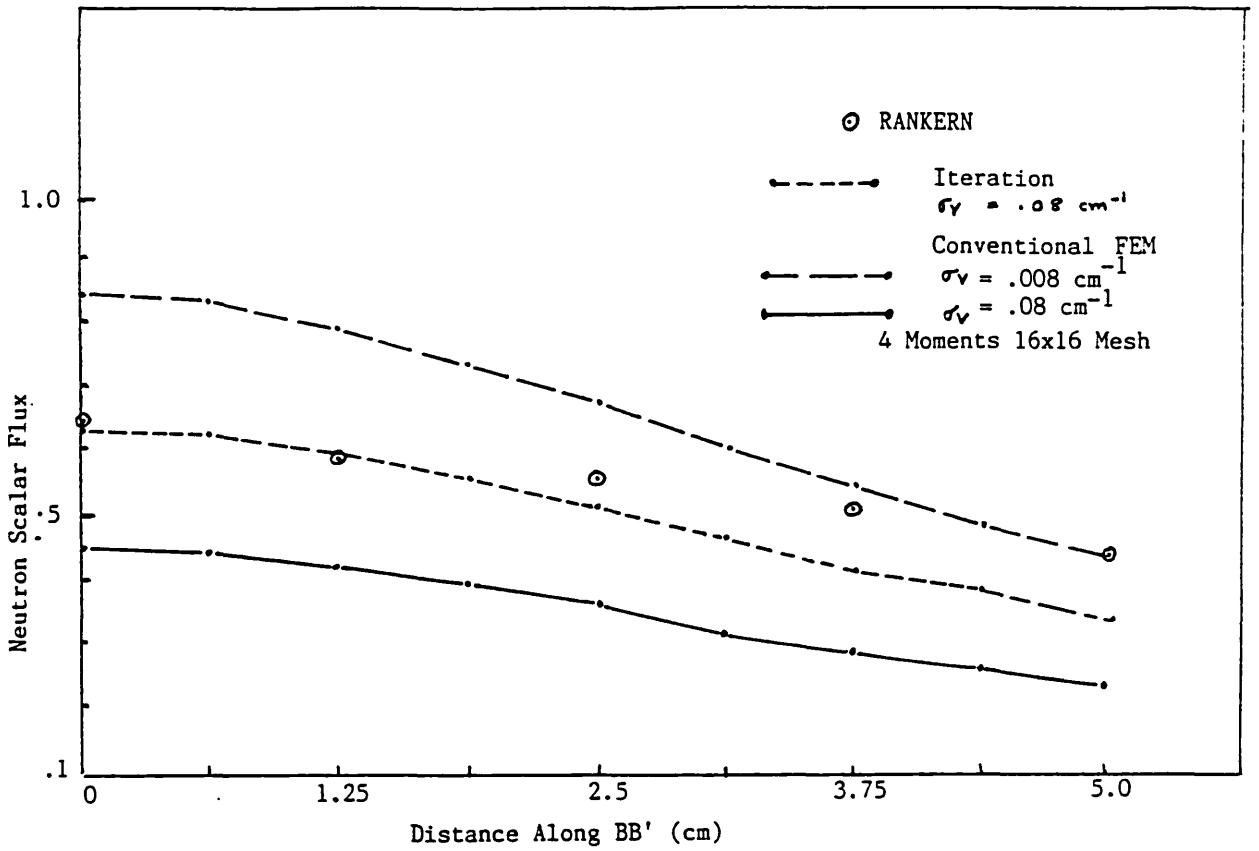


Fig. 5.21 RANKERN, Global Extrapolation and McBEND (Monte Carlo) Solutions at the Outer Boundary AA'.

Fig. 5.22(a) RANKERN, Iteration and Conventional Finite Element Solutions Along the Void Boundary BB'.



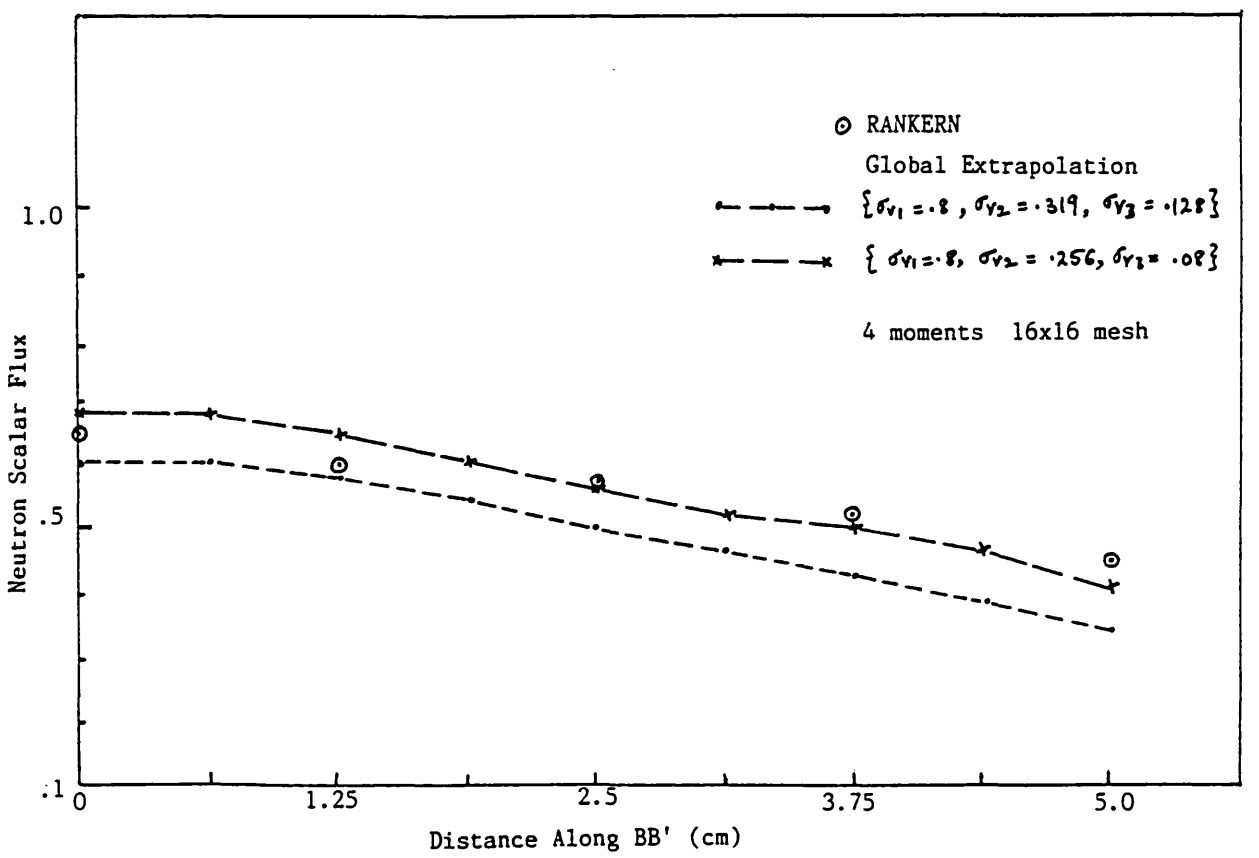


Fig. 5.22(b) RANKERN and Global Extrapolation Solutions Along the Void Boundary BB'.

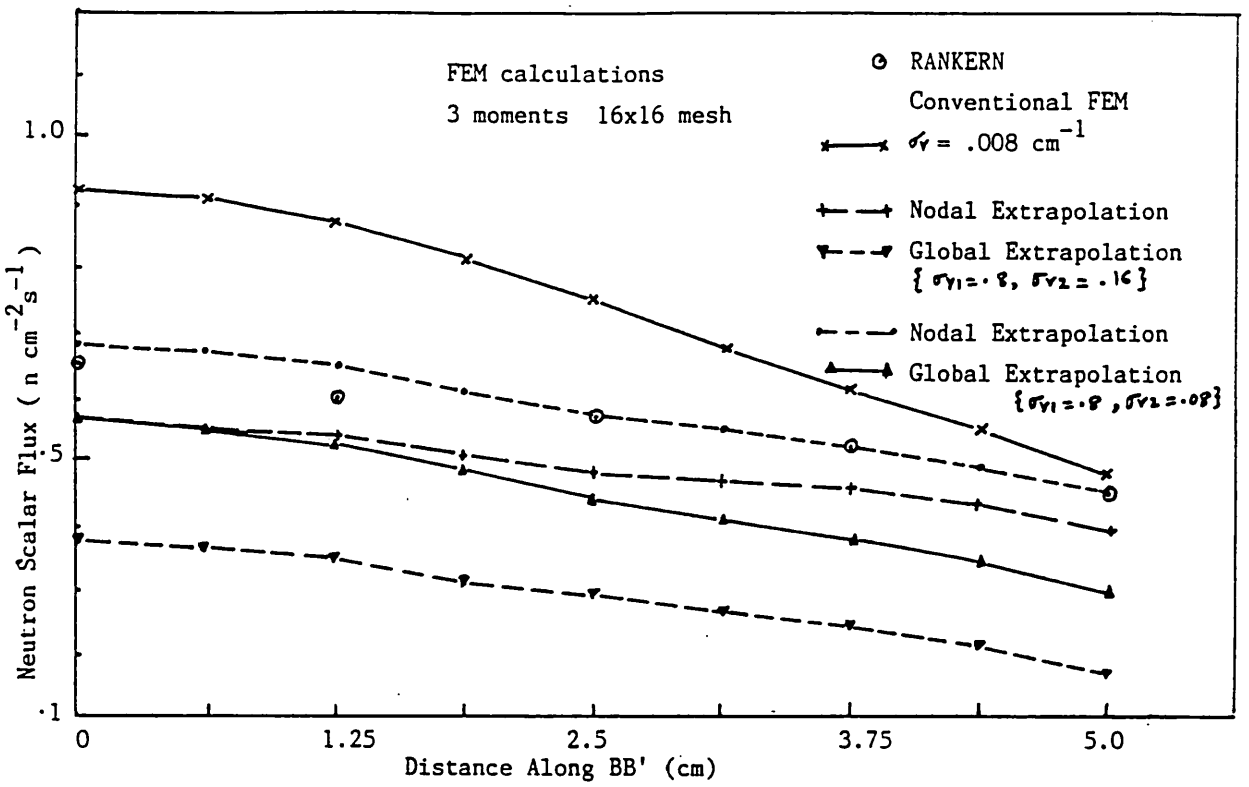


Fig. 5.23(a) RANKERN, Conventional Finite Element, Nodal and Global Extrapolation Solutions Along Void Boundary BB'.

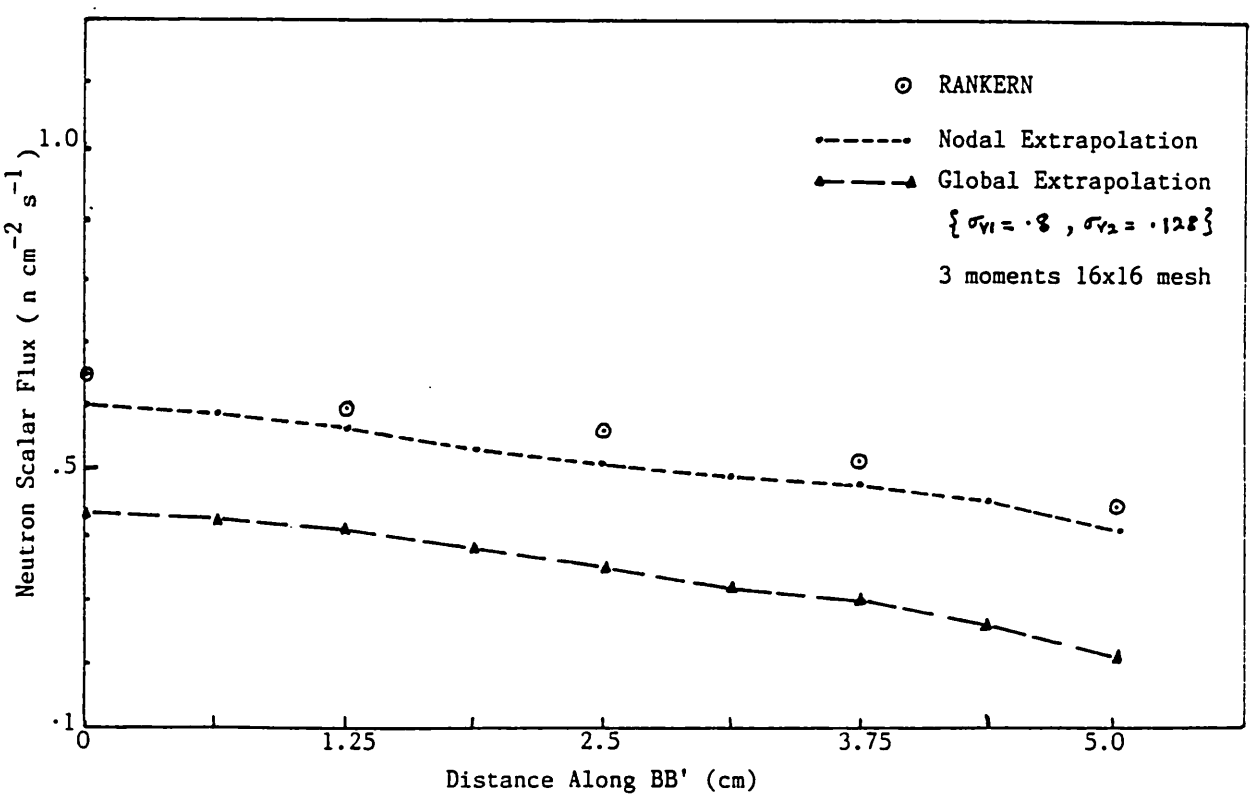


Fig. 5.23(b) RANKERN, Nodal and Global Extrapolation Solutions Along Void Boundary BB'.

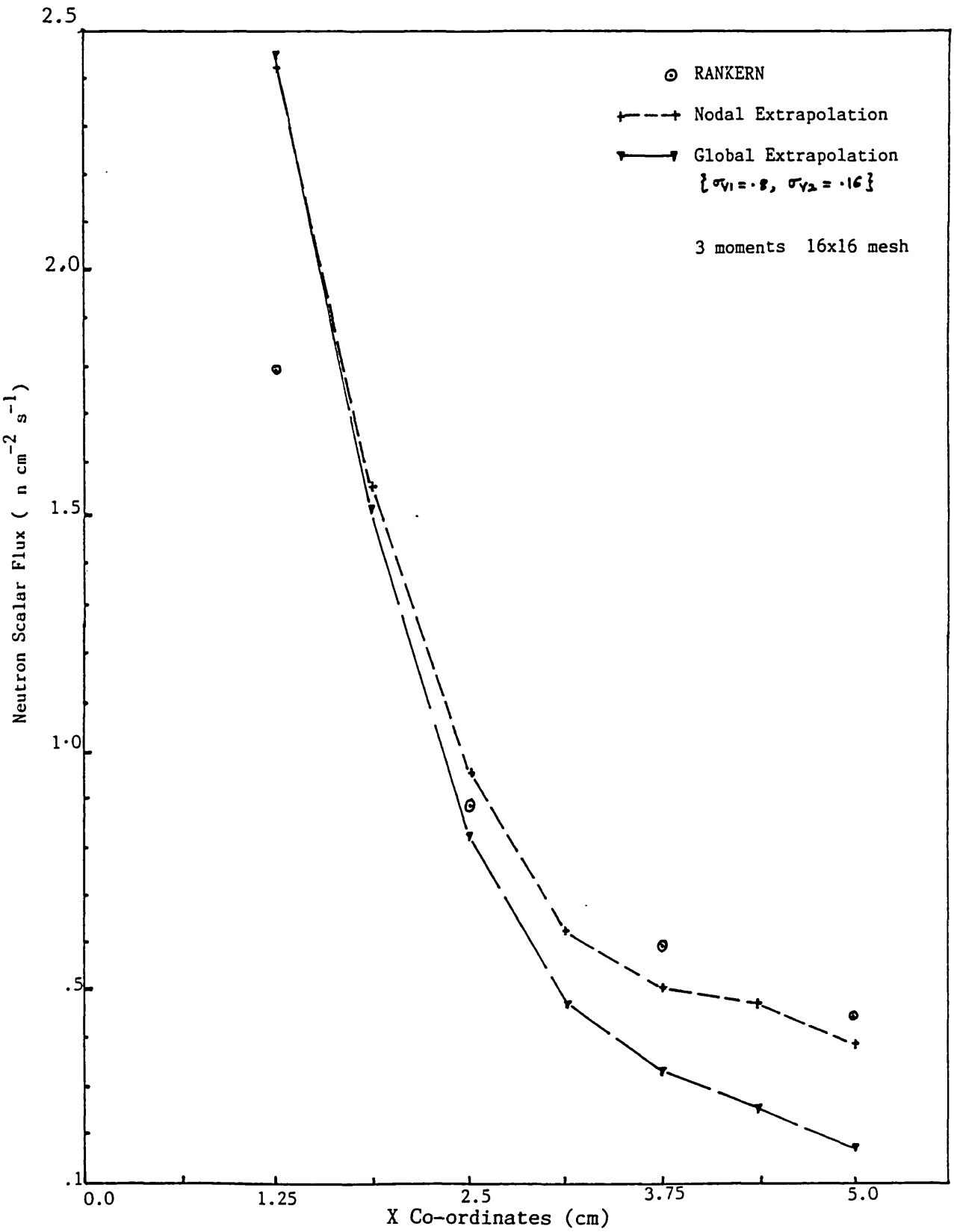


Fig. 24(a) RANKERN, Nodal and Global Extrapolation in Void Along OB'.

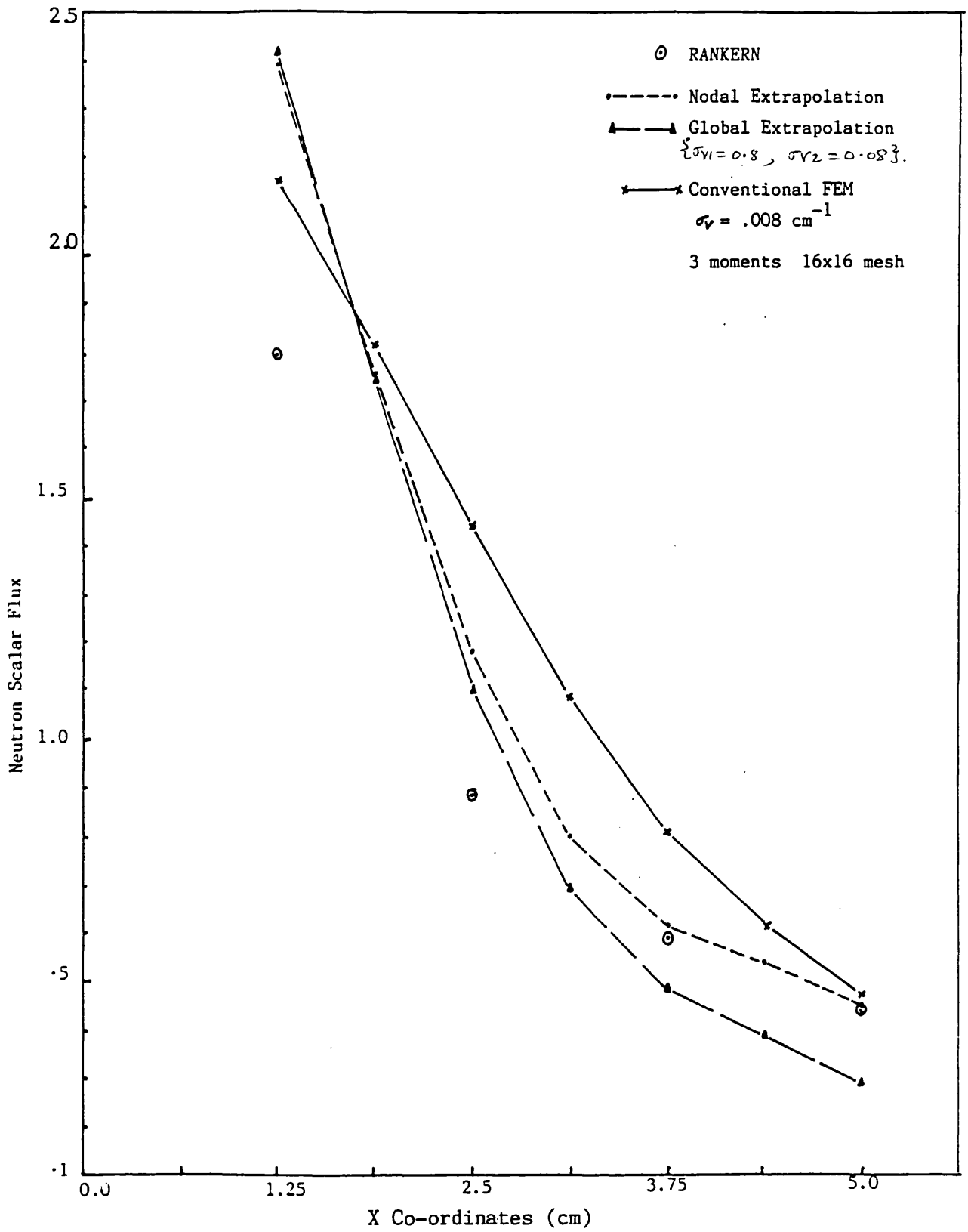


Fig. 24(b) RANKERN, Nodal and Global Extrapolation and Conventional Finite Element Solutions in Void Along OB'.

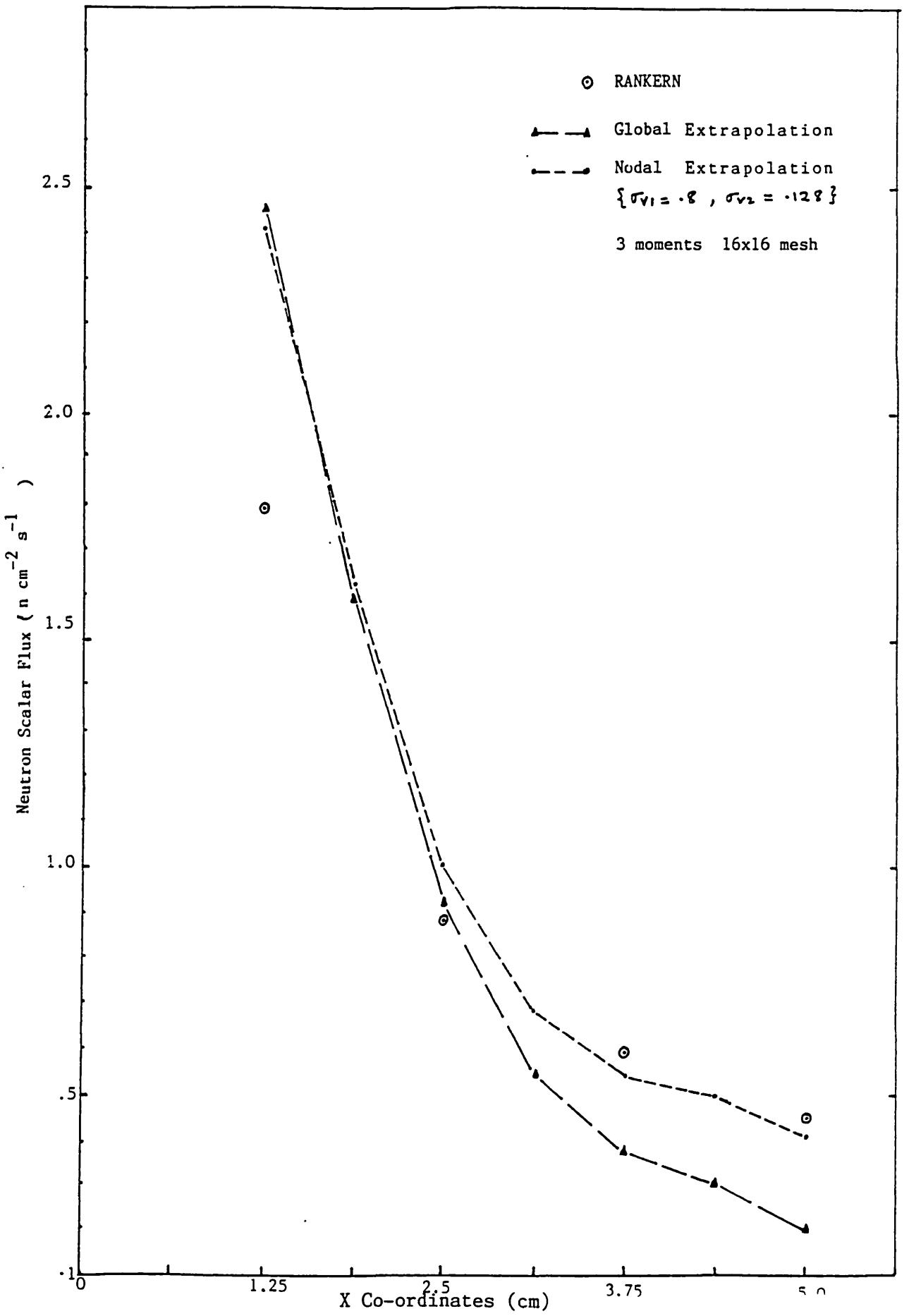


Fig. 5.25 RANKERN, Nodal and Global Extrapolation Solutions in Void Along OB'.

5.5.2 Straight Duct Source Problem with Pure Absorber

The straight duct in a wall (a reactor shield) with a source at one end of the duct is a more representative shield problem in reactor and auxilliary nuclear facilities. Straight duct penetrations in concrete walls can occur when some diagnostic equipment or pipes are inserted in shield walls. The problem analysed here is shown in Fig. 5.26 . The duct surrounding region is again absorbing, thus allowing RANKERN point kernel solutions to be used as reference. The lower and right hand sides of the system have bare surfaces (vacuum) while the other two sides are reflective. Again the source medium is the same as the absorbing region. Cross section data is presented in Table 5.2.

Three moments (14x18 mesh) solutions along the central axis OY, for various values of σ_Y is shown in Fig. 5.1. It is seen that the solutions for $\sigma_Y = .05$ cm^{-1} gives a reasonable flux profile but, is below the reference solution ψ_R^+. For relatively small values of σ_Y the void solution becomes distorted and physically incorrect. In Fig. 5.27 are plotted the 3 moments (28x36 mesh) solutions with $\sigma_Y = .05$ and $\sigma_Y = .005$ cm^{-1} for the conventional finite element calculation. The first solution is below ψ_R^+ while the second with $\sigma_Y = .005$ is beginning to show signs of flatness in the sense that the flux is decreasing near the source region and increasing at the duct exit.

Region	S	σ_T (cm^{-1})	σ_S (cm^{-1})
1	1·0	0·5	0·0
2	0·0	· VOID	
3	0·0	0·5	0·0

Table 5.2 Cross Section Data for the Straight-Duct Source Problem

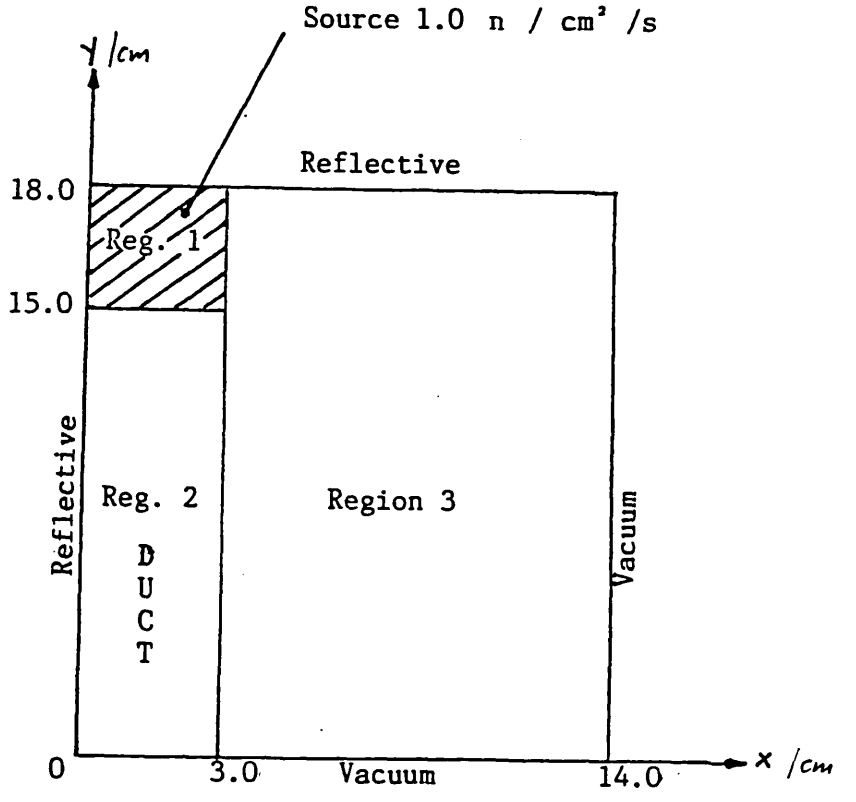


Fig. 5.26 Geometry for the Straight Duct Source Problem

In fact if we try combining the $\sigma_v = .005$ solution with others using higher values of σ_{vi} for an extrapolated solution the final solution ψ_E^+ will go above ψ_R^+. Hence, it is better to use a higher value of σ_{vi} in the void so as to keep all the trial functions, in the extrapolation method, lower bounds to ψ_R^+. A three trial function solution with $\{\sigma_{vi}\}_{i=1,2,3} = \{0.5, 0.16, 0.05\}$ is shown in Fig.5.28. This solution is in fairly good agreement with ψ_R^+ except near the bare-surface (duct exit) where it is lower than ψ_R^+. Iteration solution with $\sigma_v = .05$ is also shown in Fig.5.28. Again this is lower than ψ_R^+ towards the exit of the duct. Solutions along outer boundary of the system (OX) for the conventional calculation are shown in Fig.5.29. Towards the right hand lower corner of the system even the $\sigma_v = .05$. solution is above ψ_R^+. This should not be the case in theory. A finer local mesh and higher moments for $\psi_i(x, \Delta)$ should bring this solution below ψ_R^+. The $\sigma_v = .005$ solution is significantly above ψ_R^+ in this region. ψ_E^+ along the outer boundary with elementary or global extrapolation, is shown in Fig.5.30. As expected ψ_E^+ is higher than ψ_R^+ beyond x= 8.0 cms.

With global or elementary extrapolation we cannot expect to obtain a good solution everywhere in a void system since only a single parameter (for two trial functions) or two parameters (for three trial functions) are used globally. A better way would be to adjust the component solutions locally, i.e. node-wise. Hence the nodal extrapolation method. Calculations were

carried out using the nodal extrapolation method with two trial functions. Only the void nodal calculation is coded in FELTRAN at present hence. the solutions are restricted to the void region. Calculations were performed for 3 moments and 14x18 mesh. In Fig. 5.31 the conventional ($\sigma_v = .005$ cm^{-1}) global and nodal extrapolation solutions for $\{\sigma_{vi}\} = \{0.5, 0.005\}$ are compared along the central axis of the duct. In this case the $\sigma_v = .005$ cm^{-1} component solution is dominating and so the global and nodal extrapolation solutions do not adjust the $\sigma_v = .005$ solution significantly. Further reduction of σ_{v2} would raise the extrapolated solution, global or nodal, to above ψ_g^+ . Although it is easy to see this in this case whether or not ψ_g^+ is above or below the exact solution for the system, this will not be true in general for practical problems. Here the void surrounding media may have scattering included in which case solutions generated by the global and nodal extrapolation methods can only be compared, say with Monte Carlo calculations.

If the cross section set $\{0.5, 0.05\}$ is used in the void then there is a significant improvement on the $\sigma_v = .05$ component and the global extrapolation solution as seen in Fig. 5.32.

In order to check the sensitivity of the nodal extrapolation solution several calculations were carried out. Firstly, σ_{v2} was varied with σ_{v1} constant. The results are

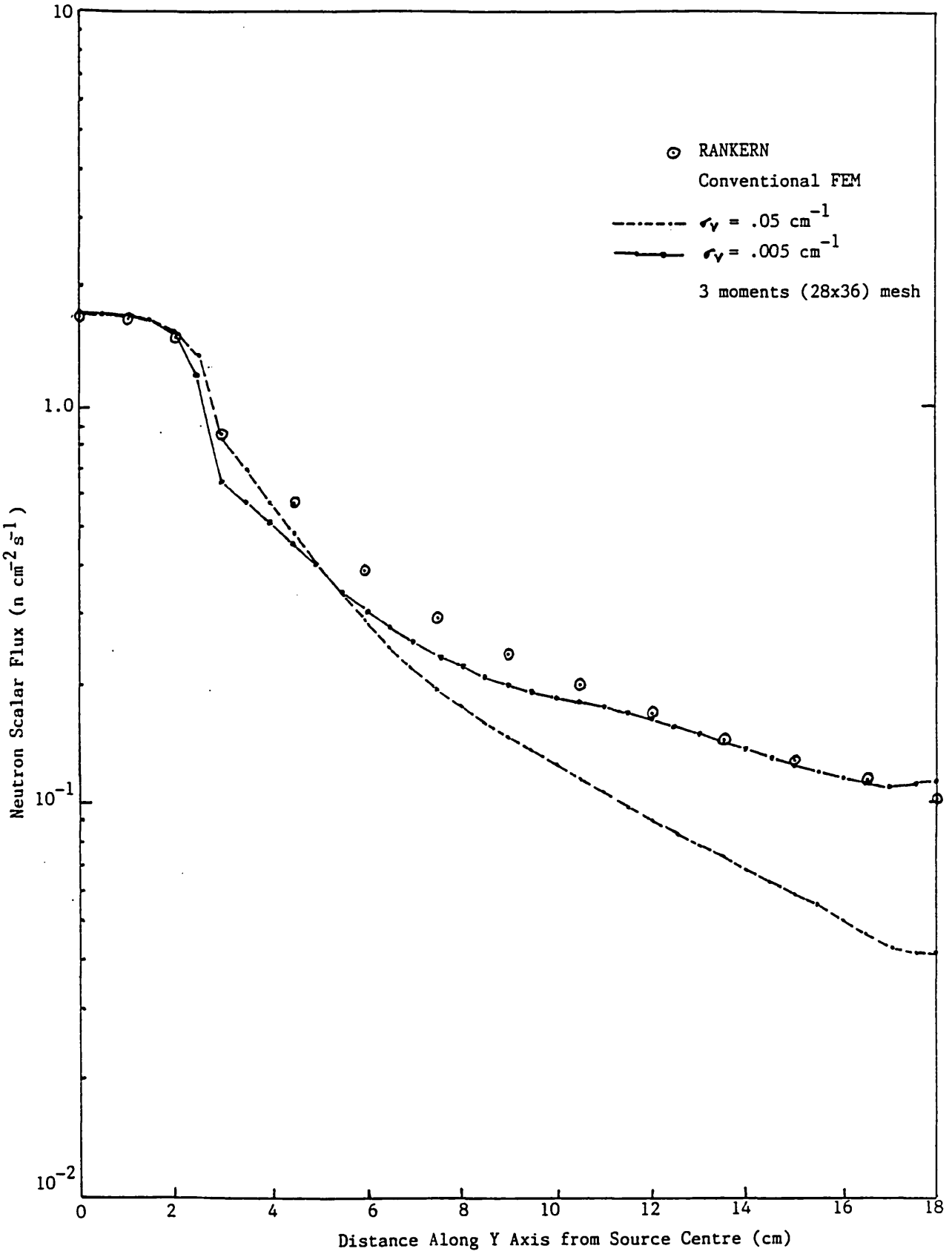


Fig. 5.27 RANKERN and Conventional Finite Element Solutions Along Central Axis of Duct.

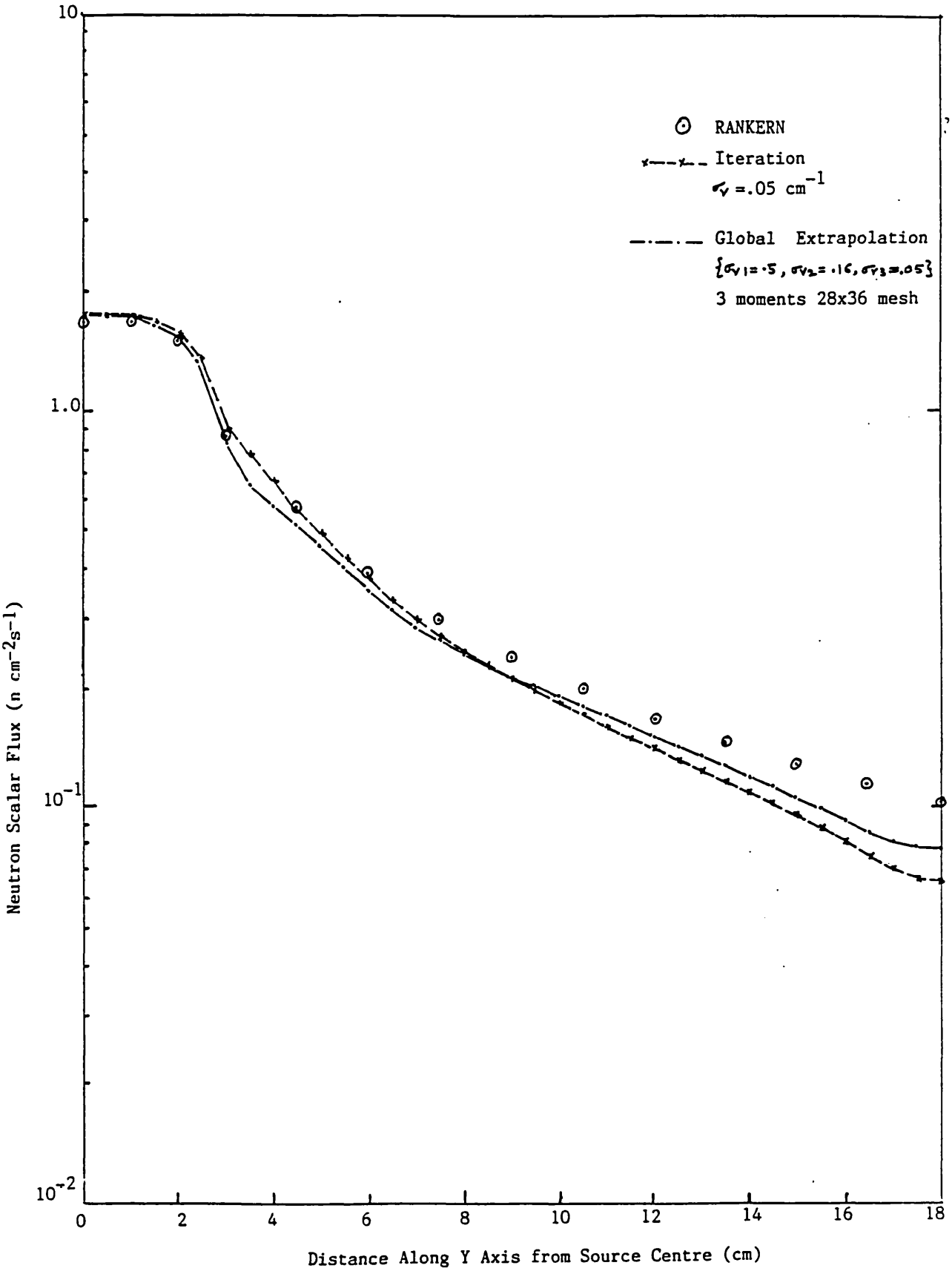


Fig. 5.28 RANKERN, Iteration and Global Extrapolation Solutions Along Central Axis of Duct.

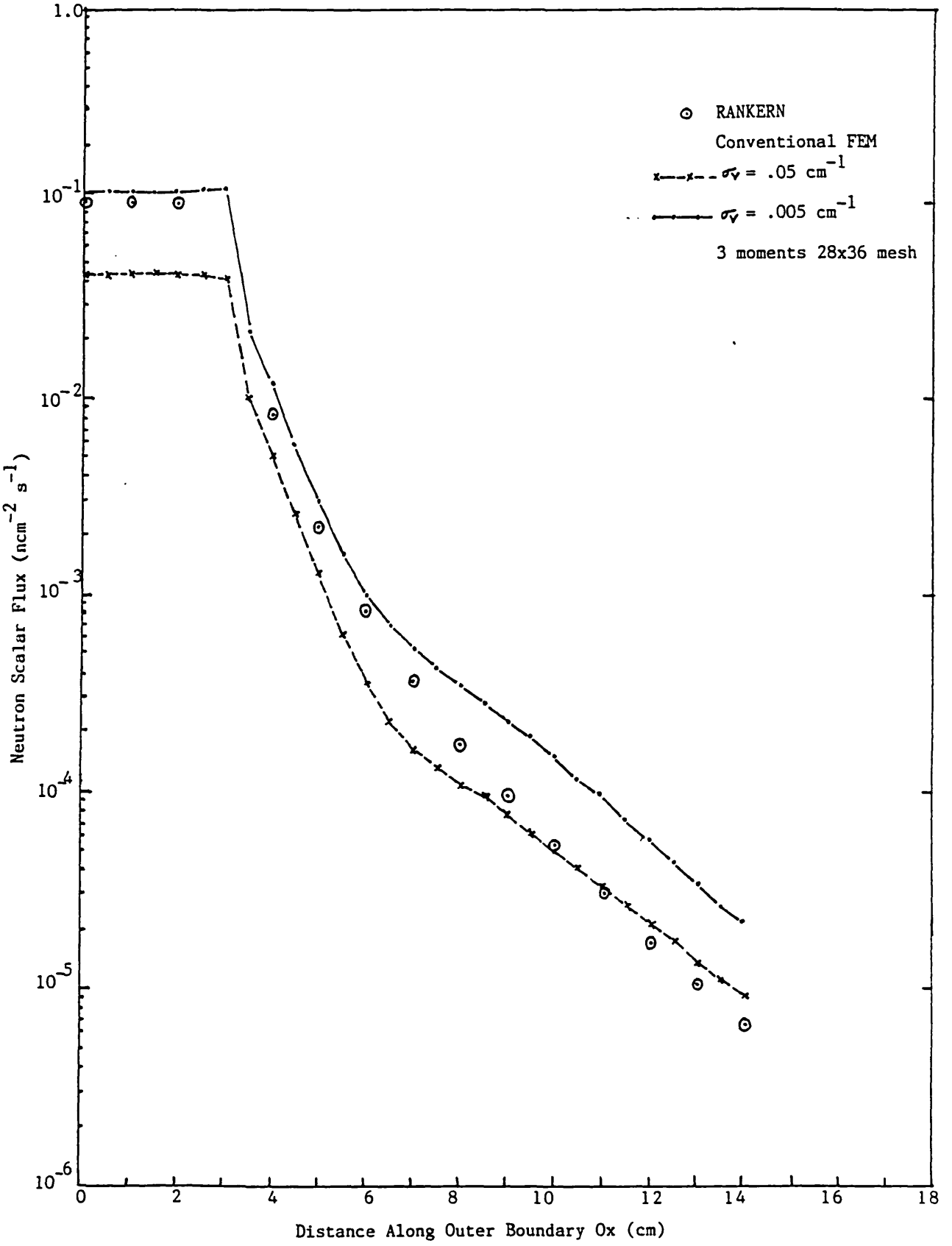


Fig. 5.29 RANKERN and Conventional Finite Element Solutions Along Outer Boundary OX.

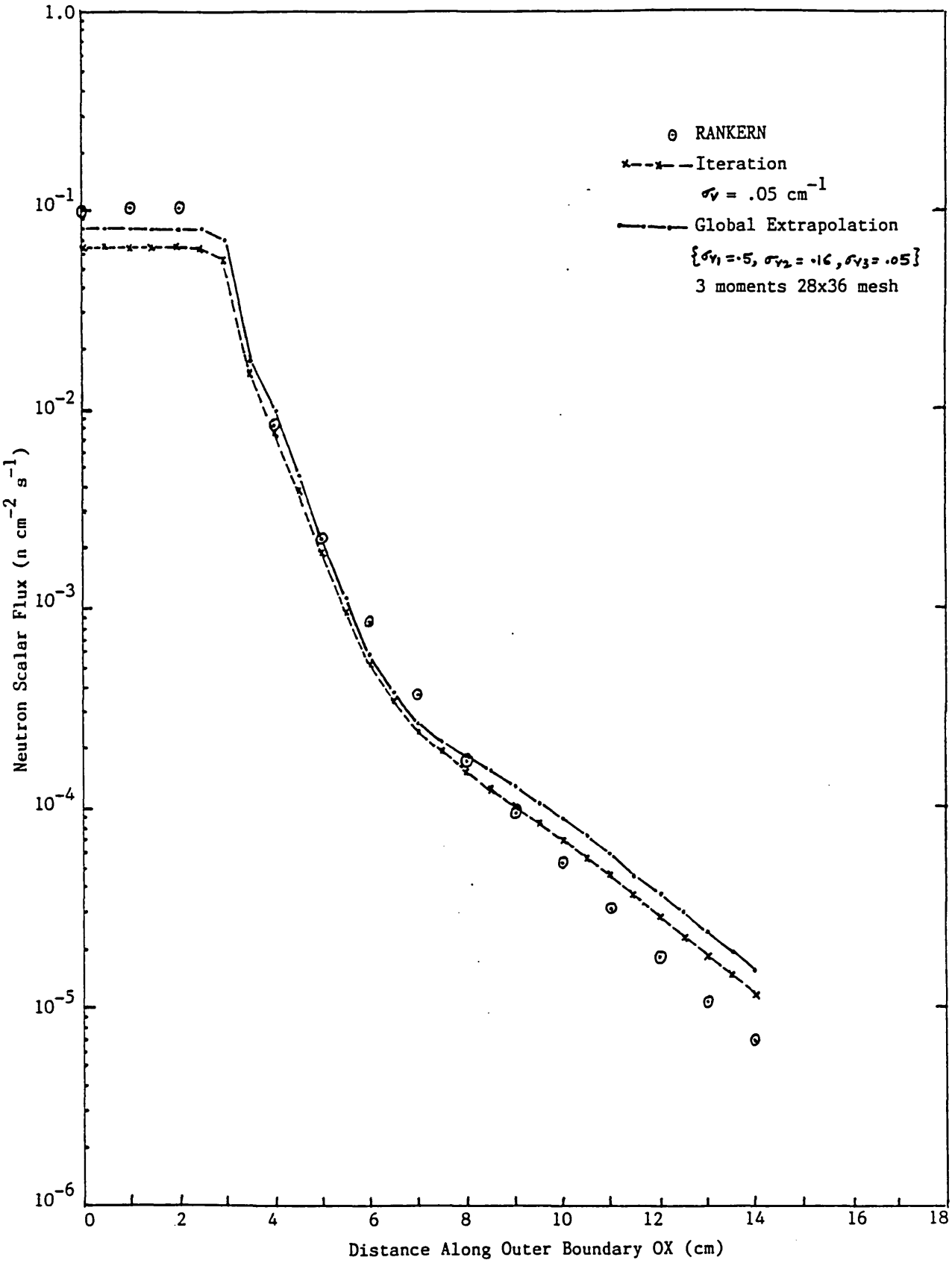


Fig. 5.30 RANKERN, Iteration and Global Extrapolation Solutions Along Outer Boundary OX.

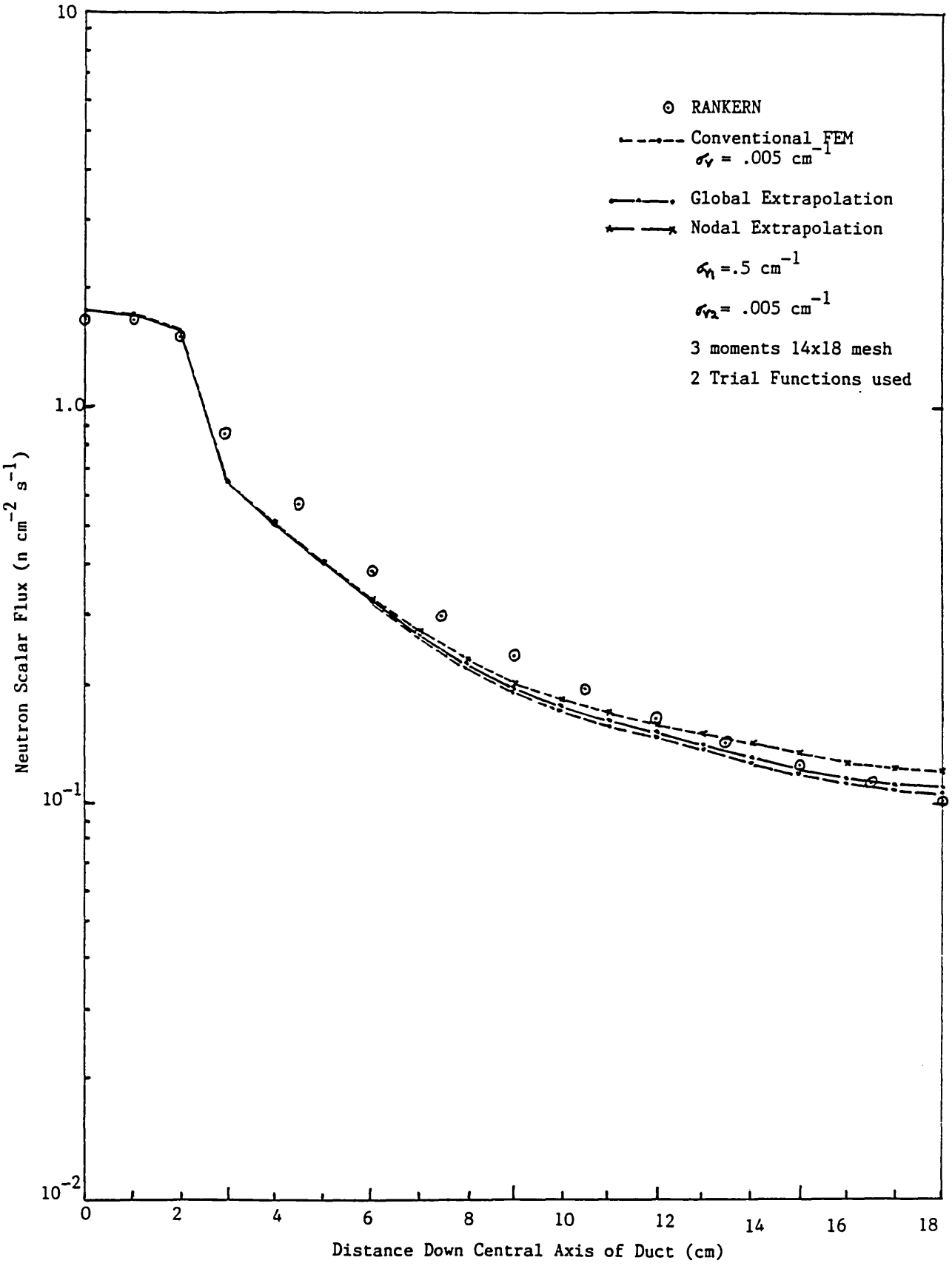


Fig. 5.31 RANKERN, Conventional Finite Element, Global and Nodal Extrapolation Solutions Along Central Axis of Duct.

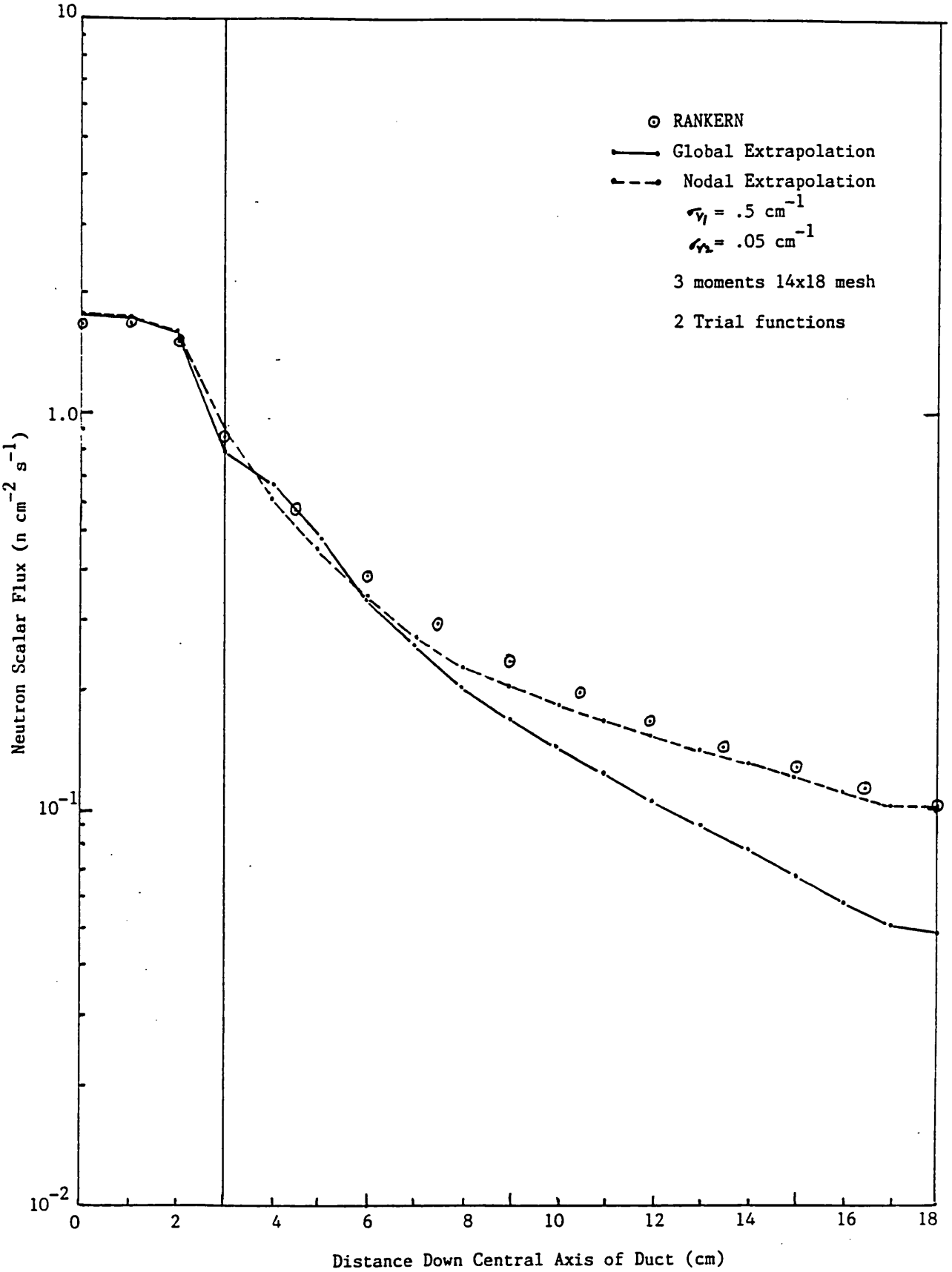


Fig. 5.32 RANKERN, Nodal and Global Extrapolation Solutions Along Central Axis of Duct.

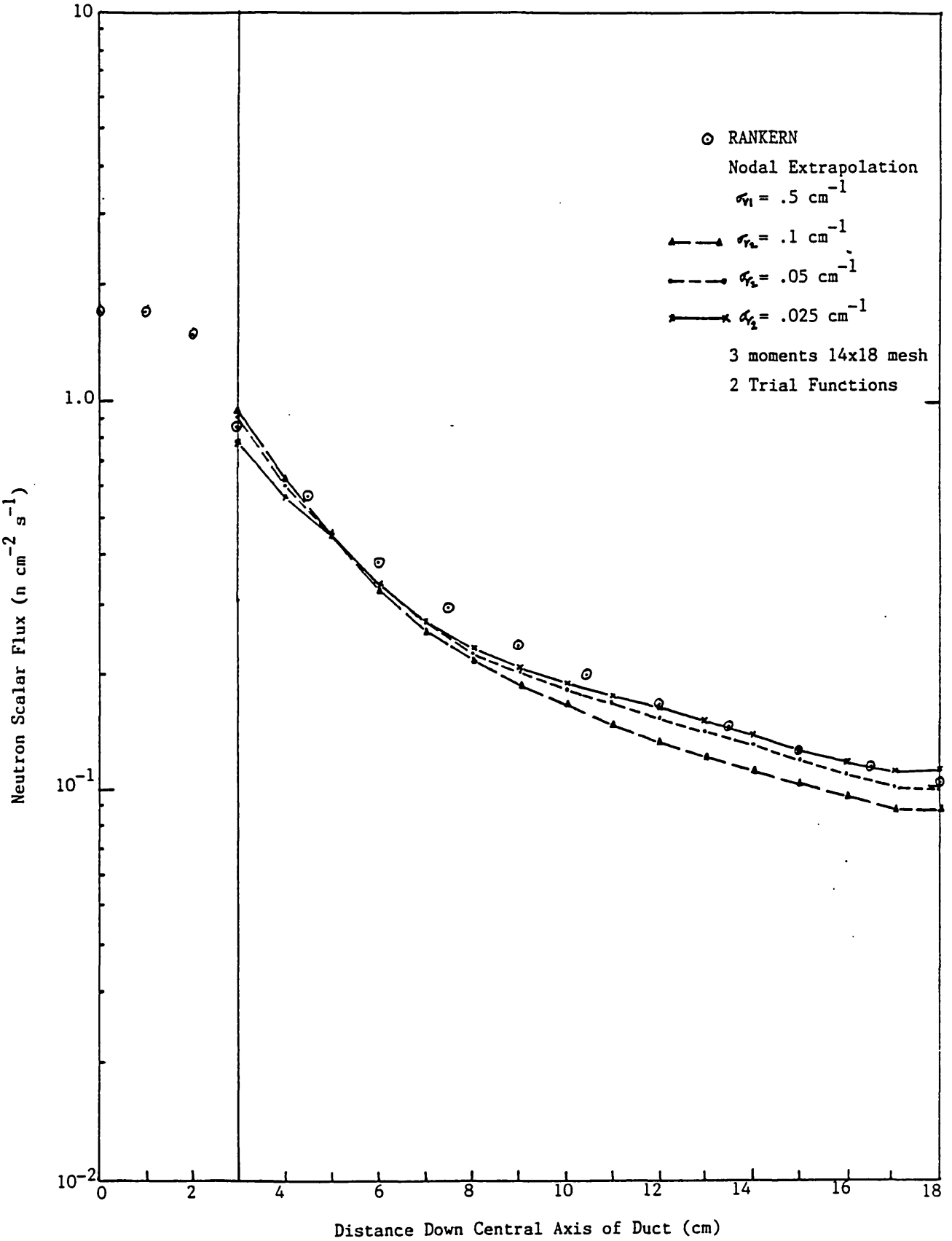


Fig. 5.33 RANKERN and Nodal Extrapolation Solutions Along Central Axis of Duct with Varying σ_{r_2}.

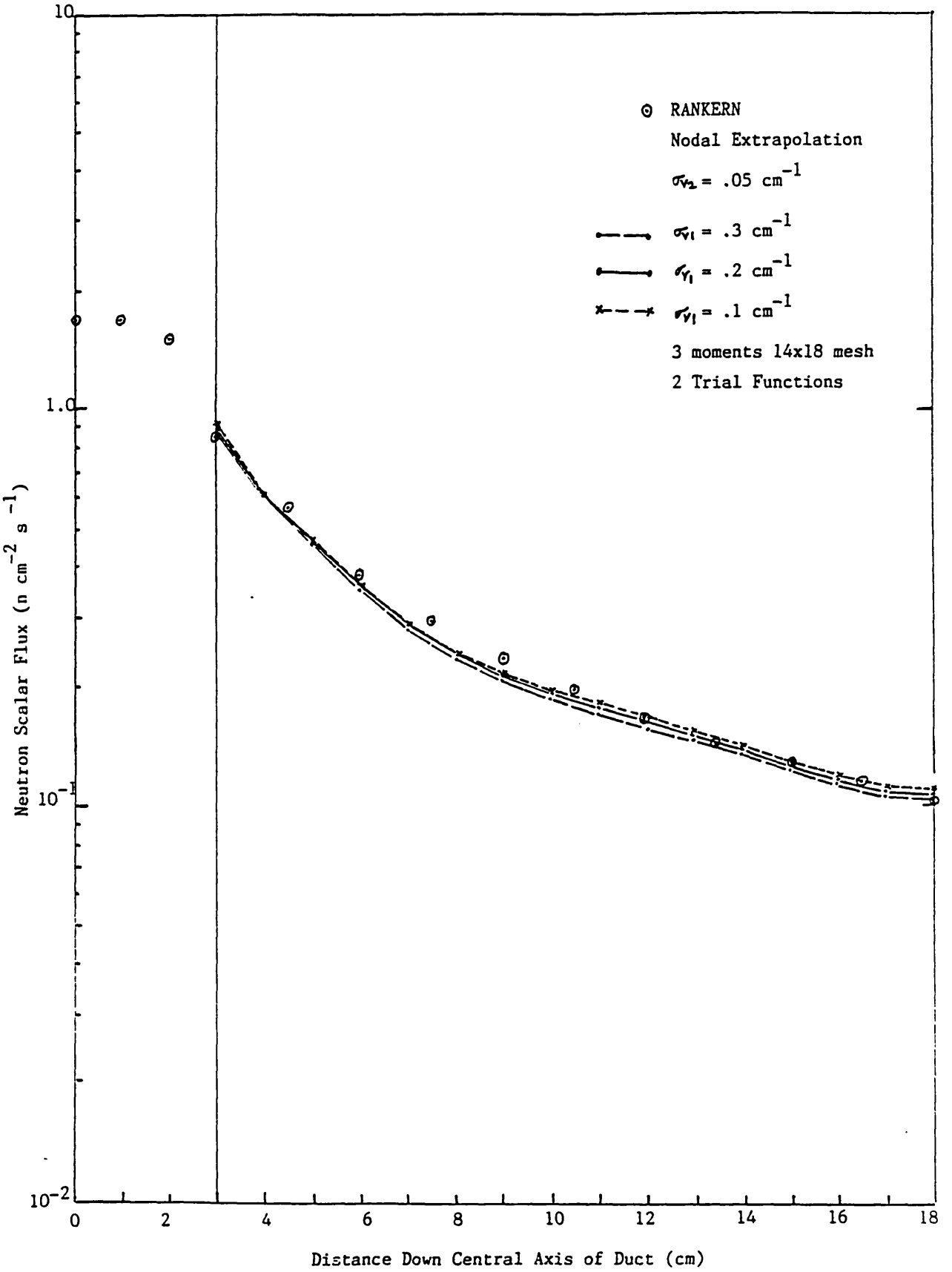


Fig. 5.34 RANKERN and Nodal Extrapolation Solutions Along Central Axis of Duct with Varying σ_{Y_1}

shown in Fig. 5.33. Hence, variation of σ_{v_2} does alter the final solution to some extent as expected. Next σ_{v_1} was varied with σ_{v_2} fixed at 0·05 cm^{-1}. The results are shown in Fig. 5.34. In this case it is seen that there is no significant variation in the final nodal extrapolation results.

5.5.4 Dog-Leg Duct Source Problem with Pure Absorber

This is a source problem in X-Y geometry with two right angled bends. The geometry is similar to that of the straight duct problem. A dog-leg duct, as it is more commonly known, allows incident source neutrons to scatter off the first wall, then off other walls until finally the neutrons emerge at the duct exit. In this way some neutrons are lost due to absorption and others which emerge at the duct exit after multiple scattering have reduced energy and a modified angular distribution. In the problem reported here, the void surrounding regions are kept purely absorbing. Full geometry of the problem is shown in Fig. 5.35. Table 5.3 gives the relevant cross section data.

In this problem, as with the straight duct, some difficulty was experienced in obtaining accuracy and convergence in the lower right half of the system. In addition it was difficult to get a satisfactory solution near and along the outer boundary OX of the system. Scalar fluxes were compared along AA' and OX. Solutions from the conventional

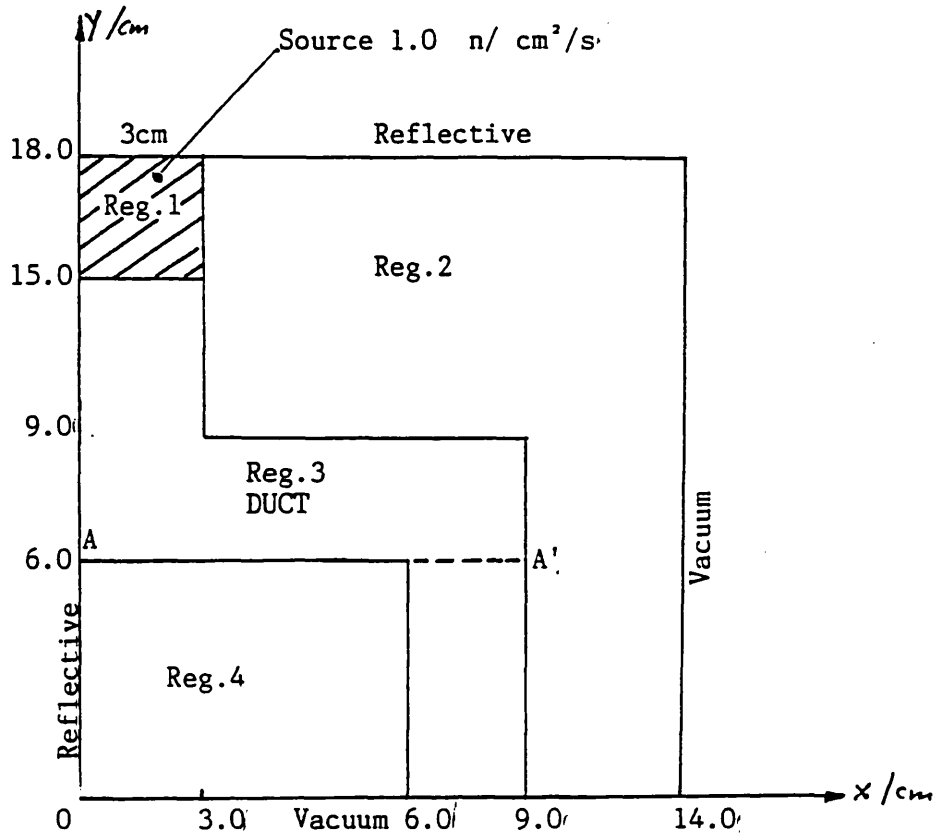


Fig. 5.35 Geometry for the Dog-Leg Duct Source Problem

finite element method along AA' for 3 moments (28x36 rectangular mesh) are shown in Fig. 5.36 for $\sigma_V = .05$ and $\cdot 005\ cm^{-1}$. Although the first solution is lower than ψ_R^+ along AA', it is closer to ψ_R^+ towards x=8·0 cm. The second solution starts off closer to ψ_R^+ upto x=5·00 cm. Beyond this point it diverges away from ψ_R^+ . Fig. 5.37 shows the iteration (3) results with $\sigma_V = .05 cm^{-1}$ and DOT (S8) results. Here DOT shows the typical oscillations and has the physically incorrect flux gradient, at x=0·0, the perfect reflector surface. The iteration solution shows overall improvement on the conventional finite element solutions. It is still below ψ_R^+ upto x=5·0 cm. Three iterations were considered in order to get a direct comparison with three trial function elementary extrapolation solutions. The solutions of the latter with $\{\sigma_{Vi}\}_{i=1,2,3} = \{0.5, 0.16, 0.05\}$ for 3 and 4 moments are shown in Fig. 5.38. These are more satisfactory than the results of the other methods. The kink in the solution at x=6·0 cm may be eliminated by local mesh refinement at absorber-void interfaces. McBEND, Monte Carlo values are plotted in Fig.5.39. These results are in good agreement with ψ_R^+ although McBEND tends to underestimate the flux more upto x=4cm.

Along the outer boundary of the system (OX) there is significant variation in ψ_R^+ from x=0·0 to 14·0cm, as shown in Fig.5.40. Conventional finite element solutions are also shown here. It is seen that the σ_V=.05 solution underestimates

Region	$S_{n\ cm^{-2}s^{-1}}$	σ_T (cm^{-1})	σ_S (cm^{-1})
1	1·0	0·5	0·0
2	0·0	0·5	0·0
3	0·0	VOID	
4	0·0	0·0	0·0

Table 5.3 Cross Section Data for the Dog-Leg Duct Source Problem.

Region	$S_{n\ cm^{-2}s^{-1}}$	σ_T (cm^{-1})	σ_S (cm^{-1})
1	6·4	0·2	0·19
2	0·0	VOID	
3	0·0	0·2	0·19

Table 5.4 Cross section Data for Square Source Problem with Scattering.

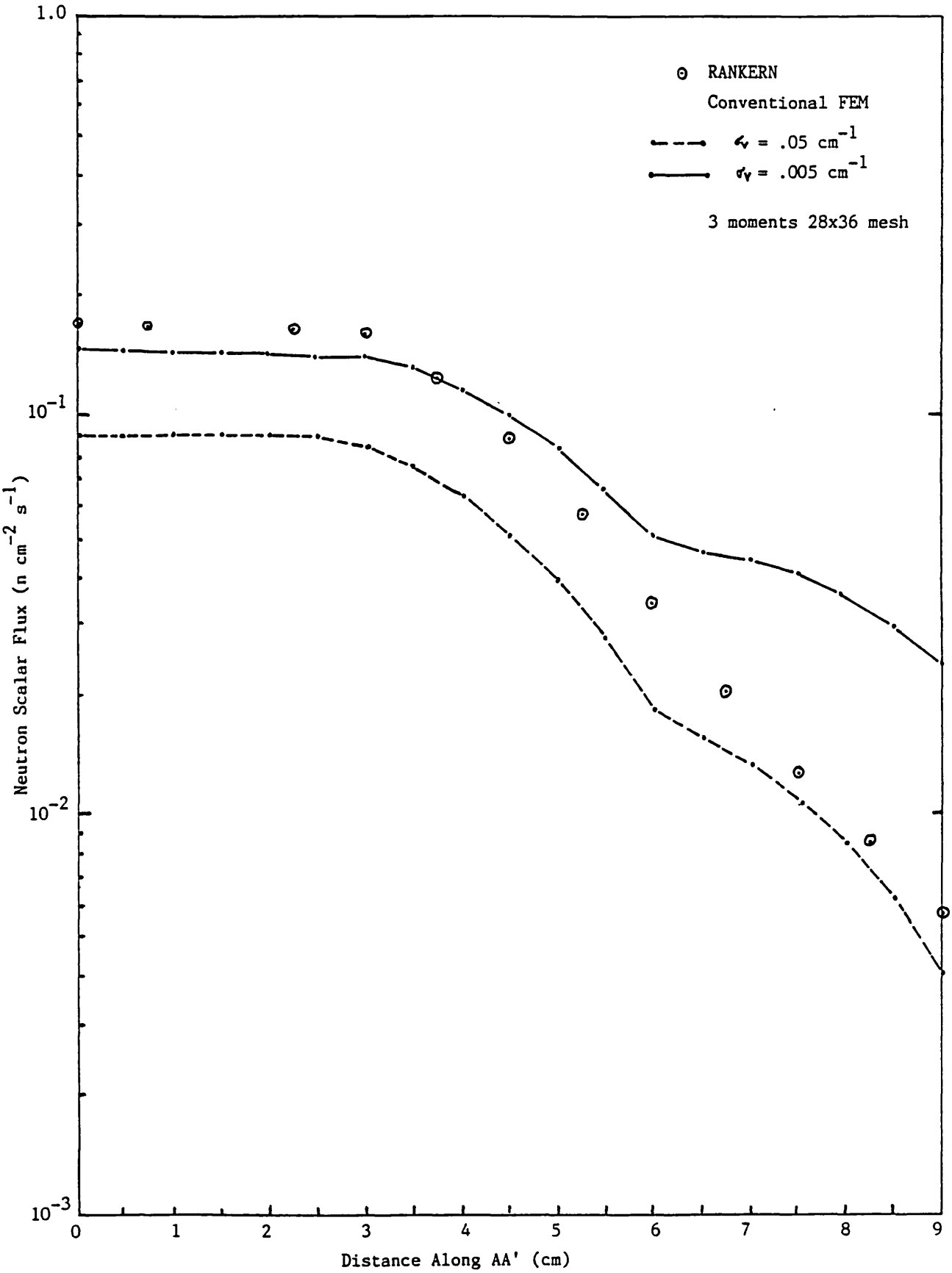


Fig. 5.36 RANKERN and Conventional Finite Element Solutions Along AA' for the Dog-Leg Duct Problem.

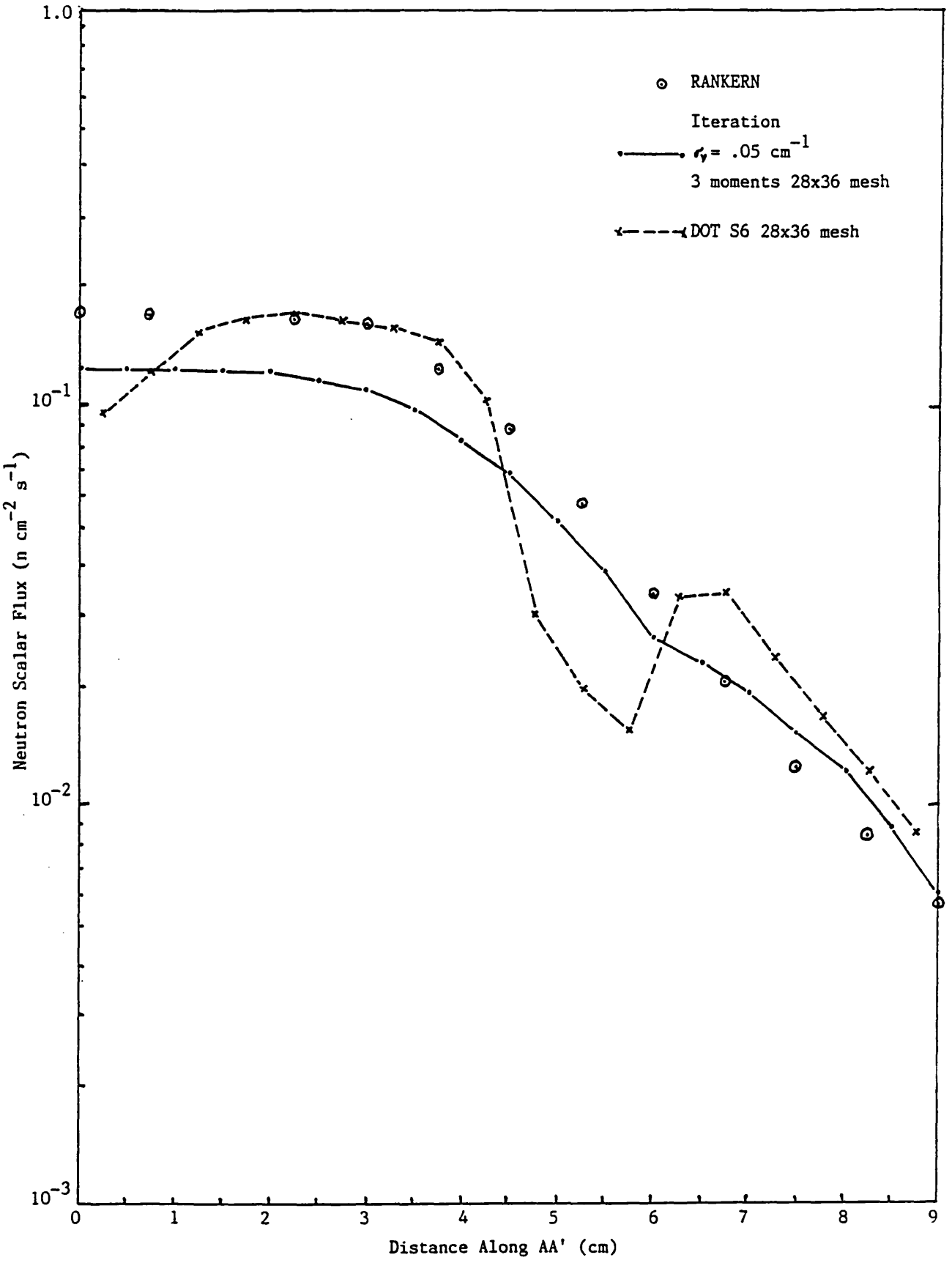


Fig. 5.37 RANKERN, Iteration and DOT Solutions Along AA'.

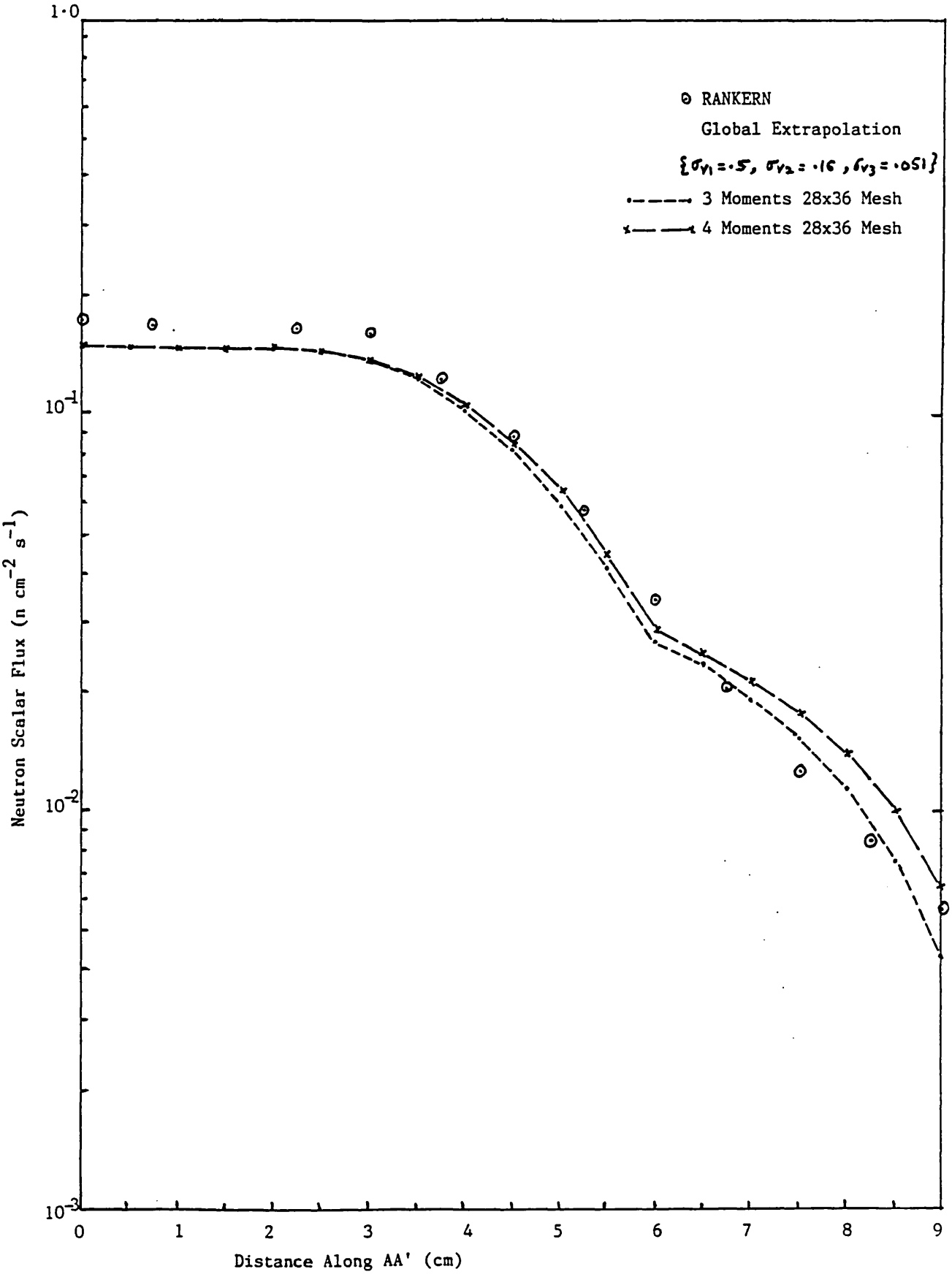


Fig. 5.38 RANKERN and Global Extrapolation Solutions Along AA'.

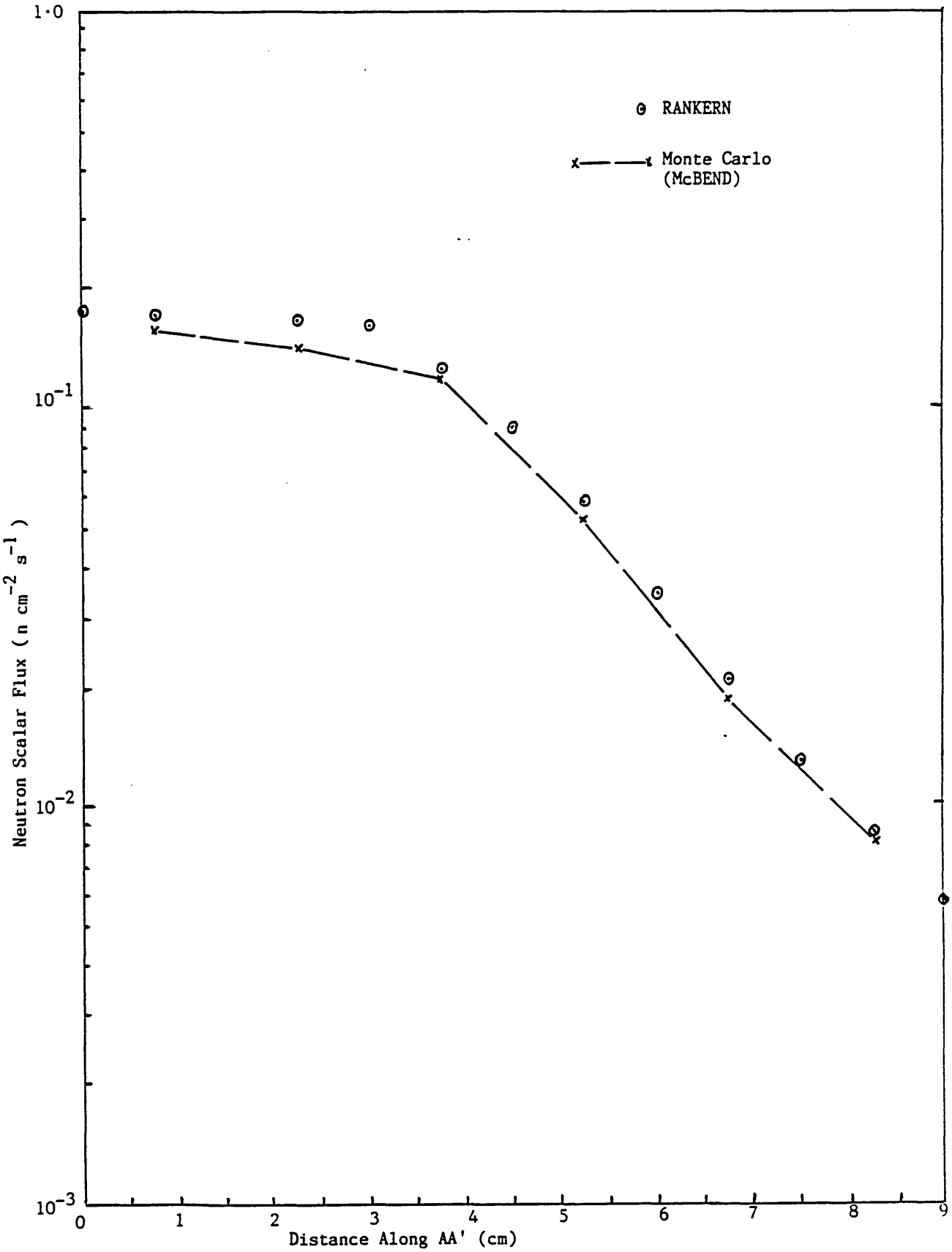


Fig. 5.39 RANKERN and McBEND (Monte Carlo) Solutions Along AA'.

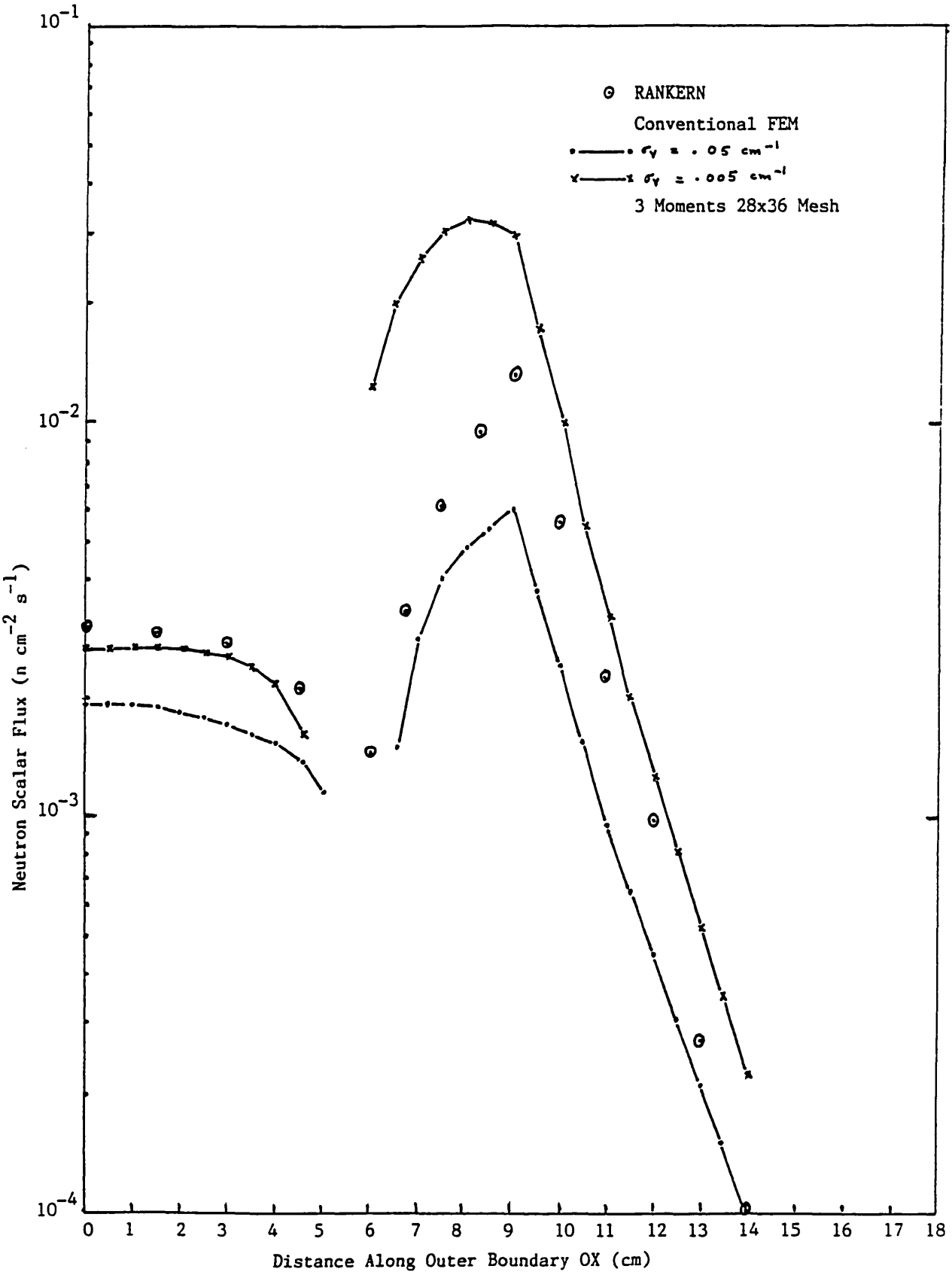


Fig. 5.40 RANKERN and Conventional Finite Element Solutions Along Outer Boundary OX.

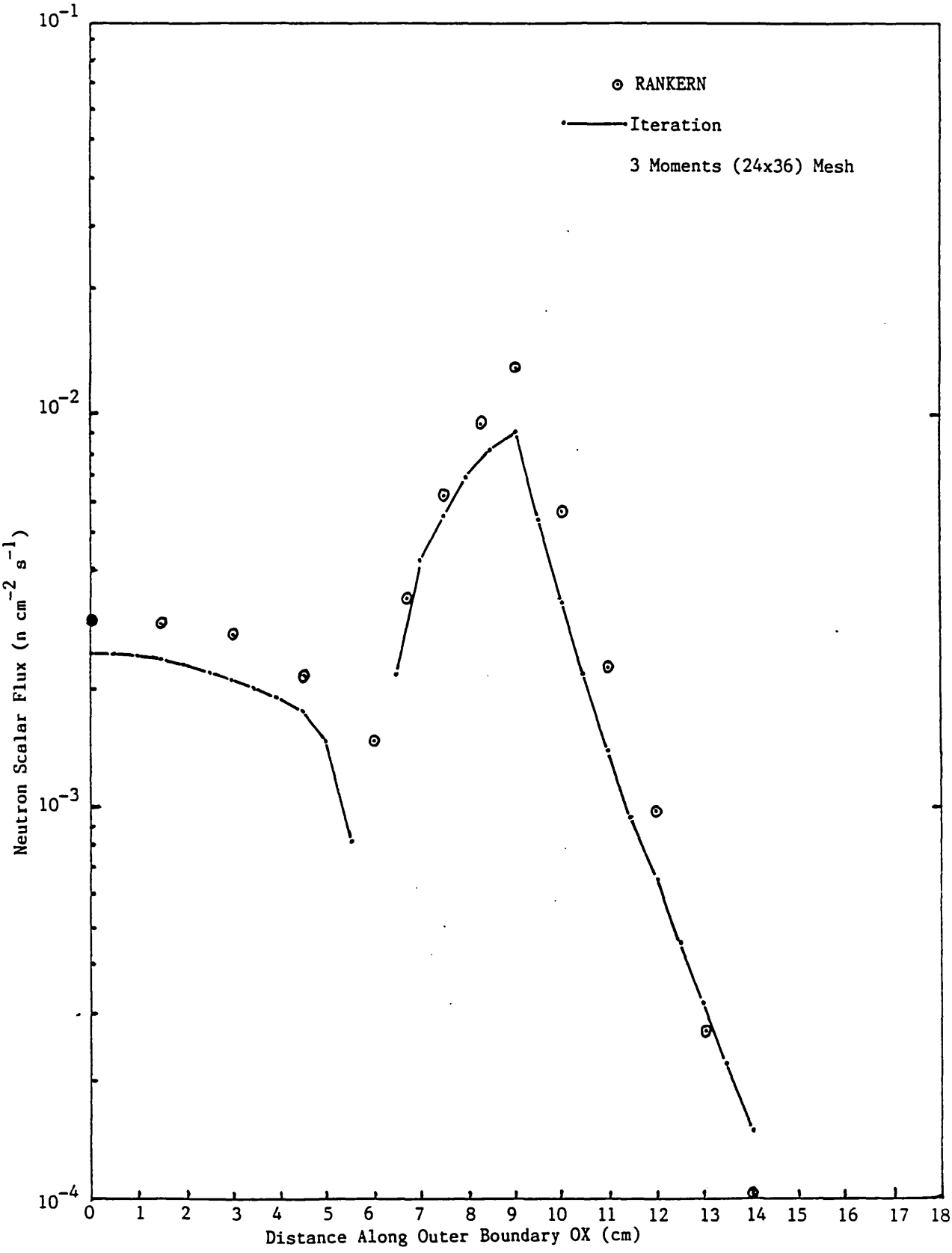


Fig. 5.41 RANKERN and Iteration Solutions Along Outer Boundary OX.

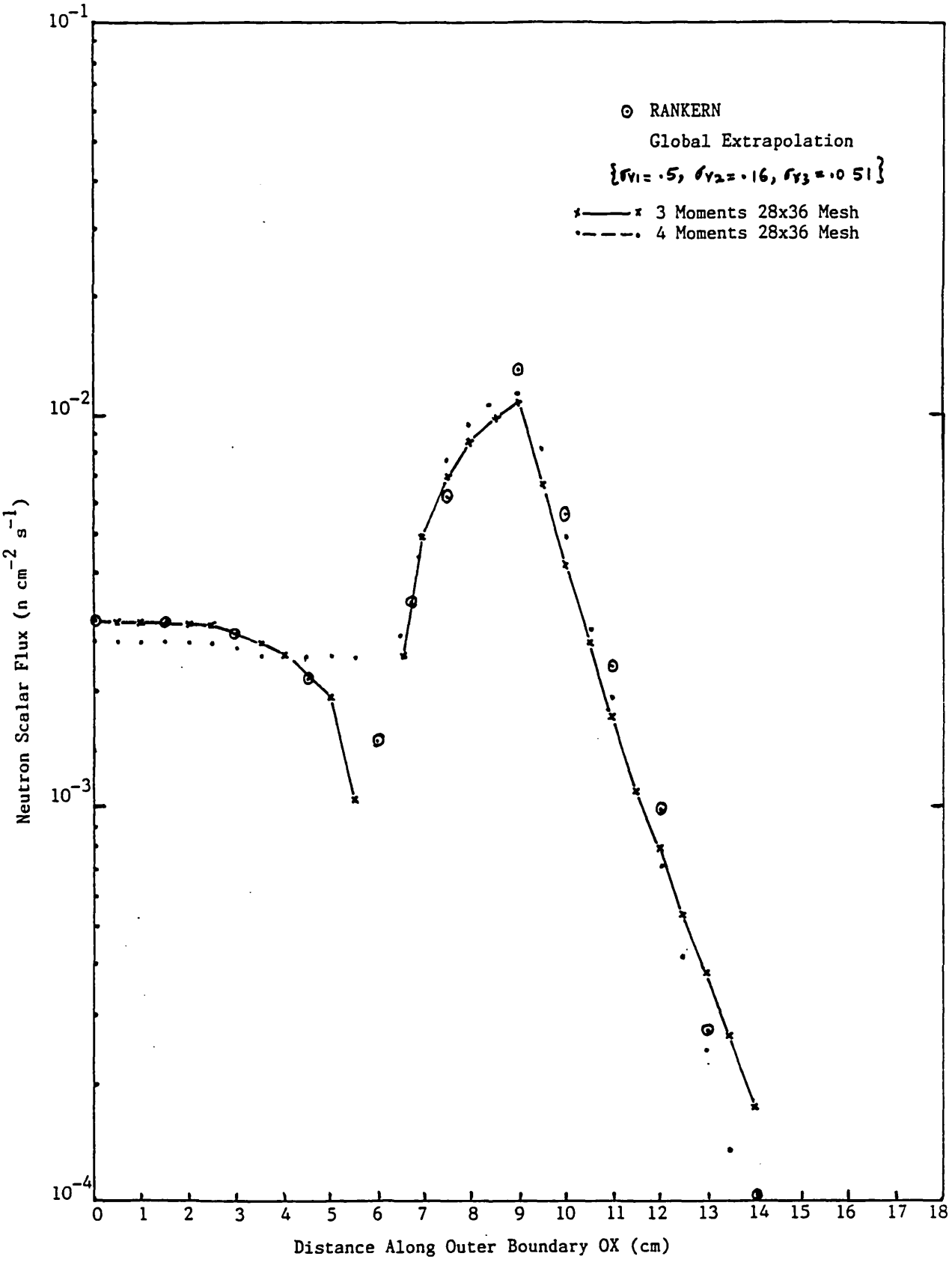


Fig. 5.42 RANKERN and Global Extrapolation Solutions Along Outer Boundary OX.

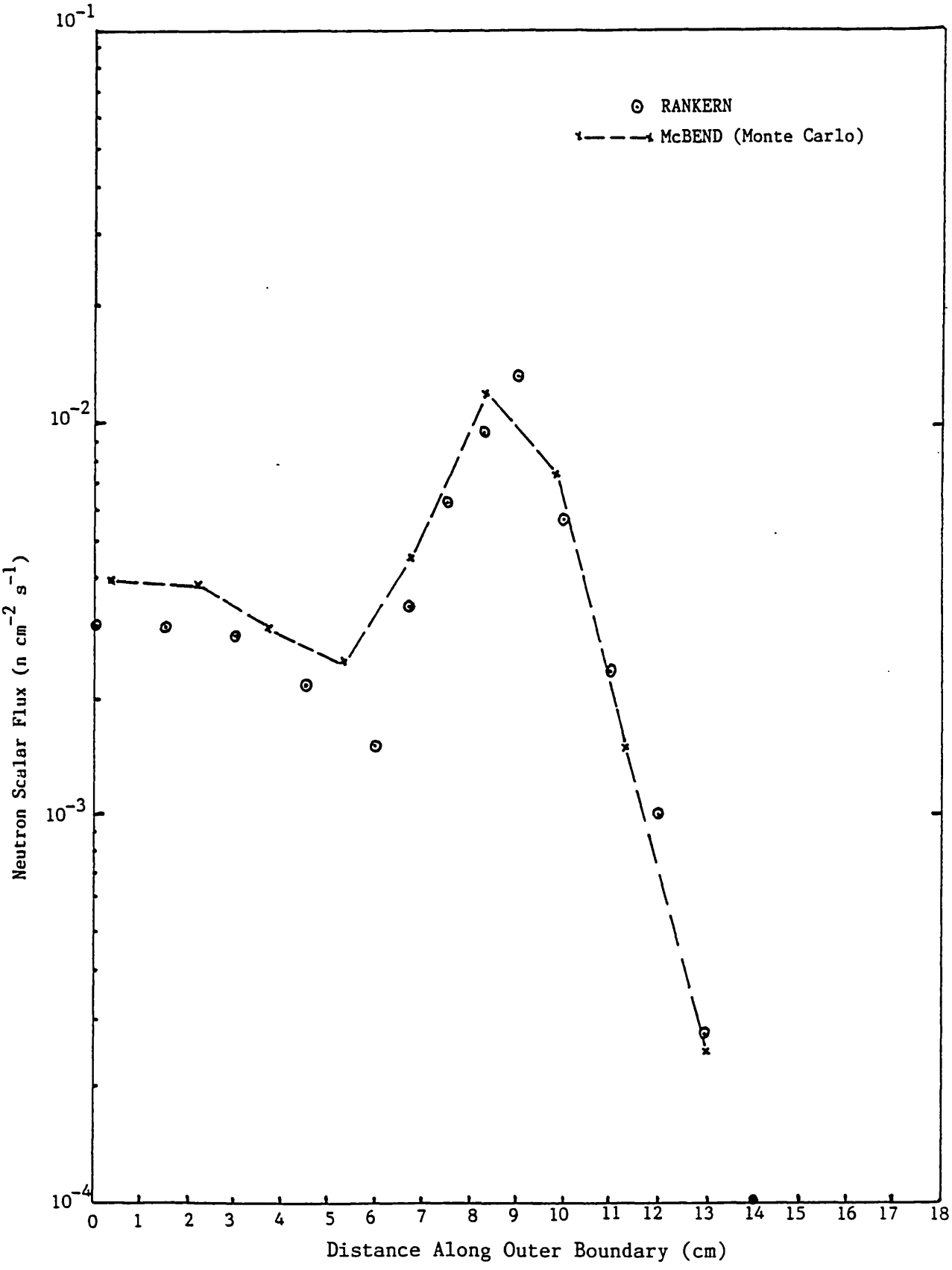


Fig. 5.43 RANKERN and McBEND (Monte Carlo) Solutions Along Outer Boundary OX.

the scalar flux everywhere along OX. The other solution with $\sigma_V = .005$ is too high near and at the exit of the duct. Difficulty was experienced in obtaining a sensible flux value near x=6·0cm where the flux dips significantly. Again a local mesh refinement here will improve the results in this region. In Fig. 5.41 are shown the iteration method results. Again three iterations were used with $\sigma_V = .05 cm^{-1}$. Overall the iterations solution is lower than ψ_R^+ nearly everywhere along OX, but, does show improvements on the conventional finite element solutions.

A three trial funciton global extrapolation solution with $\{\sigma_{Vi}\} = \{0.5, 0.16, 0.05\}$ is shown in Fig. 5.42 for three and four moments and 28x36 mesh. Overall, these solutions are closer to ψ_R^+ than any of the previous solutions. Finally McBEND Monte Carlo results are compared with RANKERN values in Fig. 5.43. Upto x=8·0 cm·McBEND overestimates the scalar flux, while beyond 10 cms it is in good agreement with RANKERN.

5.5.5 Square Source Void Problem With Scattering Media

This square source void problem was analysed by Watanabe and Maynard [12]. In this case, the geometry is the same as that of Problem 5.5.2 but, the non-void regions are now mainly scattering. The cross section data is given in Table 5.4. Watanabe and Maynard used their discrete cones method, a modified form of the discrete ordinates method, in analysing

this void problem. They compared their results along x= 5.625 cm with Monte Carlo and discrete ordinates methods. The results were shown in graphical form. See Fig. 5.44. It can be seen here that the S8 solution gives oscillations, whereas the discrete cones method, while eliminating the oscillations, still produces an incorrect flux gradient at x =0.0, the perfect reflector. Watanabe [14] also did independent Monte Carlo calculations using the MCNP code. In Fig. 5.45 results of MCNP calculations and global extrapolation calulations are compared along x= 5.625 cm. The global extrapolation calculation used three trial functions with $\{\sigma_{Vi}\} = \{0.2, 0.064, 0.021\}$. Overall there is excellent agreement with the MCNP results. The maximum standard deviation associated with the Monte Carlo results along x= 5.625 cm was 1.0%. Fig. 5.46 shows actual values of various calculations in the top right hand corner of the system. Here excellent agreement is obtained between the iteration, global extrapolation and MCNP results.

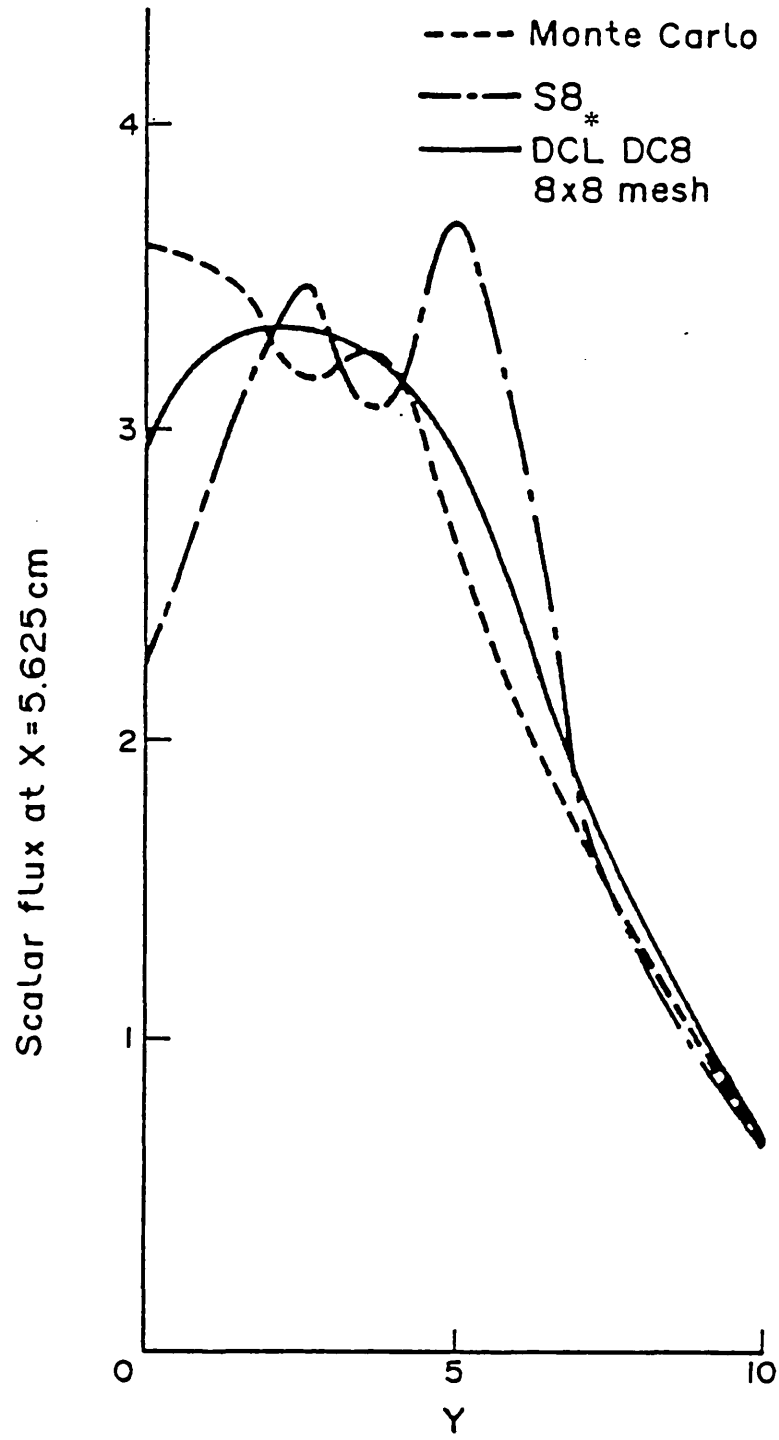


Fig. 5.44 Discrete Ordinates and Discrete Cones Method Solutions Along x= 5.625 cm for Problem 5.5.5

* DCL-Discrete Cones Method

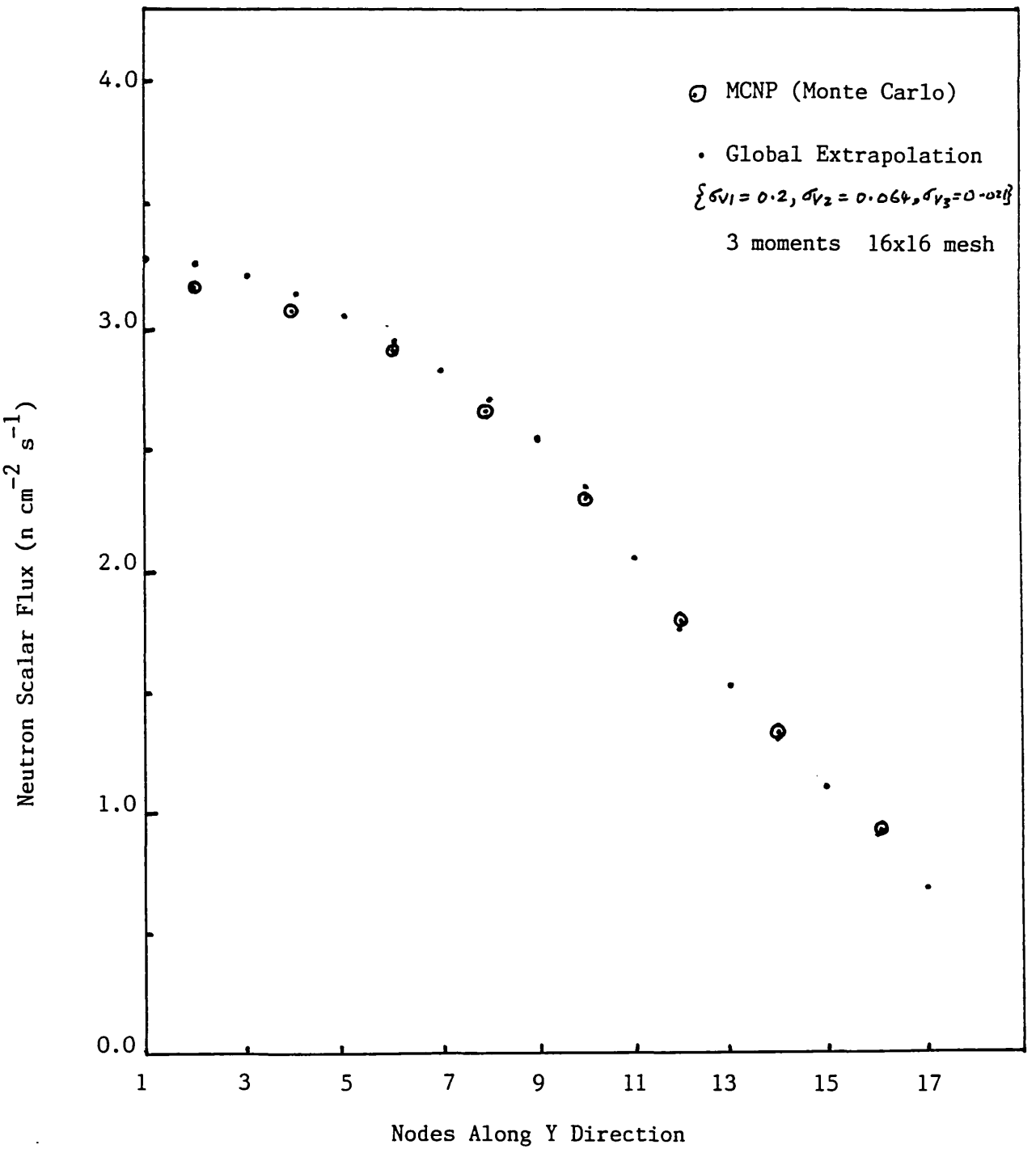


Fig 5.45 MCNP (Monte Carlo) and Global Extrapolation Solutions Along x= 5.625 cm for Problem 5.5.5.

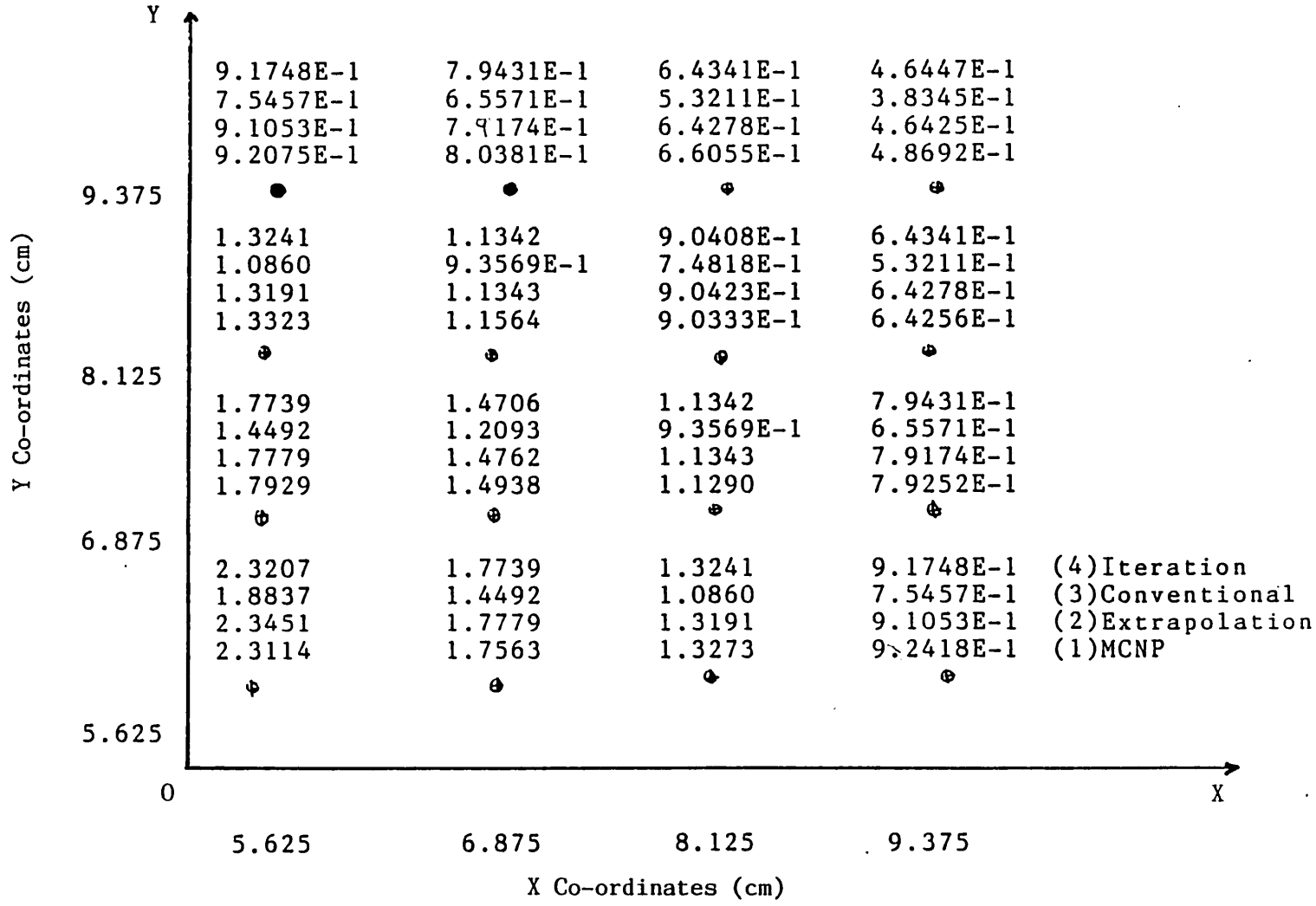


Fig. 5.46 Conventional Finite Element, Iteration, Global Extrapolation and MCNP Solutions in the Top Right Quadrant of the System.

REFERENCES TO CHAPTER 5

1. ACKROYD, R.T.
"The Why and How of Finite Elements"
Ann. Nucl. Energy, 8, p539 (1981)

2. KREYZIG, E.,
"Introductory Functional Analysis With Applications"
John Wiley and Sons (1978)

3. PRENTER, P.M.,
"Splines and Variational Methods"
John Whiley and Sons (1975)

4. CAREY G.F., and ODEN, J.T.
"The Texas Finite Element Series Vol II. A Second Course".
Prentice Hall (1983)

5. ACKROYD, R.T.
"Private Communication" (1987)

6. ACKROYD, R.T.
"Least-Squares Derivation of Extremum and Weighted-Residual Methods for Equations of Reactor Physics -I
Ann. Nucl. Energy, 10, p65 (1983)

7. MILLER, P.C., and SUMNER, V.
"RANKERN - A Point Kernel Code for Complicated Geometry Problem"
AEEW - R131, (1980)

8. RHOADES, W.A. and MYNATT, F.R.
"The DOT - II Two Dimensional Discrete Ordinates Transport Code"
ORNL - TM-4280. Oak Ridge National Laboratory.

9. BENDALL, D.E. and BRISSENDEN, R.T.
"McBEND Program User's Guide"
(Unpublished) UKAEA, Winfrith

10. STRAKER, E.A., STEVENS, P.N., IRVING, D.C. and CHAIN. V.R.
"The MORSE Code - A Multigroup Neutron and Gamma Ray Transport Code"
ORNL - 4585 (1970)

11. WATANABE, Y., and MAYNARD, C.W.
"The Discrete Cones Method for Two Dimensional Neutron Transport Computation in General Media"
Univ. of Wisconsin, Report UWFDM - 599

12. WATANABE, Y., and MAYNARD, C.W.
"The Discrete Cones Method in Two Dimensional Neutron Transport Computation"
Univ. of Wisconsin, Report UWFDM - 574

13. WATMOUGH, M.H.
"Private Communication"
(1986)

14. WATANABE, Y.
"Private Communication"
(1986)

CHAPTER 6

6. HYBRID VARIATIONAL PRINCIPLES FOR THE FINITE ELEMENT METHOD

6.1 Introduction

6.2 Least Squares Method for Hybrid Variational Principles

- 6.2.1 A Hybrid Maximum Principle for Diffusion Theory
- 6.2.2 Classical Maximum Principle
- 6.2.3 Minimum Principle

6.3 Hybrid Principles for Transport Theory

- 6.3.1 The $H^{+-}(\phi^+,\phi^-)$ Maximum Principle
- 6.3.2 Neutron Conservation
- 6.3.3 The $E^{+-}(\phi^+,\phi^-)$ Minimum Principle
- 6.3.4 The $E^{-+}(\theta^-,\theta^+)$ Minimum Principle
- 6.3.5 The $N^{+-}(\phi^+,\phi^-)$ Functional

6.4 Generating Higher Moment Solutions from Lower Moments

- 6.4.1 Maximisation of $H^{+-}(\phi^+,\phi^-)$
- 6.4.2 Synthesis Method
- 6.4.3 Synthesis Method in One Dimensional Slab Geometry
- 6.4.4 Synthesis Using $N^{+-}(\phi^+,\phi^-)$

References to Chapter 6

6. HYBRID VARIATIONAL PRINCIPLES FOR FINITE ELEMENT NEUTRON TRANSPORT

6.1 Introduction

In the following sections hybrid variational principles as applied to finite element neutron transport are discussed. Some illustrations for one dimensional slab geometry are given. Hybrid principles, recently developed are due to Ackroyd [1]. The classical $K^+(\phi^+)$ maximum principle, for instance involved only one trial function ϕ^+. With hybrid principles two quantities (unknown) are used; a trial function ϕ^+ with a trial vector $\underline{\phi}^+$ or ϕ^+ and ϕ^-. Hybrid principles for both diffusion and transport theory are discussed below.

Advantages and disadvantages in using hybrid principles for two and three dimensions and their relationship with nodal (cell) methods is also discussed. Subsequently, complementary hybrid principles are used to obtain the synthesis method for neutron transport. This method uses ϕ^+ and ϕ^- from the parity equations. An optimum solution for each higher moment using the previous moments may be obtained using the multiparameter extrapolation technique developed for void systems. This is illustrated for one dimensional slab geometry. Preliminary results using the synthesis method for a multi-layered shield problem are shown in Fig. 6.1. These are obtained by Nanneh [9]. See also Ackroyd et al [2].

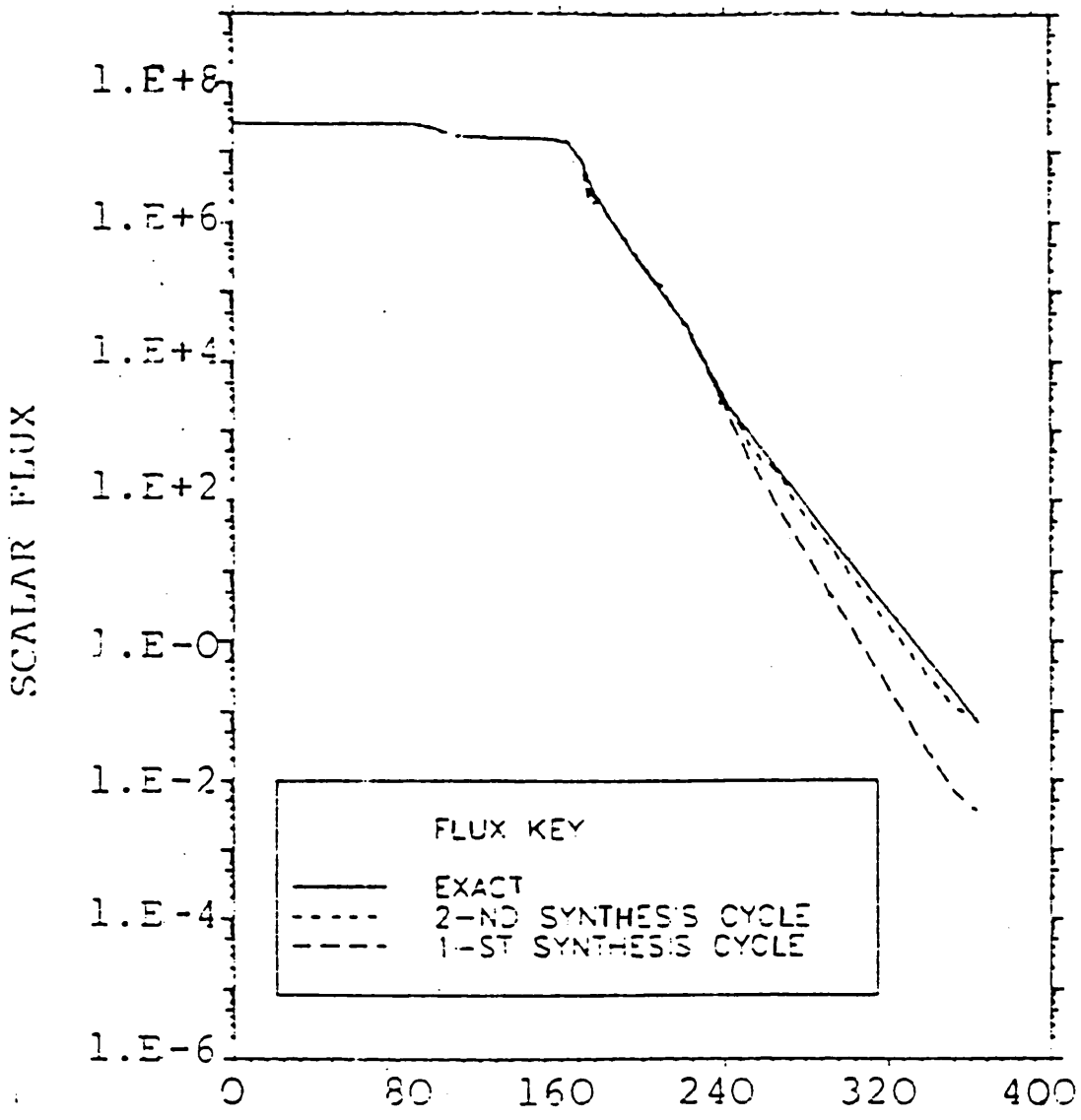


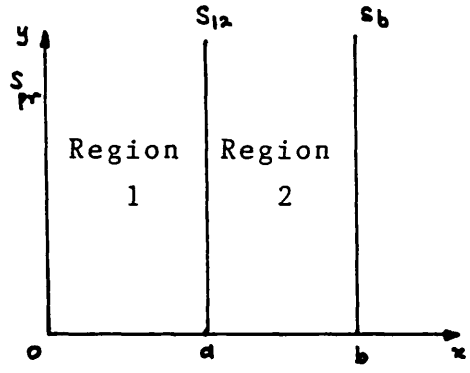
Fig. 6.1 Neutron Scalar Flux for a Multi-layered* Shield Problem.

*Results by Nanneh from Reference 2.

6.2 Least Squares Method for Hybrid Variational Principle

6.2.1 A Hybrid Maximum Principle for Diffusion Theory

Here the hybrid maximum principle is derived for one dimensional slab geometry using the generalised least squares method. Consider, for instance the diffusion equation for a system consisting of two regions.



Assume that there exists a perfect reflector at x=o and a bare surface at x=b. Write the diffusion equation as

$$\frac{d J_{ox}}{dx} + \sigma_R \phi_o(x) = S(x) \qquad (6.2\text{-}1)$$

and

$$J_{ox} = - D \frac{d \phi_o(x)}{dx} \qquad (6.2\text{-}2)$$

where Jox is the net neutron current and $\phi_o(x)$ is the exact scalar flux. The boundary conditions at the interface S_{12} and the bare surface S_b are:

$\phi_o(x)$ and J_{ox} are continuous across S_{12}.

$$\phi_o(x) - \alpha^2 J_{ox} \Big|_{x = S_b} = 0 \qquad (6.2\text{-}3)$$

where α^2 is a constant.

Let $\phi(x)$ and J_x be approximations to $\phi_0(x)$ and $J_{0x}(x)$, respectively. We are interested in local errors occuring in a least squares sense due to the approximations made. More specifically consider the residuals

$$R_1^2 = \left(\frac{dJ_x}{dx} + \sigma_R \phi - S \right)^2 \qquad (6.2\text{-}4)$$

and

$$R_2^2 = \left(J_x + D \frac{d\phi(x)}{dx} \right)^2 \qquad (6.2\text{-}5)$$

within each region. Error incurred on the bare surface can be measured in terms of

$$R_B^2 = (\phi - \alpha^2 J_x)^2 \qquad (6.2\text{-}6)$$

Across the interface, S_{12}, it is assumed that both ϕ and J_x are continuous. The global least squares error that is incurred by approximating (ϕ_0, J_{0x}) by the pair (ϕ, J_x) is given by the following functional

$$\hat{H}(\phi, J_x) = \int_V \left\{ \frac{1}{\sigma_R} \left(\frac{dJ_x}{dx} + \sigma_R \phi - S \right)^2 + \frac{1}{D} \left(J_x + D \frac{d\phi}{dx} \right)^2 \right\} dv$$

$$+ \int_{S_b} \frac{1}{\alpha^2} (\phi - \alpha^2 J_x)^2 \, ds \qquad (6.2\text{-}7)$$

Weights $\frac{1}{\sigma_r}$, $\frac{1}{D}$ and $\frac{1}{\alpha^2}$ have been used with R_1^2, R_2^2 and R_B^2 respectively, thus, generating a generalised least squares functional $\hat{H}(\phi, J_x)$. Expanding terms in $\hat{H}(\phi, J_x)$ we get

$$\hat{H}(\phi, J_x) = \int_V \left\{ \frac{1}{\sigma_R}\left(\frac{dJ_x}{dx}\right)^2 + \sigma_R \phi^2 + \frac{S^2}{\sigma_R} + 2\phi\left(\frac{dJ_x}{dx}\right) - 2\phi S - \frac{2S}{\sigma_R}\left(\frac{dJ_x}{dx}\right) \right\} dv$$

$$+ \int_V \frac{1}{D}\left\{ J_x^2 + 2D J_x \frac{d\phi}{dx} + D^2\left(\frac{d\phi}{dx}\right)^2 \right\} dv$$

$$+ \int_{S_b} \frac{1}{\alpha^2}\left\{ \phi^2 - 2\alpha^2 \phi J_x + \alpha^4 J_x^2 \right\} ds$$

(6.2-8)

We can write the term

$$2\left(\phi \frac{dJ_x}{dx} + J_x \frac{d\phi}{dx}\right) \quad \text{as}$$

$$2\frac{d}{dx}\left[\phi J_x\right]$$

(6.2-9)

In general this will be div ($\phi \underline{J}$). The volume or spatial integral for this term can then be converted to a surface integral term with the use of the divergence theorem, viz.,

$$\int_V \text{div } \underline{F}\, dv = \int_S \underline{F}.\underline{n}\, dS$$

(6.2-10)

$\hat{H}(\phi, J_x)$ then becomes

$$\int_V \left\{ \frac{1}{\sigma_R}\left(\frac{dJ_x}{dx} - S\right)^2 + \frac{1}{D}(J_x)^2 \right\} dv$$
$$+ \int_V \left\{ -2\phi S + D\left(\frac{d\phi}{dx}\right)^2 + \sigma_R \phi^2 \right\} dv$$
$$+ \int_{S_b} \left(\phi^2/\alpha^2 - 2\phi J_x + \alpha^2 J_x^2 \right) ds$$
$$+ 2\int_{S_b} \phi J_x\, ds$$

(6.2-11)

Hence, some cancellation takes place in the surface terms because of the weights chosen in constructing $\hat{H}(\phi, J_x)$. We can write

$$\hat{H}(\phi, J_x) = \hat{E}(J_x) - \hat{K}(\phi) \tag{6.2-12}$$

where

$$\hat{E}(J_x) = \int_V \left\{ \frac{1}{\sigma_R} \left(\frac{dJ_x}{dx} - S \right)^2 + \frac{1}{D} (J_x)^2 \right\} dV + \int_{S_b} \alpha^2 (J_x)^2 \, ds \tag{6.2-13}$$

and

$$\hat{K}(\phi) = \int_V \left\{ 2\phi S - D \left(\frac{d\phi}{dx} \right)^2 - \sigma_T \phi^2 \right\} dV - \int_{S_b} \frac{\phi^2}{\alpha^2} \, ds \tag{6.2-14}$$

$$\therefore \quad \hat{K}(\phi) - \hat{E}(J_x) + \hat{H}(\phi, J_x) = 0 \tag{6.2-15}$$

Since, $\hat{H}(\phi, J_x)$ is positive definite by definition on construction, then

$$\hat{E}(J_x) - \hat{K}(\phi) \geq 0$$

i.e.
$$\hat{K}(\phi) - \hat{E}(J_x) \leq 0 \tag{6.2-16}$$

This result implies a hybrid maximum principle since both ϕ and J_x are involved in the inequality.

6.2.2 The Classical Maximum Principle

The classical maximum principle [3,4] may be obtained

from the above by setting $J_x = J_{ox}$, the exact neutron current. Then

$$\hat{H}(\phi, J_{ox}) + \hat{K}(\phi) = \hat{E}(J_{ox}) \tag{6.2-17}$$

where

$$\hat{H}(\phi, J_{ox}) = \int_V \left[\sigma_R (\phi - \phi_o)^2 + D \left[\frac{d(\phi - \phi_o)}{dx} \right]^2 \right] dV + \int_{S_b} \frac{(\phi - \phi_o)^2}{\alpha^2} ds \tag{6.2-18}$$

and

$$\hat{E}(J_{ox}) = \int_V \left[D \left(\frac{d\phi_o}{dx} \right)^2 + \sigma_R \phi_o^2 \right] dV + \int_{S_b} \frac{\phi_o^2}{\alpha^2} ds \tag{6.2-19}$$

Since $\hat{H}(\phi, J_{ox})$ is positive definite, then

$$\hat{K}(\phi) \leq \int_V \left\{ D \left(\frac{d\phi_o}{dx} \right)^2 + \sigma_R \phi_o^2 \right\} dV + \int_{S_b} \frac{\phi_o^2}{\alpha^2} ds$$

$$\therefore \quad \hat{K}(\phi) \leq F(\phi_o, \phi_o) \tag{6.2-20}$$

Here the right hand side is simply the bilinear functional defined as

$$F(\phi, \psi) = \int_V \left\{ \frac{d\phi}{dx} D \frac{d\psi}{dx} + \phi \sigma \psi \right\} dV + \int_{S_b} \frac{\psi \phi}{\alpha^2} ds \tag{6.2-21}$$

$\hat{K}(\phi)$ is simply $K^+(\phi^+)$ the classical maximum principle for diffusion theory.

6.2.3 Minimum Principle

Above the classical maximum principle was obtained by

making the net current exact, i.e. Jox. In order to generate a minimum principle, set $\phi = \phi_o$, the exact scalar flux. Then

$$\hat{E}(J_x) = \hat{K}(\phi_o) + \hat{H}(\phi_o, J_x) \tag{6.2-22}$$

This can also be written as

$$\hat{E}(J_x) = F(\phi_o, \phi_o) + \int_V \left\{ \frac{1}{\sigma_R} \left(\frac{d}{dx}(J_x - J_{ox}) \right)^2 + \frac{1}{D}(J_x - J_{ox})^2 \right\} dV$$

$$+ \int_{S_b} \alpha^2 \left\{ (J_x - J_{ox})^2 \right\} dS \tag{6.2-23}$$

Since all terms on the right hand side of (6.2-23) are positive, then

$$\hat{E}(J_x) \geq F(\phi_o, \phi_o) . \tag{6.2-24}$$

This then defines a complementary minimum principle. Hence,

$$\hat{K}(\phi) \leq F(\phi_o, \phi_o) \leq \hat{E}(J_x) .$$

In the $\hat{K}(\phi)$ principle ϕ needs to be continuous across interfaces, whereas in the $\hat{E}(J_x)$ principle J_x must be continuous across interfaces. In addition both ϕ and J_x are required to have continuous first derivatives, i.e. they belong to the class C^1 of admissible functions, in each region.

6.3 Hybrid Principles for Transport Theory

6.3.1 The $H^{+-}(\phi^+, \phi^-)$ Maximum Principle

Before deriving the $H^{+-}(\phi^+, \phi^-)$ maximum principle it is appropriate to state the restrictions imposed on the trial functions ϕ^+ and ϕ^- which approximate ϕ_o^+ and ϕ_o^-, respectively.

(i) Trial Functions ϕ^+ and ϕ^- are continuous and have continuous first spatial derivatives for all $\underline{\Omega}, \underline{r}$ lying within each element.

(ii) ϕ^+ need not satisfy any interface or boundary conditions.

(iii) ϕ^- is continuous across interfaces for all $\underline{\Omega}$ crossing the interface.

(iv) On a perfect reflector S_{pr}.

$$\phi^-(\underline{r}, \underline{\Omega}) = \phi^-(\underline{r}, \underline{\Omega}^*) \quad \text{for all} \quad \underline{\Omega} \cdot \underline{n} = -\underline{\Omega}^* \cdot \underline{n} \neq 0 \tag{6.3-1}$$

where $\underline{n}$ is the outward normal to S_{pr}.

Another quantity required is $\overline{W}^{+-}(\phi^+, \phi^-)$ which is a special case of the functional $W^{+-}(\phi^+, \phi^-)$ of Ackroyd [4] defined in Chapter 3. We have

$$\overline{W}^{+-}(\phi^+, \phi^-) = I(\phi^+, \phi^-) + J(\phi^+, \phi^-) + I_b(\phi^+, \phi^-) + I_s(\phi^+, \phi^-) \tag{6.3-2}$$

where the quantities involved on the right hand side have been defined previously. $\overline{W}^{+-}$ gives an overall least squares

measure of the errors incurred by ϕ^+ and ϕ^- in not satisfying the parity equations within each element and in addition not meeting the imposed boundary conditions for S_b and S_s . $\overline{W}^{+-}$ can be written more explicitly as

$$\overline{W}^{+-}(\phi^+,\phi^-) = \int_V \langle \varsigma [\underline{\Omega}\cdot\nabla\phi^+ + \varsigma^{-1}\phi^- - s^-],\ \underline{\Omega}\cdot\nabla\phi^+ + \varsigma^{-1}\phi^- - s^- \rangle dv$$
$$+ \int_V \langle c^{-1}[\underline{\Omega}\cdot\nabla\phi^- + c\phi^+ - s^+],\ \underline{\Omega}\cdot\nabla\phi^- + c\phi^+ - s^+ \rangle dv \qquad (6.3\text{-}3)$$
$$+ \int_{S_b} \Big\{ \int_{\underline{\Omega}\cdot\underline{n}>0} |\underline{\Omega}\cdot\underline{n}|\,(\phi^+ - \phi^-)^2\, d\underline{\Omega} + \int_{\underline{\Omega}\cdot\underline{n}<0} |\underline{\Omega}\cdot\underline{n}|\,(\phi^+ - \phi^-)^2\, d\Omega \Big\} ds$$
$$+ \int_{S_s} \Big\{ \int_{\underline{\Omega}\cdot\underline{n}>0} |\underline{\Omega}\cdot\underline{n}|\,(\phi^+ - \phi^- - T(r_1,-\underline{\Omega}))^2\, d\Omega + \int_{\underline{\Omega}\cdot\underline{n}<0} |\underline{\Omega}\cdot\underline{n}|\,(\phi^+ + \phi^- - T(r,\underline{\Omega}))^2\, d\Omega \Big\} ds$$

This leads to the following identity involving

$$K^+(\phi^+) + K^-(\phi^-) + L(\phi^+,\phi^-) + M(\phi^+,\phi^-) + \overline{W}^{+-}(\phi^+,\phi^-)$$
$$\equiv \int_V \{ \langle c^{-1}s^+, s^+ \rangle + \langle \varsigma s^-, s^- \rangle \}\, dv \qquad (6.3\text{-}4)$$
$$+ 2\int_{S_s}\int_{\underline{\Omega}\cdot\underline{n}<0} |\underline{\Omega}\cdot\underline{n}|\, T^2\, d\Omega\, ds = 2\alpha \ \text{(known)}$$

Here K^+ and K^- are the classical maximum principles and L, M are defined as

$$L(\phi^+,\phi^-) = -2\int_{US_i}\int_{\Omega} \underline{\Omega}\cdot\underline{n}_i\, \phi^+\phi^-\, d\Omega\, ds \qquad (6.3\text{-}5)$$

and

$$M(\phi^+,\phi^-) = -2\int_{S_{pr}}\int_{\Omega} \underline{\Omega}\cdot\underline{n}\, \phi^+\phi^-\, d\Omega\, ds \qquad (6.3\text{-}6)$$

These terms compensate for the I and J expansion surface terms obtained by using the divergence theorem on terms involving $(\underline{\Omega}\cdot\nabla\phi^+)\phi^-$. The identity, (6.3-4) is used in deriving hybrid principles. We start by defining a functional $H^{+-}(\phi^+,\phi^-)$ as

$$H^{+-}(\phi^+,\phi^-) = K^+(\phi^+) + K^-(\phi^-) - 2\int_{US_i}\int_{\Omega} \underline{\Omega}\cdot\underline{n}_i\,\phi^+\phi^-\,d\Omega\,ds$$

$$-\lambda\int_{S_b US_s}\int_{\Omega} \omega(\underline{r},\underline{\Omega})\,|\underline{\Omega}\cdot\underline{n}|\,[c\phi^+ - s^+ + \underline{\Omega}\cdot\nabla\phi^-]$$

$$-\lambda'\int_{S_{pr}}\int_{\Omega}\omega(\underline{r},\underline{\Omega})\,|\underline{\Omega}\cdot\underline{n}|\left[s^+(\underline{r},\underline{\Omega}) - s^+(\underline{r},\underline{\Omega}^*) + \underline{\Omega}^*\cdot\nabla\phi^+(\underline{r},\underline{\Omega}^*) - \underline{\Omega}\cdot\nabla\phi^-(\underline{r},\underline{\Omega})\right]^2 d\Omega\,ds \qquad (6.3\text{-}7)$$

where $\omega(\underline{r},\underline{\Omega})$ is a positive weight function and λ and λ' are positive parameters. We then have

$$H^{+-}(\phi^+,\phi^-) \leq 2\alpha \qquad (6.3\text{-}8)$$

using (6.3-4) and assuming that ϕ^+ and ϕ^- satisfy the conditions stated earlier. The above maximum principle can be derived using the identity, (6.3-4). We get

$$H^{+-}(\phi^+,\phi^-) + \lambda\int_{S_b US_s}\int_{\Omega}\omega(\underline{r},\underline{\Omega})\,|\underline{\Omega}\cdot\underline{n}|\left[c\phi^+ - s^+ + \underline{\Omega}\cdot\nabla\phi^-\right]^2 d\Omega\,ds + \lambda'\int_{S_{pr}}\int_{\Omega}\omega(\underline{r},\underline{\Omega})\,|\underline{\Omega}\cdot\underline{n}|$$

$$\left[s^+(\underline{r},\underline{\Omega}) - s^+(\underline{r},\underline{\Omega}^*) + \underline{\Omega}^*\cdot\nabla\phi^-(\underline{r},\underline{\Omega}^*) - \underline{\Omega}\cdot\nabla\phi^-(\underline{r},\underline{\Omega})\right]^2 d\Omega\,ds + \overline{W}^{+-}(\phi^+,\phi^-) \qquad (6.3\text{-}9)$$

When $\phi^+ = \phi_o^+$ and $\phi^- = \phi_o^-$ then equality holds in (6.3-8). Otherwise there is the inequality due to the fact that $\overline{W}^{+-}$ and the surface terms involving $S_b US_s$ and S_{pr} are non-negative. If equality is assummed in (6.3-8) then the sum of the λ, λ' and $\overline{W}^{+-}$ terms vanish.

This may be seen as follows. The volume terms of $\overline{W}^{+-}$ vanish hence,

$$\underline{\Omega}\cdot\nabla\phi^+ + \varsigma^{-1}\phi^- = s^-$$
$$\underline{\Omega}\cdot\nabla\phi^- + c\,\phi^+ = s^+$$

the parity equations within each element. Hence

$$-\underline{\Omega}.\nabla\left[c^{-1}\underline{\Omega}.\nabla\phi^{-}\right] + \varsigma^{-1}\phi^{-} = s^{-} - \underline{\Omega}.\nabla\left[c^{-1}s^{+}\right] \qquad (6.3\text{-}10)$$

which is the second order odd parity equation for ϕ^{-}. Vanishing of the surface terms of $\overline{W}^{+-}$ give

$$\phi^{-} + c^{-1}\left[s^{+} - \underline{\Omega}.\nabla\phi^{-}\right] = 0 \quad \text{for } \underline{\Omega}.\underline{n} < 0$$
$$\phi^{-} - c^{-1}\left[s^{+} - \underline{\Omega}.\nabla\phi^{-}\right] = 0 \quad \text{for } \underline{\Omega}.\underline{n} > 0 \qquad \text{on } S_b$$

and
$$\phi^{-} + c^{-1}\left[s^{+} - \underline{\Omega}.\nabla\phi^{-}\right] = T(r,\Omega) \quad \text{for } \underline{\Omega}.\underline{n} < 0$$
$$\phi^{-} - c^{-1}\left[s^{+} - \underline{\Omega}.\nabla\phi^{-}\right] = T(r,-\Omega) \quad \text{for } \underline{\Omega}.\underline{n} > 0 \qquad \text{on } S_s$$

$$c^{-1}\left[s^{+}(r,\Omega) - s^{+}(r,\Omega^{*}) + \Omega^{*}.\nabla\phi^{-}(r,\Omega^{*}) - \Omega.\nabla\phi^{-}(r,\Omega)\right] = 0 \text{ for all } \underline{\Omega}.\underline{n} = -\underline{\Omega}^{*}.\underline{n} \neq 0 \text{ on } S_{pr}.$$

In addition since ϕ^{-} satisfies the interface continuity condition and reflective condition, together with Eqn. (6.3-10) imply $\phi^{-} = \phi_o^{-}$, the exact odd parity solution. Similar arguments give $\phi^{+} = \phi_o^{+}$.

This means that when ϕ^{+} and ϕ^{-} are independent trial functions, equality in (6.3-8) is only obtained when $\phi^{+} = \phi_o^{+}$ and $\phi^{-} = \phi_o^{-}$. In trying to obtain good approximations for ϕ_o^{+} and ϕ_o^{-}, $H^{+-}(\phi^{+},\phi^{-})$ is maximised by suitable choice of ϕ^{+}, ϕ^{-} with $\omega(r,\Omega)$, λ and λ' specified. Maximisation of H^{+-} is given in Section 6.4.1. For a discussion on the choice of penalty parameters λ, λ' See Ackroyd [3].

6.3.2 Neutron Conservation

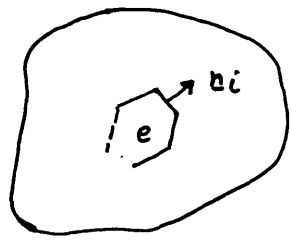
We have seen that in the $H^{+-}(\phi^+, \phi^-)$ maximum principle the trial function ϕ^+ does not have to satisfy any interface or boundary conditions. This means that ϕ^+ for one element is independent of the ϕ^+ for all other elements of a system. So in a particular element e we can specify ϕ_e^+ as

$$\phi_e^+ = \bar{\phi}_e + \psi_e^+(\underline{r}, \underline{\Omega}) \tag{6.3-11}$$

where $\bar{\phi}_e$ is the average scalar flux in e and

$$\int_{V_e}\int_{\Omega} \psi_e^+(\underline{r}, \underline{\Omega})\, d\Omega\, dV = 0 \tag{6.3-12}$$

Consider an element that lies totally within a system as shown below.



Then maximising $H^{+-}(\phi^+, \phi^-)$ with respect to the average scalar flux $\bar{\phi}_e$ gives

$$\frac{\partial}{\partial \bar{\phi}_e}\left[\int_{V_e}\int_{\Omega}\left[2\phi^+ S^+ + \underline{\Omega}\cdot\nabla\phi^+ \chi S^- - \underline{\Omega}\cdot\nabla\chi(\underline{\Omega}\cdot\nabla\phi^+) - \phi^+ C\phi^+\right] d\Omega\, dV - 2\int_{VS_i}\int_{\Omega} \underline{\Omega}\cdot\underline{n}_i\, \phi^+\phi^-\, d\Omega\, dS\right] = 0 \tag{6.3-13}$$

Hence

$$\int_{V_e}\int_{\Omega} [s^+ - C\phi^+]\, d\Omega dV = \int_{US_i}\int_{\Omega} \underline{\Omega}.\underline{n}_i\, \phi^-\, d\Omega ds \qquad (6.3\text{-}14)$$

since C is self adjoint. The right hand side of this equation implies net flow of neutrons per unit time out of element e. See the definition of neutron flow involving ϕ^- in Section 2.2. In the case of constant macroscopic absorption, scattering and total cross sections we have

$$\left(\int_{V_e}\int_{\Omega} s^+\, d\Omega dV\right) - \sigma_a V_e \bar{\phi}_e = \int_{US_i}\int_{\Omega} \underline{\Omega}.\underline{n}_i\, \phi^-\, d\Omega ds \qquad (6.3\text{-}15)$$

= Net flow of neutrons per unit time out of e.

This is a conservation equation for neutrons in element e and occurs quite naturally in the maximisation of the $H^{+-}(\phi^+, \phi^-)$ principle. See Ackroyd [7].

6.3.3 The $E^{+-}(\phi^+, \phi^-)$ Minimum Principle

The $E^{+-}(\phi^+, \phi^-)$ minimum principle can be used to obtain the method of synthesis of solutions, described later in Section 6.4. By changing the roles of ϕ^+ and ϕ^- denoted by θ^+, θ^- we can obtain $E^{-+}(\theta^+, \theta^-)$ minimum principle. This is described in Section 6.3.4. The functional $E^{+-}(\phi^+, \phi^-)$ is defined to be

$$E^{+-}(\phi^+, \phi^-) = K^+(\phi^+) - 2\int_{U_{Si}}\int_{\Omega} \phi^+ \phi^- \, d\Omega \, ds - 2\int_{S_{pr}}\int_{\Omega} \underline{\Omega}.\underline{n}\, \phi^+\phi^- \, d\Omega \, ds$$
$$+ \bar{W}^{+-}(\phi^+, \phi^-) + \int_V \langle \underline{\mathcal{T}}(\underline{\Omega}.\nabla\phi^- + c\phi^+ - s^+), \underline{\Omega}.\nabla\phi^- + c\phi^+ - s^+ \rangle dV \qquad (6.3\text{-}16)$$

where $\mathcal{T}$ is a positive operator. E^{+-} defines a minimum principle since

$$F^+(\phi_o^+, \phi_o^+) \leq E^{+-}(\phi^+, \phi^-) \qquad (6.3\text{-}17)$$

for trial functions ϕ^+ and ϕ^- satisfying the conditions stated earlier. As before equality is obtained in (6.3-17) above if and only if

$$\phi^+ = \phi_o^+$$
$$\phi^- = \phi_o^- .$$

Derivation of the E^{+-} minimum principle is given below. On using the expressions for L and M and the fact that

$$F^+(\phi_o^+, \phi_o^+) + F^-(\phi_o^-, \phi_o^-) = 2\alpha \qquad (6.3\text{-}18)$$

(See Ackroyd [4]) we have

$$K^+(\phi^+) + K^-(\phi^-) - 2\int_{US_i}\int_{\Omega} \underline{n}\cdot\underline{n}_i\,\phi^+\phi^-\,d\Omega\,ds - 2\int_{S_{pr}}\int_{\Omega} \underline{n}\cdot\underline{n}\,\phi^+\phi^-\,d\Omega\,ds$$

$$+ \overline{W}^{+-}(\phi^+,\phi^-) = 2\alpha = F^+(\phi_o^+,\phi_o^+) + F^-(\phi_o^-,\phi_o^-) \qquad (6.3\text{-}19)$$

Next we can use this result and the identity

$$K^-(\phi^-) + F^-(\epsilon^-,\epsilon^-) = 2\alpha - F^+(\phi_o^+,\phi_o^+) \qquad (6.3\text{-}20)$$

where $\epsilon^- = (\phi^- - \phi_o^-)$, to obtain

$$K^+(\phi^+) - 2\int_{US_i}\int_{\Omega} \underline{n}\cdot\underline{n}_i\,\phi^+\phi^-\,d\Omega\,ds - 2\int_{S_{pr}}\int_{\Omega} \underline{n}\cdot\underline{n}\,\phi^+\phi^-\,d\Omega\,d\underline{s} + \overline{W}^{+-}(\phi^+,\phi^-)$$

$$= F^+(\phi_o^+,\phi_o^+) + F^-(\epsilon^-,\epsilon^-)\,. \qquad (6.3\text{-}21)$$

E^{+-} can then be written as

$$E^{+-}(\phi^+,\phi^-) = F^+(\phi_o^+,\phi_o^+) + F^-(\epsilon^-,\epsilon^-) +$$

$$\int \langle \underline{P}(\underline{n}\cdot\nabla\epsilon^- + c\epsilon^+),\ \underline{n}\cdot\nabla\epsilon^- + c\epsilon^+\rangle\,dv \qquad (6.3\text{-}22)$$

here $\epsilon^+ = (\phi^+ - \phi_o^+)$.

Since $F^+(\phi_o^+,\phi_o^+)$ is positive and each of the other terms in (6.3-22) are non-negative, then

$$E^{+-}(\phi^+,\phi^-) \geq F^+(\phi_o^+,\phi_o^+) > 0$$

is the minimum principle as required.

In fact E^{+-} and K^{+}, the classical maximum principle, are complementary principles in the sense

$$K^{+}(\phi^{+}) \leq F^{+}(\phi_{o}^{+}, \phi_{o}^{+}) \leq E^{+-}(\phi^{+}, \phi^{-}) \tag{6.3-23}$$

ϕ^{+} satisfies the continuity conditions at interface and the reflection condition on S_{pr}. So E^{+-}, the hybrid minimum principle, is complementary to $K^{+}(\phi^{+})$.

6.3.4 The $E^{-+}(\theta^{+}, \theta^{-})$ Minimum Principle

The E^{-+} principle differs from the E^{+-} minimum principle in that the roles of ϕ^{+} and ϕ^{-} are changed. In this case let θ^{+} and θ^{-} be approximations to ϕ_{o}^{+} and ϕ_{o}^{-} respectively. The conditions on the trial functions θ^{+} and θ^{-} are as follows:

(i) θ^{-} does not have to satisfy any interface or boundary conditions

(ii) θ^{+} has to satisfy the continuity condition for interfaces and reflection condition on S_{pr}

The $E^{-+}(\theta^{-}, \theta^{+})$ functional is defined as

$$E^{-+}(\theta^{-}, \theta^{+}) = K^{-}(\theta^{-}) - 2\int_{USi}\int_{n} \theta^{+}\theta^{-}\, \underline{\Omega}\cdot\underline{n}_{i}\, dn\, ds - 2\int_{S_{pr}}\int_{n} \underline{\Omega}\cdot\underline{n}\, \theta^{+}\theta^{-}\, dn\, ds$$
$$+ \overline{W}^{+-}(\theta^{+}, \theta^{-}) + \int_{V} \langle \underline{\alpha}\,(\underline{\Omega}\cdot\nabla\theta^{+} + \varsigma^{-1}\theta^{-} - s^{-}),\ \underline{\Omega}\cdot\nabla\theta^{+} + \varsigma^{-1}\theta^{-} - s^{-}\rangle\, dV \tag{6.3-24}$$

where $\underline{\underline{a}}$ is another positive definite operator. The minimum principle in this case is

$$F^-(\phi_o^-, \phi_o^-) \leq E^{-+}(\theta^-, \theta^+) \tag{6.3-25}$$

Equality holds in (6.3-25) if

$$\theta^+ = \phi_o^+$$

and

$$\theta^- = \phi_o^- .$$

This minimum principle may be derived by letting

$$\zeta^+ = \theta^+ - \phi_o^+$$

and

$$\zeta^- = \theta^- - \phi_o^- .$$

Then

$$K^-(\theta^-) - 2\int_{VS_i}\int_{\Omega} \underline{\Omega}\cdot\underline{n}_i\, \theta^+\theta^-\, d\Omega\, dS - 2\int_{S_{pr}}\int_{\Omega} \underline{\Omega}\cdot\underline{n}\, \theta^+\theta^-\, d\Omega\, dS$$

$$+ \bar{W}^{+-}(\theta^+, \theta^-) = F^-(\phi_o^-, \phi_o^-) + F^+(\zeta^+, \zeta^+) \tag{6.3-26}$$

On using the parity equations (Section 2.2) this gives

$$E^{-+}(\theta^-, \theta^+) = F^-(\phi_o^-, \phi_o^-) + F^+(\zeta^+, \zeta^+) + \int_V \left\langle \underline{a}\,(\underline{\Omega}\cdot\nabla\zeta^+ + \zeta^{-1}\zeta^-),\ \underline{\Omega}\cdot\nabla\zeta^+ + \zeta^{-1}\zeta^- \right\rangle dV$$

Here $F^-(\phi_o^-, \phi_o^-)$ is positive and all other terms are non-negative. Hence,

$$E^{-+}(\theta^-, \theta^+) \geq F^-(\phi_o^-, \phi_o^-) .$$

6.3.5 The $N^{+-}(\phi^+, \phi^-)$ Functional

The N^{+-} functional is a generalisation of the Dilber-Lewis [5,6] functional used for finite element based nodal schemes. Their functional had the form

$$F(\phi^+) = \int_V \left\{ \int_\Omega \left[\frac{1}{\sigma_T} (\underline{\Omega}\cdot\nabla\phi^+)^2 + \sigma_T \phi^{+2} \right] d\Omega - \sigma_S \phi^{+2} - 2\phi^+ S \right\} dV$$

$$+ 2 \int_S \int_\Omega \underline{n}\cdot\underline{\Omega}\ \phi^+ \phi^-\ d\Omega\, d\underline{S}$$

where $$\phi^- = -\frac{1}{\sigma_T}\underline{\Omega}\cdot\nabla\phi^+.$$

The treatment was restricted to isotropic scattering. The more general $N^{+-}(\phi^+,\phi^-)$ functional can handle anisotropic scattering. N^{+-} is defined as

$$N^{+-}(\phi^+,\phi^-) = K^+(\phi^+) - 2\int_{VS_i}\int_\Omega \underline{\Omega}\cdot\underline{n}_i\ \phi^+\phi^-\ d\Omega\, dS - 2\int_{S_{pr}}\int_\Omega \underline{\Omega}\cdot\underline{n}\ \phi^+\phi^-\ d\Omega\, dS \qquad (6.3\text{-}27)$$

This functional can be used to formulate a nodal method and also to begin the method of synthesis as different from using $K^+(\phi^+)$ and $K^-(\phi^-)$ globally as the starting procedure. This is illustrated in Section 6.4.4, for one dimensional slab geometry. Further discussion and details of $N^{+-}(\phi^+,\phi^-)$ are given by Ackroyd [7].

6.4 Generating Higher Moment Solutions from Lower Moments

6.4.1 Maximisation of $H^{+-}(\phi^+, \phi^-)$

Suppose that the trial functions $\phi^+(x,\mu)$ and $\phi^-(x,\mu)$ are expanded, in one dimensional slab geometry, as

$$\phi^+(x,\mu) = \sum_{k=1}^{K} q_k^+ f_k^+(x,\mu) \qquad (6.4\text{-}1)$$

and

$$\phi^-(x,\mu) = \sum_{l=1}^{L} q_l^- f_l^-(x,\mu) \qquad (6.4\text{-}2)$$

where q_k^+ and q_l^- are the unknown coefficients and f^+, f^- are basis functions. These are products of say, Legendre polynomials in μ and finite element shape functions in x, i.e. $P_i(\mu)\,\psi_j(x)$. Since $\phi^+(x,\mu)$ does not need to satisfy any interface or boundary conditions in $H^{+-}(\phi^+,\phi^-)$, then we can allow greater flexibility in the spatial specification of $f_k^+(x,\mu)$ than $f_l^-(x,\mu)$. Maximising $H^{+-}(\phi^+,\phi^-)$ with respect to the unknown coefficients q_k^+ and q_l^- we get the following set of equations:

$$\sum_{k=1}^{K'} A_{lk}^{+} \hat{q}_k^+ = \sum_{k=1}^{K'} S_{lk}^{+} s_k^+ - \sum_{m=1}^{M} B_{lm} \hat{q}_m^- \qquad (6.4\text{-}3)$$

and

$$\sum_{m=1}^{M} A_{mn}^{-} \hat{q}_m^- = \sum_{k=1}^{K'} S_{nk}^{-+} s_k^+ - \sum_{k=1}^{K} B_{kn} \hat{q}_k^+ \qquad (6.4\text{-}4)$$

Here we have assumed an isotropic extraneous source and no surface source. The coefficients above are given by

$$A^{+}_{lk} = \int_V \left\{ \left\langle \mu \frac{df_l^+}{dx}, g\left(\mu \frac{df_k^+}{dx}\right) \right\rangle + \langle f_l^+, c f_k^+ \rangle \right\} dx$$

$$S^{+}_{lk} = \int_V \langle f_l^+, f_k^+ \rangle \, dx$$

$$B_{lm} = \int_{US_i} \int_{\mu} \mu_i f_l^+ f_m^- \, d\mu$$

$$A^{-}_{mn} = \int_V \left\{ \left\langle \mu \frac{df_n^-}{dx}, c^{-1}\left(\mu \frac{df_m^-}{dx}\right) \right\rangle + \langle f_n^-, g^{-1} f_m^- \rangle \right\} dx$$

$$+ \int_{S_b US_s} |\mu| f_n^- f_m^- \, d\mu$$

(6.4-5)

and $$S^{-+}_{nk} = \int_V \left\langle \mu \frac{df_n^-}{dx}, c^{-1} f_k^+ \right\rangle dx \, .$$

The above maximisation of $H^{+-}(\phi^+, \phi^-)$ is done with respect to both the unknown coefficients of ϕ^+ and ϕ^-. A simpler way to carry out the maximisation, see Ackroyd [7], is to use two stages in the process. Firstly, the optimised odd parity flux $\hat{\phi}^-$ may be obtained from $K^-(\phi^-)$. Then

$$\hat{\phi}^-(x,\mu) = \sum_m \hat{b}^-_m f_m^- \qquad (6.4\text{-}6)$$

where $\hat{b}^-_m$ are the values of b^-_m, the unknown coefficients, obtained using $K^-(\phi^-)$. Secondly, maximise $H^{+-}(\phi^+, \hat{\phi}^-)$ with respect to a^+_k to give coefficients $\hat{b}^+_k$ such that

$$\sum_{k=1}^{K} A^{+}_{lk} \hat{b}^+_k = \sum_{k=1}^{K'} S^{+}_{lk} s^+_k - \sum_{m=1}^{M} B_{lm} \hat{b}^-_m \qquad (6.4\text{-}7)$$

where $\hat{\psi}^{+} = \sum_{k=1}^{K} \hat{b}_k^{+} f_k^{+}$.

Since ϕ^{+} does not have to satisfy any interface or boundary conditions, then ϕ^{+} can be calculated at a local (element) level if required. Initially we may calculate ϕ^{-} using $K^{-}(\phi^{-})$ say a P_1 calculation, and use (6.4-7) to obtain a P_2 approximation for ϕ^{+}. Having calculated $\hat{\phi}^{+}(P_2)$ then we can use (6.4-4) to get a P_3 approximation. This process can be carried on until the required order of expansion is reached. In this way the solution is built up starting at say, a P_1 approximation. Since ϕ^{+} is independent in each element then the neutron conservation condition holds in each element as shown earlier.

6.4.2 Synthesis Method

Below, the synthesis method is outlined*. The idea of this method is to obtain a P_0 approximation for $\phi_0^{+}(x,\mu)$ using $K^{+}(\phi^{+})$ and a P_1 approximation to $\phi_0^{-}(x,\mu)$ using $K^{-}(\phi^{-})$ and to then start building up higher moment approximations as described later. This method differ from the direct use of the $H^{+-}(\phi^{+},\phi^{-})$ functional in that at later stage the approximations are not necessarily optimum but, are optimised by a nodal, i.e. multi-parameter, extrapolation method. Here $E^{+-}(\phi^{+},\phi^{-})$ and $E^{-+}(\theta^{-},\theta^{+})$ hybrid minimum principles are applied to obtain high order transport theory solutions. The advantages of the synthesis method for large systems is the fact that at any stage of

*Initial theoretical work on the synthesis method was carried out in collaboration with R.T. Ackroyd and M.M. Nanneh.

the calculation, only one unknown per spatial node is involved in the calculation. Hence, it is a diffusion theory type calculation.

The synthesis solution may be obtained in cycles and each cycle after the first has two phases. So for instance, after the nth cycle, a P_{2n} and P_{2n-1} approximations for ϕ_o^+ and ϕ_o^- are obtained. The first phase produces an optimised combination of the even parity outputs of the previous cycle, using smoothing and weighting operations together with K^+ maximum principle. Then the corresponding ϕ^- approximation is obtained from E^{-+} minimum principle. In the second phase the K^- principle is used in conjunction with smoothing and weighting to obtain an optimised combination of the odd parity output of the previous cycle and the odd parity flux of phase of the current cycle. This optimised ϕ^- approximation can be used in E^{+-} to give a second ϕ^+ approximation of the cycle. The procedure is given below.

Cycle 1

Phase 1

Here θ_1^+ is a P_0 approximation for $\phi_o^+(x,\mu)$. θ_1^+ satisfies the continuity condition for interfaces and reflection conditions on S_{PT}. Hence, θ_1^+ can be admissible in $K^+(\theta^+)$. Output of Phase 1 is $\hat{\theta}_1^+$ the maximiser of $K^+(\theta_1^+)$

Phase 2

ψ_1^- is a P_1 approximation for $\phi_o^-(x,\mu)$. Again ψ_1^- satisfies the same condition as θ_1^+ to be admissible in $K^-(\psi^-)$ principle. Calculate $\hat{\psi}_1^-$

the maximiser of $K^-(\psi_1^-)$.
Then the approximation for $\phi_0^+(x,\mu)$ is

$$\check{\psi}_1^+ = c^{-1}\left[s^+ - \mu \frac{d\hat{\psi}_1^-}{dx}\right]$$

which is a P_2 approximation, but not necessarily optimised.

Cycle 2

Phase 1

First perform smoothing operation on $\check{\psi}_1^+$ of phase 2 above, since $\check{\psi}_1^+$ will be discontinuous at element interfaces, in general. Next optimise this smoothed $\check{\psi}_1^+$ using nodal extrapolation

$$\hat{\theta}_{2i}^+ = f_i (\$_A \hat{\theta}_1^+)_i + (1-f_i)\$_B \check{\psi}_1^+$$

at each node i. *

where $\$_A$ and $\$_B$ are smoothing operators and f_i is the extrapolation parameter, which can be obtained by maximising $K^+(\theta_2^+)$.

In the smoothing operation we may for instance, take the mean of two $\check{\psi}_1^+$ separate values at interface nodes. Similarly for perfect reflector nodes.

Having carried out the smoothing operation for $\hat{\theta}_1^+$ and $\check{\psi}_1^+$ of cycle 1, then the optimum θ_2^+ i.e. $\hat{\theta}_2^+$ is obtained by nodal extrapolation using f_i and $(1-f_i)$ at each node i. Next the $\hat{\theta}_2^+$, a P_2 approximation, generates a P_3, $\check{\theta}_2^-$, approximation as

$$\check{\theta}_2^- = S\left[s^- - \mu \frac{d\hat{\theta}_2^+}{dx}\right]$$

for $\phi_0^-(x,\mu)$. Again $\check{\theta}_2^-$ will be discontinuous. Hence the process of smoothing is performed.

Phase 2

Here we get a P_3 trial function which is optimised

$$\hat{\psi}_{2i}^- = f_i \hat{\psi}_{1i}^- + (1-f_i)\check{\theta}_{2i}^-$$

*Justification of differentiation and smoothing is given by Ackroyd and Nanneh [8].

The f_i are calculated using K^- principle.

Next a P_4 approximation for $\phi_0^+(x,\mu)$ is obtained as

$$\overset{v}{\psi}{}_2^+ = c^{-1}\left[S^+ - \mu \frac{d\hat{\psi}_2^-}{dx}\right]$$

and the above process of smoothing and optimising are repeated.

The above is one possible way of obtaining a solution.

6.4.3 Synthesis Method in One Dimensional Slab Geometry

In this Section, the synthesis method is illustrated for one dimensional slab geometry. See Nanneh [9]. The even parity flux moments can be determined from

$$\phi_{2l}^+(x) = \frac{S_{2l}^+(x)}{(\sigma_T - \sigma_{s2l})} - \frac{1}{(4l+1)(\sigma_T - \sigma_{s2l})}\left[2l\,\frac{d\phi_{2l-1}^-}{dx} + (2l+1)\,\frac{d\phi_{2l+1}^-}{dx}\right] \tag{6.4-8}$$

and the odd parity flux moments from

$$\phi_{2l+1}^-(x) = \frac{-1}{(4l+3)(\sigma_T - \sigma_{s(2l+1)})}\left[(2l+1)\,\frac{d\phi_{2l}^+}{dx} + (2l+2)\,\frac{d\phi^+(2l+2)}{dx}\right] \tag{6.4-9}$$

assuming an isotropic extraneous source. In the synthesis method then, the optimised even and odd parity fluxes are expanded as

$$\overset{v}{\psi}{}_n^+(x,\mu) = \sum_{l=0}^{\infty}\left(\frac{4l+1}{4\pi}\right)\overset{v}{\psi}{}_{n(2l)}^+(x)\,P_{2l}(\mu) \tag{6.4-10}$$

and

$$\overset{\vee}{\theta}{}^{-}_{n}(x,\mu) = \sum_{l=0}^{\infty} \left(\frac{4l+3}{4\pi}\right) \overset{\vee}{\theta}{}^{-}_{n(2l+1)}(x)\, P_{(2l+1)}(\mu) \qquad (6.4\text{-}11)$$

for each angle.

Similarly, for the optimised solutions. Having obtained a P_0 solution $\hat{\theta}_1^+$ from K^+, and a P_1 solution $\hat{\psi}_1^-$ from K^-, and a P_2 solution calculated from (6.4-8) above, and smoothed, then

$$\hat{\theta}_{2i}^{+} = f_i\, \hat{\theta}_{i}^{+} + (1-f_i)\, \overset{\vee}{\psi}{}^{+}_{i} \; .$$

This is then substituted into the functional $K^+(\theta_2^+)$ to obtain the coefficients f_i.

Consider for instance the $\sigma_T \int_0^h \int_{-1}^{1} (\theta_2^+)^2 d\mu\, dx$ term in the K^+ principle, for a simple linear element, i.e.

$$\frac{\sigma_T}{16\pi^2} \sum_{i=1}^{2} \int_0^h \Big[f_i \Big\{ \int_{-1}^{1} \Big[\bar{\hat{\theta}}^{+}_{1i(0)} P_0 - \big(\bar{\overset{\vee}{\psi}}{}^{+}_{1i(0)} P_0 + \bar{\overset{\vee}{\psi}}{}^{+}_{1i(2)} P_2 \big) \Big] d\mu + \int_{-1}^{1} \Big[\bar{\overset{\vee}{\psi}}{}^{+}_{1i(0)} P_0 + \bar{\overset{\vee}{\psi}}{}^{+}_{1i(2)} P_2 \Big] d\mu \Big\} \psi_i(x) \Big]^2 dx \qquad (6.4\text{-}12)$$

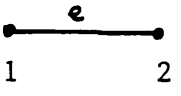
where

$$\hat{\theta}_2^{+}(x,\mu) = \frac{1}{4\pi} \sum_{i=1}^{2} f_i \Big(\bar{\hat{\theta}}^{+}_{1i(0)} P_0 - \bar{\overset{\vee}{\psi}}{}^{+}_{1i(0)} P_0 - 5\, \bar{\overset{\vee}{\psi}}{}^{+}_{1i(2)} P_2 \Big) \psi_i(x) + \Big(\bar{\overset{\vee}{\psi}}{}^{+}_{K(0)} P_0 + \bar{\overset{\vee}{\psi}}{}^{+}_{1i(2)} P_2 \Big) \psi_i(x) \; . \qquad (6.4\text{-}13)$$

is the optimised P_2 solution. By letting

$$\alpha_i = \bar{\hat{\theta}}^{+}_{1i(0)} P_0 - \left(\bar{\hat{\psi}}^{+}_{1i(0)} P_0 + \bar{\hat{\psi}}^{+}_{1i(2)} P_2 \right)$$

$$\beta_i = \left(\bar{\hat{\psi}}^{+}_{1i(0)} P_0 + \bar{\hat{\psi}}^{+}_{1i(2)} P_2 \right)$$



we can write (6.4-12) as

$$\frac{\sigma_T}{16\pi^2} \sum_{i=1}^{2} \int_0^h \left\{ \int_{-1}^{1} \left[(\beta_i \alpha_i + \beta_i) \psi_i \right]^2 d\mu \right\} dx$$

$$= \frac{\sigma_T}{16\pi^2} \int_0^h \int_{-1}^{1} \left[(\beta_1 \alpha_1 + \beta_1) \psi_1 + (\beta_2 \alpha_2 + \beta_2) \psi_2 \right]^2 d\mu \, dx \qquad (6.4\text{-}14)$$

Maximising with respect to β_1 and β_2 gives

$$\iint (\beta_1 \alpha_1 + \beta_1) \alpha_1 \psi_1 \cdot \psi_1 + \iint (\beta_2 \alpha_2 + \beta_2) \alpha_1 \psi_1 \psi_2 \,.$$

$$\iint (\beta_1 \alpha_1 + \beta_1) \alpha_2 \psi_1 \cdot \psi_2 + \iint (\beta_2 \alpha_2 + \beta_2) \alpha_2 \psi_2 \cdot \psi_2 \,.$$

In matrix form this can be written as:

$$\begin{bmatrix} \iint \alpha_1^2 \psi_1^2 & \iint \alpha_1 \alpha_2 \psi_1 \psi_2 \\ \iint \alpha_1 \alpha_2 \psi_1 \psi_2 & \iint \alpha_2^2 \psi_2^2 \end{bmatrix} \begin{bmatrix} \beta_1 \\ \beta_2 \end{bmatrix} + \begin{bmatrix} \iint (\alpha_1 \beta_1 \psi_1^2 + \alpha_1 \beta_2 \psi_1 \psi_2) \\ \iint (\alpha_2 \beta_2 \psi_2^2 + \beta_1 \alpha_2 \psi_1 \psi_2) \end{bmatrix}$$

(6.4-15)

In terms of the angular and spatial matrices already known we can write the above as

$$\begin{bmatrix} S_{11}[\alpha_1\ \alpha_2]\,A\begin{bmatrix}\alpha_1\\ \alpha_2\end{bmatrix}_{node1} & S_{12}[\alpha_1\ \alpha_2]\,A\begin{bmatrix}\alpha_1\\ \alpha_2\end{bmatrix}_{node2} \\ S_{21}[\alpha_1\ \alpha_2]\,A\begin{bmatrix}\alpha_1\\ \alpha_2\end{bmatrix}_{node1} & S_{22}[\alpha_1\ \alpha_2]\,A\begin{bmatrix}\alpha_1\\ \alpha_2\end{bmatrix}_{node2} \end{bmatrix} \begin{bmatrix} f_1 \\ f_2 \end{bmatrix} +$$

$$\begin{bmatrix} S_{11}[\alpha_1\ \alpha_2]\,A\begin{bmatrix}\beta_1\\ \beta_2\end{bmatrix}_{node1} + S_{12}[\alpha_1\ \alpha_2]\,A\begin{bmatrix}\beta_1\\ \beta_2\end{bmatrix}_{node2} \\ S_{21}[\alpha_1\ \alpha_2]\,A\begin{bmatrix}\beta_1\\ \beta_2\end{bmatrix}_{node1} + S_{22}[\beta_1\ \beta_2]\,A\begin{bmatrix}\beta_1\\ \beta_2\end{bmatrix}_{node2} \end{bmatrix}$$

Where s_{ij} are elements of the removal spatial matrix, A is the removal term angular constants matrix.

Similarly, contributions are obtained for the leakage term. Over an element where there is a source and/or bare surface again these contributions are included. The global matrix for the f_i calculation is then built up in the usual way to get a global matrix equation

$$M\underline{f} = \underline{S} \quad .$$

There is only one unknown f_i at each node i of the system. The coefficients α at the nodes will contain the optimised P_0 nodal fluxes and the unoptimised P_0 and P_2 nodal fluxes, while the coefficients β will contain only the latter. Once the optimised P_2 solution has been found, then the unoptimised P_3 odd parity solution $\check{\theta}_2^-$ can be found from

(6.4- 9) which may then be optimised in the above manner, but, this time using the K^- principle.

6.4.4 Synthesis Using $N^{+-}(\phi^+, \phi^-)$

The $N^{+-}(\phi^+, \phi^-)$ allows ϕ^+ to be independent in each element of the system since ϕ^+ does not need to satisfy interface continuity and boundary conditions. This allows local calculations to be carried out for ϕ^+ . The synthesis scheme using N^{+-} may be carried out as follows:

Carry out a P_1, ϕ^- calculation using $K^-(\phi^-)$ principle. This will be a global calculation. Next use the optimised P_1 solution in the $N^{+-}(\phi^+, \phi^-)$ functional to obtain ϕ^+ locally i.e. for an element. ϕ^+ can be expanded to any order but, only the P_0 and P_2 components will directly couple the P_1, ϕ^- solution.

$$N^{+-}(\phi^+, \hat{\phi}^-) = K^+(\phi^+) - 2\int_{V_{S_i}}\int_{-1}^{1} \mu_i \, \phi^+ \hat{\phi}^- \, d\mu \, ds - \int_{S_{pr}}\int_{-1}^{1} \mu_i \, \phi^+ \hat{\phi}^- \, d\mu \, ds$$

(6.4-16)

This preserves neutrons in each element. We could for instance obtain a P_2 approximation for ϕ^+ . The latter will be discontinuous at element interface nodes. A smoothing process is then carried out. Next an unoptimised ϕ^-, P_3 solution can be obtained from $\hat{\phi}^+, P_2$ solution. This can then be optimised using nodal extrapolation. After obtaining $\hat{\phi}^-$ a P_3 optimised approximation, $N^{+-}(\phi^+, \hat{\phi}^-)$ can again be used to obtain optimised local $\hat{\phi}^+$ solutions. Consider the N^{+-} calculation

and assume that the coefficients are known. For a linear element shown below, with interfaces A and B



we have for the surface terms

$$2\int_{-1}^{1} \sum_{ll'} \mu \left(\frac{4l+3}{4\pi}\right)\left(\frac{4l'+1}{4\pi}\right) P_{2l+1}(\mu)\, P_{2l'}(\mu)\, \hat{\phi}^{-}_{2l+1}(x)\, \phi^{+}_{2l'}(x)\, d\mu \tag{6.4-17}$$

at A

and

$$-2\int_{-1}^{1} \sum_{ll'} \mu \left(\frac{4l+3}{4\pi}\right)\left(\frac{4l'+1}{4\pi}\right) P_{2l+1}(\mu)\, P_{2l'}(\mu)\, \hat{\phi}^{-}_{2l+1}(x)\, \phi^{+}_{2l'}(x)\, d\mu \tag{6.4-18}$$

at B.

Note that $\underline{n}\cdot\underline{n}_i = -\mu$ at A

and $\underline{n}\cdot\underline{n}_i = \mu$ at B.

Hence, we have

$$\pm \frac{1}{4\pi^2} \sum_{l=0}^{\infty} \left[2l\, \hat{\phi}^{-}_{2l-1}\, \phi^{+}_{2l} + (2l+1)\, \hat{\phi}^{-}_{2l+1}\, \phi^{+}_{2l} \right]_B^A \tag{6.4-19}$$

So for $l=0$:

$$\pm \frac{1}{4\pi^2} \left[\hat{\phi}^{-}_{1}\, \phi^{+}_{0} \right]$$

$l=0,1$:

$$\pm \frac{1}{4\pi^2} \left[\hat{\phi}^{-}_{1}\, \phi^{+}_{0} + 2\, \hat{\phi}^{-}_{1}\, \phi^{+}_{2} + 3\, \hat{\phi}^{-}_{3}\, \phi^{+}_{4} \right]$$

$l=0,1,2$:

$$\pm \frac{1}{4\pi^2} \left[\hat{\phi}^{-}_{1}\, \phi^{+}_{0} + (2\hat{\phi}^{-}_{1} + 3\hat{\phi}^{-}_{3}) + 4\, \hat{\phi}^{-}_{3}\, \phi^{+}_{4} \right]$$

In the case of two even moments expansion for $\phi^+(x,\mu)$, maximisation of N^{+-} gives the usual contribution from $k^+(\phi^+)$ and in addition a 'source' term

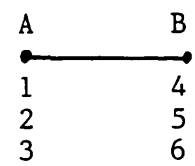
$$\frac{1}{4\pi^2}\begin{bmatrix} \hat{\phi}_1^- \\ 2\hat{\phi}_1^- \\ -\hat{\phi}_3^- \\ -2\hat{\phi}_3^- \end{bmatrix} \begin{matrix} \\ \\ \\ \text{at node 3,4} \end{matrix} \quad \text{at node 1,2}$$



Local node numbering for 2 moments

The ϕ^- approximation is P_1. For a P_4, ϕ^+ calculation, including say a P_3, ϕ^- calculation, we get

$$\frac{1}{4\pi^2}\begin{bmatrix} \hat{\phi}_1^- \\ (2\hat{\phi}_1^- + 3\hat{\phi}_2^-) \\ 4\hat{\phi}_2^- \\ -\hat{\phi}_4^- \\ -(2\hat{\phi}_4^- + 3\hat{\phi}_5^-) \\ -4\hat{\phi}_5^- \end{bmatrix}$$



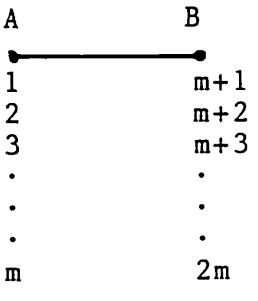
Local node numbering for 3 moments.

as the 'ϕ^- source' vector for the element. If only a P_1 approximaiton was used for ϕ^- then the 'ϕ^-source' vector would be

$$\frac{1}{4\pi^2}\begin{bmatrix} \hat{\phi}_1^- \\ 2\hat{\phi}_1^- \\ 0 \\ -\hat{\phi}_4^- \\ -2\hat{\phi}_4^- \\ 0 \end{bmatrix} .$$

The entries in the 'ϕ^- source' vector are of course nodal values. In general we can write for the 'ϕ^- source' vector,

$$\frac{1}{4\pi^2}\begin{bmatrix} \hat{\phi}_1^- \\ (2\hat{\phi}_1^- + 3\hat{\phi}_2^-) \\ (4\hat{\phi}_2^- + 5\hat{\phi}_3^-) \\ \vdots \\ (2L\hat{\phi}_{m-1}^- + (2L+1)\hat{\phi}_m^-) \\ \hat{\phi}_{m+1}^- \\ -(2\hat{\phi}_{m+1}^- + 3\hat{\phi}_{m+2}^-) \\ -(4\hat{\phi}_{m+2}^- + 5\hat{\phi}_{m+3}^-) \\ \vdots \\ (2L\hat{\phi}_{2m-1}^- + (2L+1)\hat{\phi}_{2m}^-) \end{bmatrix}$$



Here m refers to the number of even moments used for $\phi^{+}(x,\mu)$ and hence, gives the element numbering scheme. L refers to the order of angular expansion for ϕ^{+} and ϕ^{-}.

REFERENCES TO CHAPTER 6

1. ACKROYD, R.T.
"A Finite Element Method for Diffusion Theory Embracing Nodal and Difference Methods".
Prog. Nucl. Energy, 18, 1/2 p7 (1986)

2. ACKROYD, R.T., ISSA, J.G., RIYAIT, N.S. and NANNEH, M.M.
"Projection and Conservation Methods for Neutron Transport".
MAFELAP Conference, Brunel University, Uxbridge, U.K.
April (1987)

3. ACKROYD, R.T.
"Generalised Least Squares as a Generator of Variational Principles and Weighted Residual Methods for FEM Neutron Transport Methods"
Prog. Nucl. Energy, 18, 1/2 p45 (1986)

4 ACKROYD, R.T.
"The Why and How of Finite Elements"
Ann. Nucl. Energy, 6, p563 (1981)

5. LEWIS, E.E. and DILBER, I.
"Variational Nodal Methods for Neutron Transport"
Nucl. Sci. Engng. 91, p132 (1985)

6. LEWIS, E.E., and DILBER, I.
"Finite Element, Nodal and Response Matrix Methods: A Variational Synthesis for Neutron Transport"
Prog. Nucl. Energy, 18, 1/2 p63 (1986)

7. ACKROYD, R.T.
"A Unified Treatment of Least Squares, Variational and Weighted Residual Methods for the First, Parity and Second Order Forms of the Boltzmann Equation"
To be Published.

8. ACKROYD, R.T. and NANNEH, M.M.
"Upper and Lower Bounds for Disadvantage Factors".
To be published in Annals of Nuclear Energy.

9. NANNEH,M.M.
Internal Report, Nuclear Power Section, Imperial College. (1987).

CHAPTER 7

7. CONCLUSIONS AND RECOMMENDATIONS

7.1 Discussion
7.2 Recommendations for Further Study

7. CONCLUSIONS AND RECOMMENDATIONS

7.1 Discussion

This thesis has been mainly concerned with the treatment of multigroup anisotropic scattering and new methods for solution of void problems, using the finite element method. There was also a brief discussion about hybrid principles in neutron transport and synthesis of solutions.

In the case of multigroup anisotropic scattering, proof tests on one dimensional, one group and multigroup, severe anisotropic scattering problems show that the finite element method gives accurate results. In the one group forward scattering problem a nine even-moment calculation gives a percentage error of less than one percent when compared with the analytical result. For the two group backward-forward-isotropic scattering source problem close agreement for the scalar fluxes is reached with the analytical results. The two group P_3 scattering source problem and the P_1 scattering multiregion source problem, both with large attenuation, also demonstrate the accuracy of the finite element method. Overall, the theory of multigroup anisotropic scattering for the even parity transport equation has been illustrated and it has been demonstrated that the finite element method for the even parity transport equation can handle multigroup anisotropic scattering quite successfully.

With the solution of the even parity transport equation for systems with void/ducts, two new methods were presented. The methods were termed (a) iteration and (b) extrapolation methods. The latter was further divided into elementary (global) and multiparameter (nodal) extrapolation. The theory of these methods was presented and the methods were tested on quite severe void test problems. The problems were severe in the sense that the regions surrounding the void were purely absorbing, except for one test problem, and hence, the angular flux was highly anisotropic. The results presented in Chapter 5, indicate that the iteration technique can give better results than the conventional finite element method. Further, global extrapolation is superior to the iteration technique. The nodal extrapolation method predicts the scalar flux even more accuratly even when using only two trial functions. The results of test problems with these methods indicate that the new methods can be used for shield design scoping studies and for more accurate definitive calculations.

7.2 Recommendations for Further Study

At the present the nodal extrapolation technique has only been inplemented in FELTRAN for a single void region. The next stage is to code the method for multiple void and non-void regions. Subsequently, nodal extrapolation (and the other methods) need to be tested on a number of void problems,

which should include systems with a significant percentage of void. In addition, there is a technique for generating a variable cross section profile within the void region which can be used as a basis for a conventional or extrapolation calculation. This needs invesigation.

As seen in Chapter 6, the nodal extrapolation technique may be used in the method of synthesis using N^{+-} functional. By starting with the lowest order angular approximation in a single element, the higher order solutions may be built up within each element. The optimised higher order solution being obtained by the nodal extrapolation technique. N^{+-} with extrapolation will reduce computer storage requirements. This work is currently in progress in one dimensional slab geometry* and if successful, can be used in higher spatial dimension, where it will be of greatest benefit.

Another technique to be investigated concerns the K^{+-} functional. Discontinuous finite elements have been used with the $K^{+-}(\phi^{+},\phi^{-})$ functional to obtain different order angular approximations in different regions. This requires the use of both $K^{+}(\phi^{+})$ and $K^{-}(\phi^{-})$ functionals where as the $K_{\lambda}^{o+}(\phi^{+})$ functional does not require ϕ^{-}, the odd parity angular flux. This method can be investigated in one dimensional slab geometry.

* See Reference 9 of Chapter 6 .

Some theoetical investigation is required into maximum and minimum principles for the equations of electromagnestism and solutions of these equations by the finite element method, especially in three dimensional geometry. Another area of work includes the solution of Maxwell's equations in plasmas (for plasma containment in a fusion reactor) by the finite element technique.

APPENDICIES

APPENDIX A

Derivation of the Even Parity Equations for the Iteration Method

In the case of constant $\sigma_v = \sigma'$ in the void region (V_v) the first order equations for the iteration scheme are:

$$
\begin{aligned}
&\underline{\Omega}\cdot\nabla\psi_1 + \sigma'\psi_1 = 0\\
&\underline{\Omega}\cdot\nabla\psi_2 + \sigma'\psi_2 = \sigma'\psi_1\\
&\underline{\Omega}\cdot\nabla\psi_3 + \sigma'\psi_3 = \sigma'\psi_2\\
&\underline{\Omega}\cdot\nabla\psi_4 + \sigma'\psi_4 = \sigma'\psi_3\\
&\quad\vdots\\
&\underline{\Omega}\cdot\nabla\psi_m + \sigma'\psi_m = \sigma'\psi_{m-1}\\
&\quad\vdots\\
&\underline{\Omega}\cdot\nabla\psi_M + \sigma'\psi_M = \sigma'\psi_{M-1}
\end{aligned}
\qquad \text{(A1)}
$$

In the non-void region V_R we have

$$
\begin{aligned}
&\underline{\Omega}\cdot\nabla\psi_1 + \Sigma\psi_1 = S\\
&\underline{\Omega}\cdot\nabla\psi_2 + \Sigma\psi_2 = 0\\
&\underline{\Omega}\cdot\nabla\psi_3 + \Sigma\psi_3 = 0\\
&\underline{\Omega}\cdot\nabla\psi_4 + \Sigma\psi_4 = 0\\
&\quad\vdots\\
&\underline{\Omega}\cdot\nabla\psi_m + \Sigma\psi_m = 0\\
&\quad\vdots\\
&\underline{\Omega}\cdot\nabla\psi_M + \Sigma\psi_M = 0
\end{aligned}
\qquad \text{(A2)}
$$

where $\psi = \psi(r,\underline{\Omega})$, $S = S(r,\underline{\Omega})$ and Σ is the operator defined in Section 5.4.5. M is the number of iterations and ψ_m is the m^{th} component of the iteration solution.

The boundary conditions for ψ_m are:

$$\psi_m = 0 \quad \text{on } S_b \text{ for } \underline{\Omega}\cdot\underline{n} < 0 .$$

$$\psi_m \text{ continuous across interfaces for } \underline{\Omega}\cdot\underline{n} \neq 0. \qquad \text{(A3)}$$

$$\psi_m(\underline{r},\underline{\Omega}) = \psi_m(\underline{r},\underline{\Omega}^*) \text{ on } S_{pr} \text{ for } \underline{\Omega}\cdot\underline{n} = -\underline{\Omega}^*\cdot\underline{n} \neq 0 .$$

m=1,2,3.....,M.

The even and odd parity components of (A2) give

$$\begin{aligned}
&\underline{\Omega}\cdot\nabla\psi_1^- + c\,\psi_1^+ = s^+ \\
&\underline{\Omega}\cdot\nabla\psi_1^+ + \varsigma^{-1}\psi_1^- = s^- \\
&\underline{\Omega}\cdot\nabla\psi_2^- + c\,\psi_2^+ = 0 \\
&\underline{\Omega}\cdot\nabla\psi_2^+ + \varsigma^{-1}\psi_2^- = 0 \\
&\vdots \\
&\underline{\Omega}\cdot\nabla\psi_m^- + c\,\psi_m^+ = 0 \\
&\underline{\Omega}\cdot\nabla\psi_m^+ + \varsigma^{-1}\psi_m^- = 0 \\
&\vdots \\
&\underline{\Omega}\cdot\nabla\psi_M^- + c\,\psi_M^+ = 0 \\
&\underline{\Omega}\cdot\nabla\psi_M^+ + \varsigma^{-1}\psi_M^- = 0
\end{aligned} \qquad \text{(A4)}$$

where c and ς^{-1} have been defined previously. Eliminating the odd parity flux components from (A4) for V_R gives

$$\begin{aligned}
&-\underline{\Omega}\cdot\nabla\left[\varsigma\,(\underline{\Omega}\cdot\nabla\psi_1^+)\right] + c\,\psi_1^+ = s^+ - \underline{\Omega}\cdot\nabla\varsigma s^- \\
&-\underline{\Omega}\cdot\nabla\left[\varsigma\,(\underline{\Omega}\cdot\nabla\psi_2^+)\right] + c\,\psi_2^+ = 0 \\
&\vdots \\
&-\underline{\Omega}\cdot\nabla\left[\varsigma\,(\underline{\Omega}\cdot\nabla\psi_M^+)\right] + c\,\psi_M^+ = 0
\end{aligned} \qquad \text{(A5)}$$

with the boundary conditions

$$\psi_m^+ \text{ continuous across interfaces for } \underline{\Omega}\cdot\underline{n} \neq 0 .$$

$$\begin{aligned}
&\psi_1^+ - \varsigma\left[s^- - \underline{\Omega}\cdot\nabla\psi_1^+\right] = 0 && \text{for } \underline{\Omega}\cdot\underline{n} > 0. \\
&\psi_1^+ + \varsigma\left[s^- - \underline{\Omega}\cdot\nabla\psi_1^+\right] = 0 && \text{for } \underline{\Omega}\cdot\underline{n} < 0 \text{ on } S_b,
\end{aligned} \qquad \text{(A6)}$$

and for m=2,3,4,.....,M

$$\begin{aligned} &\psi_m^+ + \varsigma\,(\underline{\Omega}\cdot\nabla\psi_m^+) = 0 \qquad \text{for} \quad \underline{\Omega}\cdot\underline{n} > 0 \\ &\psi_m^+ - \varsigma\,(\underline{\Omega}\cdot\nabla\psi_m^+) = 0 \qquad \text{for} \quad \underline{\Omega}\cdot\underline{n} < 0 \end{aligned} \tag{A7}$$

on S_b .

On a perfect reflector, S_{pr},

$$\psi_m^+(\underline{r},\underline{\Omega}) = \psi_m^+(\underline{r},\underline{\Omega}^*) \qquad \text{for} \quad \underline{\Omega}\cdot\underline{n} = -\underline{\Omega}^*\cdot\underline{n} \neq 0.$$

m=1,2,3,.....,M.

I.e.

$$\varsigma\left[\, S^-(\underline{r},\underline{\Omega}) - \underline{\Omega}\cdot\nabla\psi_1^+(\underline{r},\underline{\Omega}) - S^-(\underline{r},\underline{\Omega}^*) + \underline{\Omega}^*\cdot\nabla\psi_1^+(\underline{r},\underline{\Omega}^*)\,\right] = 0 \tag{A8}$$

for m=1, and

$$\varsigma\left[\, \underline{\Omega}^*\cdot\nabla\psi_m^+(\underline{r},\underline{\Omega}^*) - \underline{\Omega}\cdot\nabla\psi_m^+(\underline{r},\underline{\Omega})\,\right] = 0$$

for $m \geq 2$.

The even and odd parity components of (A1) give

$$\begin{aligned}
&\underline{\Omega}\cdot\nabla\psi_1^- + \sigma^1\psi_1^+ = 0 \\
&\underline{\Omega}\cdot\nabla\psi_1^+ + \sigma^1\psi_1^- = 0 \\
&\underline{\Omega}\cdot\nabla\psi_2^- + \sigma^1\psi_2^+ = \sigma^1\psi_1^+ \\
&\underline{\Omega}\cdot\nabla\psi_2^+ + \sigma^1\psi_2^- = \sigma^1\psi_1^- \\
&\vdots \\
&\underline{\Omega}\cdot\nabla\psi_m^- + \sigma^1\psi_m^+ = \sigma^1\psi_{m-1}^+ \\
&\underline{\Omega}\cdot\nabla\psi_m^+ + \sigma^1\psi_m^- = \sigma^1\psi_{m-1}^- \\
&\vdots \\
&\underline{\Omega}\cdot\nabla\psi_M^- + \sigma^1\psi_M^+ = \sigma^1\psi_{M-1}^+ \\
&\underline{\Omega}\cdot\nabla\psi_M^+ + \sigma^1\psi_M^- = \sigma^1\psi_{M-1}^-
\end{aligned} \tag{A9}$$

Eliminating the odd parity components from (A9) gives, in V_v,

$$\begin{aligned}
&\frac{-\underline{\Omega}\cdot\nabla\left(\underline{\Omega}\cdot\nabla\,\psi_1^+\right)}{\sigma^1} + \sigma^1\,\psi_1^+ = 0 \\
&\frac{-\underline{\Omega}\cdot\nabla\left(\underline{\Omega}\cdot\nabla\,\psi_2^+\right)}{\sigma^1} + \sigma^1\,\psi_2^+ = 2\sigma^1\,\psi_1^+ \\
&\frac{-\underline{\Omega}\cdot\nabla\left(\underline{\Omega}\cdot\nabla\,\psi_3^+\right)}{\sigma^1} + \sigma^1\,\psi_3^+ = 2\sigma^1\,\psi_2^+ - \sigma^1\,\psi_1^+
\end{aligned} \tag{A10}$$

and for m=4,5,6,.....,M

$$\frac{-\underline{\Omega}\cdot\nabla\left(\underline{\Omega}\cdot\nabla\,\psi_m^+\right)}{\sigma^1} + \sigma^1\,\psi_m^+ = 2\sigma^1\,\psi_{m-1}^+ - \sigma^1\,\psi_{m-2}^+ \,.$$

Here the right hand side of (A10) needs to be positive in order that $\psi_m^+(r,\underline{\Omega})$ is positive. This means that the condition $\psi_{m-1}^+ > \frac{1}{2}\,\psi_{m-2}^+$ is required for $\psi_m^+ > 0$.

Eliminating the absorption sources in the first two and then the first three equations in (A10) above gives

$$\frac{-\underline{\Omega}\cdot\nabla\left(\underline{\Omega}\cdot\nabla\left(\psi_1^+ + \frac{1}{2}\,\psi_2^+\right)\right)}{\sigma^1} + \sigma^1\left(\frac{\psi_2^+}{2}\right) = 0 \tag{A11}$$

and

$$\frac{-\underline{\Omega}\cdot\nabla\left(\underline{\Omega}\cdot\nabla\left(\psi_1^+ + \frac{2}{3}\,\psi_2^+ + \frac{1}{3}\,\psi_3^+\right)\right)}{\sigma^1} + \sigma^1\left(\frac{\psi_3^+}{3}\right) = 0 \tag{A12}$$

In general for $m \geq 1$ the following equation for V_v is obtained

$$-\underline{\Omega}\cdot\nabla\left[\,\underline{\Omega}\cdot\nabla\left(\psi_1^+ + \frac{m-1}{m}\,\psi_2^+ + \cdots + \frac{(m-k+1)}{m}\,\psi_k^+ + \cdots + \frac{\psi_m^+}{m}\right)\right] + \frac{\sigma^1\,\psi_m^+}{m} = 0$$

In deriving the above equation it has been assumed that each iterative component solution ψ_i^+ is exact so that all the

above equations are also exact. In practice the equations will be satisfied approximately since the ψ_i^+ will be approximate.

Let

$$\theta_M^+(r,\underline{\Omega}) = \sum_{i=1}^{M} \left(\frac{M-i+1}{M}\right) \psi_i^+(r,\underline{\Omega}) \tag{A13}$$

i.e. the solution obtained after M iterations. Then θ_M^+ satifies

$$\frac{-\underline{\Omega}\cdot\nabla(\underline{\Omega}\cdot\nabla\theta_M^+)}{\sigma} + \sigma\frac{\psi_M^+}{M} = 0 \tag{A14}$$

in V_v.

In addition let $\xi_M^+ = \phi_0^+ - \theta_M^+$, where $\phi_0^+ = \phi_0^+(r,\underline{\Omega})$ is the exact solution in V_v. Then ξ_M^+ satisfies the following equation, in V_v,

$$\frac{-\underline{\Omega}\cdot\nabla(\underline{\Omega}\cdot\nabla\xi_M^+)}{\sigma} = \frac{\sigma\psi_M^+}{M} \quad . \tag{A15}$$

Similarly for V_R

$$-\underline{\Omega}\cdot\nabla[\varsigma(\underline{\Omega}\cdot\nabla\theta_M^+)] + c\theta_M^+ = s^+ - \underline{\Omega}\cdot\nabla\varsigma s^- \tag{A16}$$

and

$$-\underline{\Omega}\cdot\nabla[\varsigma(\underline{\Omega}\cdot\nabla\phi_0^+)] + c\phi_0^+ = s^+ - \underline{\Omega}\cdot\nabla\varsigma s^-$$

Hence

$$-\underline{\Omega}\cdot\nabla[\varsigma(\underline{\Omega}\cdot\nabla\xi_M^+)] + c\xi_M^+ \qquad \text{in } V_R \tag{A17}$$

ξ_M^+ also satisfies the bare surface, perfect reflector and interface conditions. Hence ξ_M^+ is the even parity flux due to a source $\frac{\sigma\psi_M^+}{M}$ in the void region. From (A15) $\xi_M^+ > 0$, i.e. $\theta_M^+ < \phi_0^+$. So the M iteration solution θ_M^+ is bounded above by ϕ_0^+. As $M \to \infty$ the source in (A15) tends to zero, i.e. $\lim_{M\to\infty} \xi_M^+ = 0$ or $\lim_{M\to\infty} \theta_M^+ = \phi_0^+$.

APPENDIX B

Theoretical Lower Bounds to the Even Parity Flux

In Appendix A it was shown that the M iteration solution

$$\theta_M^+ = \sum_{l=1}^{M} \left(\frac{M-l+1}{M}\right) \psi_l^+ \tag{B1}$$

was a lower bound to ϕ_0^+ . If we let

$$\phi_M^+ = \sum_{l=1}^{M} \psi_l^+ \tag{B2}$$

i.e. the right hand side of (B1) with coefficient $\left(\frac{M-l+1}{M}\right)$ equal to unity, then the following inequality is obtained

$$\theta_M^+ < \phi_M^+ < \phi_0^+ .$$

ϕ_M^+ is obtained from (A10) but without the cancellation of absorption sources as was the case with θ_M^+ . The inequality $\phi_M^+ < \phi_0^+$ follows from $\phi_M < \phi_0$. The solution $\bar{\phi}_3^+ = \bar{\psi}_1^+ + \bar{\psi}_2^+ + \bar{\psi}_3^+$ is also a lower bound to $\phi_0^+(x,\mu)$. This is shown below. Consider the case of three iterations. Then in V_v

$$\frac{L\psi_1^+}{\sigma^1} + \sigma^1 \psi_1^+ = 0 \tag{B3}$$

$$\frac{L\psi_2^+}{\sigma^1} + \sigma^1 \psi_2^+ = 2\sigma^1 \psi_1^+ \tag{B4}$$

$$\frac{L\psi_3^+}{\sigma^1} + \sigma^1 \psi_3^+ = 2\sigma^1 \psi_2^+ - \sigma^1 \psi_1^+ \tag{B5}$$

where the operator L is given by

$$L \equiv -\mu \cdot \nabla (\mu \cdot \nabla) .$$

Equations (B3) and (B4) give

$$\frac{L}{\sigma_1}\left(\psi_1^+ + \psi_2^+/2\right) + \sigma_1 \psi_2^+/2 = 0 \qquad \text{(B6)}$$

and (B4) and (B5) give

$$\frac{L}{\sigma_1}\left(\psi_3^+ + \psi_2^+/2\right) + \sigma_1\left(\psi_3^+ + \psi_2^+/2\right) = 2\sigma_1 \psi_2^+ \qquad \text{(B7)}$$

Eliminating the absorption source $2\sigma_1\psi_2^+$ from (B6) and (B7) leads to

$$\frac{L}{\sigma_1}\left[\left(\psi_1^+ + \psi_2^+/2\right) + 1/4\left(\psi_3^+ + \psi_2^+/2\right)\right] + \frac{\sigma_1}{4}\left(\psi_3^+ + \psi_2^+/2\right) = 0 \qquad \text{(B8)}$$

Since $L\phi_0^+(r,\Omega) = 0$, then

$$\frac{L}{\sigma_1}\left\{\phi_0^+ - \left[\left(\psi_1^+ + \psi_2^+/2\right) + 1/4\left(\psi_3^+ + \psi_2^+/2\right)\right]\right\} = \frac{\sigma_1}{4}\left(\psi_3^+ + \psi_2^+/2\right) \qquad \text{(B9)}$$

Hence $\left\{\phi_0^+ - \left(\psi_1^+ + 5/8\,\psi_2^+ + \psi_3^+/4\right)\right\} \geq 0$, as it is the even parity angular flux induced by the positive source $\frac{\sigma_1}{4}\left(\psi_3^+ + \psi_2^+/2\right)$. Comparing the solution $\left(\psi_1^+ + 5/8\,\psi_2^+ + 1/4\,\psi_3^+\right)$ with that obtained ($\bar{\phi}_3^+$) by simply using positive absorption sources $\sigma_1\psi_1^+$, $\sigma_1\psi_2^+$, $\sigma_1\psi_3^+$ etc. in (B5), we have

$$\begin{aligned} \psi_1^+ &= \bar{\psi}_1^+ \\ \psi_2^+ &= 2\bar{\psi}_2^+ \\ \psi_3^+ + \psi_2^+/2 &= 4\bar{\psi}_3^+ \end{aligned} \qquad \text{(B10)}$$

$$\therefore \quad \bar{\phi}_3^+ = \psi_1^+ + 5/8\,\psi_2^+ + 1/4\,\psi_3^+$$

and

$$\phi_3^+ = \psi_1^+ + \frac{2}{3}\psi_2^+ + \frac{1}{3}\psi_3^+ .$$

Hence $\phi_0^+ - \left(\bar{\psi}_1^+ + \bar{\psi}_2^+ + \bar{\psi}_3^+\right) \geq 0$, i.e. $\bar{\phi}_3^+ < \phi_0^+$.

Hence $\bar{\phi}_3^+$ is bounded above by ϕ_0^+, the exact solution in V_v.

In the case of four iterations, the equation analogous to (B8) above is

$$\frac{L}{\sigma^{-1}}\left[\left(\psi_1^+ + \psi_2^+/2\right) + 1/4\left(\psi_3^+ + \psi_2^+/2\right) + 1/8\left(\psi_3^+ + \psi_2^+/2 + \psi_4^+\right)\right] + \frac{\sigma^{-1}}{8}\left(\psi_3^+ + \psi_2^+/2 + \psi_4^+\right) = 0 \tag{B11}$$

Hence

$$\begin{aligned}\bar{\phi}_4^+ &= \bar{\psi}_1^+ + \bar{\psi}_2^+ + \bar{\psi}_3^+ + \bar{\psi}_4^+ \\ &= \left(\psi_1^+ + \psi_2^+/2\right) + 1/4\left(\psi_3^+ + \psi_2^+/2\right) + 1/8\left(\psi_3^+ + \psi_2^+/2 + \psi_4^+\right)\end{aligned} \tag{B12}$$

is bounded above by ϕ_0^+ . So

$$\bar{\phi}_4^+ = \psi_1^+ + \frac{11}{16}\psi_2^+ + \frac{3}{8}\psi_3^+ + 1/8\,\psi_4^+$$

and

$$\phi_4^+ = \psi_1^+ + \frac{3}{4}\psi_2^+ + \frac{1}{2}\psi_3^+ + \frac{1}{4}\psi_4^+$$

Solutions of the form $\bar{\phi}_m^+$ as in (B12) have been used in the iteration method presented in Section 5.3.

APPENDIX C

Derivation of Parameters for Elementary Extrapolation

Two Trial Functions

The functional for the void problem, where the void is filled with material of absorption cross section σ_v is

$$K^+(\psi_E^+) = \int_{V_R}\int_{\Omega} \left\{ 2\psi_E^+ S^+ - \left[\underline{\Omega}.\nabla \psi_E^+ \, \underline{\Omega}.\nabla \psi_E^+ + \psi_E^+ \, C \, \psi_E^+ \right] \right\} d\underline{\Omega}\, dv$$

$$- \int_{V_V}\int_{\Omega} \left[\frac{(\underline{\Omega}.\nabla\psi_E^+)^2}{\sigma_v} + \sigma_v (\psi_E^+)^2 \right] d\Omega\, dv$$

$$- \int_{S_b}\int_{\Omega} |\underline{\Omega}.\underline{n}| \, (\psi_E^+)^2 \, d\Omega\, ds \qquad \text{(C1)}$$

where

$$\psi_E^+(r, \underline{\Omega}) = \alpha \psi_1^+(r, \underline{\Omega}) + (1-\alpha)\psi_2^+(r, \underline{\Omega})$$

is the extrapolated solution using two trial functions ψ_1^+, ψ_2^+. These are obtained by solving the given system with the void filled with material of cross sections σ_{v1} and σ_{v2} respectively. Substituting for $\psi_E^+(r, \underline{\Omega})$ in (C1) and maximising $K^+(\psi_E^+)$ with respect to the parameter α gives

$$\sigma_v \int_{V_R}\int_{\Omega} \left\{ \left[\psi_1^+ - \psi_2^+ \right] S^+ - \left(\alpha \underline{\Omega}.\nabla \left[\psi_1^+ - \psi_2^+\right] + \underline{\Omega}.\nabla \psi_2^+ \right) \underline{\Omega}.\nabla \left(\psi_1^+ - \psi_2^+\right) \right.$$
$$\left. - \left(\alpha \left[\psi_1^+ - \psi_2^+\right] + \psi_2^+ \right) C \left(\psi_1^+ - \psi_2^+\right) \right\} d\Omega\, dv$$
$$- \int_{V_V}\int_{\Omega} \left\{ \left(\alpha \underline{\Omega}.\nabla \left[\psi_1^+ - \psi_2^+\right] + \underline{\Omega}.\nabla \psi_2^+ \right) \underline{\Omega}.\nabla \left(\psi_1^+ - \psi_2^+\right) \right.$$
$$\left. + \sigma_v^2 \left(\alpha \left[\psi_1^+ - \psi_2^+\right] + \psi_2^+ \right) C \left(\psi_1^+ - \psi_2^+\right) \right\} d\Omega\, dv \qquad \text{(C2)}$$
$$- \sigma_v \int_{S_b}\int_{\Omega} |\underline{\Omega}.\underline{n}| \left(\alpha \left[\psi_1^+ - \psi_2^+\right] + \psi_2^+ \right) \left(\psi_1^+ - \psi_2^+\right) d\Omega\, ds = 0$$

Expanding α in a power series in σ_v as

$$\alpha = \alpha(\sigma_v) = a_0 + a_1\sigma_v + a_2\sigma_v^2 + \cdots\cdots\cdots \tag{C3}$$

Substituting for α in (C2) and equating powers of σ_v gives

$$\hat{a}_0 = \frac{-\int_{V_v}\int_{\Omega} \underline{\Omega}\cdot\nabla\psi_2^+ \,\underline{\Omega}\cdot\nabla(\psi_1^+ - \psi_2^+)\, d\Omega\, dV}{\int_{V_v}\int_{\Omega} \left[\underline{\Omega}\cdot\nabla(\psi_1^+ - \psi_2^+)\right]^2 d\Omega\, dV} \tag{C4}$$

$$\hat{a}_1 = \frac{\begin{aligned}&\int_{V_R}\int_{\Omega} \Big\{ \left[\psi_1^+ - \psi_2^+\right] S^+ - \left(\hat{a}_0\,\underline{\Omega}\cdot\nabla\left[\psi_1^+ - \psi_2^+\right] + \underline{\Omega}\cdot\nabla\psi_2^+\right) G\,\underline{\Omega}\cdot\nabla\left[\psi_1^+ - \psi_3^+\right] \\ &\quad - \left(\hat{a}_0\left[\psi_1^+ - \psi_2^+\right] + \psi_2^+\right) C\left[\psi_1^+ - \psi_2^+\right] \Big\}\, d\Omega\, dV \\ &- \int_{S_b}\int_{\Omega} |\underline{\Omega}\cdot\underline{n}|\left(\hat{a}_0(\psi_1^+ - \psi_2^+) + \psi_2^+\right)\left[\psi_1^+ - \psi_2^+\right] d\Omega\, dS\end{aligned}}{\int_{V_v}\int_{\underline{\Omega}} \left(\underline{\Omega}\cdot\nabla\left[\psi_1^+ - \psi_2^+\right]\right)^2 d\underline{\Omega}\, dV} \tag{C5}$$

$$\hat{a}_2 = \frac{\begin{aligned}&\hat{a}_1\int_{V_R}\int_{\Omega} \Big\{ -\underline{\Omega}\cdot\nabla\left[\psi_1^+ - \psi_2^+\right] G\,\underline{\Omega}\cdot\nabla\left[\psi_1^+ - \psi_3^+\right] - \left[\psi_1^+ - \psi_2^+\right] C\left[\psi_1^+ - \psi_2^+\right] \\ &\quad - \left(\hat{a}_0\left[\psi_1^+ - \psi_2^+\right] + \psi_2^+\right) C\left[\psi_1^+ - \psi_2^+\right] \Big\}\, d\Omega\, dV \\ &- \hat{a}_1\int_{S_b}\int_{\Omega} |\underline{\Omega}\cdot\underline{n}|\left[\psi_1^+ - \psi_2^+\right]^2 d\Omega\, dS\end{aligned}}{\int_{V_v}\int_{\Omega} \left(\underline{\Omega}\cdot\nabla\left[\psi_1^+ - \psi_2^+\right]\right)^2 d\Omega\, dV} \tag{C6}$$

Hence $$\psi_E^+(\underline{r},\underline{\Omega}) = \hat{\psi}_0^+ + \hat{\psi}_1^+ \sigma_v + \hat{\psi}_2^+ \sigma_v^2 + \cdots\cdots$$

where

$$\begin{aligned} \hat{\psi}_1^0 &= \hat{a}_0 (\psi_1^+ - \psi_2^+) + \psi_2^+ \\ \hat{\psi}_1^+ &= \hat{a}_1 (\psi_1^+ - \psi_2^+) + \psi_2^+ \\ \hat{\psi}_2^+ &= \hat{a}_2 (\psi_1^+ - \psi_2^+) \qquad \text{etc.} \end{aligned} \tag{C7}$$

Three Trial Functions

In the case of three trial functions, the extrapolated solution is

$$\psi_E^+(\underline{r},\underline{\Omega}) = \alpha\psi_1^+ + \beta\psi_2^+ + (1-\alpha-\beta)\psi_3^+ \tag{C8}$$

Each of the coefficients is expanded in a power series involving σ_v. Substituting for ψ_E^+ in the K^+ functional gives

$$\begin{aligned} K^+(\psi_E^+) = \int_{V_R}\int_{\Omega} \Big\{ & 2(\alpha\psi_1^+ + \beta\psi_2^+ + (1-\alpha-\beta)\psi_3^+) S^+ \\ & - [\underline{\Omega}\cdot\nabla(\alpha\psi_1^+ + \beta\psi_2^+ + (1-\alpha-\beta)\psi_3^+)] G [\underline{\Omega}\cdot\nabla(\alpha\psi_1^+ + \beta\psi_2^+ + (1-\alpha-\beta)\psi_3^+)] \\ & - (\alpha\psi_1^+ + \beta\psi_2^+ + (1-\alpha-\beta)\psi_3^+) C (\alpha\psi_1^+ + \beta\psi_2^+ + (1-\alpha-\beta)\psi_3^+) \Big\} d\Omega\, dV \end{aligned}$$

$$- \int_{V_v}\int_{\Omega} \left\{ \frac{1}{\sigma_v} (\underline{\Omega}\cdot\nabla(\alpha\psi_1^+ + \beta\psi_2^+ + (1-\alpha-\beta)\psi_3^+))^2 + \sigma_v (\alpha\psi_1^+ + \beta\psi_2^+ + (1-\alpha-\beta)\psi_3^+)^2 \right\} d\Omega\, d$$

$$- \int_{S_b}\int_{\Omega} (\alpha\psi_1^+ + \beta\psi_2^+ + (1-\alpha-\beta)\psi_3^+)^2 |\underline{\Omega}\cdot\underline{n}|\, d\Omega\, dS$$

where $\alpha = a_0 + a_1 \sigma_v + a_2 \sigma_v^2 + \cdots\cdots$

and $\beta = b_0 + b_1 \sigma_v + b_2 \sigma_v^2 + \cdots\cdots$

Differentiating with respect to α and β and setting $\frac{\partial K^+}{\partial \alpha}$ and $\frac{\partial K^+}{\partial \beta}$ to zero gives

$$0 = \int_{V_R}\int_{\Omega} \Big\{ 2\,(\psi_1^+ - \psi_3^+)S^+ - \big[\underline{\Omega}\cdot\nabla\,(\alpha\psi_1^+ + \beta\psi_2^+ + (1-\alpha-\beta)\psi_3^+)\,\varsigma\,(\underline{\Omega}\cdot\nabla(\psi_1^+ - \psi_3^+)) + \underline{\Omega}\cdot\nabla\,(\psi_1^+ - \psi_3^+)\,\varsigma\,\big[\underline{\Omega}\cdot\nabla\,(\alpha\psi_1^+ + \beta\psi_2^+ + (1-\alpha-\beta)\psi_3^+)\big] - \big[(\alpha\psi_1^+ + \beta\psi_2^+ + (1-\alpha-\beta)\psi_3^+)\,C\,(\psi_1^+ - \psi_3^+) + (\psi_1^+ - \psi_3^+)\,C\,(\alpha\psi_1^+ + \beta\psi_2^+ + (1-\alpha-\beta)\psi_3^+)\big] \Big\}\, d\Omega\, dv \qquad (C9)$$

$$-2\int_{S_b}\int_{\Omega} |\underline{\Omega}\cdot\underline{n}|\,(\alpha\psi_1^+ + \beta\psi_2^+ + (1-\alpha-\beta)\psi_3^+)\,(\psi_1^+ - \psi_3^+)\, d\Omega\, ds$$

$$-2\int_{V_V}\int_{\Omega} \Big\{ \frac{1}{\sigma_v}\,(\underline{\Omega}\cdot\nabla\,(\alpha\psi_1^+ + \beta\psi_2^+ + (1-\alpha-\beta)\psi_3^+)\,\underline{\Omega}\cdot\nabla\,(\psi_1^+ - \psi_3^+)) + \sigma_v\,(\alpha\psi_1^+ + \beta\psi_2^+ + (1-\alpha-\beta)\psi_3^+)\,(\psi_1^+ - \psi_3^+) \Big\}\, d\Omega\, dv$$

$$0 = \int_{V_R}\int \Big\{ 2\,(\psi_2^+ - \psi_3^+)S^+ - 2\big[\underline{\Omega}\cdot\nabla\,(\alpha\psi_1^+ + \beta\psi_2^+ + (1-\alpha-\beta)\psi_3^+)\,\varsigma\,(\psi_2^+ - \psi_3^+)\big] - 2\big[(\alpha\psi_1^+ + \beta\psi_2^+ + (1-\alpha-\beta)\psi_3^+)\,C\,(\psi_2^+ - \psi_3^+) \Big\}\, d\Omega\, dv \qquad (C10)$$

$$-\int_{V_V}\int_{\Omega} 2\Big\{ \frac{1}{\sigma_v}\,(\underline{\Omega}\cdot\nabla\,(\alpha\psi_1^+ + \beta\psi_2^+ + (1-\alpha-\beta)\psi_3^+)\,\underline{\Omega}\cdot\nabla(\psi_2^+ - \psi_3^+) + \sigma_v\,(\alpha\psi_1^+ + \beta\psi_2^+ + (1-\alpha-\beta)\psi_3^+)\,(\psi_2^+ - \psi_3^+) \Big\}\, d\Omega\, dv$$

$$-\int_{S_b}\int_{\Omega} 2\,|\underline{\Omega}\cdot\underline{n}|\,(\alpha\psi_1^+ + \beta\psi_2^+ + (1-\alpha-\beta)\psi_3^+)\,(\psi_2^+ - \psi_3^+)\, d\Omega\, ds$$

Substituting for α and β and equating powers of σ_v^* gives

$$\hat{a}_0 \int_{V_V}\int_{\Omega} [\underline{\Omega}.\nabla(\psi_1^+ - \psi_3^+)]^2 d\underline{\Omega}\, dV + \hat{b}_0 \int_{V_V}\int_{\Omega} \underline{\Omega}.\nabla(\psi_2^+ - \psi_3^+)\, \underline{\Omega}.\nabla(\psi_1^+ - \psi_3^+)\, d\underline{\Omega} dV$$
$$= -\int_{V_V}\int_{\Omega} \underline{\Omega}.\nabla\psi_3^+\, \underline{\Omega}.\nabla(\psi_1^+ - \psi_3^+)\, d\underline{\Omega} dV \qquad (C11)$$

$$\hat{a}_0 \int_{V_V}\int_{\Omega} \underline{\Omega}.\nabla(\psi_1^+ - \psi_3^+)\, \underline{\Omega}.\nabla(\psi_2^+ - \psi_3^+)\, d\underline{\Omega} dV + \hat{b}_0 \int_{V_V}\int_{\Omega} [\underline{\Omega}.\nabla(\psi_2^+ - \psi_3^+)]^2 d\Omega\, dV$$
$$= -\int_{V_V}\int_{\Omega} \underline{\Omega}.\nabla\psi_3^+\, \underline{\Omega}.\nabla(\psi_2^+ - \psi_3^+)\, d\Omega\, dV$$

Hence

$$\hat{a}_0 = \frac{(c_2 d_{12} - c_1 d_{22})}{(d_{21} d_{12} - d_{11} d_{22})}$$
$$\hat{b}_0 = \frac{(c_2 d_{11} - c_1 d_{21})}{(d_{11} d_{22} - d_{12} d_{21})} \qquad (C12)$$

where

$$d_{11} = \int_{V_V}\int_{\Omega} [\underline{\Omega}.\nabla(\psi_1^+ - \psi_3^+)]^2 d\Omega\, dV$$

$$d_{12} = d_{21} = \int_{V_V}\int_{\Omega} \underline{\Omega}.\nabla(\psi_1^+ - \psi_3^+)\, \underline{\Omega}.\nabla(\psi_2^+ - \psi_3^+)\, d\Omega\, dV$$

$$d_{22} = \int_{V_V}\int_{\Omega} [\underline{\Omega}.\nabla(\psi_2^+ - \psi_3^+)]^2 d\underline{\Omega}\, dV$$

$$c_1 = -\int_{V_V}\int_{\Omega} \underline{\Omega}.\nabla\psi_3^+ \cdot \underline{\Omega}.\nabla(\psi_1^+ - \psi_3^+)\, d\Omega\, dV$$

$$c_2 = -\int_{V_V}\int_{\Omega} \underline{\Omega}.\nabla\psi_3^+ \cdot \underline{\Omega}.\nabla(\psi_2^+ - \psi_3^+)\, d\Omega\, dV$$

Four Trial Functions

In this case the trial function is given by

$$\psi_\epsilon^+(\underline{r},\underline{\Omega}) = \alpha\,\psi_1^+ + \beta\,\psi_2^+ + \gamma\,\psi_3^+ + \delta\,\psi_4^+ \qquad \text{(C13)}$$

where $\alpha+\beta+\gamma+\delta = 1$.

The optimised coefficients are as follows:

$$\hat{a}_0 = \frac{b_1}{a_{11}} - \frac{a_{12}}{a_{11}}\hat{b}_0 - \frac{a_{13}}{a_{11}}\hat{c}_0 \qquad \text{(C14)}$$

$$\hat{b}_0 = \frac{\left(\frac{b_1}{a_{11}} - \frac{b_2}{a_{21}}\right)}{\left(\frac{a_{12}}{a_{11}} - \frac{a_{22}}{a_{21}}\right)} - \frac{\left(\frac{a_{13}}{a_{11}} - \frac{a_{23}}{a_{21}}\right)}{\left(\frac{a_{12}}{a_{11}} - \frac{a_{22}}{a_{21}}\right)}\hat{c}_0 \qquad \text{(C15)}$$

$$\hat{c}_0 = \frac{\left[\frac{\left(\frac{b_1}{a_{11}} - \frac{b_2}{a_{21}}\right)}{\left(\frac{a_{12}}{a_{11}} - \frac{a_{22}}{a_{21}}\right)} - \frac{\left(\frac{b_2}{a_{21}} - \frac{b_3}{a_{31}}\right)}{\left(\frac{a_{22}}{a_{21}} - \frac{a_{32}}{a_{31}}\right)}\right]}{\left[\frac{\left(\frac{a_{13}}{a_{11}} - \frac{a_{23}}{a_{21}}\right)}{\left(\frac{a_{12}}{a_{11}} - \frac{a_{32}}{a_{31}}\right)} - \frac{\left(\frac{a_{23}}{a_{21}} - \frac{a_{33}}{a_{31}}\right)}{\left(\frac{a_{22}}{a_{21}} - \frac{a_{32}}{a_{31}}\right)}\right]} \qquad \text{(C16)}$$

where

$$b_1 = -\int_W\int_\Omega \underline{\Omega}\cdot\nabla\psi_4^+\;\underline{\Omega}\cdot\nabla\left(\psi_1^+ - \psi_4^+\right)\,d\Omega\,dV$$

$$b_2 = -\int_{V_V}\int_{\Omega} \underline{\Omega}\cdot\nabla\,\psi_4^+\;\underline{\Omega}\cdot\nabla\left(\psi_2^+ - \psi_4^+\right) d\Omega\, dV$$

$$b_3 = -\int_{V_V}\int_{\Omega} \underline{\Omega}\cdot\nabla\,\psi_4^+\;\underline{\Omega}\cdot\nabla\left(\psi_3^+ - \psi_4^+\right) d\Omega\, dV$$

$$a_{11} = \int_{VV}\int_{\Omega} \underline{\Omega}\cdot\nabla\left(\psi_1^+ - \psi_4^+\right)\underline{\Omega}\cdot\nabla\left(\psi_1^+ - \psi_4^+\right) d\Omega\, dV$$

$$a_{12} = \int_{VV}\int_{\Omega} \underline{\Omega}\cdot\nabla\left(\psi_2^+ - \psi_4^+\right)\underline{\Omega}\cdot\nabla\left(\psi_1^+ - \psi_4^+\right) d\Omega\, dV = a_{21}$$

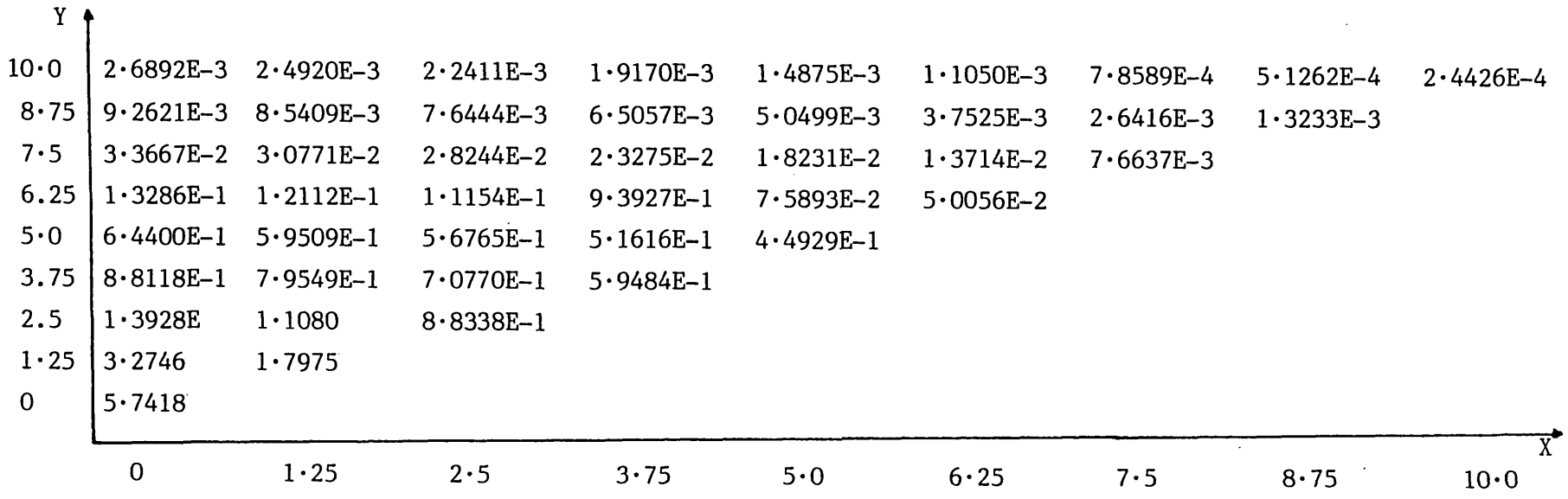
$$a_{13} = \int_{VV}\int_{\Omega} \underline{\Omega}\cdot\nabla\left(\psi_3^+ - \psi_4^+\right)\underline{\Omega}\cdot\nabla\left(\psi_1^+ - \psi_4^+\right) d\Omega\, dV = a_{31}$$

$$a_{22} = \int_{VV}\int_{\Omega} \underline{\Omega}\cdot\nabla\left(\psi_2^+ - \psi_4^+\right)\underline{\Omega}\cdot\nabla\left(\psi_2^+ - \psi_4^+\right) d\Omega\, dV$$

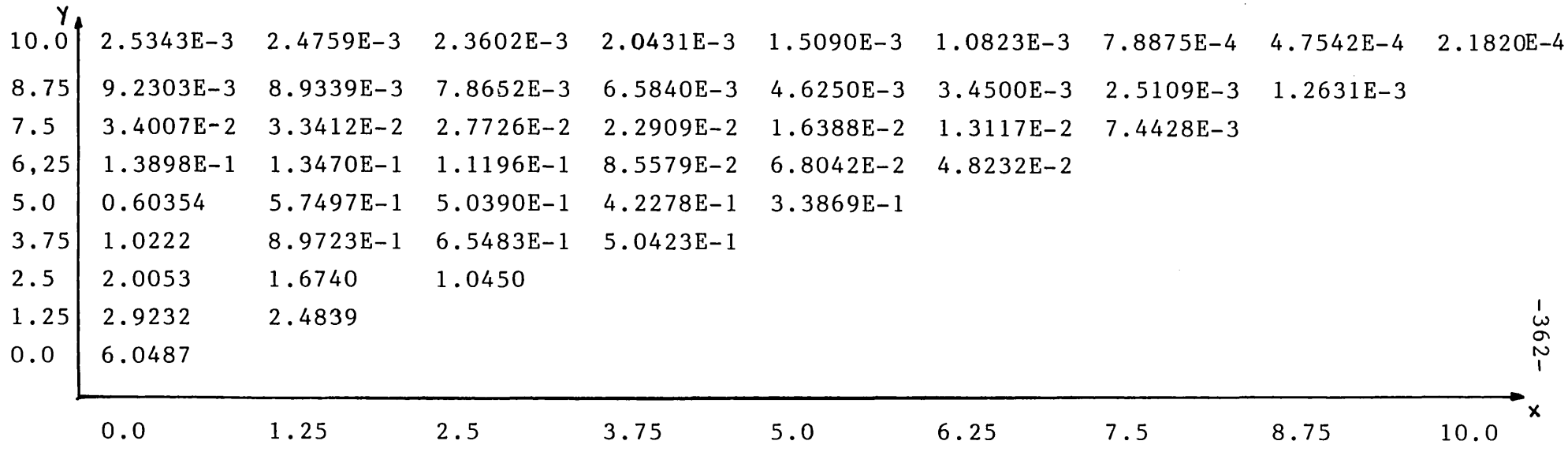
$$a_{32} = \int_{VV}\int_{\Omega} \underline{\Omega}\cdot\nabla\left(\psi_3^+ - \psi_4^+\right)\underline{\Omega}\cdot\nabla\left(\psi_2^+ - \psi_4^+\right) d\Omega\, dV = a_{23}$$

$$a_{33} = \int_{VV}\int_{\Omega} \underline{\Omega}\cdot\nabla\left(\psi_3^+ - \psi_4^+\right)\underline{\Omega}\cdot\nabla\left(\psi_3^+ - \psi_4^+\right) d\Omega\, dV \;.$$

APPENDIX D



RANKERN Solutions for the Square Source Problem With Pure Absorber.



Co-ordinates Along OX

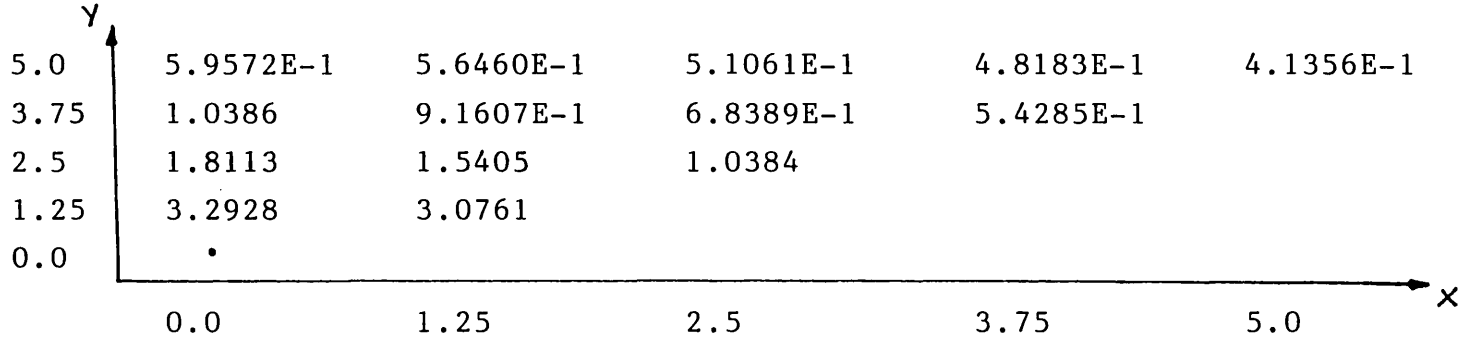
3 Trial Functions, 4 Moments, 16x16 mesh.

$\psi_E = \alpha\phi_1^+ + \beta\phi_2^+ + (1-\alpha-\beta)\phi_3^+$

$\alpha = 0.53747, \quad \beta = -2.15757$

$\sigma_{v1} = 0.8, \quad \sigma_{v2} = 0.319, \quad \sigma_{v3} = 0.128$

Global Extrapolation Results for Square Source Void Problem with Pure Absorber



Co-ordinates Along OX (cm)

Nodal Extrapolation Results(in Void) for Square Source Void Problem with Pure Absorber

3 moments, 16x16 mesh

$\sigma_{v1} = 0.8$, $\sigma_{v2} = 0.128$ cm^{-1}

y		
	8.8589E-1	6.6228E-1
14.0	6.2655E-1	5.4959E-1
	4.7863E-1	4.3705E-1
12.0	3.6161E-1	3.5001E-1
	2.8525E-1	2.8905E-1
10.0	2.3969E-1	2.4837E-1
	2.1179E-1	2.2108E-1
8.0	1.9209E-1	2.0140E-1
	1.7594E-1	1.8534E-1
6.0	1.6183E-1	1.7054E-1
	1.4935E-1	1.5589E-1
4.0	1.3789E-1	1.4108E-1
	1.2659E-1	1.2666E-1
2.0	1.1543E-1	1.1442E-1
	1.0734E-1	1.0814E-1
0.0	1.1067E-1	1.1207E-1
	0.0	3.0 (x)

Co-ordinates Along OX

Nodal Extrapolation Results (in void)
for the Straight Duct Source Problem.

3 Moments, 14x18 mesh
$\sigma_{\gamma_1} = 0.2$ and $\sigma_{\gamma_2} = 0.05$ cm^{-1}.

List of Joint Publications

1. Treatment of Voids in Finite Element Transport Methods.
   R.T. Ackroyd, J.G. Issa and N.S. Riyait.
   Progress in Nuclear Energy 18, 1/2. (1986)

2. Comparison of Numerical Solution to Predict Neutron Streaming in Shield Design for Re-Processing plants.
   A.K. Ziver, J.G. Issa, N.S. Riyait and M.H. Watmough.
   Progress in Nuclear Energy 18, 1/2. (1986)

3. Multigroup Application of the Anisotropic FEM Code FELTRAN to One, Two, Three-Dimensions and R-Z Problems.
   J.G. Issa, N.S. Riyait, A.J.H. Goddard and G.E. Stott.
   Progress in Nuclear Energy, 18, 1/2 (1986)

4. The Finite Element Method for Multigroup Neutron Transport: Anisotropic Scattering in 1-D Slab Geometry.
   N.S. Riyait and R.T. Ackroyd.
   Annals of Nuclear Energy, 14, 3 (1987)

5. Projection and Conservation Methods for Neutron Transport.
   R.T. Ackroyd, J.G. Issa, N.S. Riyait and M.M. Nanneh.
   The Mathematics of Finite Elements and Applications, Brunel University, April 28 - May 1, 1987.

6. The Finite Element Code FELTRAN: Its Structure and Benchmarking (Poster Session)
   R.T. Ackroyd, A.J.H. Goddard, J.G. Issa and N.S. Riyait.
   MAFELAP, Brunel University, 1987.

7. The Finite Element Transport Code FELTRAN: Its Structure and Benchmarking.
R.T. Ackroyd, A.J.H. Goddard, J.G. Issa, N.S. Riyait and M.H. Watmough.
Topical Meeting on Advances in Reactor Physics, Mathematics and Computation. Paris 1987.

8. Iteration and Extrapolation Methods for the Approximate Solution of the Even Parity Transport Equation for Systems with Voids.
R.T. Ackroyd and N.S. Riyait
To be published in Annals of Nuclear Energy.